2022

Models and Optimal Controls for Smart Homes and their Integration into the Electric Power Grid

Huangjie Gong
University of Kentucky, huangjie.gong@uky.edu
Author ORCID Identifier:
https://orcid.org/0000-0002-5726-9006
Digital Object Identifier: https://doi.org/10.13023/etd.2022.053

STUDENT AGREEMENT:

I represent that my thesis or dissertation and abstract are my original work. Proper attribution has been given to all outside sources. I understand that I am solely responsible for obtaining any needed copyright permissions. I have obtained needed written permission statement(s) from the owner(s) of each third-party copyrighted matter to be included in my work, allowing electronic distribution (if such use is not permitted by the fair use doctrine) which will be submitted to UKnowledge as Additional File.

I hereby grant to The University of Kentucky and its agents the irrevocable, non-exclusive, and royalty-free license to archive and make accessible my work in whole or in part in all forms of media, now or hereafter known. I agree that the document mentioned above may be made available immediately for worldwide access unless an embargo applies.

I retain all other ownership rights to the copyright of my work. I also retain the right to use in future works (such as articles or books) all or part of my work. I understand that I am free to register the copyright to my work.

REVIEW, APPROVAL AND ACCEPTANCE

The document mentioned above has been reviewed and accepted by the student's advisor, on behalf of the advisory committee, and by the Director of Graduate Studies (DGS), on behalf of the program; we verify that this is the final, approved version of the student's thesis including all changes required by the advisory committee. The undersigned agree to abide by the statements above.

Huangjie Gong, Student

Dr. Dan M. Ionel, Major Professor

Dr. Daniel Lau, Director of Graduate Studies

Models and Optimal Controls for Smart Homes and their Integration into the Electric Power Grid

DISSERTATION

A dissertation submitted in partial fulfillment of the requirements for the degree of Doctor of Philosophy in the College of Engineering at the University of Kentucky

By

Huangjie Gong

Lexington, Kentucky

Director: Dr. Dan M. Ionel, Professor and L. Stanley Pigman Chair in Power

Lexington, Kentucky 2022

ABSTRACT OF DISSERTATION

Models and Optimal Controls for Smart Homes and their Integration into the Electric Power Grid

Smart homes can operate as a distributed energy resource (DER), when equipped with controllable high-efficiency appliances, solar photovoltaic (PV) generators, electric vehicles (EV) and energy storage systems (ESS). The high penetration of such buildings changes the typical electric power load profile, which without appropriate controls, may become a "duck curve" when the surplus PV generation is high, or a "dragon curve" when the EV charging load is high. A smart home may contribute to an optimal solution of such problems through the energy storage capacity, provided by its by battery energy storage system (BESS), heating, ventilation, and air conditioning (HVAC) system, and electric water heater (EWH), and the advanced controls of an home energy management (HEM). The integrated modeling of home energy usage and electric power distribution system, developed as part of this dissertation research, provides a testbed for HEM control methods and prediction of long-term scenarios.

A hybrid energy storage system including batteries and a variable power EWH was proposed. It was demonstrated that when the operation of the proposed hybrid energy storage system was coordinated with PV generation, the required battery capacity would be substantially reduced while still maintaining the same functionality for smart homes to operate as dispatchable generators. A newly developed co-simulation framework, INSPIRE+D, enables the dynamic simulation of smart homes and their connection to the grid.

The equivalent thermal model of a reference house was proposed with parameters based on the systematic study of experimental data from fully instrumented field demonstrators. Energy storage capacity of HVAC systems was calculated and an equivalent state-of-charge (SOC) was defined. The aggregated HVAC load was calculated based on special HVAC parameters and a sequential DR scheme was proposed to reduce both ramping rate and peak power, while maintaining human comfort according to ASHRAE standards. A long short-term memory (LSTM) method was

applied to for the identification of HVAC system from the aggregated data.

The generic water heater load curves based on the data retrieved from large experimental projects for resistive EWHs and heat pump water heaters (HPWHs) were created. A community-level digital twin with scalability has been developed to capture the aggregated hot water flow and average hot temperature in the tanks. The potential electricity saving of shifting from EWH to HPWH was calculated. The energy storage capacities for both EWHs and HPWHs were calculated.

Long term load prediction by considering different fractions of smart homes with HEM for at the power system was provided based on one of the largest rural field smart energy technology demonstrators located in Glasgow, KY, US. Also demonstrates was the ability of EWH to provide ancillary services while maintaining customer comfort. The minimum participation rates for EWH and batteries were calculated and compared with respect to different peak reduction targets.

The aggregated charging load for EV in a community was calculated based on data from the National Travel Household Survey (NHTS). The EV charging and RESS operation were scheduled to reduce the daily utility charge. Building resilience was quantified by analyzing the self-sustainment duration for all possible power outages throughout an entire year based on the annual electricity usage of a typical California residence. The influence of factors such as energy use behavioral patterns, BESS capacity, and an availability of EV was evaluated.

A concept of generalized energy storage (GES) model for BESS, EWH and HVAC systems was proposed. The analogies, including SOC versus water/indoor temperature differential, were identified and explained, and models-in-the-loop (MIL) were introduced, which were compatible with the Energy Star and Consumer Technology Association (CTA)-2045 general specifications and command types. A case study is included to illustrate that the "energy content" and "energy take" for BESS and EWH.

The main original contributions of this dissertation include the comprehensive simulation of the total building energy usage and the development of the co-simulation framework incorporating building and power system simulators. Another contribution of the dissertation is the quantification of building resilience based on the building energy usage model. The dissertation also contributes to the concept of GES which regards the HVAC and EWH as virtual energy storage and their unified controls with BESS. The GES facilitates the employment of industrial standards, e.g., CTA-2045, and the hybrid ESS reduces required BESS capacity.

This dissertation contributes to the modeling of aggregated load for EWH, HVAC, and EV using different methods and long term forecasting of power profile at the system level. The aggregated generic load for EWH was calculated based on large amount of field data, the aggregated EV charging load was estimated based on na-

tional survey results, and the aggregated HVAC load was simulated based on the modeling of every residences, where the model parameters were populated according to special distributions. The methods based LSTM for the identification of HVAC power from the aggregated load was developed.

KEYWORDS: Smart home, Generalized energy storage (GES), Electric vehicle (EV), Home energy management (HEM), Long short-term memory (LSTM)

Huangjie Gong

April 21, 2022

Models and Optimal Controls for Smart Homes and their Integration into the Electric Power Grid

By
Huangjie Gong

Dr. Dan M. Ionel
Director of Dissertation

Dr. Daniel Lau
Director of Graduate Studies

April 20, 2022
Date

ACKNOWLEDGMENTS

I am most grateful to my Ph.D. advisor, Professor Dan M. Ionel, Ph.D., FIEEE, L. Stanley Pigman Chair in Power, who has been my strongest supporter during my studies at Universities of Kentucky in Lexington, KY. Professor Ionel has always been a constant source of scientific knowledge, encouragement, and inspiration. He closely guided me through detailed technical subject matters and helped me to step into new areas with his broad knowledge. I am very thankful to him as he trusted me and inspired me for continued progress and achievements. He taught me how to work diligently and efficiently as an independent researcher, as well as a team member and leader. From Professor Ionel, I learned to be open to the fast-changing world and always be ready for new things. From him, I understood the importance of coordination and communication. I am most grateful to Professor Ionel for setting up the SPARK group, a true academic family, and for making us feel at home on a daily basis, and with the occasional surprises and celebrations.

At UK, I am especially thankful for the advice and feedback received from my Ph.D. Committee members Drs. Donald Colliver, Nicholas Jewell, Yuan Liao, Peng Wang, YuMing Zhang, and external examiner Professor Michael Renfro. I would also like to extend my sincere thanks to Dr. Jiangbiao He.

I am deeply indebted to my postdoc mentor, Dr. Vandana Rallabandi, for all her help and guidance, going back to my early days in the Ph.D. program. I would also like to thank all my colleagues in the SPARK Lab, in approximate chronological order: Narges, Akeyo, Yibin, Murat, Naser, Damien, Evan, Rosemary, Donovin, Gerald, Yaser, Ali, and Badewa, and senior postdoc colleagues: Drs. Peng Han and Abdullah Al Hadi, for their special collaboration and friendship.

The continued support of University of Kentucky, the L. Stanley Pigman endowment is gratefully acknowledged. The support of the Department of Energy (DOE), projects #DE-EE0009021 and #DE-EE0008352, and of the National Science Foundation (NSF), award #1936131 is also gratefully acknowledged. My great appreciation is also due for the continued support of A. O. Smith Corp., Flex Power Controls, Inc., Louisville Gas & Electric Company and Kentucky Utilities (LG&E and KU), and Tennessee Valley Authority (TVA).

At A. O. Smith, special thanks are due to Brian Branecky and Tim Rooney for their continued collaboration ranging from the detailed modeling of electric and heat pump water heaters to the broad industrial practical perspectives. At Flex Power Controls, I am very thankful to Gregory Smith and May Jang for their project leadership and technical insights. At LG&E and KU, special thanks are due to Aron Patrick and Nicholas Jewell for their advice and support on topics of power systems and renewable energy, including access to experimental data, coding scripts, and powerful computers. At TVA, special thanks are due to Andrew Frye for his collaboration on smart buildings and grids.

I would like to thank my mother and father, Lijun Huang and Zhengren Gong, for their unlimited love and support. They have always been my best teachers for life and sources of courage. "Who will say that the inch of grass in his heart is gratitude enough for all the sunshine of spring?" I also would like to thank Daniel F. Grant, the best landlord who cared me a lot while my staying in Lexington. Great thanks to my girlfriend, Lijiao Huang for her continued support.

Huangjie Gong

March, 2022

Table of Contents

List of Tables

List of Figures

Chapter 1

Introduction

1.1 Background

According to the U.S. Department of Energy, a net zero energy (NZE) home is a residence for which the total amount of energy used on an annual basis is less than or equal to the amount of renewable energy generated on site [1]. Due to the high energy usage and concerns over greenhouse gas emissions, efforts have been made to implement more NZE homes both in the USA and worldwide. For instance, as per the California Public Utilities Commission, the plan was for residential constructions to be NZE by the year 2020 [2]. The "Nearly zero-energy buildings" proposed by European Commission required all EU Member States to have all new buildings to be nearly zero-energy by the end of 2020 [3]. As a result, a growing number of US states and countries have started to build NZE residences at different scales, varying from single homes to big neighborhoods, and their objectives range from reduced energy usage to net positive energy input to the grid.

The NZE homes typically incorporate solar photovoltaic (PV) systems as the

main source of renewable energy. Solar PV generation is largely dependent by external environment conditions, leading to unpredictability and stochastic properties. The mismatch between the peaks of PV generation and residential load leads to variations in the net power flow, which may cause the "duck curve" phenomenon for example [4]. Such challenges are further exacerbated when a number of PV systems are congregated in the same neighborhood comprising NZE homes [5].

Battery energy storage systems (BESS) provides increased flexibility to the NZE residences. The sizing for BESS is mainly determined by factors including building characteristics, utility tariffs and the BESS operating schedule [6–8]. Apart from the BESS, an electric water heater (EWH) can be regarded as a uni-directional energy storage system.

The ubiquity of EWHs make them one of the most advantageous appliances for participation in the virtual power plant (VPP) operation for residential buildings. The EWHs have large thermal masses of water in their tanks and can be regarded as both heat reservoirs and energy sinks. Nevertheless, the unpredictability of customer behavior makes quantifying the benefits of controlling EWHs difficult. Demand response implementations must carefully balance the water temperature in the tank for the maximum grid benefit between two bounds, i.e., it must be kept high enough to meet the user demand while not exceeding the stipulated safety reference. Fortunately, technologies such as mixing valves may be used to allow the water to be safely stored up to 145F and still meet safety requirements [9, 10].

EWHs can be used to absorb surplus PV generation, or to, for a short period of time, be turned OFF for load shedding while maintaining the water temperature at

the reference temperature. As PV penetration advances, there are multiple benefits of incorporating EWHs into home energy management. Recent research indicates that battery capacity may be reduced by up to 30% when batteries are coordinated with EHW, which were regarded as "uni-directional" energy storage [11].

The heating, ventilation, and air conditioning (HVAC) systems are widely perceived as solely energy-consuming in the power grid. This view is being re-assessed in the field of home energy management (HEM) as recent research from the Oak Ridge National Laboratory (ORNL) demonstrates that the HVAC system can be regarded as an equivalent energy storage device and be conveniently controlled by a similar charging/discharging procedure [12]. For example, a commercial building with multiple zones can be modeled to operate as an equivalent energy storage device and can be controlled by adjusting zonal airflow rates [13]. As claimed in [14], the round trip efficiency of the HVAC-based equivalent energy storage can be near 100%.

Utilizing HVAC systems as demand response (DR) devices has great opportunity to yield significant energy savings, especially at an aggregated level. To properly study the simulated implementation of HVAC DR schemes, a suitable model of HVAC power and energy use is required. Aggregated modeling for a community of air conditioning loads has been proven effective for the study of large-scale DR implementation [15]. Commercial HVAC system modeling employs statistical methods that are also highly accurate [16].

The DR studies with residential-level HVAC models, however, are more recent and have yet to reach this degree of confidence due to the strong link among HVAC energy use, random user behavior, and external weather conditions. To ensure adequate

thermal comfort, the HVAC control follows Standard 55 of the American Society of Heating, Refrigerating and Air-Conditioning Engineers (ASHRAE), in terms of external and internal temperature, relative humidity, individual metabolic rate, etc. [17]. The ASHRAE Standards quantify the comfort of the space using a numerical scale called the Predicted Mean Vote (PMV) that was derived from survey results where participants ranked their comfort from -3, very cold, to 3, very hot. This allows for an association between a range of environmental conditions to a comfortable status within a home that can be calculated as a PMV between -0.5 and 0.5, which may be used to control heating and cooling systems without affecting thermal comfort.

In the rapidly evolving electric power system, in which new renewable and distributed energy resources are being connected and fossil fuel based generators are being retired at a growing rate, it is increasingly more important to ensure a continued and reliable supply of electricity. For example, approximately 8,000 MW may need to be imported to avoid blackouts in California by filling in gaps caused by renewable energy generation variability and increased power demand. Another major threat to energy supply reliability are large natural disasters, such as, in recent years, wide-spread wild fires [18]. In 2020, there were more than 8 thousand fires in California alone resulting in almost 1.5 million burnt out acres and significant power system damage [19]. In a winter storm in 2021, approximately 2 million homes suffered power outages in Texas which substantially increased electricity demand due to record-breaking low temperatures [20]. Worse still, about 34,000 MW of renewable wind generation capability within Texas was lost during this storm as freezing

temperatures forced power plants offline in quick succession [21]. It is very important to ensure power system reliability through whatever means possible under such conditions to protect residents from environmental health risks.

The growing trend of electric vehicles (EV) provides the potential to boost the energy capacity of residential energy storage systems (ESS). Hence, research towards the development of smart energy management in residential houses using home ESS and EV battery systems is in progress [22, 23]. Residences with EV can help to improve the load factor in communities, reducing costs related to the maintenance of transformers, feeders, etc. [24]. A previous study using data from the National Household Travel Survey (NHTS) found that most cars commute around 20 miles daily, resulting in 90% of SOC remaining on average for EVs when they return home [25].

Depending on the user preferences and applications of the EV, the additional energy storage can expand the residential ESS, but may not be available at the residence when the outage occurs. For example, according to recent reports, the very large 90kWh battery installed on the most recent EV model of the Ford F-150 truck can be controlled to supply up to 10 days of electricity for a connected home [26]. Other factors including user behavior regarding residential load, the capacity of the residential ESS, renewable energy generation, etc., should all be taken into consideration for systematically quantifying building resilience.

For modern smart appliances and devices, a new standard was developed as Consumer Technology Association (CTA) 2045 [27],[28]. This initiative aims at meeting the challenges of the large deployment of smart devices, including differences between

products across manufacturers and data streaming. In principle, the Energy Star [29] and CTA-2045 standard define a set of functional requirements such as "normal operation", "shed", "load up", etc., and a set of specifications and concepts such as "energy capacity", "energy content", and "energy take". Those specifications and functional requirements may be extended to any energy storage device, enabling a unified approach at the system level. For EWH, success has been reported at the individual residential and utility aggregated levels [30, 31].

In the past decade the penetration of smart metering in the United States has rapidly increased from less than 5% in 2008 to over 60% in 2019 [32] with more than 90 million devices installed. The increase in smart meter infrastructure represents a major shift in smart grid equipment deployment, but regulatory and demand flexibility barriers still exist in utilizing the smart meters in DR programs such as time-of-use (ToU) pricing. Furthermore, to assess load specific information from HVAC systems and water heaters, the pro-dominant use devices, through field measurements requires additional direct load control (DLC) instrumentation such as [33] on top of smart meters, which poses a substantial cost and implementation barrier, including data management and processing challenges [34].

1.2 Literature Review

A brief literature review is provided in this section with more details being included in each of the dissertation chapters. Starting with the concept of smart home, this is one of the enabling ideas for building a pathway towards a sustainable power system in the future by facilitating the participation of every power generation entity.

The futuristic smart homes not only integrate information technology but also provide the opportunity to incorporate other innovative technologies such as PV, smart devices, and energy storage. Due to such technological advancements, smart homes can enhance energy efficiency, and improve both stability and reliability by allowing owners to regulate electricity usage [35–37]. They may also have a positive impact on the electric utility overall residential load by minimizing both energy usage and peak demand in the residences [38–41].

Most research works report simulation of the residential electricity consumption by either mathematical models or building energy simulation software. The mathematical house energy usage models sum the typical household loads [42–51]. Coupling factors including solar illumination, radiant energy from appliances and people, impact of airflow, and etc. add complexities to the mathematical models. There is a trade-off between the accuracy and complexity of such models. Other research works use building energy simulation software to produce the static house load profiles. The software tools such as EnergyPlus, Building Energy Optimization (BEopt), eQUEST, etc., are able to model houses with various characteristics in different locations[52–59]. The Integrated District Energy Assessment (IDEA) reports another method to model and control the building energy usage considering the environment, networks and building characteristics [60].

Some technical challenges are associated with the high penetration of PV in the residences, one of which is the "duck curve". This phenomenon occurs when the net power demand fluctuates with a large deviation within a short period, typically during the hours between the afternoon and the evening [4]. For ensuring local voltage

support, it is necessary to maintain a minimum generation of electricity by the utility plants. Hence, the reliability of the power system is compromised when the generation of power is minimized during the mid-day to allow high PV generation [61]. To match with the fast increasing power demand in the evening, high-cost high-ramp rate generators are required when PV generation becomes unavailable [62]. Electrical energy storage systems can be divided into three categories: electrochemical, mechanical, and ultracapacitors [63]. A deferrable load can be redefined as an energy storage device by three integral properties: "the volume of energy that can be stored, the rate at which energy can be absorbed, and the rate at which energy can be released" [64]. This uniformity enables a single HEM strategy across electric energy storage devices and deferrable energy loads [11, 22].

The EWHs are also capable of providing ancillary services due to the large thermal mass of the water tank, as well as their presence in most households [65, 66]. The potential of water heater related technologies was widely appreciated in the annual conference of Hot Water Forum held by the American Council for an Energy-Efficient Economy (ACEEE) [67]. Most EWH manufacturers allow the CTA-2045 modules in their new products or offer refurbishments to enable real-time communication and control [68, 69]. Previous research showed that a smart home may achieve comparable functionality with a smaller battery energy capacity, given that special EWH and associated controls are incorporated in a hybrid energy storage system [11]. These services could improve the reliability of the grid and offer monetary benefits to both the grid and residences while maintaining user comfort [70–74]. The potential regulation capacity of water heaters is impacted by factors including ambient temperature,

hot water usage, and setpoint [75–78].

The electric power profile of water heaters is dependent of user behavior. In previous studies, the hot water draws for 48 representative days were evaluated based on measured data from California homes [79]. The proposed schedules are used in the California Building Energy Code Compliance for Residential buildings (CBECC-Res) [80]. In another study, the aggregated EWH load was calculated by analyzing the hot water usage schedules [81]. A typical aggregated load for EWHs has a morning and evening peak, as shown in the study involving 50 water heaters [82]. The aggregated load curve for the resistive EWHs was proposed in a previous conference paper by the same group of authors [83].

Ancillary services, such as those described in [84], are employed in order to enhance the capabilities of the electric power system. Smart homes can be used as virtual energy storage by utilizing various thermal components such as the HVAC systems, EWH for circumventing peak demand [85]. Residence can support the ancillary services with its energy flexibility, which depends on factors including the capacity of the HVAC system [86]. The aggregated HVAC systems can be used to improve power quality efficient in DR [87]. At the aggregated level, the HVAC systems can be controlled in a sequential way to reduce the peak demand while maintaining the user comfort [88].

Studies reported multiple demonstrations for the effectiveness of HVAC systems as DR devices through control or price-based schemes [81]. A study in which indoor temperature of an individual simulated building was controlled based on electricity retail prices found that heating and cooling energy use was reduced by 12% and 21%

for the coldest and hottest months, respectively [89]. A bonus-based DR approach that employs Stackelberg game theory to reduce mismatch between residential energy use and renewable generation also yielded significant results with a reduced deviation ranging from about 32% to 43% [90]. A bi-level optimal control study including residential HVAC systems resulted in as much as 22% in energy savings [91]. An internet-based survey involving 1,600 members found that approximately 70% of the residential participants would allow the utility to control their switches or thermostats when proper incentives were available [92].

In lack of specific measured data, the HVAC power can be alternatively estimated through software that models the entire building energy usage, such as eQuest [93], BEopt [94], EnergyPlus [11], and OpenStudio [95], or is based on R-C equivalent circuit models, e.g. [96]. Based on a collection of representative building models and assuming a statistical distribution, the HVAC power load at the community level can be aggregated on methods such as Gaussian Kernel Density Estimation (GKDE) [97]. Substantial developing effort and uncertainties, inclusive of those associated with the physical characteristics of construction materials and different human behaviour that result in questionable accuracy and generality, continue to be considered typical challenges for the computational models.

Recent research shows that EV batteries can operate as a voltage source or offline uninterruptible power supply (UPS) for a home in an outage [98, 99]. A well managed energy storage system with BESS and EV support could provide good performance during both transient and steady-state operation, considering the voltage waveform and current harmonics distortion [100]. Different operation modes of EV in smart

homes have been proposed and explored, and it was shown that depending on the usage preferences of the user, EV batteries can act as a power source to feed residential appliances during a power outage [98]. When energy not supplied (ENS) or system average interruption duration index (SAIDI) is taken into consideration, the participation of a EV connected to the home improved resilience the most [101].

The vehicle-to-home (V2H) capability of EV realizes the outage management and cost reduction for a smart home [102, 103]. EV systems can potentially adopt the same method introduced in [104] allowing the battery system to switch between input PV energy harvesting mode and output V2H mode for emergency situations. V2H functionality also improves power system resilience factors including load restoration, reactive power supply, and peak reduction, etc. [105–109]. Bidirectional wireless power transfer will further facilitate V2H applications by enabling higher power transfer and easing the barrier to entry for the consumer [110].

Utilities have electric power monitoring capabilities mostly at the aggregated community level, as recent smart meter-type technologies are yet to be widely deployed in the field at building level and substantially contribute to the historic collection of big-data. As such, there is continued interest in community studies based on a variety of methods such as Multivariate Quantile Regression [111], Deep Neural Networks (DNN) [112], Quantile Regression Averaging on Sister Forecasts [113], and more recently Long Short-Term Memory (LSTM) neural networks, e.g. [114, 115].

Extensive literature review on more detailed aspects of smart homes and their integration in the electric power grid is distributed throughout this dissertation and included in each chapter. These include the co-simulation frameworks in Chapter

2, modeling and control for EWH and HPWH in Chapters 3, modeling and control for VPP in Chapter 4, EV studies in Chapter 5, and the application of artificial intelligence and machine learning methods in Chapter 6.

1.3 Research Objectives and Original Contributions

Research objectives

The increasing penetration of smart homes brings challenges to the power system. The house types are switching from conventional to more advanced. The co-simulation framework is developed for the dynamic analysis of controls for smart homes. The co-simulation framework utilizes OpenDSS, EnergyPlus, and Python. The software framework provides a virtual building, and offers a platform for the testing of various energy storage operating schedules to meet the specified objectives, as introduced in Chapter 2. With the dynamic modeling of building energy usage and power system, the long term forecasting for power demand at system level with increasing penetration of smart homes is enabled.

The solar generation and power demand are mismatched in a typical smart home. The modeling and prediction for PV generation and building load are required for the coordination of the local solar generation and power demand. Challenges in a uniform approach arise because the energy usage in houses differs due to weather, location, human behavior and other factors. As described in Chapter 2, the power demand for smart homes was modeled using whole building modeling software and

validated against experimental data. Systematic guidelines for the sizing of solar PV and energy storage systems to achieve NZE operation are proposed based on the building energy models.

At the power system level, the generic curve for large amount of EWHs is created based on experimental data, as explained in Chapter 3. A representative power profile for aggregated water heater load that can be scaled to any number is developed. Also, EWHs and HPWHs have very different characteristics so they need to be analyzed separately. While inlet and outlet temperatures are easy to measure, they do not represent stored energy well as the temperature inside the water tank is stratified [30].

Most HVAC system models require parameters that are challenging to acquire. It becomes increasingly difficult for aggregated HVAC load modeling considering additional parameters for the multiple buildings. In Chapter 4, the aggregated HVAC load is modeled while monitoring the room temperatures for individual buildings. The proposed model allowed DR control and maintain user comfort.

The aggregated EV charging power is modeled based on the NHTS 2017 data, considering the distribution of arrival home time and daily mileage, as explained in Chapter 5. EV provides larger energy storage and can be used to improve the building resilience. Both battery, EWH, HVAC, and EV are modeled as generalized energy storage complying to CTA-2045 standards.

The quantification for building residence is proposed in Chapter 5. The building resilience for smart homes should consider different time occurrences for power

outages. Residences with solar PV generation would be less dependent on electricity from the grid during the daytime and could self-sustain longer if outages occur at times when electricity usage is low. The building resilience for residences with varying electricity usage, PV generation capability, and BESS capacities need to be analyzed in order to provide a reference for all types of house owners.

The BESS, EV, EWH, and HVAC systems can be described as generalized energy storage (GES) and controlled uniformly using a set of specifications and concepts such as "energy capacity", "energy content", and "energy take". A set of functional requirements defined by the CTA-2045 standards and Energy Star specifications such as "normal operation", "shed", "load up", etc. can be applied to the GES. The proposed GES can potentially meet the challenges in the large employment of smart devices, including differences between products across manufacturers to supply HEM.

Fewer studies into aggregated HVAC load separation of entire distribution circuits including hundreds to thousands of homes were found. The newly developed machine learning method explained in Chapter 6 addresses at the community level the timely topic of day-ahead forecast with a view at enabling optimal energy controls and utility planning. This is possible through the introduction of new key temperature indicators corresponding to the stand-by zero-power operation for the HVAC systems for summer cooling and winter heating and an innovative additional run of the trained LSTM model with such constant temperature and zero irradiance.

Original contributions

The major contributions of the dissertation are summarized as:

- development of a co-simulation framework capable of modeling of electric distribution system and building power flow, demonstrated on case studies with hundreds of homes and appliances
- modeling and control of large-scale virtual power plants using smart homes and appliances as distributed energy resources
- modeling of aggregated power for electric water heaters, HVAC systems, and electric vehicles based on computational and experimental data
- definition of generalized energy storage for electric water heater, HVAC system, battery, and electric vehicle, according to CTA-2045 based conceptions
- disaggregation of HVAC power and baseload using machine learning, the long short-term memory methods, for large communities.

1.4 Dissertation Outline

Following the introduction, co-simulation frameworks for the analysis of the distribution power flow and smart homes are introduced in Chapter 2. In Chapter 2, the residential power systems are sized for smart homes to operate as dispatchable generator or load. The generic load curve and optimal control for aggregated power of EWH and HPWH are developed in Chapter 3. The energy storage capacity of EWH and HPWH are calculated based on the generic load curve. The virtual power plant operation for large residential communities with increasing smart homes is discussed in Chapter 4. The modeling for large scale HVAC load and the DR control for peak

reduction are introduced in the Chapter 4 as well. In Chapter 5, the EV operation at aggregated level for charging (G2V), V2H, and V2G power are analyzed based on survey data and the building resilience is quantified and improved by EV. The application of LSTM machine learning methods for the separation of HVAC power and baseload is presented in Chapter 6. The dissertation is concluded in the last chapter.

1.5 Publications

The main elements of this dissertation have been peer-reviewed and published in the following journal papers:

- **H. Gong**, E. S. Jones, R. Alden, A. G. Frye, D. Colliver, and D. M. Ionel, "Virtual power plant control for large residential communities using HVAC systems for energy storage," *IEEE Transactions on Industry Applications*, Vol. 58, No. 1, pp. 622-633, 2022.

- **H. Gong**, T. Rooney, O. M. Akeyo, B. T. Branecky, and D. M. Ionel, "Equivalent electric and heat-pump water heater models for aggregated community-level demand response virtual power plant controls," *IEEE Access*, Vol. 9, pp. 141233–141244, 2021.

- **H. Gong** and D. M. Ionel, "Improving the power outage resilience of buildings with solar PV through the use of battery systems and EV energy storage," *Energies*, Vol. 14, No. 18, pp. 5749, 2021.

- R. E. Alden, **H. Gong**, E. S. Jones, C. Ababei, and D. M. Ionel, "Artificial intelligence method for the forecast and separation of total and hvac loads with

application to energy management of smart and nze homes," *IEEE Access*, Vol. 9, pp. 160497–160509, 2021.

- **H. Gong**, V. Rallabandi, M. L. McIntyre, E. Hossain, and D. M. Ionel, "Peak reduction and long term load forecasting for large residential communities including smart homes with energy storage," *IEEE Access*, Vol. 9, pp. 19345–19355, 2021.

- **H. Gong**, V. Rallabandi, D. M. Ionel, D. Colliver, S. Duerr, and C. Ababei, "Dynamic modeling and optimal design for net zero energy houses including hybrid electric and thermal energy storage," *IEEE Transactions on Industry Applications*, Vol. 56, No. 4, pp. 4102–4113, 2020.

Additional peer-reviewed conference proceedings papers have been published and are listed in the following:

- **H. Gong**, E. S. Jones, A. Jakaria, A. Huque, A. Renjit, and D. M. Ionel, "Generalized energy storage model-in-the-loop suitable for energy star and CTA-2045 control types," *2021 IEEE Energy Conversion Congress and Exposition (ECCE)*, pp. 814–818, 2021.

- **H. Gong**, O. M. Akeyo, T. Rooney, B. Branecky, and D. M. Ionel, "Aggregated generic load curve for residential electric water heaters," *2021 IEEE Power Energy Society General Meeting (PESGM)*, pp. 1–5, 2021.

- **H. Gong** and D. M. Ionel, "Combined use of EV batteries and PV systems for

improving building resilience to blackouts," *2021 IEEE Transportation Electrification Conference & Expo (ITEC)*, pp. 584–587, 2021.

- **H. Gong**, E. S. Jones, R. E. Alden, A. G. Frye, D. Colliver, and D. M. Ionel, "Demand response of hvacs in large residential communities based on experimental developments," *2020 IEEE Energy Conversion Congress and Exposition (ECCE)*, pp. 4545–4548, 2020.

- **H. Gong**, E. S. Jones, and D. M. Ionel, "An aggregated and equivalent home model for power system studies with examples of building insulation and hvac control improvements," *2020 IEEE Power Energy Society General Meeting (PESGM)*, pp. 1–4, 2020.

- **H. Gong** and D. M. Ionel, "Optimization of aggregated EV power in residential communities with smart homes," *2020 IEEE Transportation Electrification Conference & Expo (ITEC)*, pp. 779–782, 2020.

- R. E. Alden, **H. Gong**, C. Ababei, and D. M. Ionel, "Lstm forecasts for smart home electricity usage," *2020 9th International Conference on Renewable Energy Research and Application (ICRERA)*, pp. 434–438, 2020.

- E. S. Jones, R. E. Alden, **H. Gong**, A. G. Frye, D. Colliver, and D. M. Ionel, "The effect of high efficiency building technologies and PV generation on the energy profiles for typical us residences," *2020 9th International Conference on Renewable Energy Research and Application (ICRERA)*, pp. 471–476, 2020.

- **H. Gong**, V. Rallabandi, M. L. McIntyre, and D. M. Ionel, "On the optimal

energy controls for large scale residential communities including smart homes," *2019 IEEE Energy Conversion Congress and Exposition (ECCE)*, pp. 503–507, 2019.

- **H. Gong**, V. Rallabandi, and D. M. Ionel, "Load variation reduction by aggregation in a community of rooftop PV residences," *2019 IEEE Power Energy Society General Meeting (PESGM)*, pp. 1–4, 2019.

- E. S. Jones, **H. Gong**, and D. M. Ionel, "Optimal combinations of utility level renewable generators for a net zero energy microgrid considering different utility charge rates," *2019 8th International Conference on Renewable Energy Research and Applications (ICRERA)*, pp. 1014–1017, 2019.

- **H. Gong**, V. Rallabandi, D. M. Ionel, D. Colliver, S. Duerr, and C. Ababei, "Net zero energy houses with dispatchable solar PV power supported by electric water heater and battery energy storage," *2018 IEEE Energy Conversion Congress and Exposition (ECCE)*, pp. 2498–2503, 2018.

- **H. Gong**, O. Akeyo, V. Rallabandi, and D. M. Ionel, "Real time operation of smart homes with PV and battery systems under variable electricity rate schedules and transactive power flow," *2018 7th International Conference on Renewable Energy Research and Applications (ICRERA)*, pp. 1392–1395, 2018.

- O. Akeyo, **H. Gong**, V. Rallabandi, N. Jewell, and D. M. Ionel, "Power utility tests for multi-mw high energy batteries," *2018 7th International Conference on Renewable Energy Research and Applications (ICRERA)*, pp. 1396–1399,

2018.

Other papers have been completed and are currently under review:

- **H. Gong**, R. E. Alden, A. Patrick, and D. M. Ionel, "Community level total load forecast and HVAC disaggregation through a new LSTM method," *Energies*, 15p, 2021, *(Submitted in Dec, 2021)*.

- **H. Gong**, E. S. Jones, A. Jakaria, A. Huque, A. Renjit, and D. M. Ionel, "Large-scale modeling and demand response control of electric water heaters with energy star and CTA-2045 control types in distribution power system," *IEEE Transactions on Industry Applications*, 10p, 2021, *(Submitted in Dec, 2021)*.

- **H. Gong**, D. M. Ionel, and R. E. Alden, "V2G Operations for Community as VPP Complying to CTA-2045 Standards Based on Stochastic EV Power Modeling," *2022 IEEE Transportation Electrification Conference & Expo (ITEC)*, 5p, 2022, *(Submitted in Jan, 2022)*.

- L. Donovin, **H. Gong**, and D. M. Ionel, "Sizing considerations for EV dynamic wireless charging systems with integrated energy storage," *2022 IEEE Transportation Electrification Conference & Expo (ITEC)*, 6p, 2022, *(Submitted in Jan, 2022)*.

Chapter 2

Co-simulation of Buildings and Electric Power Grid

2.1 Introduction

The advancement of smart home and grid technologies and the associated electric power system integration studies relies on individual and combined simulators for buildings, such as EnergyPlus, and circuit networks, e.g., OpenDSS, MATPOWER, GridLAB-D, etc. [116]. OpenDSS versions of the representative IEEE distribution system test cases, such as the IEEE 123-bus test system, are available and may be employed for studies of large scale Distributed Energy Resource (DER) implementation and demand response (DR) control [117, 118]. These distribution system models in combination with the simulation of smart devices enables the community-level study of control strategies in an aggregated manner.

A co-simulation framework named INSPIRE+D, incorporating freeware including Python, BEopt, EnergyPlus, and OpenDSS is proposed. The proposed co-simulation framework is capable of simulating the energy usage and instantaneous solar generation for a large community of net zero energy (NZE) homes, and their interconnection

with the grid. An important feature of INSPIRE+D is that it utilizes OpenDSS, widely used by the utilities, in contrast with more academic approaches based on MATPOWER. There are only very few such simulation tools available, including the authors' previous Smartbuilds, the PNNL developed GridLAB-D and the extremely recently announced HELICS by PNNL, which is yet to be used by the professional community [119]. The software framework provides virtual buildings, and offers a platform for the testing of various energy storage operating schedules to meet the specified objectives.

Another testbed, namely, the DER integration testbed, which utilizes MILs to simulate DERs, enables the study of home energy management (HEM) system implementation at the residential and community level. The testbed includes open-source simulation software, was originally developed by the Electric Power Research Institute (EPRI), comprises multiple layers for controls, devices, and circuits, and is able to communicate using protocols that are typically employed for hardware components [120, 121]. HEMs may coordinate various DERs such that energy use and cost is optimized. Algorithms developed for such optimization may shift energy usage of controllable loads, such as heating ventilation and air-conditioning (HVAC), electric water heater (EWH), and electric vehicle (EV), and utilize rooftop solar photovoltaic (PV) generation with battery energy storage system (BESS) such that the distribution system experiences a significant combined effect that may drastically reduce total energy use and peak load for the utility [122, 123]. Using this technique, the DER integration testbed can be used with a combination of real physical devices and/or

with their equivalent model-in-the-loop (MIL) software implementation. The advantages of the MIL approach include cost-effective development and testing in a realistic set-up and the ability to largely scale-up studies with minimal hardware [124, 125].

This chapter features the modeling and validation of the building energy usage within the INSPIRE+D co-simulation framework. The electricity usage is calculated for California and Kentucky, and validated using data from the California Building Energy Code Compliance (CBECC) and experimental data from the existing low-cost low-income near-NZE houses in southern Kentucky, respectively. Coupling factors including solar illumination, radiant energy from appliances and people, impact of airflow, and etc. add complexities to the mathematical models. There is a trade-off between the accuracy and complexity of such models.

The NZE homes typically incorporate solar PV systems as the main source of energy [126, 127]. Solar PV generation is largely decided by external environment conditions, leading to unpredictability and stochastic properties. The mismatch between the peaks of PV generation and residential load leads to variations in the net power flow, which causes the "duck curve" phenomenon [4]. In addition, the power flow due to surplus solar generation can potentially exceed the rated capacity of distribution lines and transformers. Curtailment of solar energy and the use of energy storage systems are common methods to overcome these challenges [128].

BESS provides increased flexibility to the NZE residences. The sizing for BESS is mainly determined by factors including building characteristics, utility tariffs and the BES operating schedule [6–8]. A placement planning scheme for the optimal combination of PV and BESS with stochastic optimization is proposed [129]. The

stability and control for a PV-BESS system were studied in recent research works [130, 131]. The stability of power converters, which are the main components of such a power electronic interface, were studied [132, 133].

Apart from the BESS, an EWH can be regarded as a uni-directional energy storage system. Research works regarding EWH as a deferrable load realize the HEM by changing its working status between "on" and "off" [134–136]. Others works have demonstrated the use of EWH in conjunction with batteries. For instance, an EWH coupled with the DC bus is used to suppress the power fluctuation in systems with large batteries [137]. This chapter proposes the control of batteries, together with water heaters to operate a community of grid connected NZE homes as dispatchable generators, which can provide constant grid power flow for specified durations of time on typical winter and summer days. It is demonstrated that the required battery capacity is reduced by utilizing the EWH along with the battery to form a hybrid PV energy storage system (HyPVESS).

In addition to the distributed optimization and control approach of these DERs, behind-the-meter (BTM) transactive control may be employed with HEMs for energy use reduction in residences by coordinating home appliances in market schemes that also consider human comfort [125]. Furthermore, optimal management methods for typical residential devices have potential to accommodate for the drastic change in that distribution load profiles will likely experience due to the increasing popularity of EVs in the automobile market [138]. When the NZE homes operate as dispatchable generator/load, the power flow at the distribution system level is relatively stable.

The co-simulation framework, INSPIRE+D, which enables the dynamic modeling

of building energy software and power system simulator, was developed and introduced in this chapter. Another testbed, the DER integration testbed, which utilizes MILs to simulate DERs, enables the study of HEM system implementation at the residential and community level was also introduced. The calculation of power flow and the mathematical basis of OpenDSS were introduced.

A method for sizing for the capacity of the solar PV and energy storage systems to meet the NZE mandate and minimize the side impact of the renewables was proposed. The proposed power electronic interface in this chapter interconnects the BESS, PV, the grid and other house loads. The example sizing case was presented based on the representative design days. A HyPVESS was proposed to realize dispatchable output for the NZE community while harvesting the maximum of PV generation with minimum BESS energy capacity.

This chapter is substantially based on the following journal papers:

- H. Gong, *et al.*, "Large-scale modeling and demand response control of electric water heaters with energy star and CTA-2045 control types in distribution power system," *IEEE Transactions on Industry Applications*, 10p, 2021, *(Submitted in Dec, 2021)*.

- H. Gong, *et al.*, "Dynamic modeling and optimal design for net zero energy houses including hybrid electric and thermal energy storage," *IEEE Transactions on Industry Applications*, Vol. 56, No. 4, pp. 4102–4113, 2020.

2.2 Co-simulation Framework–Structure, Models, and Examples

2.2.1 The INSPIRE+D Co-simulation Software Framework

The proposed co-simulation software framework comprises freeware including BEopt, EnergyPlus, OpenDSS, BCVTB, and Python (Fig. 2.1). The name for the co-simulation framework is "**I**ntegrated **N**etwork simulation for **S**mart **P**ower-flow **I**n **R**esidences using **E**nergyPlus and Open**D**SS" (INSPIRE+D, pronounced as INSPIRED). INSPIRE+D provides an improved platform for instantaneous building energy usage modeling and simulation, based on the freeware BEopt, EnergyPlus from Lawrence Livermore National Lab, and simulation of distribution power networks, using the frequency domain OpenDSS freeware from EPRI. INSPIRE+D is a Python-based co-simulation tool which allows residential load calculation, district network analysis and control realization in just one model. INSPIRE+D is capable of simulating 1000s of homes in parallel at one minute intervals. Each thread handles one EnergyPlus process and needs approximately 1GB of RAM. The time required for the whole simulation depends on the time-step and running period. A typical simulation for the entire year with a time-step of 5-minutes takes approximately 10 minutes to complete.

Solar generators, battery energy storage, control for water heater and HVAC systems can also be included in the framework. The software framework uses BEopt and EnergyPlus for building simulations, which allow both fast house energy modeling as well as dynamic instantaneous load simulation. BEopt converts the geometric data and the schedules of the appliances for the user-defined house to input data file (IDF),

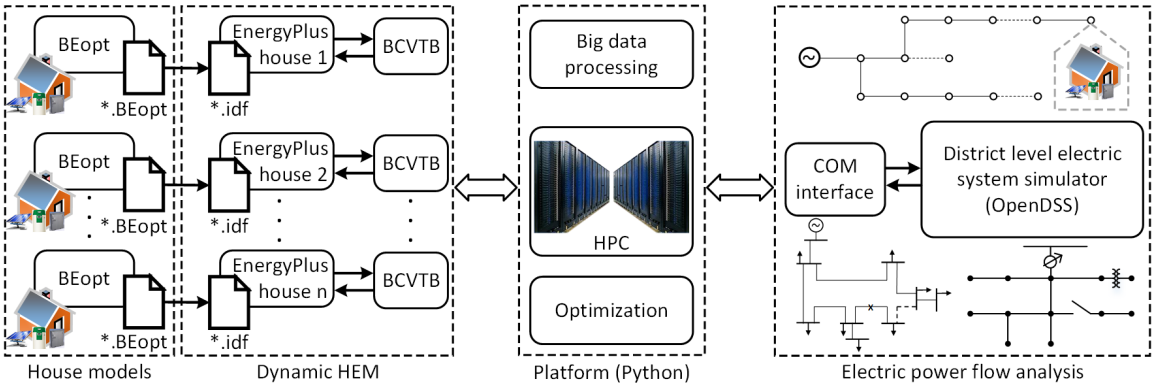

Figure 2.1: The INSPIRE+D co-simulation framework, including four parts. Thousands of single house energy models can be simulated in parallel through a high performance computing (HPC) system.

which serves as the input for the EnergyPlus software. The IDF is an ASCII file containing the data describing the building to be simulated. EnergyPlus is capable of simulating domestic energy usage to a time step of 1-minute. The Building Controls Virtual Test Bed (BCVTB) is a software environment that allows coupling different simulation programs [89, 139].

The proposed co-simulation framework is capable of running thousands of EnergyPlus processes in parallel in the platform powered by the high performance computing (HPC) system. The net power flow from all the houses form the loads of the electric power system, which is simulated by the OpenDSS software. Energy storage control algorithms to achieve different objectives can be implemented in the proposed INSPIRE+D framework, both at the single house and distribution power system levels. The calculated energy usage is validated using examples based on California Building Energy Code Compliance (CBECC) and the near-NZE subdivision in southern Kentucky (Fig. 2.2).

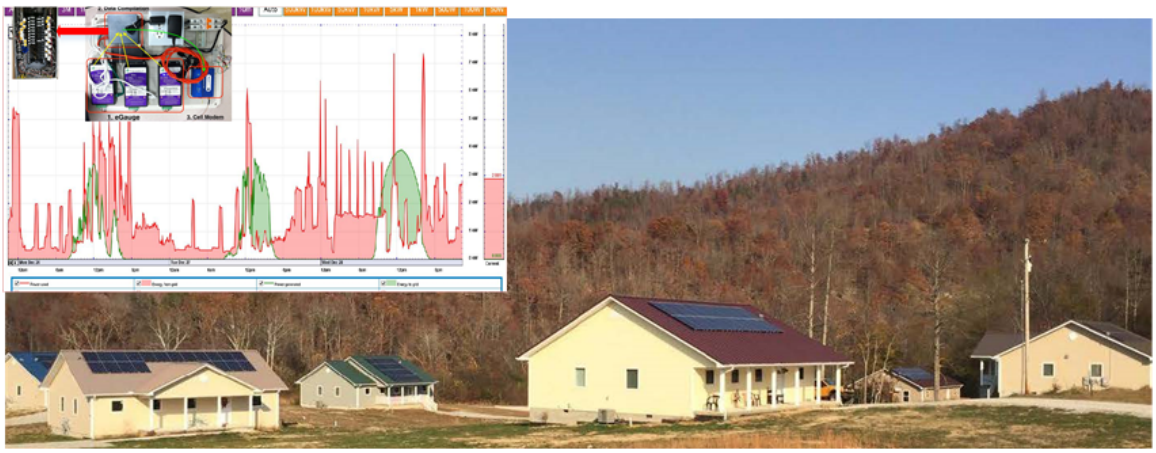

Figure 2.2: A newly developed field demonstrator with twelve near-NZE houses in southern Kentucky, which are modeled within the INSPIRE+D co-simulation framework and validated with measured load data.

2.2.2 DER Integration Virtual Testbed

The EPRI's DER integration testbed (Fig. 2.3) simulates power system models with real world communication systems and DER models. The testbed can assess the control functionality and communication interoperability of the DER Management System (DERMS) and can evaluate different control strategies for any circuit. It also supports real world communication systems by incorporating industry standard protocols, such as the CTA-2045 standard, Energy Star specifications, DNP3, and SunSpec Modbus. The testbed can simulate scenarios that include a variety of DERs, feeders, load conditions, weather, and DER penetration levels.

The DER integration testbed has four layers in its architecture: control, device, circuit, and visualization and analytics (Fig. 2.3). The circuit layer contains a power system simulator, such as OpenDSS or Cyme, to model the feeder and calculate powerflow. The visualization and analytics layer provides the user with actionable

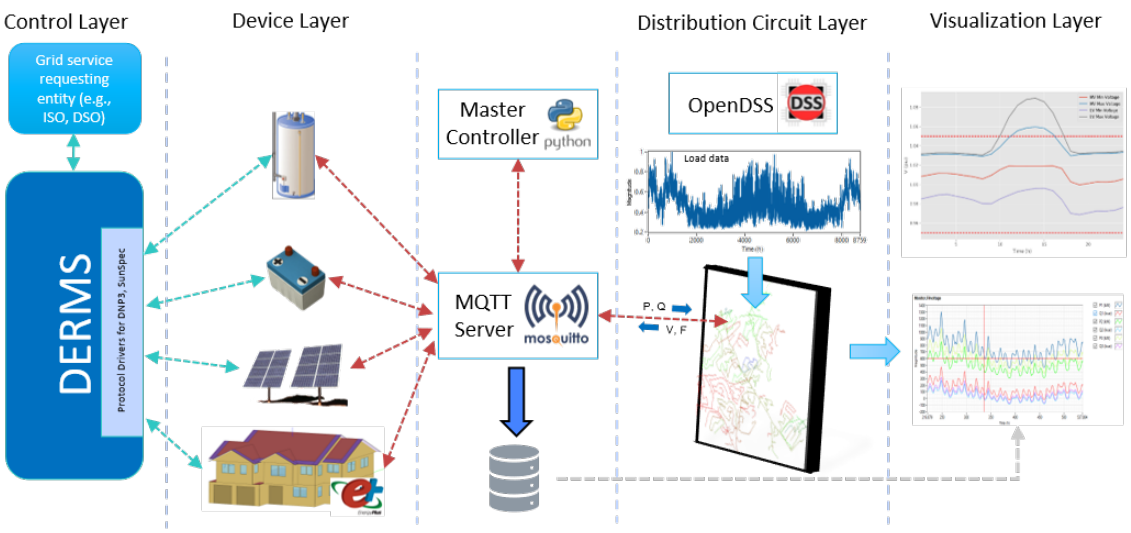

Figure 2.3: The architecture of EPRI's DER integration testbed. Models-in-the-loop (MIL) are employed at the device layer. The chapter proposes unified models for the BESS and EWH suitable for Energy Star and CTA-2045 control types, which are issued by a distributed energy resource management system (DERMS). The MILs are to communicate with the distribution system simulator, which is OpenDSS for this study, through the Message Queuing Telemetry Transport (MQTT), which enables distribution-level simulation of control schemes.

information to analyze the full system. The control layer manages DER in the device layer using control strategies that may be user-built or commercial.

OpenDERMS is an EPRI developed reference control tool that can aggregate, optimize and manage large number of DER to provide grid services while enabling customer benefits. The devices in the device layer are implemented as software simulators that emulate real world DER characteristics and incorporate built-in commercial communication interfaces for common industry protocols. The device and circuit layers communicates through the Message Queuing Telemetry Transport (MQTT) protocol, which is an effective communication tool for IoT devices and has great potential for facilitating co-simulation of multiple DER ecosystems [140]. The way in

which these layers are interconnected provides a high level of modularity and scalability to the testbed. Utilizing this tool enables distribution-level simulation of DR control schemes and co-simulation of the distribution system simulator, MIL, and other device-level simulators such as EnergyPlus, a whole building energy simulation program.

2.2.3 Modeling and Example Validation for House Energy Usage

The INSPIRE+D co-simulation framework provides instantaneous home energy usage data, based on the floorspace, occupancy, and ambient conditions, which enables testing of the developed real-time control for advanced home appliances. The building simulations are validated by comparing with experimental data from field demonstrator homes in Southern Kentucky. The calibration for the developed house energy usage models is carried out for three types of loads, respectively. The three types of loads are: the HVAC system, which reflects the influences of the external temperature; the EWH, as it is of interest for the proposed hybrid energy storage system; and the remaining loads.

The HVAC load depends on the nominal rating, thermostat set-points, ambient temperature as well as building insulation and materials. The EWH load is decided by the nominal power rating, the set point, the deadband, and the hot water draw of different equipment including clothes washer, dish washer, shower, bath, etc.

Two weeks, one in summer and the other in winter are chosen for the validation such that the house electricity consumption and PV generation under different

Table 2.1: Weekly and annual energy usage for an example California house (kWh).

Load type	Winter		Summer		Annual	
	CBECC	EP	CBECC	EP	CBECC	EP
HVAC	11	12	294	292	5,625	5,628
EWH	59	59	23	23	1,664	1,679
Other loads	101	106	88	82	4,741	4,816
Total usage	170	177	404	398	12,030	12,122

external environments are fully represented.

The reference energy usage and PV generation for a single house are from two different sites, California and southern Kentucky. The home energy model for California is validated based on the weekly energy usage complying with the California Building Energy Code Compliance Residential Standards (CBECC-Res). The reference data is simulated from the CBECC-Res 2019 software. The EnergyPlus (EP) house model is validated as it has good agreement with the CBECC-Res in both weekly and annually basis (Table 2.1).

The home energy model representing house in southern Kentucky has good agreement with the experimental data in weekly basis (Table 2.2). Due to the mild climate in Kentucky, HVAC consumption throughout the whole year is fairly low. It is worth noticing the electricity consumed by the EWH for the house in the chosen summer week is very low. The building simulation tools can be used to generate instantaneous energy usage data over the day. Daily house load profiles of the reference and simulated data in CA for the summer week and KY for the winter week have satisfactory agreement (Figs. 2.4 and 2.5). It may be noted that variations from the measured instantaneous energy usage are introduced because of consumer behavior. The energy usage from the CBECC-Res 2019 software has a) resolution of one hour, while

Table 2.2: Weekly and annual energy usage for an example Kentucky house (kWh).

Load type	Winter		Summer		Annual
	Exp	EP	Exp	EP	EP
HVAC	214	225	64	66	2,603
EWH	42	40	8	9	1,829
Other loads	182	181	93	92	6,689
Total usage	439	446	164	168	11,121

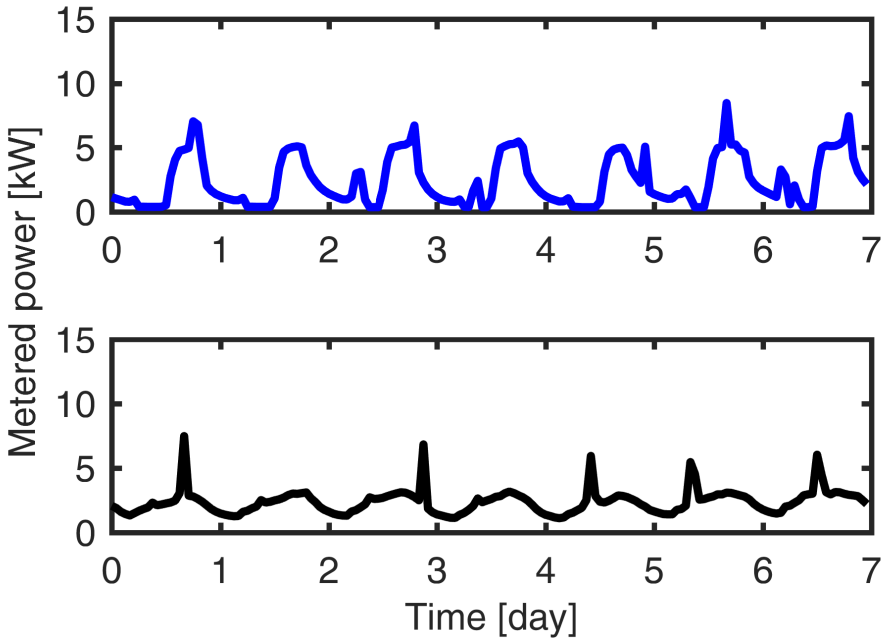

Figure 2.4: Results from two building simulation tools on the daily and weekly load for a typical 3-bedroom, 1.5 bathroom house calculated during a summer week in California with CBECC-Res 2019 (top) and EnergyPlus(bottom).

the time step for EnergyPlus is set to five minutes. The peaks from EnergyPlus are averaged through a period of an hour, for the purpose of comparison with the output from CBECC-Res, for example at hour t:

$$P_{hour}(t) = \frac{\sum_{n=1}^{n=12} P_{5min}(n) \cdot \Delta n}{60}, \tag{2.1}$$

where Δn is the time step set to five minutes.

The measured house load data has the resolution of 15 minutes (Fig. 2.5). It may

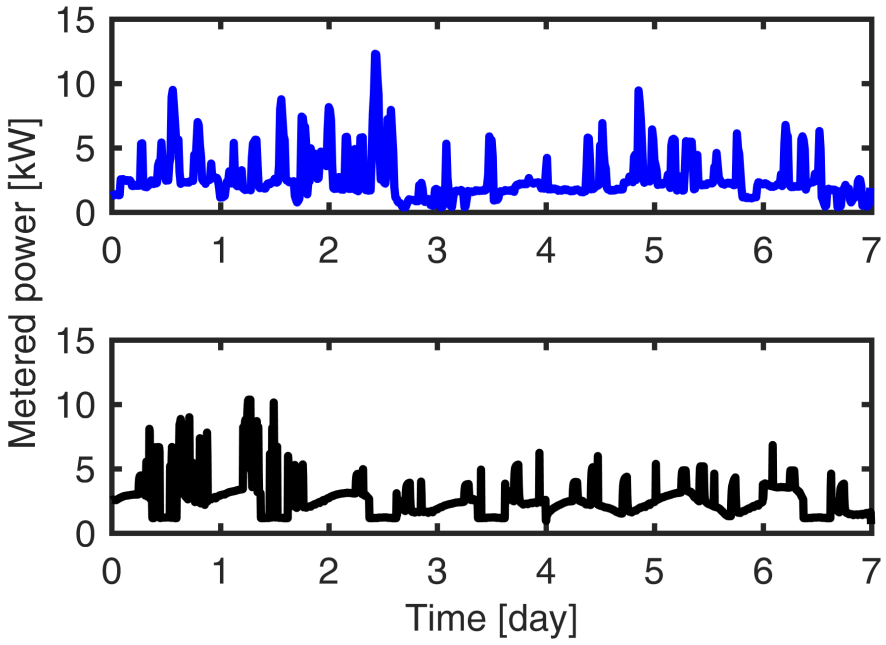

Figure 2.5: Experimental (top) and EnergyPlus simulation data for a house in southern KY in a winter week. The total weekly energy usage comply satisfactorily.

be noted that human behavior adds randomness to the house load, which accounts for the differences between the measured and simulated schedules. Human behavioral modeling and its effect on the load are beyond the scope of this work.

2.2.4 Modeling of Power System with Realistic Residential Loads–A Modified IEEE 123-bus Test Case

The modified IEEE 123-bus feeder [118] was used for the simulation of the distribution system for the community (Fig. 2.6). The original spot loads of each node were replaced by the residential loads, which was comprising of the measured data from the SET project and simulated EWH power. The bus-150 was connected to upper level transmission system, and regarded as the slack bus in the simulation.

In this study, a maximum of 10kW for residential loads was assumed. Node 2

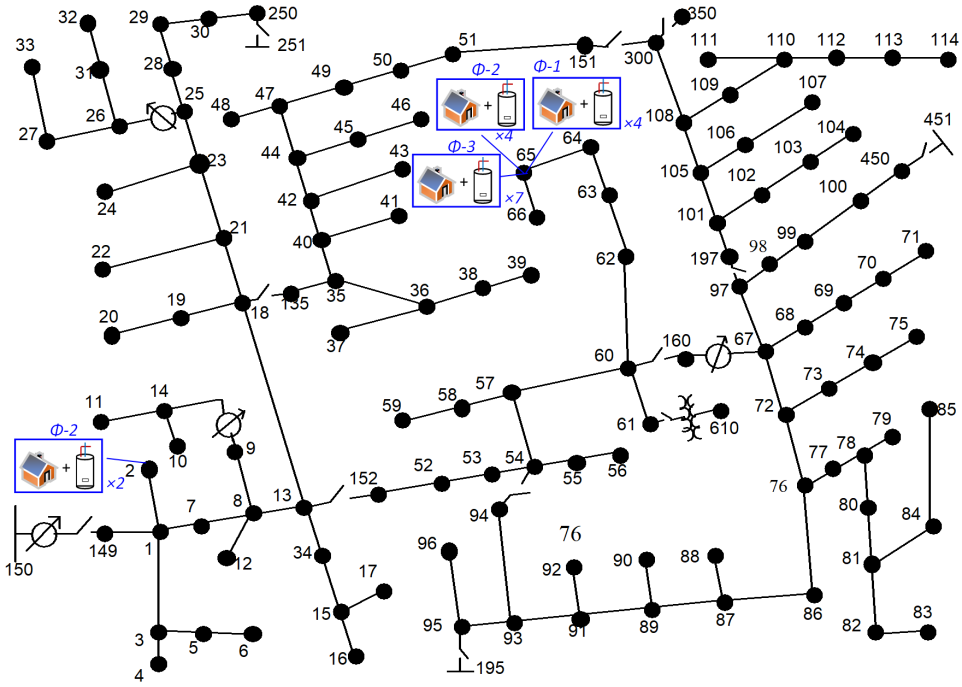

Figure 2.6: The modified IEEE 123-bus feeder. The original spot loads were replaced by the residential loads, which are comprising of measured data from the SET project and the simulated EWH power.

has 20kW in its phase-2, therefore, 2 houses were connected to Node 2 phase-2. Similarly to node 65, 4 houses to phase-1, 4 houses to phase-2, and 7 houses to phase-3 were connected. No generator bus (P-V bus) was considered in the study. The PV generation may cause negative power flow from the residence to the power grid. Even when the residence provides power, the bus is still considered a load bus (P-Q bus).

The house number was rounded to ceiling if the results for dividing the original spot load was not an integer. For example, Phase-1 of node 65 has a spot load of 35kWh. Therefore, 4 houses were connected to phase-1 of node 65. A total of 353 houses were connected to the IEEE 123-bus feeder. In this study, the power factor of 0.95 was given to all buses [141].

The differences between houses were represented by their bedroom numbers in

Table 2.3: Percentage and number of houses with different numbers of bedrooms

Bedrooms	Percentage (%)	Number
0 & 1	2.1 + 8.2	36
2	25.8	91
3	42.8	151
4	16.7	59
5+	4.5	16

this study (Table 2.3). The percentage in Table 2.3 was retrieved from the survey published by the United States Census Bureau [142]. The bedroom number was used to select the hot water draw in the study.

The workflow of the simulation is presented in Fig. 2.7. After determining the numbers of each house type (Table 2.3), the residential load profiles were selected. The SET project provides the daily loads for 5,000 residences with a resolution of 15 minutes. To protect the privacy of its residents, only the timestamp, anonymous house ID, and electricity usage are known. A total of 353 different load profiles whose daily electricity usage was between 20kWh and 40kWh were selected randomly.

Residences were attributed to each of the nodes in the IEEE 123-bus feeder. Each residence was assumed to have a 10kW maximum and the default kW value of each node was referred by [118] as "spot loads". The system was populated with the representative residences by assigning a randomly selected residence from among the 353 total to an available connection point, or node, which had belonged to pre-existing spot loads from the original IEEE 123-bus example system. This procedure ensured that a residence was connected to only one node and allowed for a node to have multiple residences.

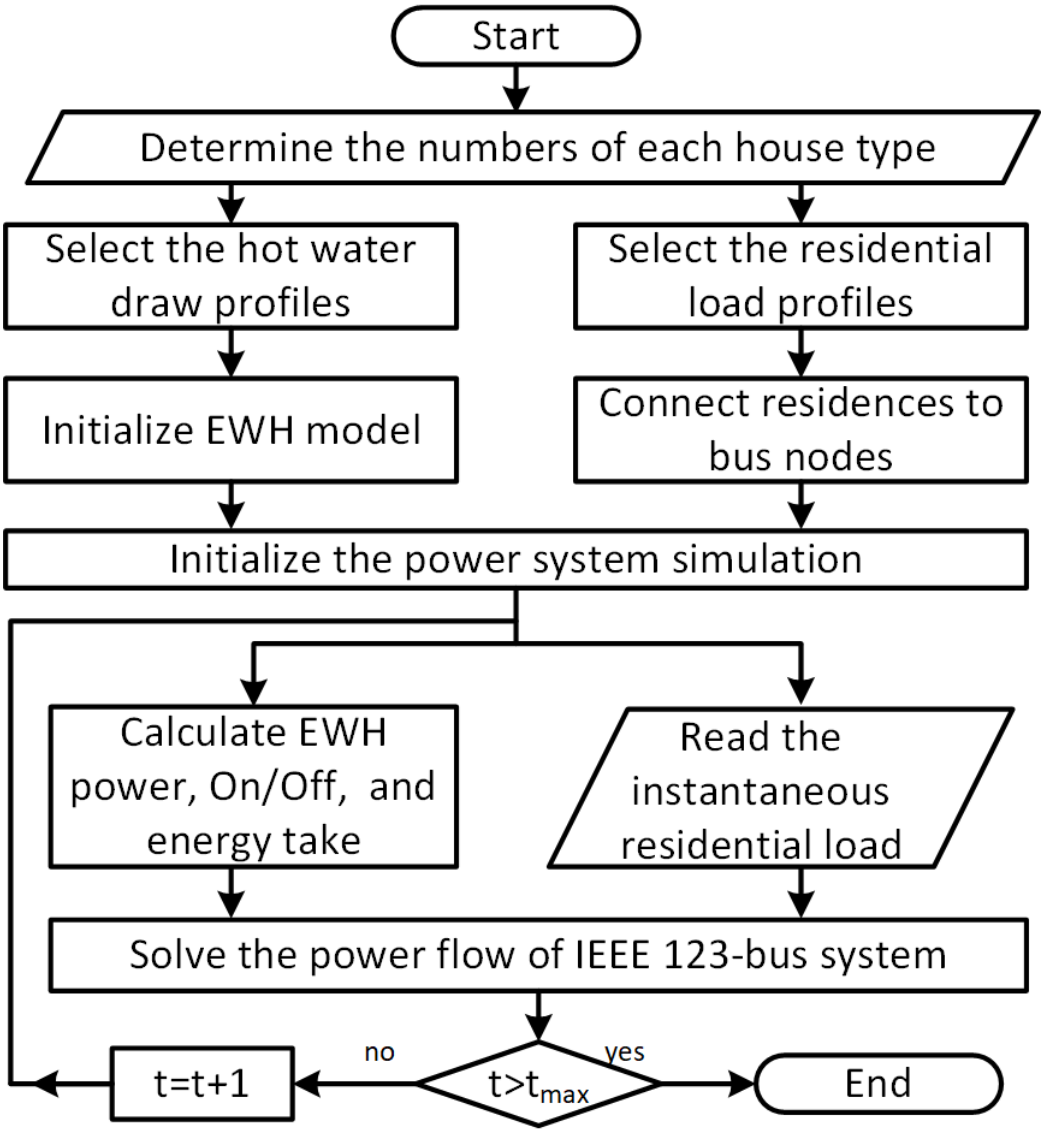

Figure 2.7: Work flow for the simulation of the modified IEEE 123-bus system with realistic residential load and water heater power.

2.3 Formulation and Solution of Electric Power Flow

2.3.1 Definition of Power Injection

The calculation of load flow is to determine the following quantities at each and every node of any power system:

1. The voltage magnitude $|V|$
2. The phase angle of the voltage σ
3. the real power injection P
4. the reactive power injection Q.

The power injected into the ith node is given by:

$$S_i = P_i + jQ_i = V_i I_i^*. \tag{2.2}$$

For a power system with n nodes, the network equation is given by the matrix equation:

$$\boldsymbol{I} = \boldsymbol{Y}\boldsymbol{V}, \tag{2.3}$$

where, $\boldsymbol{I}$ is n vectors of current injections, $\boldsymbol{Y}$ is $n \times n$ bus admittance matrix, $\boldsymbol{V}$ is n vectors of node voltages.

The current injected into the i th node can be obtained from (2.3):

$$I_i = \sum_{k=1}^{n} Y_{ik} V_k = Y_{i1} V_1 + Y_{i2} V_2 + \cdots + Y_{in} V_n. \tag{2.4}$$

Solving (2.4 and 2.2) we get:

$$S_i = P_i + jQ_i = \sum_{k=1}^{n} V_i V_{ik}^* V_k^* \tag{2.5}$$

Rewriting $V_k = |V_k| \underline{/\delta_k}$, $Y_{ik} = |Y_{ik}| \underline{/\theta_{ik}}$, (2.5) becomes:

$$S_i = \sum_{k=1}^{n} |V_i| \underline{/\delta_i} \, |Y_{ik}| \underline{/-\theta_{ik}} \, |V_k| \underline{/-\delta_k} = |V_i| |Y_{ik}| |V_k| \underline{/\delta_i - \theta_{ik} - \delta_k}. \tag{2.6}$$

Therefore, the real and reactive power injection into ith node are given by

$$P_i = Re(S_i) = \sum_{k=1}^{n} |V_i| |Y_{ik}| |V_k| cos(\delta_i - \theta_{ik} - \delta_k) \tag{2.7}$$

$$Q_i = Im(S_i) = \sum_{k=1}^{n} |V_i| |Y_{ik}| |V_k| sin(\delta_i - \theta_{ik} - \delta_k) \tag{2.8}$$

2.3.2 Calculation of Power Flow

The power injected into the nodes of a power system network consisting of n busbars from (2.5) is described by a set of complex equations given by:

$$\begin{aligned} S_i = P_i + jQ_i &= \sum_{k=1}^{n} V_i Y_{ik}^* V_k^* \\ &= V_i Y_{ii}^* V_i^* + V_i \sum_{k=1, k\neq i}^{n} Y_{ik}^* V_k^*, \quad i = 1, 2, \cdots, n \end{aligned} \tag{2.9}$$

Rewriting (2.9):

$$Y_{ii}^* V_i^* = \frac{S_i}{V_i} - \sum_{k=1, k\neq i}^{n} Y_{ik}^* V_k^* \quad i = 1, 2, \cdots, n \tag{2.10}$$

Dividing both side of (2.9) by Y_{ii}^*:

$$V_i^* = \frac{1}{Y_{ii}^*} [\frac{S_i}{V_i} - \sum_{k=1, k\neq i}^{n} Y_{ik}^* V_k^*] \quad i = 1, 2, \cdots, n \tag{2.11}$$

The complex conjugate of (2.11) is :

$$V_i = \frac{1}{Y_{ii}} [\frac{S_i^*}{V_i^*} - \sum_{k=1, k\neq i}^{n} Y_{ik} V_k] \quad i = 1, 2, \cdots, n \tag{2.12}$$

The computer algorithm for Gauss Seidel method is summarized in (algorithm. 2.1). The voltage for P-Q bus is calculated directly. For P-V bus, the magnitude needs to be adjusted while angle updated.

The flow chart of Gauss Seidel method is presented in Fig. 2.8.

Algorithm 2.1 Calculate the power flow using Gauss Seidel method

Read line data and construct the bus admittance matrix;
Read node data;
For P-V nodes, the starting values of the voltages are: $V_k^0 = \left|V_k^s\right| \angle 0 \quad k = 1, 2, \cdots, m$;
For P-Q nodes, the starting values are: $V_k^0 = 1.0 \angle 0 \quad k = m+1, m+2, \cdots, n$;
Set iteration count i=1;
while *mismatches larger than tolerance* **do**
  Set node number k=2;
  while $k<n$ **do**
    if $k>m$ **then**
      Go to line 15;
    else
      Go to lines 13;
    As a P-V busbar, compute the current: $I_k = \sum_{r=1}^{k-1} Y_{kr} V_r^i + \sum_{r=k}^{n} Y_{kr} V_r^{i-1}$;
    Compute the reactive power injection : $Q_k = Im(S_k) = Im(V_k^{i-1} I_k^*)$;
    Compute the new value of voltage: $V_k^i = \frac{1}{Y_{kk}}\left[\frac{S_k^*}{(V_k^{i-1})^*} - \sum_{k=1, k\neq i}^{n} Y_{ik} V_k\right]$;
    if $k<m$ **then**
      Calculate the voltage angle: $\delta_k = atan2(Im\{V_k^i\}, Re\{V_k^i\})$;
      As a P-V node, correct the magnitute: $V_k^i = \left|V_k^s\right| \angle \delta_k$;
    $k = k + 1$;
  end
  $i = i + 1$;
end

2.3.3 Modeling and Solving of Power System in OpenDSS

OpenDSS uses the primitive admittance, or primitive Y, matrix approach for the system modeling. A two-phased coupled impedance example is illustrated in Fig. 2.9 and defined as:

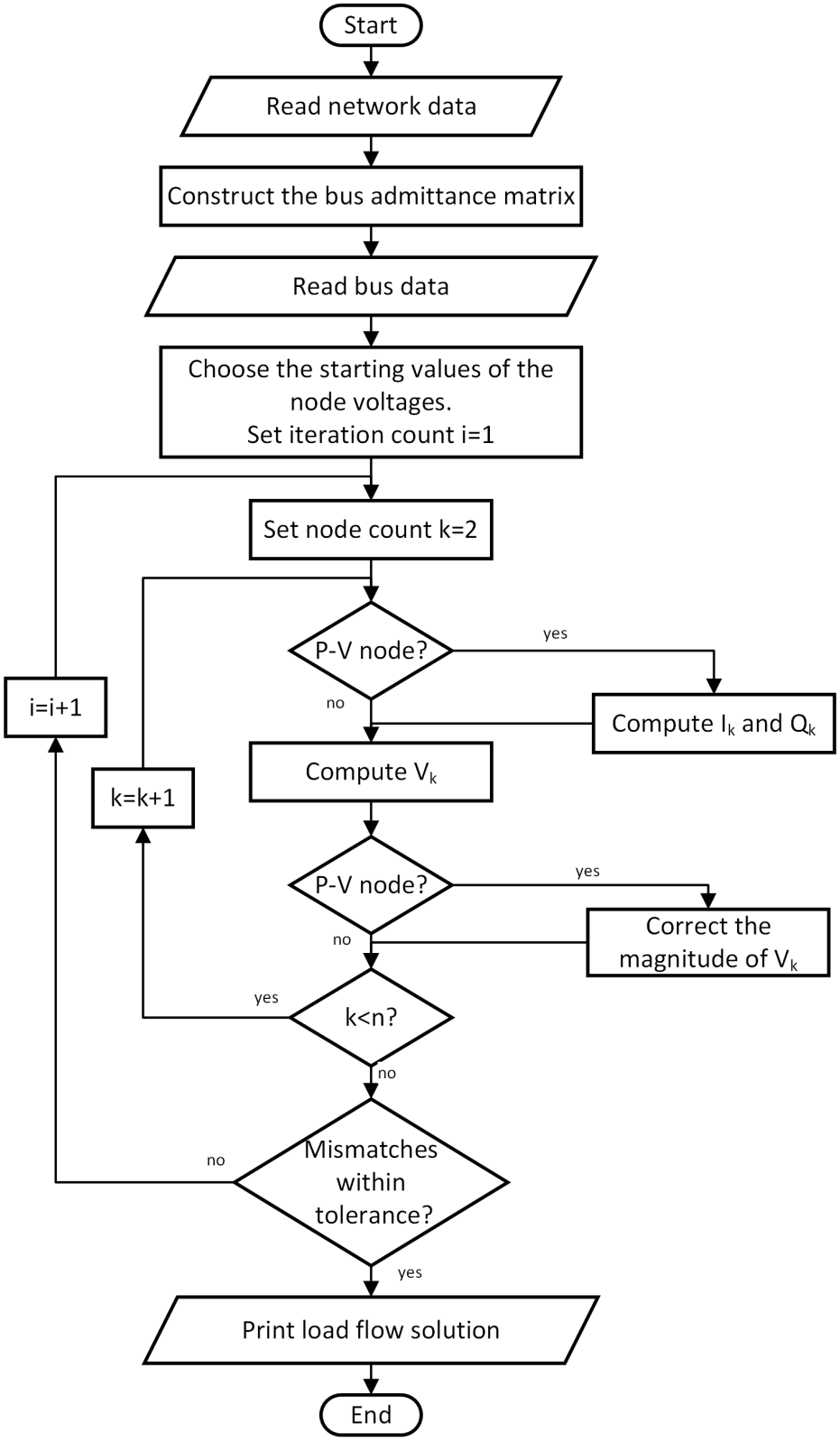

Figure 2.8: Flow chart for Using Gauss Seidel mothod to solve the power system

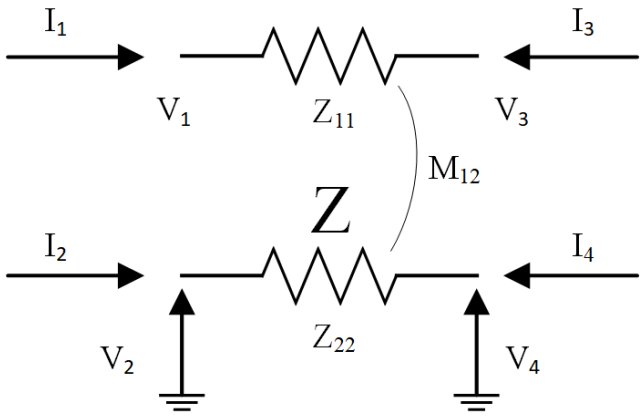

Figure 2.9: The primitive Y matrix for a two-phase coupled impedance. All voltages are with with respect to the ground.

$$\begin{bmatrix} I_1 \\ I_2 \\ I_3 \\ I_4 \end{bmatrix} = \begin{bmatrix} Z^{-1} & -Z^{-1} \\ -Z^{-1} & Z^{-1} \end{bmatrix} \begin{bmatrix} V_1 \\ V_2 \\ V_3 \\ V_4 \end{bmatrix}, \tag{2.13}$$

where the impedance characteristics, Z, are defined as:

$$Z = \begin{bmatrix} z_{11} & M_{12} \\ M_{12} & z_{22} \end{bmatrix} \tag{2.14}$$

In OpenDSS, the power line types are defined by the impedance matrix. For a three phase bus example, the impedance matrices is:

$$Z = R + jX = \begin{bmatrix} Z_{11} & Z_{12} & Z_{13} \\ Z_{21} & Z_{22} & Z_{23} \\ Z_{31} & Z_{32} & Z_{33} \end{bmatrix} \tag{2.15}$$

,

The series resistance matrix is defined as ohms per unit length:

$$R = \begin{bmatrix} R_{11} & & \\ R_{21} & R_{22} & \\ R_{31} & R_{32} & R_{33} \end{bmatrix}. \tag{2.16}$$

The series reactance matrix is defined as ohms per unit length:

$$X = \begin{bmatrix} X_{11} & & \\ X_{21} & X_{22} & \\ X_{31} & X_{32} & X_{33} \end{bmatrix}. \tag{2.17}$$

The shunt nodal capacitance matrix is defined as nanofarads per unit length:

$$C = \begin{bmatrix} C_{11} & & \\ C_{21} & C_{22} & \\ C_{31} & C_{32} & C_{33} \end{bmatrix}. \tag{2.18}$$

The screenshot from OpenDSS model file (*.DSS) in Fig. 2.10 (a) shows the example definition for power lines types with 1, 2, 3 phases, respectively. In the example *.DSS file, the "—" symbol separates the rows. Also defined for the line types are number of phase and base frequency. In OpenDSS, power lines can be created with the line types, line length, number of phase, and the terminals at the two ends, as shown in Fig. 2.10 (b).

A power system model can be created in OpenDSS with its power source (Fig. 2.10 (c)) and load. For the IEEE 123-bus system, the examples for creating the regulator and switch are shown in Fig. 2.10 (d) and Fig. 2.10 (e), respectively. OpenDSS provides other components, such as, PV generator, capacitors, and battery energy storage.

The power flow is solved in OpenDSS by the iteration loop, as shown in Fig. 2.11. The main system admittance matrix, Y, is constructed by the small nodal admittance matrices of each line. The source currents and node voltages are updated at each iteration until it converges typically 0.0001 p.u.

The Ohm's Law in matrix form with the main system admittance matrix, Y, is

```
New linecode.1 nphases=3 BaseFreq=60
~ rmatrix = [0.086666667 | 0.029545455 0.088371212 | 0.02907197 0.029924242 0.087405303]
~ xmatrix = [0.204166667 | 0.095018939 0.198522727 | 0.072897727 0.080227273 0.201723485]
~ cmatrix = [2.851710072 | -0.920293787  3.004631862 | -0.350755566  -0.585011253 2.71134756]

New linecode.7 nphases=2 BaseFreq=60
~ rmatrix = [0.086666667 | 0.02907197  0.087405303]
~ xmatrix = [0.204166667 | 0.072897727  0.201723485]
~ cmatrix = [2.569829596 | -0.52995137  2.597460011]

New linecode.9 nphases=1 BaseFreq=60
~ rmatrix = [0.251742424]
~ xmatrix = [0.255208333]
~ cmatrix = [2.270366128]
```

(a)

```
New Line.L1     Phases=1 Bus1=1.2        Bus2=2.2        LineCode=10   Length=0.175
New Line.L2     Phases=1 Bus1=1.3        Bus2=3.3        LineCode=11   Length=0.25
New Line.L3     Phases=3 Bus1=1.1.2.3    Bus2=7.1.2.3    LineCode=1    Length=0.3
New Line.L4     Phases=1 Bus1=3.3        Bus2=4.3        LineCode=11   Length=0.2
New Line.L5     Phases=1 Bus1=3.3        Bus2=5.3        LineCode=11   Length=0.325
New Line.L6     Phases=1 Bus1=5.3        Bus2=6.3        LineCode=11   Length=0.25
New Line.L7     Phases=3 Bus1=7.1.2.3    Bus2=8.1.2.3    LineCode=1    Length=0.2
New Line.L8     Phases=1 Bus1=8.2        Bus2=12.2       LineCode=10   Length=0.225
New Line.L9     Phases=1 Bus1=8.1        Bus2=9.1        LineCode=9    Length=0.225
New Line.L10    Phases=3 Bus1=8.1.2.3    Bus2=13.1.2.3   LineCode=1    Length=0.3
New Line.L11    Phases=1 Bus1=9r.1       Bus2=14.1       LineCode=9    Length=0.425
New Line.L12    Phases=1 Bus1=13.3       Bus2=34.3       LineCode=11   Length=0.15
New Line.L13    Phases=3 Bus1=13.1.2.3   Bus2=18.1.2.3   LineCode=2    Length=0.825
New Line.L14    Phases=1 Bus1=14.1       Bus2=11.1       LineCode=9    Length=0.25
New Line.L15    Phases=1 Bus1=14.1       Bus2=10.1       LineCode=9    Length=0.25
New Line.L16    Phases=1 Bus1=15.3       Bus2=16.3       LineCode=11   Length=0.375
New Line.L17    Phases=1 Bus1=15.3       Bus2=17.3       LineCode=11   Length=0.35
New Line.L18    Phases=1 Bus1=18.1       Bus2=19.1       LineCode=9    Length=0.25
```

(b)

```
New object=circuit.ieee123
~ basekv=4.16 Bus1=150 pu=1.00 R1=0 X1=0.0001 R0=0 X0=0.0001
```

(c)

```
new transformer.reg1a phases=3 windings=2 buses=[150 150r] conns=[wye wye]
    kvs=[4.16 4.16] kvas=[5000 5000] XHL=.001 %LoadLoss=0.00001 ppm=0.0
new regcontrol.creg1a transformer=reg1a winding=2 vreg=120 band=2 ptratio=20 ctprim=700 R=3 X=7.5
```

(d)

```
New Line.Sw1    phases=3  Bus1=150r   Bus2=149    r1=1e-3 r0=1e-3 x1=0.000 x0=0.000 c1=0.000 c0=0.000 Length=0.001
New Line.Sw2    phases=3  Bus1=13     Bus2=152    r1=1e-3 r0=1e-3 x1=0.000 x0=0.000 c1=0.000 c0=0.000 Length=0.001
New Line.Sw3    phases=3  Bus1=18     Bus2=135    r1=1e-3 r0=1e-3 x1=0.000 x0=0.000 c1=0.000 c0=0.000 Length=0.001
New Line.Sw4    phases=3  Bus1=60     Bus2=160    r1=1e-3 r0=1e-3 x1=0.000 x0=0.000 c1=0.000 c0=0.000 Length=0.001
New Line.Sw5    phases=3  Bus1=97     Bus2=197    r1=1e-3 r0=1e-3 x1=0.000 x0=0.000 c1=0.000 c0=0.000 Length=0.001
New Line.Sw6    phases=3  Bus1=61     Bus2=61s    r1=1e-3 r0=1e-3 x1=0.000 x0=0.000 c1=0.000 c0=0.000 Length=0.001
```

(e)

Figure 2.10: Example of OpenDSS definition for (a) line types; (b) power line; (c) source bus; (d) transformer and regulator; (e) switch.

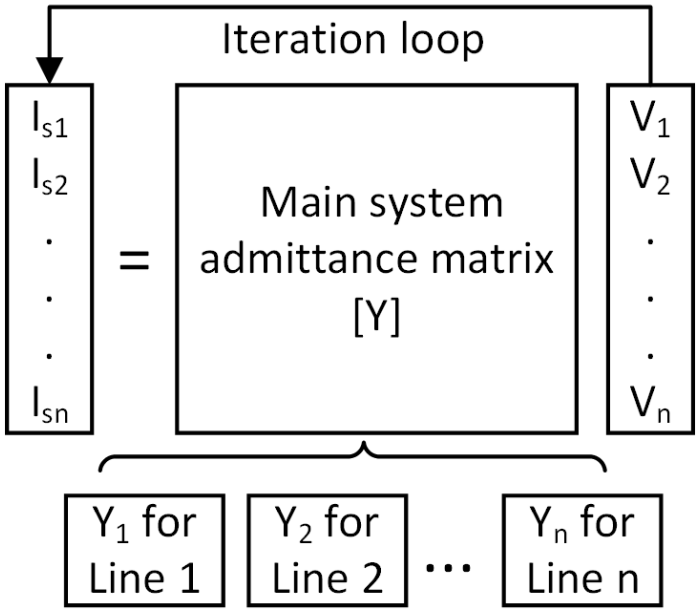

Figure 2.11: Illustration of the OpenDSS solution loop. The main system admittance matrix, Y, is constructed by the small nodal admittance matrices of each line.

expressed as:

$$\mathbf{I_s} = \mathbf{YV}, \tag{2.19}$$

where $\mathbf{I_s}$ is the source currents; $\mathbf{V}$, the node voltages. OpenDSS adopts the "flat start", i.e., all voltage angles set to zero and magnitudes set to 1.0 p.u. During the iteration, the $\mathbf{V}$ is calculated with sparse matrix solver, denoted by:

$$V_i^{(k+1)} = \frac{1}{Y_{ii}}(I_{si} - \sum_{j \neq i} Y_{ij} V_j^k). \tag{2.20}$$

Updating (2.19) with the newly calculated $\mathbf{V^{(k+1)}}$:

$$\mathbf{I_s^{k+1}} = \mathbf{YV^{k+1}} \tag{2.21}$$

.

The new $\mathbf{I_s^{k+1}}$ and $\mathbf{V^{k+1}}$ are used in (2.20) and the procedure repeats until the calculated voltages converge to 0.0001 p.u. The procedure is summarized in Algorithm. 2.2.

Algorithm 2.2 Power Flow Solution in OpenDSS

Flat start: set $V_1 = 1\angle 0°, V_1 = 1\angle 0°, ..., V_n = 1\angle 0°$
while $\exists |V_i^{(k+1)} - V_i^{(k)}| > 0.0001$ **do**
    Update node voltages according to (2.20);
    Update source currents according to (2.21);
end

2.4 Sizing and Scheduling Studies for Residential Power

The solar PV system capacity required to achieve NZE operation was calculated from the simulated annual average energy usage, based on

$$\int P_c(t)dt \geqslant E_H, \tag{2.22}$$

where P_c is the PV capacity; E_H, the total annual energy usage for the simulated house. The obtained PV system capacities to meet NZE targets for the chosen 3-bedroom 1.5-bathroom residence in CA, and the low-cost low-income house in southern KY are at least 7.2kW and 6.5kW, respectively. It may be noted that a solar PV system with a capacity substantially exceeding the annual energy usage has a higher probability of meeting the NZE mandate but may lead to a high value of grid feed-in power during the middle of the day when loads are low, and a large power demand in the evening, when loads increase and PV energy reduces. This may potentially cause the "duck curve".

The EWH typically leads to repeating load peaks (Figs. 2.4 and 2.5). A residential battery can be sized and its operation scheduled to maximize the home owner's profitability by absorbing power from the grid during low price periods, and supplying the home loads when the electricity rate is high. This would benefit the home owner. In another approach, the battery can be sized and scheduled to minimize the peak-peak grid power flow variation, which would potentially benefit the utility company. As the focus in this chapter is on mitigating the technical challenges brought forth by large NZE communities, the second sizing approach is discussed. The home electricity spending under a ToU tariff is calculated to evaluate the incentive for users to operate their energy storage systems to minimize the grid power fluctuation.

A battery may be charged during midday to absorb the solar energy surplus, and be discharged later in the day to supply the EWH load, to avoid the absorption of peak power from the utility grid. In principle, a battery can be sized to mitigate the "duck curve" and reduce the residential peak load, however, its capacity and power rating would become prohibitively high. A hybrid PV energy storage system, including both battery and EWH controls is proposed. The EWH is a 'uni-directional' energy storage, and it is expected that the solar PV generation coordinated controls of this system would reduce the residential peak load, and mitigate the "duck curve" issue with a reduced battery size. The energy stored in the EWH is

$$\Delta Q = cm\Delta T = cm(T_H - T_L), \tag{2.23}$$

where Q is the energy; $c = 4.18^{J}/_{(g \cdot k)}$, the specific heat of water; m, the mass of water; ΔT the change of water temperature.

The provision of mixing valves allows the water to be maintained at a higher temperature, thereby increasing the thermal capacity of the tank. Control parameters for the EWH include the tank temperature. In this example, the highest and lowest temperatures of water in the tank are set to 70℃ and 50℃, respectively, ensuring the continued supply of hot water as the required temperature is always achievable by mixing cold water. The mass of water is fixed for a typical tank volume of 50 gallons, which will service 3-4 people. Given the volume of 50-gallons and deadband of 20℃, the EWH can only absorb 4.4kWh thermal energy.

The control of EWH is realized, for example, by the proposed power electronic interface interconnecting the solar panels with the HyPVESS and the utility grid (Fig. 2.12). A multi-port converter inter solar PV panels, battery and variable power EWH to the DC bus, which feeds a single phase inverter connected to the utility and home loads. The converter is configured such that power flow to the PV and EWH systems is uni-directional. On the other hand, the power flow to the battery is bi-directional. In order to provide for high hot water draw, the EWH has both AC and DC elements, so that excess hot water demand can be serviced directly from the grid.

The switch S_{pv} is modulated such that the PV operates at its maximum power point. The inverter switches S_1 to S_4 are controlled to supply power to the grid and home loads at the specified voltage and frequency. The battery converter is controlled to regulate the dc bus voltage. Operation of S_{b1} and S_{b2} causes the battery to discharge and charge, respectively. The EWH absorbs the desired power from the DC bus by the modulation of S_{ewh}. The converter allows the DC bus voltage to be higher than that of the solar PV, battery and EWH.

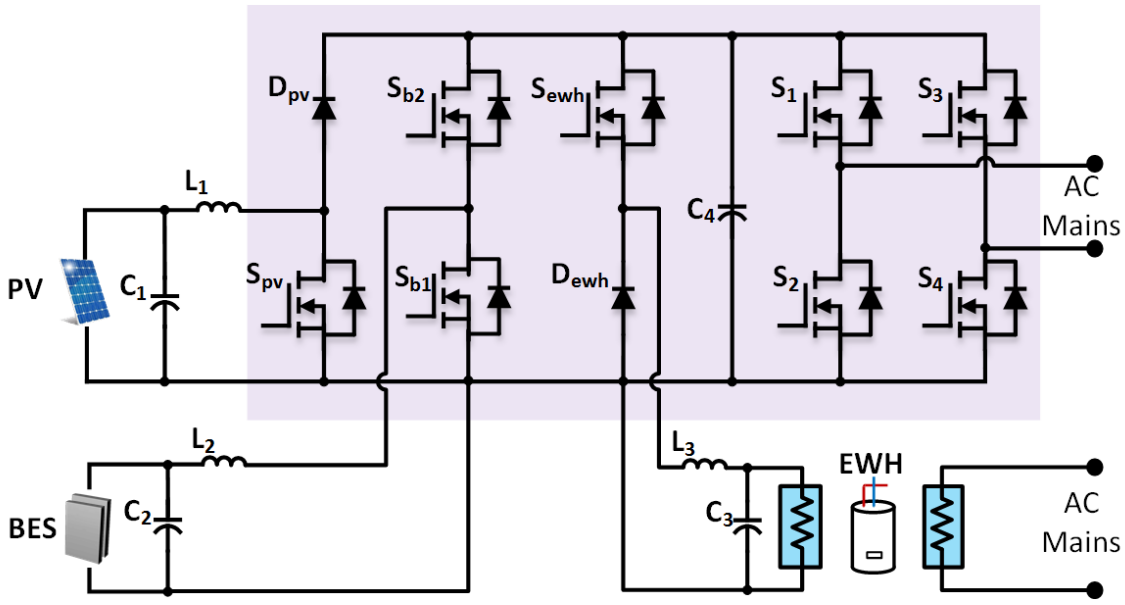

Figure 2.12: Example power electronic interface for an NZE house. The battery storage, EWH and PV array are interconnected with the DC bus via a multi-port converter.

In the traditional case, the EWH is generally equipped with conventional controls, which leads to a peak load that might not coincide with the peak of solar generation (Figs. 2.13 (a) and (b)). On the other hand, the solar PV coordinated controls of the EWH lead to the shifting of this load to a time in the middle of the day when solar power is in abundance (Figs. 2.13 (c) and (d)). This reduces the required energy capacity of the battery, which would otherwise have had to operate in the charging mode to absorb all the surplus solar power. Additionally, the use of a variable power EWH as opposed to a fixed power type reduces peak loads, which leads to a further reduction in the required energy and power ratings of the battery.

It may be noted that the energy consumed by the EWH depends on the hot water load, and is therefore the same in both fixed and variable power EWH types. Negligible heat loss, which is realized by good insulation, ensures the same EWH

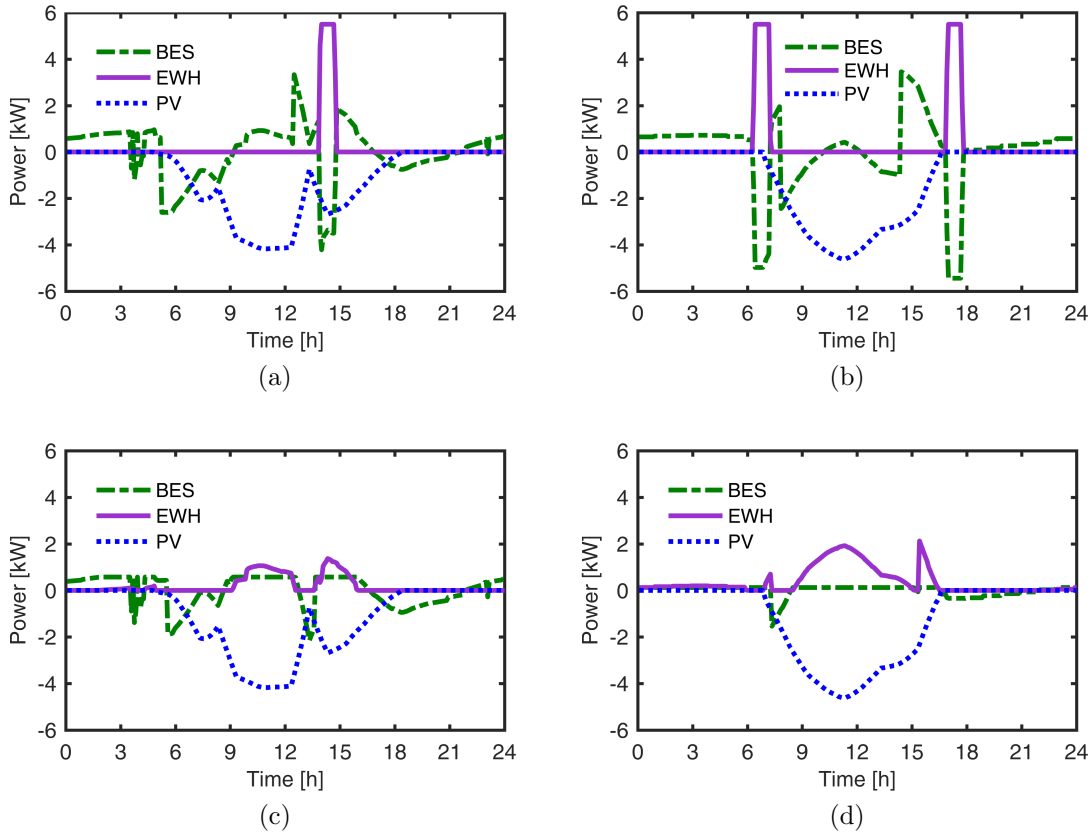

Figure 2.13: Battery and EWH schedules for the traditional case with a fixed power water heater for a representative (a) summer day and (b) winter day in California. Variable power water heater with controls co-ordinated with solar power availability for the same (c) summer day and (d) a winter day.

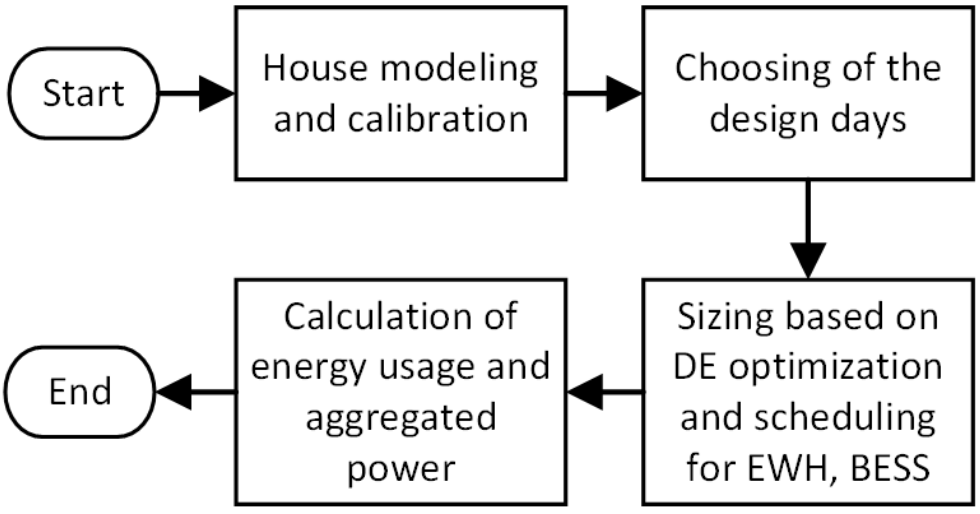

Figure 2.14: Procedure for the sizing of HyPVESS, calculation for electricity spending of NZE home and aggregated power of the distribution system.

energy consumption irrespective of the times at which it operates, therefore, the operating schedule involves distributing a fixed energy.

The procedure for the systematic sizing of the HyPVESS is shown (Fig. 2.14). Following the modeling and calibration of the house energy consumption model, representative design days for summer and winter were chosen. Based on the PV generation and energy usage data for the design days, the differential evolution (DE) method was used for BES sizing and the scheduling for BESS and EWH. Electricity spending of individual NZE homes was calculated using the ToU and buy back rate based on CA. The savings for individual homes were analyzed comparing the different electricity spendings caused by HyPVESS for the same house at the same day. The benefits of HyPVESS at distribution power system level were analyzed by comparing the peak power reduction.

The power balance for each home is expressed as:

$$\begin{aligned} P_M(t) &= P_{PV}(t) + P_{BES}(t) \cdot \eta + P_R(t) \quad , \\ P_R(t) &= P_{EWH}(t) + P_{R1}(t) \quad , \end{aligned} \tag{2.24}$$

where, $P_M(t)$ is the metered power; $P_{PV}(t)$, the PV power generation; $P_{BES}(t)$, the battery power; η, the battery efficiency (which, unless specified otherwise, is considered to be 100% considered for simplicity. A study of the real efficiency effects is later on included); $P_R(t)$, the residential load power; $P_{EWH}(t)$, the EWH load power; and $P_{R1}(t)$, the residential load power excluding the EWH.

The ideal grid power flow would be constant throughout the day, however, such profiles are not practical due to solar power variability and peak loads. Therefore, each house is considered to deliver or absorb constant power to and from the grid for

a certain time during the day in order to minimize the grid power fluctuation, and mitigate issues related to solar power variability Therefore, the power is fixed at two levels, as defined below,

$$P_M(t) = \begin{cases} P_1 & 0 \le t \le t_1, \\ P_2 & t_1 \le t \le t_2, \\ P_1 & t_2 \le t \le 24. \end{cases} \tag{2.25}$$

With two such power levels considered, only 4-parameters are required to define $P_M(t)$, i.e., P_1, P_2, t_1, t_2. It may be noted that when this analysis is combined maximum profitability considerations, the metered power variation will change accordingly. The battery size and metered power would depend on the weather conditions. In this study, two representative summer and winter days are considered.

In the simulation, the battery is assumed to have the same amount of energy in the end as the beginning. Upon the integration of (2.24) over the whole day, taking the efficiency $\eta = 1$ and setting $\int P_{BES}(t) \cdot \eta dt = 0$ yields

$$\int P_M(t)dt = E_{PV} + E_R, \tag{2.26}$$

where, E_{PV} and E_R are energy generation by the solar PV system, and home energy usage over a day, respectively. Both these terms are fixed for given weather and residential load data, and thus, the term $\int P_M(t)dt$ can be calculated. This can be used to eliminate one of the 4-parameters composing the grid power definition using

$$\int P_M(t)dt = P_1 \cdot t_1 + P_2 \cdot (t_2 - t_1) + P_1 \cdot (24 - t_2). \tag{2.27}$$

The variation in grid power flow is defined as:

$$\Delta P = |P_1 - P_2|. \tag{2.28}$$

A multi-objective optimization problem using P_1, P_2 and t_1 as variables is set up. The objectives considered are minimizing the battery energy capacity (C_B), variation in grid output power (ΔP), and maximum battery power (P_B), as follows:

$$\text{Min}(C_B, \Delta P, P_B), \tag{2.29}$$

where (2.29) is subject to (2.24-2.27).

At each instant of time, for a specified value of P_M, and knowing the values of P_{PV} and P_{R1}, the term $P_{BES} - P_{EWH}$ can be calculated using (2.24). The battery and water heater schedules are separated considering that the water heater is capable of only energy absorption, unlike the battery which can sink or source power. The EWH tank size and power rating are decided based on the requirements of typical single water heater homes. Furthermore, the EWH schedule is coordinated with the PV power generation such that as far as possible it operates when solar energy is in abundance.

Other objectives including the financial profitability for the house owner can be stated as follows:

$$\text{Min}(\sum_{i}^{t}(P_M^t \cdot r_c^t - P_M^t \cdot r_b^t)), \tag{2.30}$$

where, P_M^t is the discrete form of $P_M(t)$ from (2.24); r_c^t, the utility charge rate at time t, and r_b^t, the utility buy back rate at time t.

2.5 Studies Optimal Power Flow at System Level with Minimum Battery Energy Capacity

2.5.1 Control of House Net Power with the PV Hybrid Energy Storage System

The ratings of the battery and EWH systems for each day are determined from an optimization study, using typical meteorological year (TMY) weather data and design days, which are representative of typical winter and summer days. A more exhaustive sizing methodology may involve a consideration of different weather conditions for a specific location, and sorting of the similar days of a year.

Several thousand candidate values of these optimization variables are considered, and the process is exemplified for home load and PV generation on a summer's and winter's day in California (Fig. 2.15). It is seen that a battery rated for 3.5kWh/2.2kW would achieve power delivery to the grid with a maximum fluctuation of 2.3kW in summer, and a battery rated for 1.4kWh/1.5kW would have a fluctuation for output power of 2.4kW in winter. A battery rated for larger capacity, i.e., 3.5kWh/2.2kW for the summer case in CA is chosen in order to handle the worst case. This battery rating is approximately a quarter of that marketed by commercial battery manufacturers [143].

The results of optimal sizing for southern Kentucky, where the EWH electricity consumption is fairly low (Table 2.2) on the representative summer day show that even in this case, the proposed HyPVESS reduces the battery size required. The required minimal BESS capacity C_B is reduced from 5.8kWh/6.3kW of the PVBES

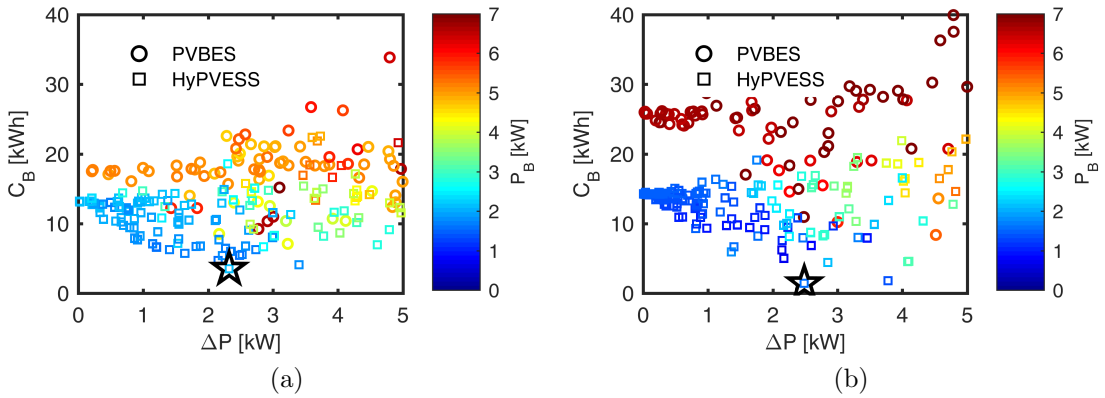

Figure 2.15: The variation of battery energy capacity, C_B with grid power fluctuation, ΔP evaluated for several thousand values of P_1, P_2 and t_1 in NZE homes equipped with only BESS and PV (PVBES), and the hybrid PV energy storage system (HyPVESS) on a representative (a) summer's day and (b) winter's day for California.

to 4.1kWh/1.3kW through the use of the EWH with the proposed controls. The two cases are marked with a ☆ and a ◇, respectively (Fig. 2.16 (a)).

The detailed net power flow for the best cases of California on both summer and winter days are based on the optimization results (Fig. 2.15). In the absence of energy storage, peak load are serviced by the absorption of power from the utility grid (Figs. 2.17 (a) and (b)). The time-of-use (ToU) utility charge rates and the buy back rate, which is 3.8 cents/kWh for the case studies are based on CA [144, 145]. The electricity spending (ES) were calculated for the power flows (Fig. 2.17). Assuming the BESS efficiency is 100%, the daily electricity spending for the same summer weekday were \$10.08 and \$8.91, without and with HyPVESS scheduling, respectively (Fig. 2.17 (a) and (c)). The electricity spending for the same winter weekday were reduced from \$3.46 to \$1.80 with the HyPVESS scheduling (Fig. 2.17 (b) and (d)). This analysis shows that the operation scheduling of the HyPVESS to operate each home as a dispatchable generator is able to reduce the electricity spending to benefit the

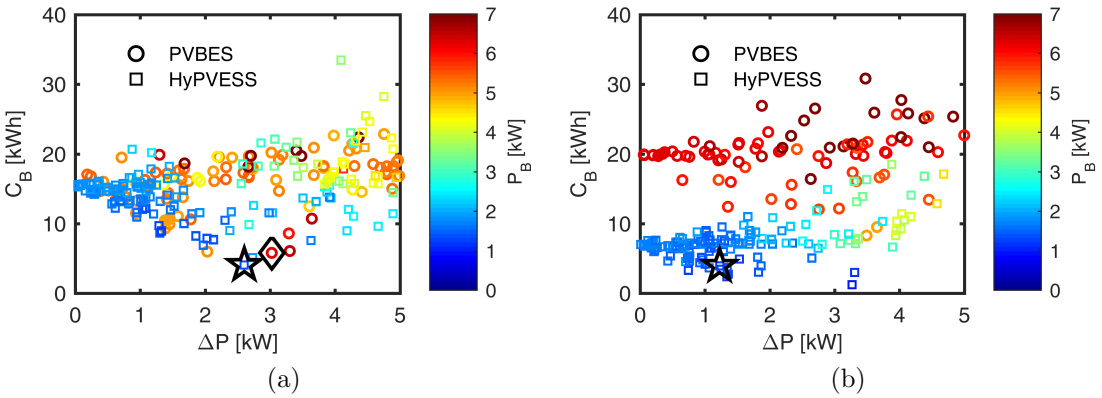

Figure 2.16: The DE results of battery sizing for southern Kentucky on a representative (a) summer's day and (b) winter's day. A battery rated for 4.1kWh/1.3kW is chosen based on the summer case and marked with a ☆. The sized battery has a maximum output power fluctuation of 2.6kW and 1.2kW for the summer and winter days, respectively. Though better choices are available on the winter day, the limitation is set by the summer.

individual houses. This would serve as an incentive to home owners to operate the HyPVESS so that each house behaves like a dispatchable generator.

The effects of BESS efficiency on the proposed HyPVESS is studied (Table 2.4). In line with expectations, for both the studied summer and winter weekdays, energy losses decrease as BESS efficiency increases. It is observed that the daily electricity spending does not vary significantly with the changes in BESS efficiency. This is due to the fact that the proposed sizing method enables the minimum BESS energy capacity with fewer BESS operations.

On the other hand, in NZE residences equipped with the HyPVESS, the operating schedules can ensure that the home provides dispatchable power to the grid, or behaves like a controllable load for relatively long duration of time (Figs. 2.17 (c) and (d)). The variation of power flow to the grid is determined by the solar PV

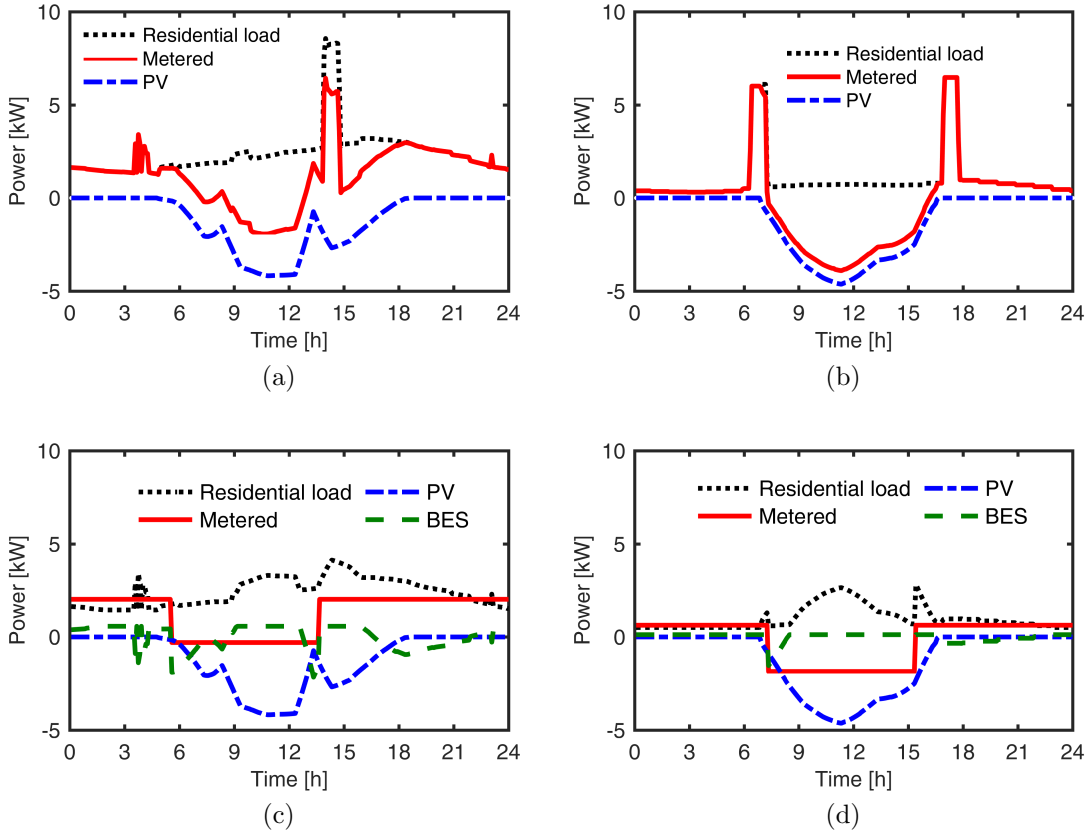

Figure 2.17: Power flow in a home equipped with a solar panel, but no storage, on (a) a summer's day, and (b) a winter's day. Power flow in a home with solar panels and coordinated control of energy storage systems on the same (c) summer's day and, (d) winter's day.

Table 2.4: The impact of BESS efficiency on system loss and electricity spending

BESS efficiency (%)	Energy loss (kWh) summer weekday	Energy loss (kWh) winter weekday	Daily ES ($) summer weekday	Daily ES ($) winter weekday
80	2.73	0.81	8.97	1.80
85	2.05	0.61	8.95	1.80
90	1.37	0.41	8.94	1.80
95	0.68	0.20	8.92	1.80
100	0.00	0.00	8.91	1.80

Total daily energy usage, summer: 58.13kWh; winter: 24.25kWh

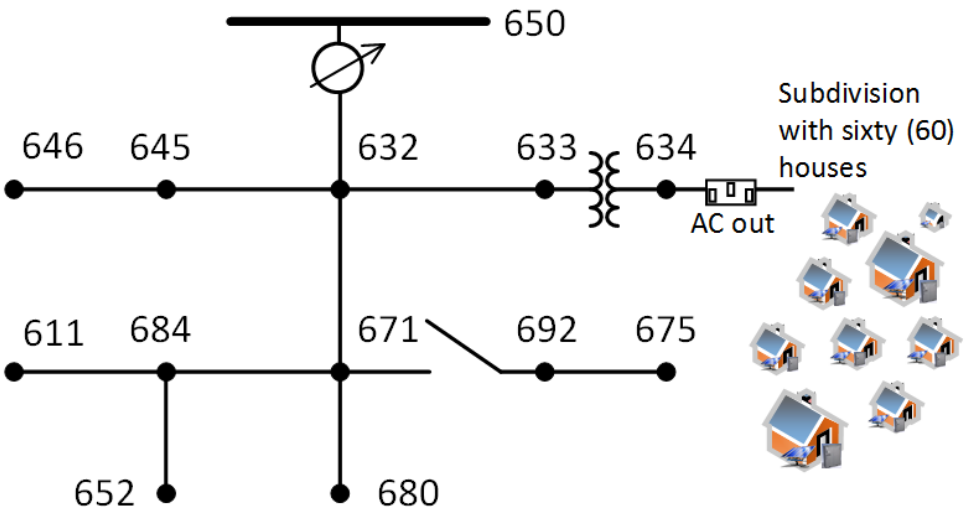

Figure 2.18: The IEEE 3-phase single line diagram 13-node feeder test case is adopted for the district level simulation. Sixty NZE houses are linked to node 634.

generation, as well as by the rating and operating schedule of the energy storage system, and more particularly that of the battery. The calculated battery ratings would minimize the power flow fluctuations on typical winter and summer days. Increased battery ratings may be required if the number of cloudy days per year are higher, which may be the case in Kentucky, though not in California.

2.5.2 Optimal Power Flow at Power Distribution System Level

In order to evaluate the effect of the proposed home energy storage scheduling on an aggregated level, the behavior of the NZE homes at the district level is modeled by interconnection with an IEEE-13 node test feeder system, which is described in [146]. Sixty NZE homes with residential load and PV generation profiles modified according to the number of occupants and local weather variations are connected to node 634 (Fig. 2.18).

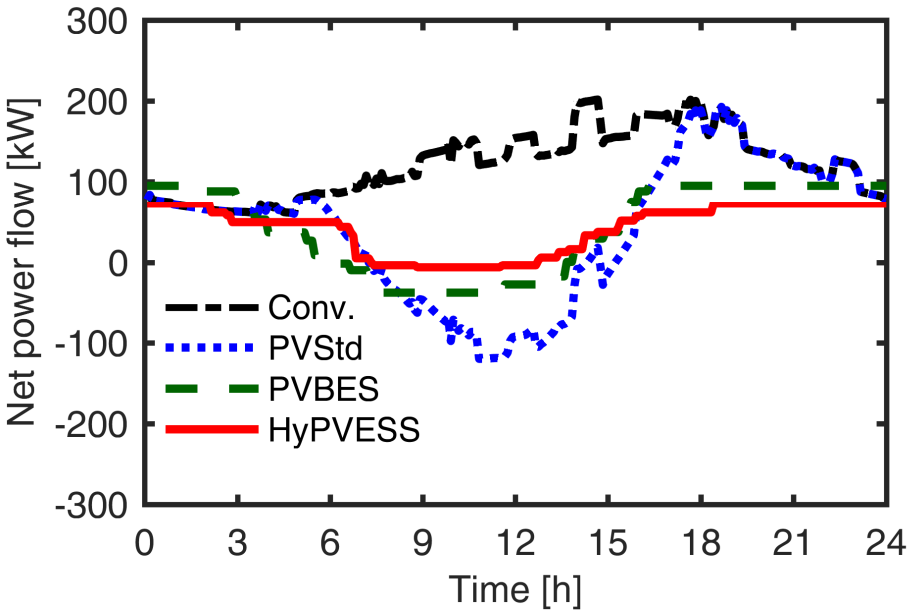

Figure 2.19: Power flow profile at node 634 of the IEEE 13-bus test system from Fig. 2.18 on a summer day.

Four types of homes, conventional i.e., without solar PV and BES; PVStd, including solar PV and conventional EWH but no batteries; PVBES, equipped with solar PV, conventional EWH, and batteries of the sized energy capacity; and the proposed HyPVESS containing both solar panels, batteries, and EWH with controls co-ordinated with solar PV generation are examined to verify the benefits of the proposed HyPVESS at the district level (Figs. 2.19 and 2.20) . In case of the HyPVESS homes, the battery and EWH schedules and ratings are derived for each home as detailed in Section IV. The active power at the node 634 is monitored.

Homes of the PVStd type, which contain no storage can achieve NZE targets by feeding power to the utility during periods of plentiful solar power, and absorbing it when solar generation reduces. One of the limitations associated with this type of operation is that PV generation and load peaks are not coincident, leading to an excess

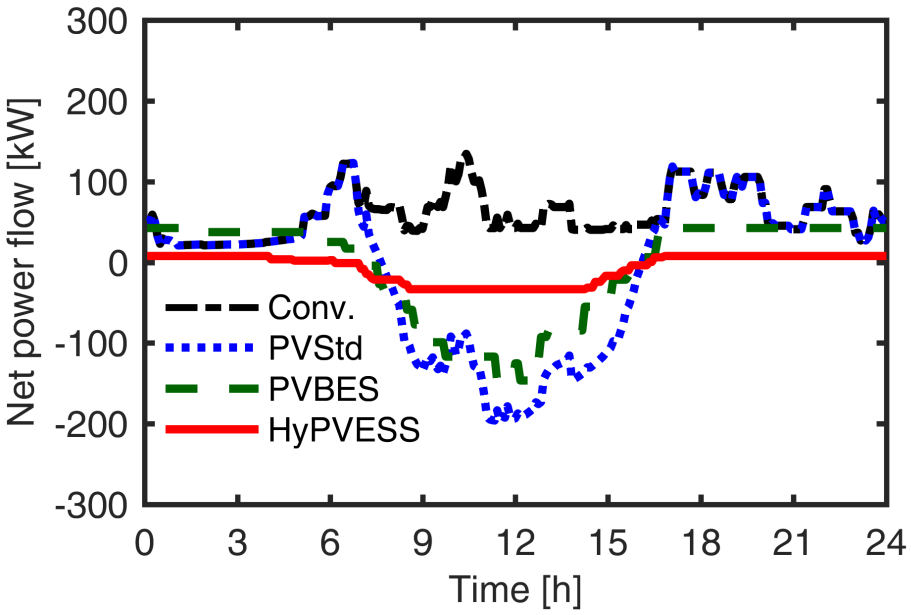

Figure 2.20: Power flow profile at node 634 of the IEEE 13-bus test system from Fig. 2.18 on a winter day.

inflow of power into the utility at and around midday. In contrast, during the evening, PV generation diminishes, and load rise, therefore excess power is absorbed from the utility grid at this time. This type of behavior leads to the "duck curve", which would be exacerbated for high PV penetration communities (Figs. 2.19 and 2.20). For large PV communities, a power system incorporating a number of fast responding gas plants would be required to service this rate of change of load, requiring tremendous investment. The peaks of power inflow and outflow could also potentially cause issues including overloading of distribution lines, transformers, and excessive voltage drop.

The PVBES homes, i.e., homes with batteries and conventional EWH systems can theoretically eliminate the "duck curve" and offset the peaks, however, the batteries required to achieve these objectives would have large energy capacities, and lead to high cost. In the HyPVESS case, i.e., homes with the variable power controllable

EWH as well as batteries the "duck curve" is alleviated and peak demand is reduced, with a smaller size battery. When the homes are equipped with the HyPVESS, each one is controlled to deliver dispatchable power (Figs. 2.19 and 2.20). It is observed that peaks and the "duck curve" of the power flow to the grid are the minimum in all the cases for both summer and winter days (Figs. 2.19 and 2.20). Thus, these case studies demonstrate that the proposed hybrid PV and BESS and controls can potentially mitigate the issues stemming from solar power variability, with a relatively small battery size. The proposed schedules for the battery and EWH can be combined with economic analysis and modified accordingly in order to maximize profitability for the consumer, in order to motivate more consumers to install home energy storage systems.

2.6 Conclusion

This chapter introduces a co-simulation framework called INSPIRE+D, which is capable of modeling the instantaneous energy usage and solar generation of a large community of buildings, and simulating their interconnection with the grid. Also introduced was the DER integration testbed, which enables the study of HEM system implementation at both the residential and community levels. An example community for 353 residences was modeled using the IEEE 123-bus feeder case with filed measured data. This example community will be further used for the verification smart devices, which are able to react to DR signals complying to CTA-2045 standards.

The energy usage models within the co-simulation framework are used to predict the electricity consumption for California and Kentucky, and validated based on the

California Building Energy Code Compliance Residential Standards, and experimental data from southern Kentucky, respectively. A method to identify the minimum size of the solar PV panels in order to achieve NZE operation based on the simulated annual average energy usage was proposed. An energy storage system using batteries along with water heaters was proposed to alleviate the duck curve caused due to non coincident solar generation and load demands. It was demonstrated through simulation studies on a large community of grid connected NZE homes that home energy storage systems can be controlled such that the grid power flow fluctuation can be minimized on typical winter and summer days, thereby mitigating technical challenges associated with solar power variability.

A methodology based on multi-objective differential evolution for sizing and scheduling the operations of the hybrid energy storage system on typical winter and summer days was outlined. The objectives include the energy capacity and power ratings of the BESS, and the fluctuation of the net metered power. Simulation studies show that the distribution power system operated as dispatchable generator/load with a 30% smaller battery through the use of the proposed controlled variable power water heaters. Furthermore, the sizing for BESS could be extended to consider charging/discharging patterns for different weather conditions over the year. For a case considering the ToU tariff and buy back rates from California, it is found that the electricity spending costs can be reduced significantly for representative summer and winter days through this control of the hybrid energy storage system.

Chapter 3

Electric Water Models including Energy Storage Characteristics and Demand Response Applications

3.1 Introduction and Problem Formulation

The electric water heater (EWH) accounts for a substantial portion of a typical house electric power consumption [147]. However, the unpredictability of customer behavior makes quantifying the benefits of controlling EWHs difficult. Demand response (DR) implementations must carefully balance the water temperature in the tank to provide the maximum grid benefit between two bounds, i.e., it must be kept high enough to meet the user demand while not exceeding the stipulated safety reference. Fortunately, technologies such as mixing valves may be used to allow the water to be safely stored up to 145F and still meet safety requirements [9, 10].

The ubiquity of EWHs make them one of the most advantageous appliances for

participation in the virtual power plant (VPP) operation for residential buildings. The EWHs have large thermal masses of water in their tanks and can be regarded as both heat reservoirs and energy sinks to provide ancillary services with relatively low-cost [22, 31]. Their effective tank insulation gives high equivalent thermal resistance compared to pipes, resulting in less energy loss associated with water heater tanks than distribution systems [148]. These properties allow EWHs to, for a short period of time, be turned Off for load shedding while maintaining the water temperature at the reference temperature. Furthermore, EWHs can be used to absorb surplus PV generation. These services could improve the reliability of the grid and provide monetary benefits to both the grid and residences while maintaining user comfort [70–74]. The potential regulation capacity of water heaters is impacted by factors including ambient temperature, hot water usage, and setpoint [75–78].

Energy storage devices and systems, which can be electric, such as battery energy storage systems (BESS), or thermal, such as EWH or heating, ventilation and air conditioning (HVAC) systems, are essential in order to ensure an optimal energy management and power flow within the modern grid with DER. This method of hybrid energy storage can reduce required BESS capacity by up to 30% while providing the same capability [11]. To support technology development and standard-type implementation that would enable wide scale industrial and utility deployment, Energy Star, a program conducted by the Environmental Protection Agency (EPA) and Department of Energy (DOE), provides general specifications for energy parameters and DR functionalities [29].

For EWH, these specifications are typically implemented using the Consumer

Technology Association (CTA) 2045 standard [27], and success has been reported at the individual residential and utility aggregated levels [30], [31]. In principle, the combined Energy Star and CTA-2045 specifications and concepts such as "energy capacity", "energy content", and "energy take" and DER commands, such as "load up", "shed", etc., can be extended to any energy storage device and system, enabling a unified approach at the system level. For EWH, success has been reported at the individual residential and utility aggregated levels [30, 31].

Modeling of EWH energy use at the individual level to be employed in a DER testbed may be performed through different means, including grey-box modeling which employs a combination of white-box (theory-based) and black-box (data-driven) methods. For example, [149] employs physics-based equations to model the thermal losses to the environment and water consumption as well as for the contribution from the heating element. In addition to these mathematical representations, estimation through measured data was utilized to determine certain parameters of the physical model.

Regardless of the model type, the common input for an EWH MIL is the total domestic hot water (DHW) usage of end use appliances. Typical DHW schedules, such as those provided by the CBECC-Res Compliance Software Project [80], are very useful resources for performing realistic community-level simulation studies. An internet-based survey involving 1,600 members found that approximately 70% of the residential participants would allow the utility to control their switches or thermostats when proper incentives were provided [92]. The potential of water heater related technologies was widely appreciated in the annual conference of Hot Water Forum

held by the American Council for an Energy-Efficient Economy (ACEEE) [67].

The power profile of water heaters is largely decided by user behavior. In previous studies, the hot water draws for 48 representative days were evaluated based on measured data from California homes [79]. The proposed schedules are used in the California Building Energy Code Compliance for Residential buildings (CBECC-Res) [80]. In another study, the aggregated EWH load was calculated by analyzing the hot water usage schedules [81]. A typical aggregated load for EWHs has a morning and evening peak, as shown in the study involving 50 water heaters [82].

The problems addressed in this chapter include water heater as generalized energy storage, thermodynamics of water heater when DR is applied, the total energy storage capacity of EWHs and HPWH, and impact of DR controls on the distribution power system. Each of the problems are defined in the subchapters: water heater as generalized energy storage in section 3.2.1, thermodynamics of water heater, and the total energy storage capacity of EWHs and HPWH in section 3.3, and impact of DR controls on the distribution power system in section 3.4.

In this chapter, the EWH was modeled using the equivalent circuit with parameters calibrated against measured data. A representative power profile for aggregated water heater generic load curve that can be scaled to any number was developed based on public data. The potential of water heaters as energy storage at the power system level was estimated based on the generic curve. Also, EWH and heat pump water heater (HPWH) have very different characteristics and were analyzed separately. A total number of 353 EWH were modeled separately and connected to a modified IEEE 123-bus feeder, which also included the realistic residential load from measurement.

DR signals complying to CTA-2045 standards were applied to the EWHs and their impacts were monitored at the power system, including power flow and voltage at each bus.

This chapter is substantially based on the following journal papers:

- H. Gong, *et al.*,"Equivalent electric and heat-pump water heater models for aggregated community-level demand response VPP controls," *IEEE Access*, Vol. 9, pp. 141233–141244, 2021.

- H. Gong, *et al.*, "Large-scale modeling and demand response control of EWH with energy star and CTA-2045 control types in distribution power system," *IEEE Transactions on Industry Applications*, 10p, 2021, *Submitted in Dec, 2021.*

3.2 Multi-physics Models for EWHs

3.2.1 Energy Storage Generalized Concepts based on CTA-2045

The EPRI's DER integration testbed for energy storage systems is of particular interest for this study as it was utilized for the simulation of an EWH that is treated as an energy storage system [121]. The simulator is capable of various smart functions, such as connection/disconnection, charging/discharging, volt-VAR curve input, and generation level and power factor adjusting. The EWH MIL was simulated in the chapter and connected to EPRI's DER integration testbed (Fig. 3.1).

The Generalized Energy Storage (GES) in a residence includes BESS, EWH, and the HVAC system. For a BESS, the "current available energy storage capacity" is

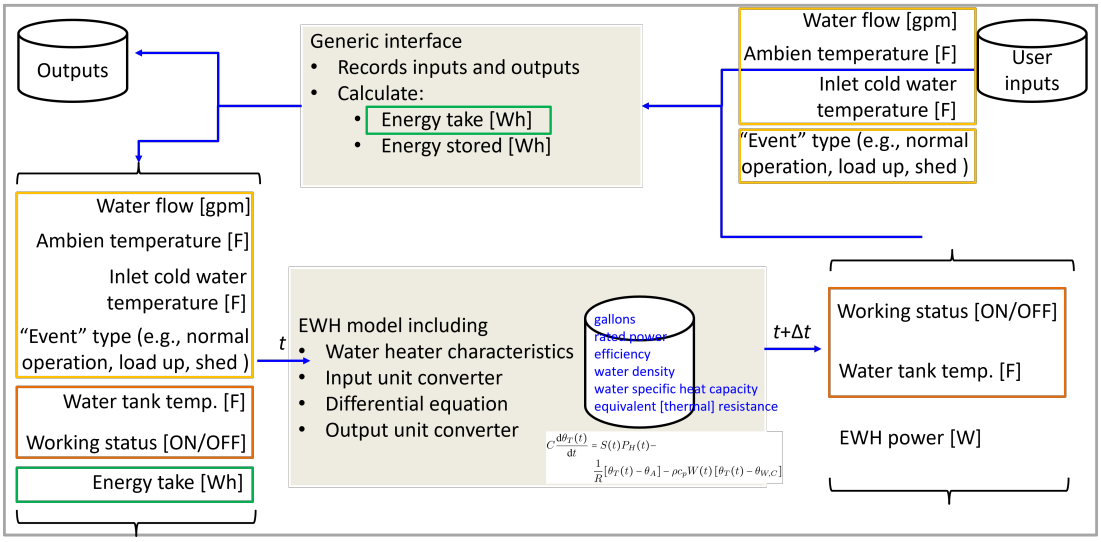

Figure 3.1: Schematic of the Model-In-the-Loop (MIL) for an Electric Water Heater (EWH). The computer code is implemented in C# under Visual Studio 2020 and communications with the EPRI's DER integration testbed follow the CTA-2045 standard for Energy Star commands.

calculated as follows:

$$E_{C,B}(t) = \overline{E_{B,R}} \cdot (SOC_{B,max} - SOC_B(t)), \tag{3.1}$$

where $\overline{E_{B,R}}$ is the rated energy capacity of the BESS; $SOC_{B,max}$, the maximum allowed SOC.

For most of the academic work, the water temperature in the tank was used to represent the current status of the energy storage for the EWH. Practically, the water temperature is hard to measure as it is stratified inside the tank. Therefore, most CA-2045 available EWH only provide the "energy take" by manufactures based on their undisclosed algorithms.

In this chapter, the "energy content of the stored water" for the EWH is defined as:

$$E_W(t) = V \rho c_p \theta_T(t), \tag{3.2}$$

where V is water tank volume; ρ, density of water; c_p, specific heat capacity of water; θ_T, the average temperature in the water tank. Based on (3.2), the "current available energy storage capacity" for a water heater is calculated by referring to the set point, as follows:

$$E_{C,W}(t) = \overline{E_{W,S}} - E_W(t), \tag{3.3}$$

where $\overline{E_{W,S}} = V\rho c_p \theta_{T,S}$ is the maximum energy capacity for the EWH, defined by $\theta_{T,S}$, the set point. The "energy take" is defined as follows:

$$E_{T,W}(t_2 - t_1) = E_W(t_2) - E_W(t_1). \tag{3.4}$$

The HVAC system is regarded as an energy storage and its equivalent SOC is defined as:

$$SOC_H(t) = \frac{\theta_{max} - \theta_I(t)}{\theta_{max} - \theta_{min}}, \tag{3.5}$$

where the θ_{max} and θ_{min} are the maximum and minimum room temperature, respectively; θ_I, the indoor temperature. The energy storage capacity of the HVAC system, $\overline{E_{H,C}}$, is defined as the input electricity needed to change the room temperature from the maximum to the minimum with a fixed outside temperature [88]. The "current available energy storage capacity" for the HVAC system calculated as:

$$E_{C,H}(t) = \overline{E_{H,C}} \cdot (1 - SOC_H(t)). \tag{3.6}$$

Two cases, which were based on experimental results, were studied to validate the EWH as a MIL in the EPRI's DER integration testbed. In the first case, the simulation results of a resistive EWH was validated against the experimental data from an EPRI performance test on a CTA-2045 compatible EWH [30]. The tank

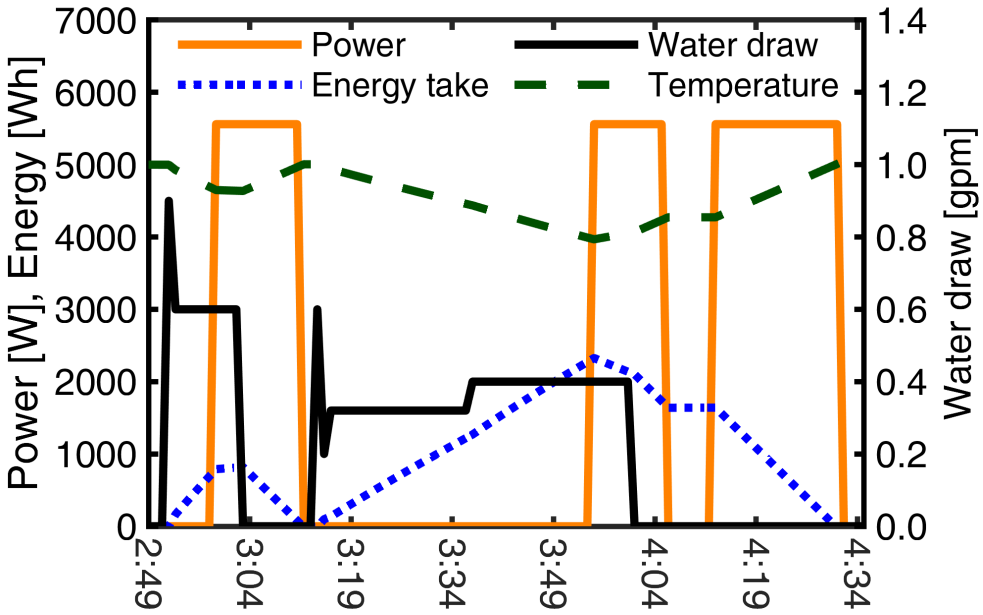

Figure 3.2: Example of simulated EWH "Shed Event" corresponding to the experimental data illustrated in Fig. 3.3. Based on DR control signals, the "energy take" capacity was increased from 900Wh to 2,200Wh, resulting in a shift/delay of the water heating process.

temperature and the "energy take" values were monitored as the EWH responded to the "Shed Event" signal (Fig. 3.2). The simulation has satisfactory results compared with the experimental data (Fig. 3.3).

The value of "energy take" has different ranges which correspond to the types of DR signal. Under normal operation, the range of "energy take" is [0, 900Wh]. When the value of "energy take" is more than 900Wh, the EWH turns On until the value reaches 0 (Fig. 3.2). The temperature and water draw are referred in p.u., where the base values for temperature and hot water flow are 140 F and 1 gallon per minute (GPM), respectively.

At 3:10, the EWH responded to the DR signal "Shed Event" by setting the "energy take" range to [2,000Wh, 2,200Wh]. The DR signal "Shed Event" postponed

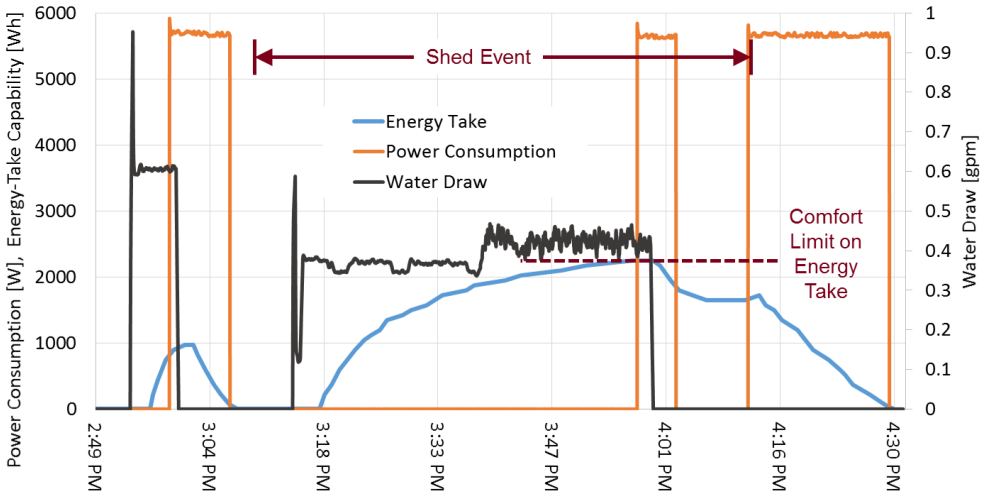

Figure 3.3: Experimental data, previously reported by NREL/EPRI [30], and employed for the satisfactory validation of the proposed EWH MIL. The "Shed Event" occurs from 3:10 to around 4:10, which causes the "energy take" range to increase and the heating process to be postponed while maintaining occupant comfort.

the heating process by allowing more energy to be taken from the tank by the hot water while maintaining occupant comfort. The "Shed Event" ended at around 4:10 and the EWH was turned On immediately to bring the "energy take" value to 0. For comparison, an illustration of the experimental data for the "Shed Event" case reported in [30] is provided in Fig. 3.3.

The second case was based on the experiment from the SHINES program, which was launched in 2016 by the DoE to develop and demonstrate technologies that enable sustainable and holistic integration of energy storage with solar PV [150]. In this chapter, the EWH loads of the two houses, as well as the BESS, solar PV, pool pump and HVAC were tested in the field. The different EWH loads and BESS charging schedule as well as the corresponding energy and aggregated power of the two EWHs are provided for a comparative study (Fig. 3.4).

The example charging schedule for the BESS resulted in a similar power rating

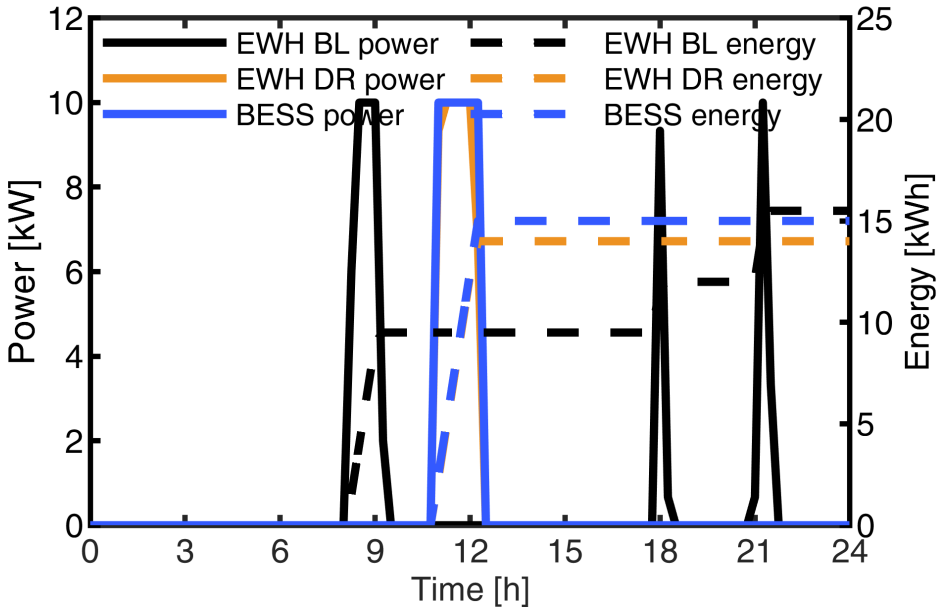

Figure 3.4: Comparative study of energy storage with BESS and EWH, including typical/normal base line (BL) and DR schedules. For BL operation, the EWH has a morning and two evening peak power cycles. The BESS schedule was adjusted to allow comparison with a EWH study for DR load shifting around noon, which may align well with PV generation, if available.

when compared to the EWH DR power. This example shows that the BESS and EWH are comparable when considering their energy content as GES. The average temperature of the water was monitored in the case studies and shown in Fig. 3.5. When the peak in the morning was shifted, the temperature in the tank was still above the commonly acceptable user comfort level, which is 115F. Mixing valve technology was used to guarantee occupant safety when the temperature in the water tank was high. The EWH under DR can be programmed at night to boost the tank temperature to the same value as the beginning of the day.

The EPRI SHINES project provides timely data with a resolution of 15 minutes for the power flow at the transformer where four houses were connected. Two of the four houses have their own solar PV installations, HVACs, pool pumps, and

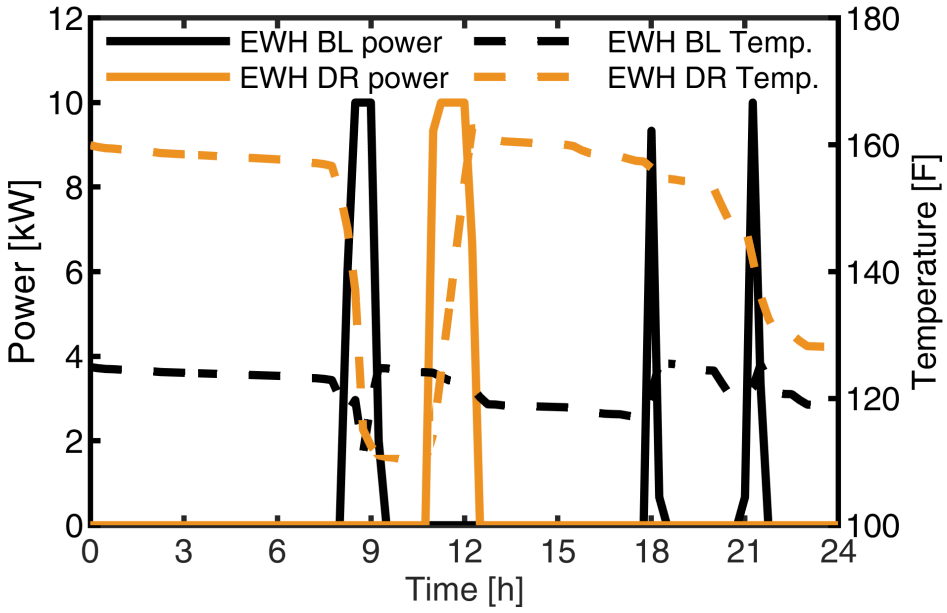

Figure 3.5: Power draw and water tank temperature for an EWH operating under BL and DR studied schedules. The high water temperature in the tank may be enabled by special mixing valve technologies.

other non-DER loads monitored by the SHINES project. The non-DER loads of the monitored houses were added to the total power of the other two houses, and were labeled as "uncontrollable loads" at the distribution level (Fig. 3.6).

The EWH provided the energy storage capacity for the surplus PV generation as the BESS (Fig. 3.4). The net flow at the aggregated level was reduced due to the DR control, as shown in Fig. 3.7. Shifting the EWH load also reduced the peaks in the afternoon and evening.

3.2.2 Water Flow and Electric Power Load

Hot water draw from the CBECC-Res data set was named as "XDY". X is the number of bedrooms and Xϵ{1,2,3,4,5}. CBECC-Res water heater draw has three

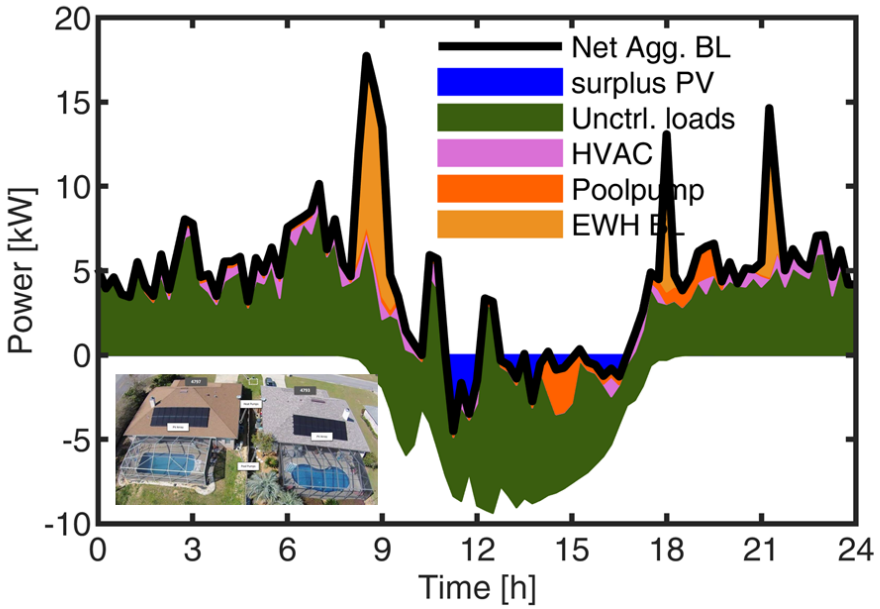

Figure 3.6: Combined experimental and simulated power flow on an example February day for two smart homes, which are located in Florida and were developed as part of the EPRI SHINES DoE project (photo inset). The EWH simulations were performed with the proposed MIL.

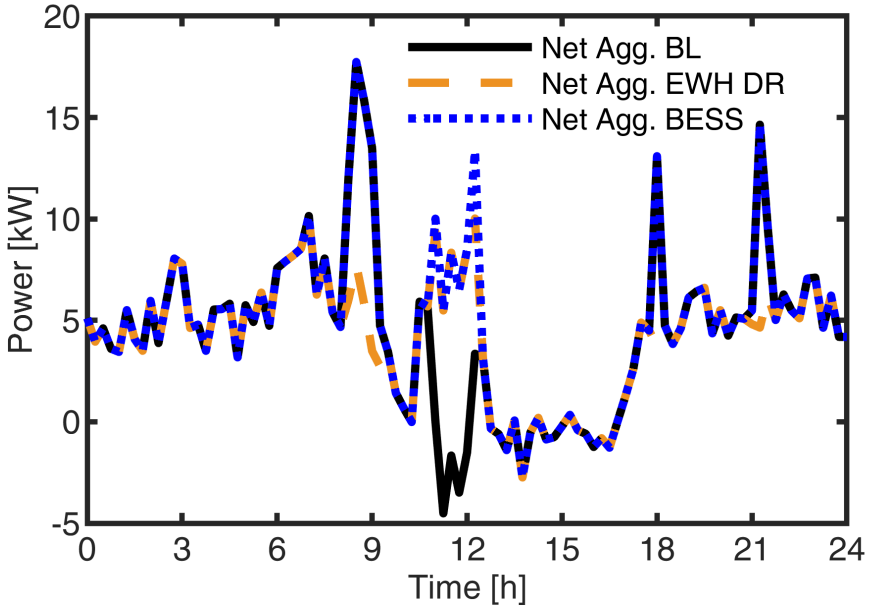

Figure 3.7: Case studies for the aggregated net power flow at the distribution level. For the proposed control, during the day, a substantial portion of the solar PV generated energy was locally stored in the EWH or BESS.

Table 3.1: Hot water fraction and end use temperature of fixtures.

End use	Hot water fraction	End use Temp. [F]
Faucet	0.50	95
Shower	0.66	105
Clothwasher	0.22	78
Bath	0.66	105
Dishwasher	1.00	125

types of days: weekdays (D), weekends (E), and holidays (H). Only type "D" was considered in this study. Y is the Y^{th} profiles for one category and Y$\in\{0,1,2,3,4,5,6,7,8,9\}$. The value for Y is only the natural sequence for different profiles and does not attribute to any specific day. For example, "3D8" is the 8^{th} weekday profile for a 3 bedroom house, and it represents a user behavior which could occur at any weekday.

In this study, there were 36 residences with 1 bedroom (Table 2.3). Therefore, 36 hot water draw were selected randomly as "1DY" (Y$\in\{0,1,2,3,4,5,6,7,8,9\}$) with repetition, i.e., some profiles were selected more than once. Similar procedures were performed for the other residences with more than 1 bedroom, and a total of 353 hot water draw profiles were selected based on the 50 representative hot water profiles from CBECC-Res.

The daily hot water draw profiles in CBECC-Res include the hot water flow at different fixtures (Fig. 3.8). Based on the hot water draw, the EWH power, tank temperature, and energy take were calculated. The temperature for hot water and cold water, and the hot water fraction of end use were concluded in [79]. The end use temperature for the fixtures were calculated (Table 3.1).

The hot water flow at the outlet of the water tank was calculated using the water

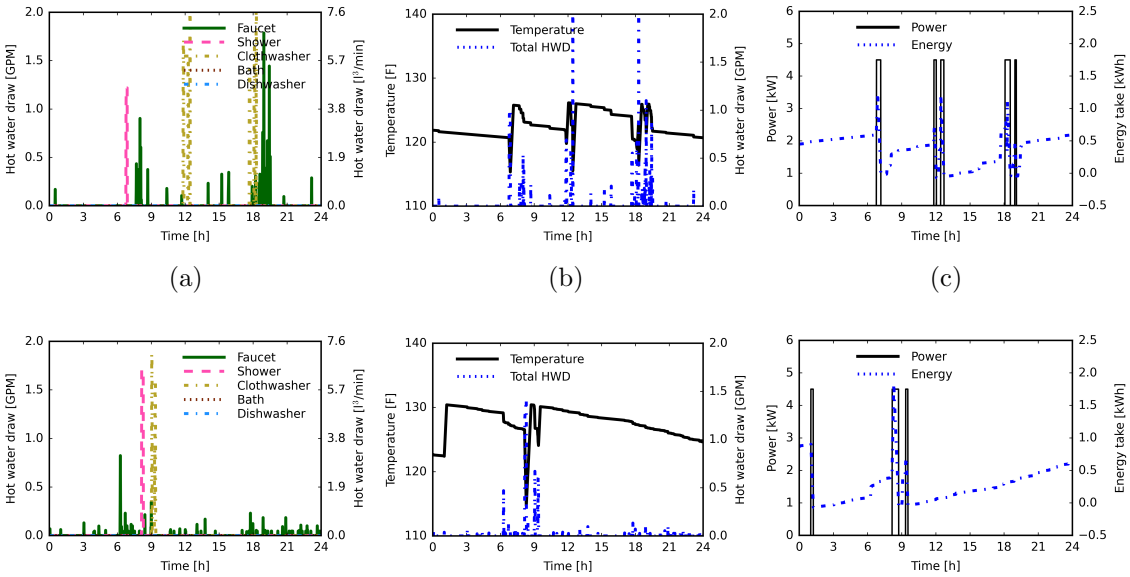

Figure 3.8: Example hot water draws from CBECC-Res data for different end use (a), (d); Calculated tank temperature and total hot water draw (b), (e); and calculated EWH power and energy take (c), (f). Shown are two example daily hot water draws corresponding to "5D3" (top), and "3D2" (bottom).

flow balance and energy balance:

$$\dot{V}_H + \dot{V}_C = \sum \dot{V}_i, \tag{3.7}$$

where $\dot{V}_H$ is the water flow at the outlet of water tank; $\dot{V}_C$, water flow of cold water; $\dot{V}_i$, water flow at fixture.

The energy balance is represented as follows:

$$\dot{V}_H \theta_T(t) + \dot{V}_C \theta_{W,C} = \sum \dot{V}_i \theta_i, \tag{3.8}$$

where $\theta_T(t)$ is the water temperature in the tank; $\theta_{W,C}$, cold water temperature; θ_i, end use temperature listed in Table 3.1.

Each EWH had different initialized water temperature and energy take value. The 1R1C gray-box model of EWH is used for the calculation of water temperature with

Table 3.2: Parameters for the equivalent EWH model.

Parameter	Value or unit
Density of water ρ	993 $^{kg}/_{m^3}$
Specific heat capacity of water c_p	4,179 $^{J}/_{kg°C}$
Room air temperature θ_A	22 °C
Temperature of cold water $\theta_{W,C}$	10 °C
Water heater heating rate P_H	kW
Water tank volume V	50 gallon
Equiv. thermal resistance R	[a]1400 $^{°C}/_{kW}$ [b]600 $^{°C}/_{kW}$
Water temperature in the tank θ_T	°C
Hot water flow W	m^3/s

[a] EWH, [b] $HPWH$

three major effects, i.e., the input electric power, the standby heat loss, and the hot water draw activities, as:

$$C\frac{\mathrm{d}\theta_T(t)}{\mathrm{d}t} = S(t)P_H(t) - \frac{1}{R}[\theta_T(t) - \theta_A] - \rho c_p W(t)\,[\theta_T(t) - \theta_{W,C}]\,. \tag{3.9}$$

The values for the parameters are listed in Table 3.2.

C and $S(t)$ are the equivalent thermal capacitance and On/Off status, defined respectively, as:

$$C = V \cdot \rho \cdot c_p. \tag{3.10}$$

$$S(t) = \begin{cases} 0, & \text{if } S(t-1) = 1 \;\&\; E_{T,W}(t) \le Q_{T,min}(t) \\ 1, & \text{if } S(t-1) = 0 \;\&\; E_{T,W}(t) \ge Q_{T,max}(t) \\ S(t-1), & \text{otherwise,} \end{cases} \tag{3.11}$$

where the $Q_{T,min}$ and $Q_{T,max}$ are the energy take levels, which differ for DR events (Table 3.3) [30]. When the energy take value is larger than the maximum energy take level, EWH has to be On in order to compensate for the lost energy. The higher

Table 3.3: Water heater condition as characterized by energy take levels

Event	Energy take levels (Q_T) [Wh]	
	Minimum	Maximum
Normal operation	0	300: ≥ 1 GPM 600: ≥ 0.3 GPM 900
Shed	1800	2250
Load up	0	300

the maximum energy take level, the more hot water allowed to be drawn without triggering on the EWH. When the energy take value is smaller than the minimum energy take level, EWH would be turned Off. The energy take at a given time point $E_{T,W}(t)$ was referred to the starting point of the simulation and (3.4) is rewritten as:

$$E_{T,W}(t) = E_W(t) - E_W(0). \tag{3.12}$$

For the Normal operation event, the maximum energy take level depends on the hot water flow. Increased hot water flow causes the energy take level to be lower. When the hot water draw is high, EWH will be On, even if the energy take value is low, so that the user comfort is guaranteed. For the shed event, the energy take levels are much higher to allow for more hot water draw. The EWH would be On during the shed event when the energy take is too high, which indicates low water temperature in the tank. For the load up event, the EWH would be On even if the energy take is low. The load up event always occurs when there is surplus PV generation.

3.3 Aggregated Generic Load Curve for EHW and HPWH

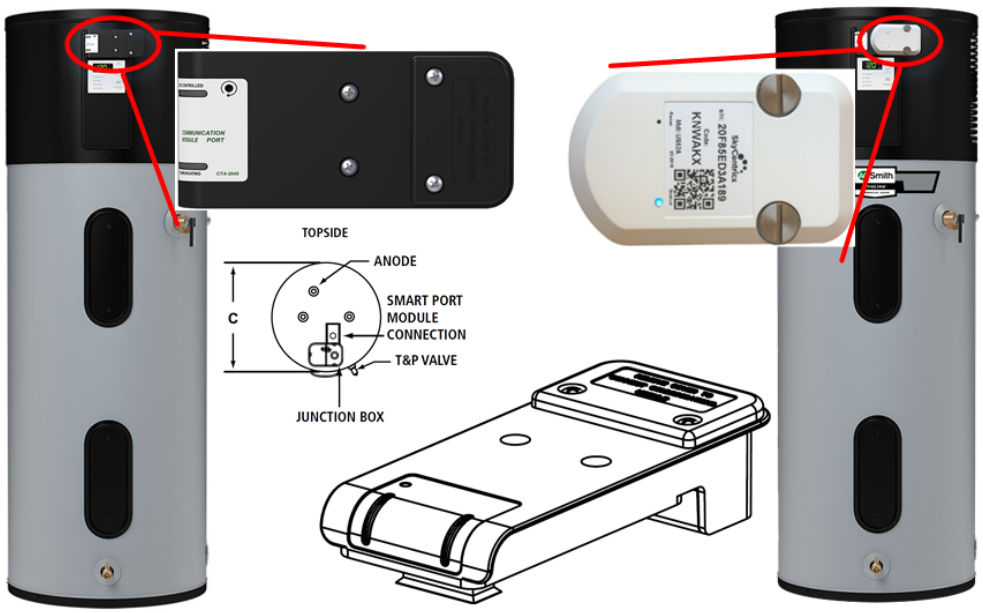

Figure 3.9: The illustrative parts of A. O. Smith "Energy Smart" model and CTA-2045 standard port. The "Energy Smart" controller is smart grid ready and implements standardized communications for DR.

3.3.1 Large Scale Experimental Study for EWH

A smart EWH that allows users to control the setpoint, the operating mode and receive alerts based on the device operation was developed by A. O. Smith. Approximately 800 anonymized units with the "Energy Smart" EWH controller were analyzed in the program, in which appliance usage data were retrieved and evaluated. The "Energy Smart" controller can be plugged into the EWH and enables the monitoring, remote control, alarming, and creating custom heating schedules [151]. The EWH heater models optionally include a CTA-2045 port adapter and utility communication module to enable smart communication with energy providers (Fig. 3.9).

Over a two-year period from 2018 to 2020, the data analyzed witnessed a growing number of participants, peaking at nearly 500 EWHs recorded per day in early 2019

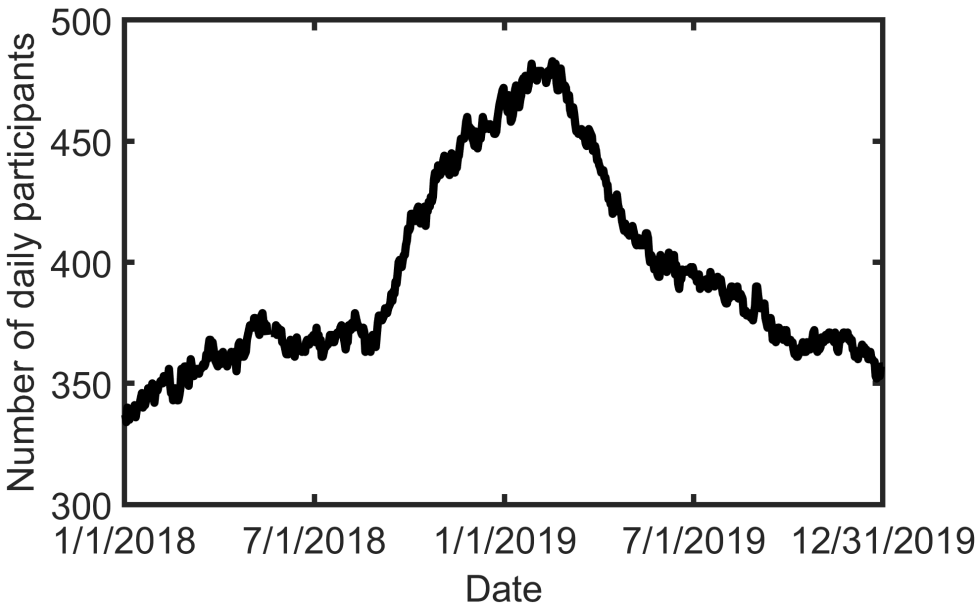

Figure 3.10: Daily number of EWH in service. Approximately 800 participants were analyzed as part of the program and an increase from 2018 till early 2019 can be observed before the gradual decline.

(Fig. 3.10). Based on the data retrieved, up to 100 participants opted out of the program at inception and 140 EWHs participated through the entire length of the project (Fig. 3.11). During the project span, approximately 350 EWHs were reporting their instantaneous power online.

The daily power profile for EWHs is determined by the user-influenced parameters such as hot water usage and the hot water temperature set point. The power profile for EWHs is also influenced by other factors including the ambient temperature, inlet water temperature, and the insulation of domestic water pipes. Hence, there is variation in the power curve from one EWH unit to the other. A typical residential EWH would normally have two or three short heating cycles daily, leading to sharp power differences throughout the day. Only when the number of EWHs being analyzed is fairly large is the aggregated EWH power relatively smooth with distinct trends.

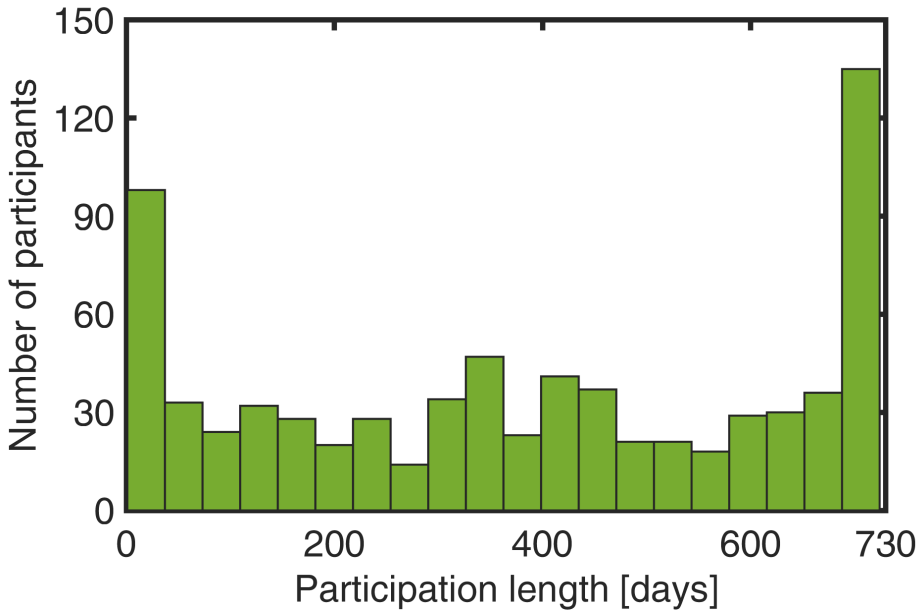

Figure 3.11: Participant engagement over the duration of the research. Reduction in the number of participants in some cases were attributed to changes in internet settings and monitoring hardware devices being disconnected

.

The experimental data was reported in Coordinated Universal Time (UTC) but the location of the EWH was not recorded. This is because all the user information had been anonymized in order to protect privacy. As the data was collected within the entire continental USA, the time zone for the experimental data is regarded as UTC-06:30, i.e., between the CST and MST.

At each minute, the aggregated EWH load was calculated by summing all the selected power together. The base power, which is used to calculate the per unit value, is defined as follows:

$$P_{base} = \frac{E \cdot N}{T}, \tag{3.13}$$

where, E is the average daily electricity usage; N, the total number of EWHs; and T, representing the number of hours to be averaged over. In this chapter, E is fixed

to 12.5kWh as the typical daily electricity usage for EWH and T is fixed to 24, for the number of hours in one day. In the case of HPWHs, E is also 12.5kWh so the per-unit load values for both EWH and HPWH are comparable. The actual energy produced by EWHs and HPWHs is assumed to be the same. For the HPWH, the COP is defined as the ratio between the power drawn out of the HPWH and the power supplied to the compressor. Due to the COP of HPWH, the electricity usage of EWH and HPWH are different.

The per unit value for the aggregated water heater load power is calculated as:

$$P_{pu}(t) = \frac{P_A(t)}{P_{base}}, \tag{3.14}$$

where P_A is the aggregated water heater power acquired from the measurements at time t.

The measured power profiles were used to develop an aggregated generic load profile to represent the typical power flow for multiple EWHs. The generic EWH load profile was defined by 8 data points for which the mathematical derivative of the load curve, i.e. ramping rate, changes drastically. The data point for hour 24 is not shown because hour 0 and hour 24 have the same value (Table 3.4). The values between those points were interpolated linearly with user defined resolution. The time step of 1-minute was used throughout this chapter if not mentioned otherwise. The generic curve captured the major characteristics of the experimental data, as the peaks, ramping rates, and the power values for different time periods were almost the same (Fig. 3.12). The aggregated EWH load curves shown in Fig. 3.12 include the per unit value and an example for 1,000 EWHs for which the base power has been

Table 3.4: The p.u. value of average EWH power

Hour	0	3	6	9	15	18	20
Power [p.u.]	0.33	0.33	1.5	1	0.75	1.25	1.25

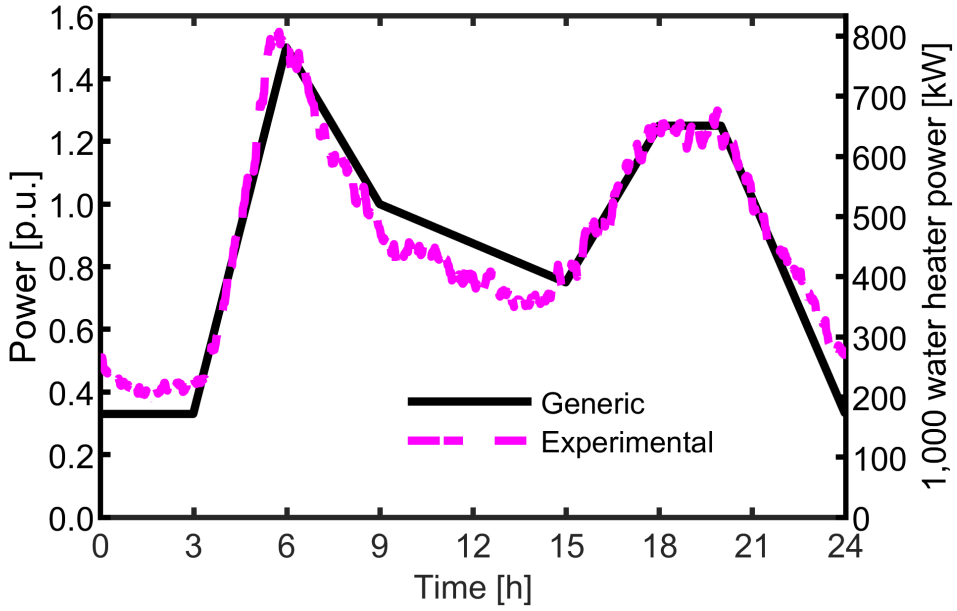

Figure 3.12: Example daily aggregated power transfer for EWH. The aggregated generic profile was developed based on data retrieved from the two-year long project.

calculated with (3.13) to be equal to 521kW.

Another experimental study, of a smaller scale with only 50 EWH, has been conducted by the researchers from the Oak Ridge National Laboratory (ORNL) [82]. The results shown in Fig. 3.13 confirm the typical timing of the morning and evening peaks, which shows the similar trend compared with the generic curve. When comparing data and considering scaling between Figs. 3.12 and 3.13, it should be kept in mind that the smaller scale study illustrates the variability due to the day of the week, which can be substantial, and also includes larger power variations possibly due to community/location specifics and the low number of EWH considered. Obtaining substantially large local data for the utility might be a challenge and the

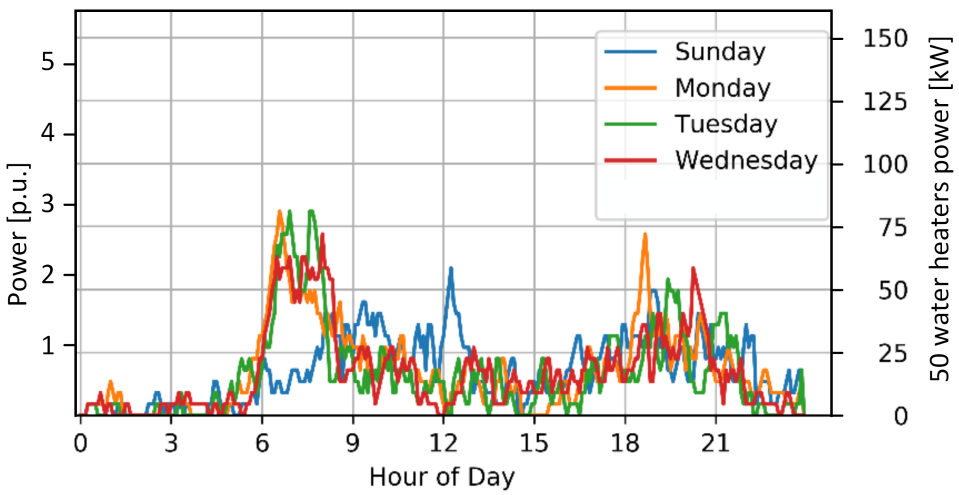

Figure 3.13: Experimental aggregated data based on a smaller scale study that included only 50 water heaters [82]. The morning and the evening peaks are approximately timed in line with expectations, as compared with the example generic curve of Fig. 3.12, and the power values illustrate the community dependent variability.

corresponding aggregated load based on the limited data might have large variation.

On the other hand, the generic curved proposed in Fig. 3.12 is artificially aggregated in time and space throughout the entire continental US, which spans four time zones, i.e., UTC-05:00 to UTC-08:00. Therefore, the aggregated load was able to represent the national trend, but needed adjustment when employed to a specific location. The learnings from the two studies can be combined with other locally based statistics to establish a specific load curve for electric power utility DR planning.

3.3.2 Large Scale Experimental Study for HPWH

The Bonneville Power Administration (BPA) has spent the recent years developing the capability to use the CTA-2045 enabled water heaters for both traditional DR and everyday applications such as renewable generation integration. The project, which delivered the experimental data used by this chapter, deployed 300 CTA-2045 enabled

HPWHs in the Pacific Northwest (PNW) over one year. The data has a resolution of 1-minute and covers January through August of 2018 [152]. The emphasis of this section has been on the modeling of HPWH not the house energy. The simulations for HPWH have been considered independent of the residential energy usage.

The data includes multiple columns, among which the `timestap`, `alias`, `curr_watts`, `curr_curtail_type` were used to generate the generic load curve for the HPWH. The `alias` records the device name and distinguishes the type of water heater. This was used in this chapter to select only the data from HPWHs. The `curr_curtail_type` records the demand control signal. In this chapter, only the days having a signal of `End Shed/Run Normal = 8` for the entire day were selected. Therefore, for the selected days, all their 1,440 records of column `curr_curtail_type` must be 8. The `timestamp` and `curr_watts` record the timestamp and the instantaneous watt reported by the water heaters. Additionally, only the business days were selected as user behavior differs on holidays and weekends.

Approximately 10,000 daily HPWH schedules were selected and each schedule had 1,440 recorded power instances. The distribution for the values of the selected instantaneous power shown in Fig. 3.14 does not include times without a power draw. When the HPWHs were On in `End Shed/Run Normal` mode all day long, the compressors were operating alone 94% of the time and, for the other 6% of the time, the resistance element was On.

The data was provided for three seasons separately, i.e., Winter: Jan-Apr, Spring: Apr-June, and Summer: June-Aug. The annual curve was calculated by using the data from all three seasons together. It is observed that, even though the peak values

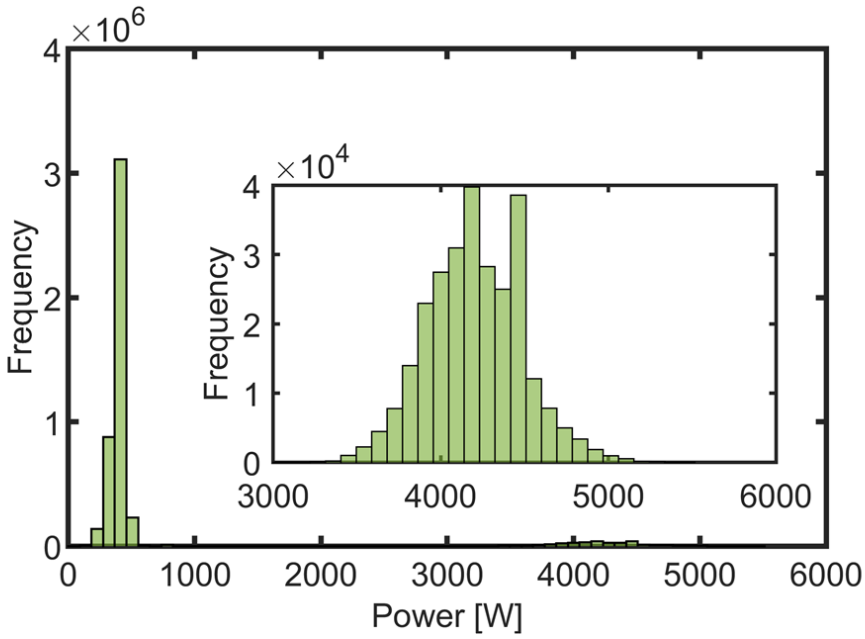

Figure 3.14: The distribution for the instances of selected power values. Two clusters stand for the compressor power only and the instances which include the resistance element, which are approximately 94% and 6%, respectively.

Table 3.5: The p.u. value of average HPWH power

Hour	0	3	5	8	15	18	21
Power [p.u.]	0.24	0.1	0.1	0.5	0.18	0.21	0.37

differ, all the daily load curves have two peaks at approximately 8am and 9pm, as shown in Fig. 3.15.

The generic HPWH load curve was created based on the annual load curve presented in Fig. 3.15 and was defined by 8 data points as in the Table 3.5. The data for hour 24 is not shown because, as at the end of the day, the value is the same as the beginning. The generic curve based on the annual data is shown in Fig. 3.16 in both per unit value and the value for 1,000 HPWH.

The experimental data and generic curves for both EWHs and HPWHs are presented together in Fig. 3.17. The peak value for EWHs is approximately 3 times

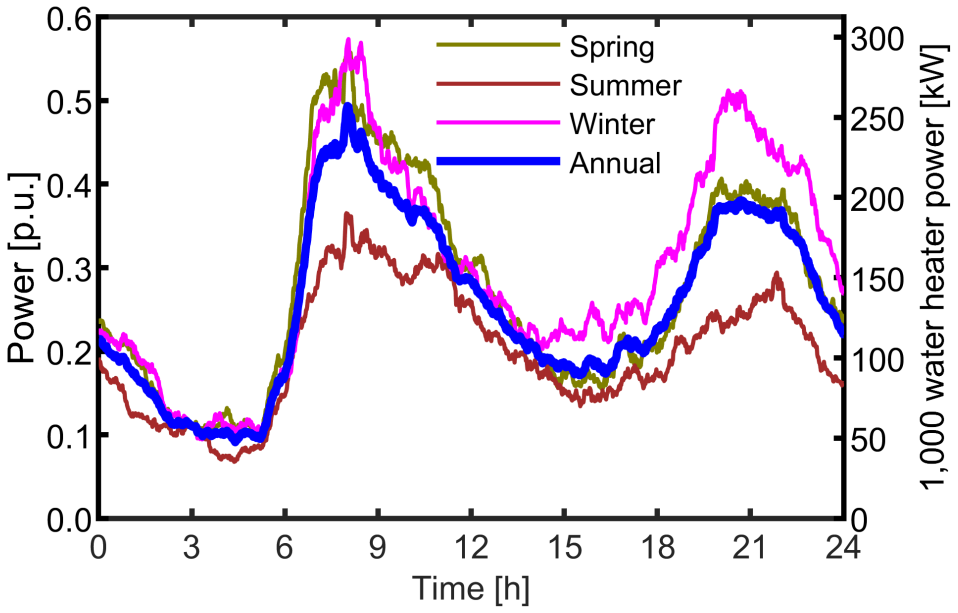

Figure 3.15: The generic power curve created based on the BPA data for Spring, Summer, and Winter for the year of 2018. The annual curve, which includes the data from the three seasons, is used to generate the generic HPWH curve.

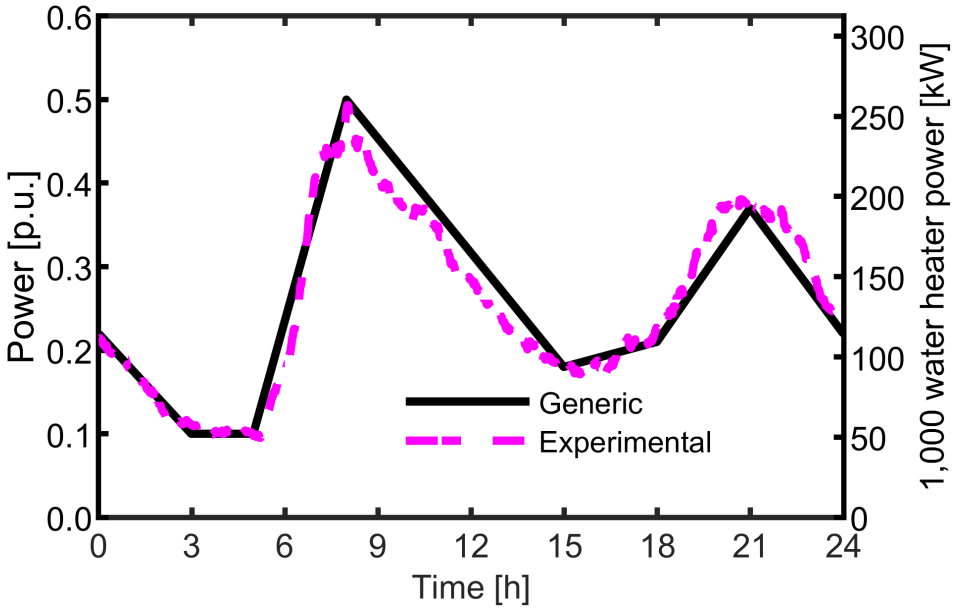

Figure 3.16: The experimental and generic curve of the daily HPWH power profile. The experimental curve is based on the same data as the annual curve shown in Fig. 3.15.

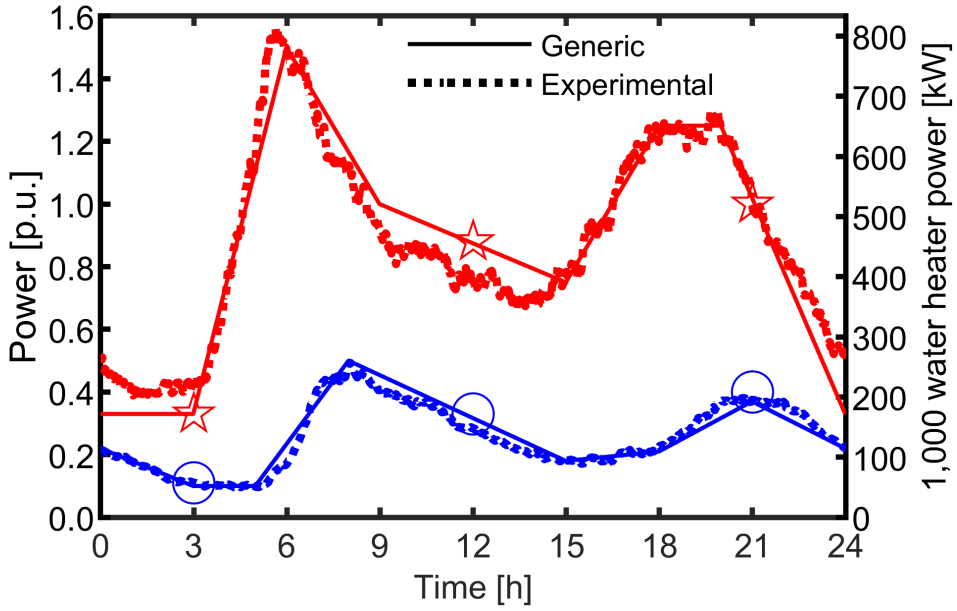

Figure 3.17: The experimental and generic curves for both EWHs (indicated with ☆) and HPWHs (indicated with ◯) in the same scale.

the peak value for HPWHs. It is observed that the peak for HPWH comes later for both morning and evening. Unless otherwise mentioned, the studies in the rest of this chapter are all based on the generic curves.

The per unit value for energy usage is deduced by integrating both side of (3.14) with respect to time:

$$\int P_{pu}(t)\mathrm{d}t = \int \frac{P_A(t)}{P_{base}}\mathrm{d}t \Rightarrow E_{pu}(t) = \frac{E_A(t)}{P_{base}}, \tag{3.15}$$

where $E_A(t)$ is the measured aggregated energy usage. In a per unit system, the base and the actual value have the same unit. Based on (3.15), the base value for the aggregated energy (MWh) has the same magnitude as P_{base} ($|E_{base}| = |P_{base}|$). The cumulative electricity usage based on the generic load curves for EWH and HPWH are shown in Fig. 3.18. At the end of the day, the aggregated electricity usage for EWH and HPWH are 21.4 p.u. and 6.3 p.u., respectively. Given 1,000 water heaters, the

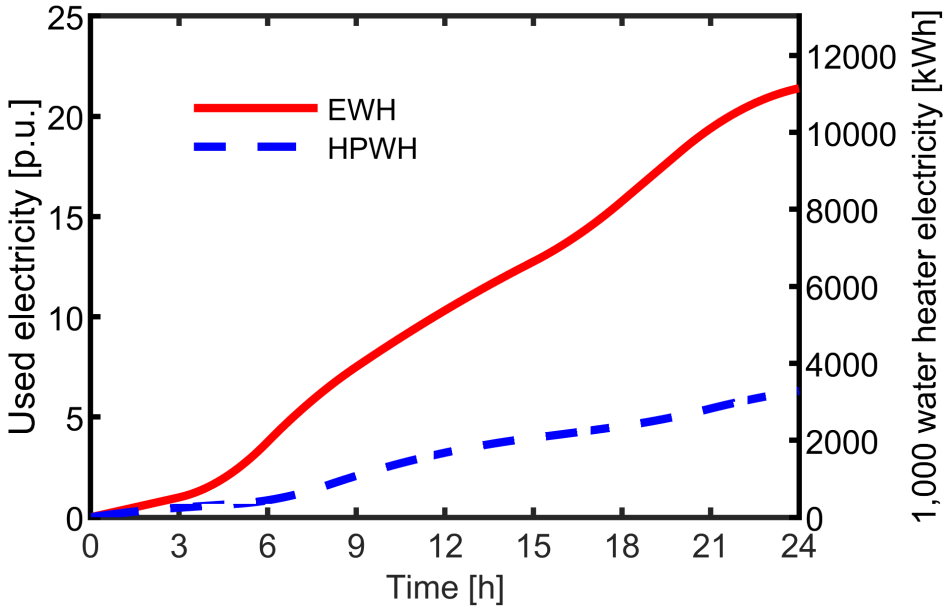

Figure 3.18: The accumulated electricity usage for the EWH and HPWH based on the generic load curves. The daily electricity usage for EWH and HPWH are 21.4 p.u. and 6.3 p.u., respectively.

daily electricity usage for an all EWH community and an all HPWH community are 11,146kWh and 3,281kWh, respectively. For a community changing from all EWH to all HPWH, the daily saving on electricity is approximately 70%.

3.3.3 Equivalent Model and Digital Twin at Aggregated Level

One simplification and two assumptions have been made in this chapter to facilitate the study. The water temperature in the tank was simplified to be uniform instead of stratified. Other models, including the "WaterHeater:Mixed" in EnergPlus [153] and the model used for International Energy Conservation Code (IECC) by the DOE and Pacific Northwest National Laboratory (PNNL) [154] all consider uniform temperature tanks appropriate. The models developed by Ecotope [155] consider

vertical stratification of the water tanks and have accurate results at the cost of performance. In this chapter, the uniform temperature in the water tank was considered as it is sufficient for the evaluation of the energy balance in the water tank.

The first assumption is that Coefficient Of Performance (COP) of the HPWH was constant for the calculation of the daily profile. COP will not change drastically when the ambient environment remains stable, which is the common case for most of residential users. The second assumption is that the average water temperature for all the EWHs whose power was used to generate the generic curve (Fig. 3.12) was constant when there was no DR control. This assumption was based on basic aggregation, that for a given point in time, some water heaters have high temperature while others have low. Based on these assumptions, the hot water usage and the temperature in the tank for the water heaters can be calculated.

An equivalent thermal model is used to calculate the daily hot water usage based on the generic load. Typically, the water temperature in the tank is stratified. In this chapter, the average water temperature is considered sufficient for the estimation of the energy storage capacity of the water heater. Therefore, the thermodynamic of the water heater is represented in a single-nodal model:

$$C\frac{\mathrm{d}\theta_T(t)}{\mathrm{d}t} = S(t)P_H(t) - \frac{1}{R}[\theta_T(t) - \theta_A] - \rho c_p W(t)\,[\theta_T(t) - \theta_{W,C}]\,. \tag{3.16}$$

It is assumed the efficiency of the resistive element is 100% for heating. The three terms on the RHS consider the effect of the input electric power, the standby heat loss, and the hot water draw activities, respectively. C and $S(t)$ are the equivalent

thermal capacitance and On/Off status, defined respectively, as:

$$C = V \cdot \rho \cdot c_p. \tag{3.17}$$

$$S(t) = \begin{cases} 0, & \text{if } S(t-1) = 1 \ \& \ \theta_T(t) \geq \theta_H(t) \\ 1, & \text{if } S(t-1) = 0 \ \& \ \theta_T(t) \leq \theta_L(t) \\ S(t-1), & \text{otherwise,} \end{cases} \tag{3.18}$$

where θ_L and θ_H are the lower and upper band of the water tank temperature. The definitions of other parameters are listed in Table 3.2. It is worth noting that the water heater heating rate P_H, the water temperature in the tank θ_T and the hot water draw W have only their units listed in the table. Also important is that the water heater heating rate P_H for the HPWH should consider its COP.

The proposed single-nodal model is scalable with its parameters represented in the per unit system. Dividing both sides of (3.16) by $P_{base}|_{N=1}$ yields:

$$\frac{C}{P_{base}|_{N=1}} \frac{\mathrm{d}\theta_T(t)}{\mathrm{d}t} = S(t) \frac{P_H(t)}{P_{base}|_{N=1}} - \frac{1}{RP_{base}|_{N=1}} [\theta_T(t) - \theta_A] - \rho c_p \frac{W(t)}{P_{base}|_{N=1}} [\theta_T(t) - \theta_{W,C}]. \tag{3.19}$$

When there is only one water heater, the aggregated power is the power of the single water heater:

$$P_A(t) = P_H(t), \tag{3.20}$$

and the per unit value for the aggregated water heater power in (3.14) becomes:

$$P_{pu} = \frac{P_H(t)}{P_{base}|_{N=1}}, \tag{3.21}$$

as $P_{base}|_{N=1} = \frac{E}{T}$, (3.19) is rewritten as:

$$\frac{CT}{E}\frac{\mathrm{d}\theta_T(t)}{\mathrm{d}t} = S(t)P_{pu}(t) - \frac{1}{RE/T}[\theta_T(t) - \theta_A] - \rho c_p \frac{W(t)T}{E}[\theta_T(t) - \theta_{W,C}]. \tag{3.22}$$

Defining the per unit values as: $C_{pu} = \left|\frac{C \cdot T}{E}\right|, R_{pu} = \left|\frac{R \cdot E}{T}\right|, W_{pu} = \left|\frac{W \cdot T}{E}\right|$, the heat transfer function of a water heater is represented as:

$$C_{pu}\frac{\mathrm{d}\theta_T(t)}{\mathrm{d}t} = S(t)P_{pu}(t) - \frac{1}{R_{pu}}[\theta_T(t) - \theta_A] - \rho c_p W_{pu}(t)[\theta_T(t) - \theta_{W,C}]. \tag{3.23}$$

The heat transfer function (3.16) holds for single water heater, therefore, it holds for the average values of $C, P_H(t), R$, and $W(t)$:

$$\overline{C}\frac{\mathrm{d}\theta_T(t)}{\mathrm{d}t} = S(t)\overline{P_H}(t) - \frac{1}{\overline{R}}[\theta_T(t) - \theta_A] - \rho c_p \overline{W}(t)[\theta_T(t) - \theta_{W,C}]. \tag{3.24}$$

Rewriting (3.24) as:

$$C_{pu}\frac{C_{base}}{N}\frac{\mathrm{d}\theta_T(t)}{\mathrm{d}t} = S(t)P_{pu}(t)\frac{P_{base}}{N} - \frac{1}{R_{pu}\frac{R_{base}}{N}}[\theta_T(t) - \theta_A] - \rho c_p W_{pu}(t)\frac{W_{base}}{N}[\theta_T(t) - \theta_{W,C}]. \tag{3.25}$$

Compared with (3.23), the equation (3.25) holds when $\left|\frac{C_{base}}{N}\right| = \left|\frac{P_{base}}{N}\right| = \left|\frac{1}{R_{base}/N}\right| = \left|\frac{W_{base}}{N}\right|$. Therefore, the base values are defined as: $|C_{base}| = |W_{base}| = |P_{base}|$, $|R_{base}| = |N^2/P_{base}|$.

In the study, it is assumed that the average temperature of all the EWHs was constant at $\theta_T(t) = 125F$ due to their fast recovery rate relative to HPWHs. Therefore, (3.23) can be re-written to calculate the per unit hot water usage:

$$W_{pu}(t) = \frac{S(t)P_{pu}(t) - \frac{1}{R_{pu}}[\theta_T(t) - \theta_A]}{\rho c_p [\theta_T(t) - \theta_{W,C}]}. \tag{3.26}$$

The generic load for EWHs is used to calculate the aggregated hot water draw, i.e., the item "$S(t)P_{pu}(t)$" is replaced by the value of the generic load of the EWH at each time point. The calculated generic hot water flow shown in Fig. 3.19 stands for the representative user behavior and does not change when the water heater is HPWH or the DR is implemented. In this study, the hot water flow has the time resolution of 1-minute and is presented in per unit value as well as gallon per minute (GPM). The daily hot water draw is calculated by integrating the hot water flow with respect to minute, and the results, i.e., the area between x-axis and the curve in Fig. 3.19 are 112 p.u., and 58,507 gallons for the 1,000 water heater example.

The generic hot water draw and the generic load curves are used to calculate the average tank temperature using (3.23). As shown in Fig. 3.20, the average tank temperature for EWH is constant as expected. The variation in the average temperature for HPWH reflects its latent nature.

The equivalent water heater model may be thought of as a digital twin for three reasons. First, all the I/O can be real-time if the data is available. Second, the model can stream data complying to the communication protocol approved by CTA-2045 standard. Third, the model is exchangeable with the hardware in a co-simulation circumstance where the EWH is involved as one of the smart components. Example

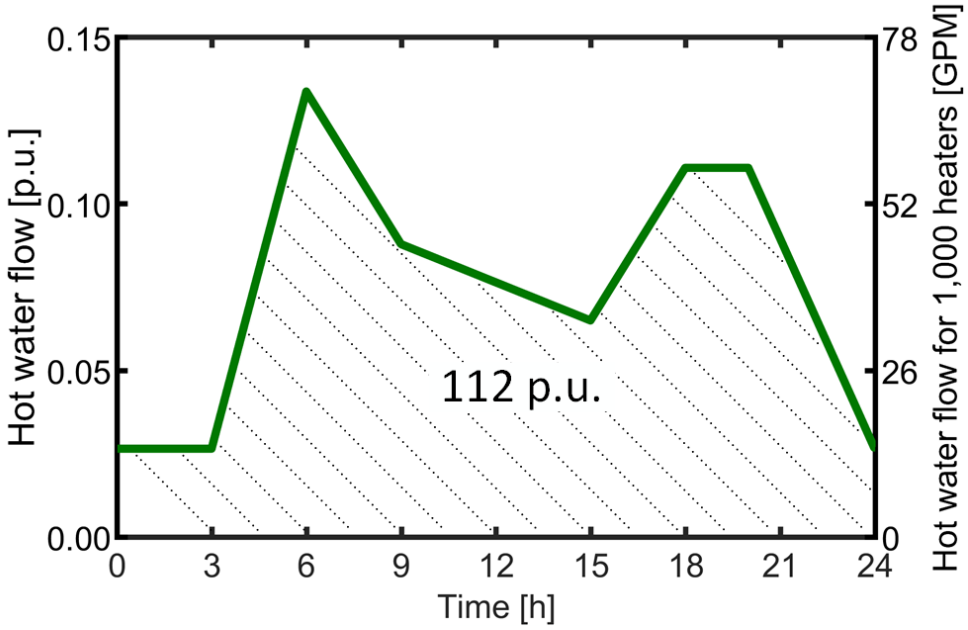

Figure 3.19: The calculated aggregated daily hot water flow. The total daily hot water usage was 112 p.u. Given 1,000 water heaters, total daily hot water usage was 58,507 gallons.

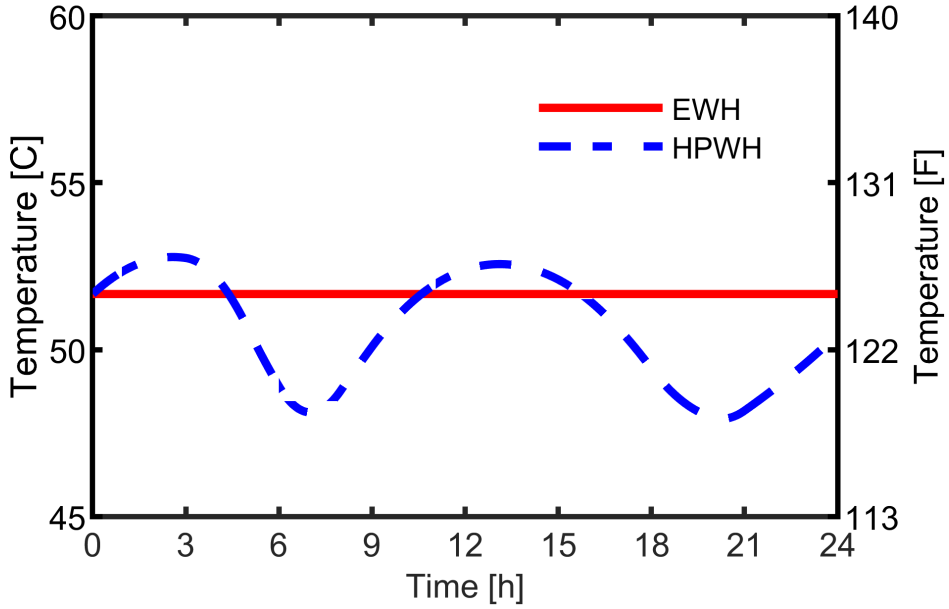

Figure 3.20: The average temperature for EWH and HPWH, which were calculated using the same hot water flow. The variation in average temperature for HPWH shows the deferring nature of the compressor.

Table 3.6: Event type and duration

Event	Duration
Shed	[7:00,10:00) ∪ [17:00,19:00)
Load up	[6:00,7:00) ∪ [11:00,16:00)
Normal operation	Other time

applications can be found in the Distributed Energy Resources (DER) integration testbed developed by EPRI [156]. This chapter focuses on the computational parts of the EWH model while the data packing and communication will be introduced in future work.

3.4 Optimal DR Case Study on a Modified IEEE 123-Bus System Co-simulated with Individual EWHs

3.4.1 Electric Water Heater Operation

In this study, example DR control was applied to all the EWHs in the distribution system introduced in Fig. 2.6. All the 353 EWHs in the simulated distribution system received and reacted to the same control signals listed in Table 3.6. A sequential control method, which spreads out the turning On operation of EWHs, might reduce the peak caused by rebound effect [96]. For utilities serving large areas, the simulated distribution system is one node at the transmission system, and the simulated EWHs could be controlled as one batch.

The initial water temperature in the tanks for all simulated EWHs were evenly distributed between 115F and 135F, noted as $\mathcal{U}(115F, 135F)$. The initial energy take

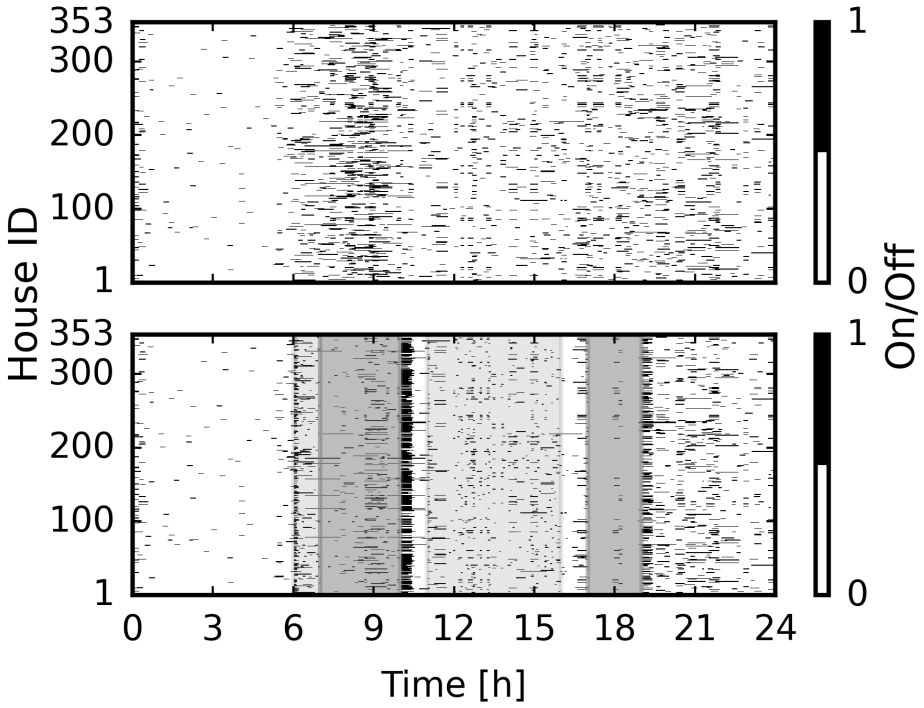

Figure 3.21: Working status of the EWHs without control (top) and with CTA-2045 control (bottom). The Shed command in the morning and evening postpone most of the EWHs to be On.

for all simulated EWHs were evenly distributed between 0 and 1000Wh, noted as $\mathcal{U}(0, 1000Wh)$. Two shed event commands were issued during 7:00–10:00 and 17:00–19:00 to reduce the peak power. The first load up event starting from 6:00 was to increase the water temperature for the coming shed event. The other load up event during 11:00–16:00 was to absorb the potential surplus PV generation from other nodes of the entire transmission power system.

The simulation results of On/Off status for all 353 EWHs demonstrate the antedated and postponed peak under CTA-2045 control (Fig. 3.21). The shadowing parts for the controlled case (bottom) indicate the duration for when the DR control signals were implemented. Many EWHs were turned On when the load up events

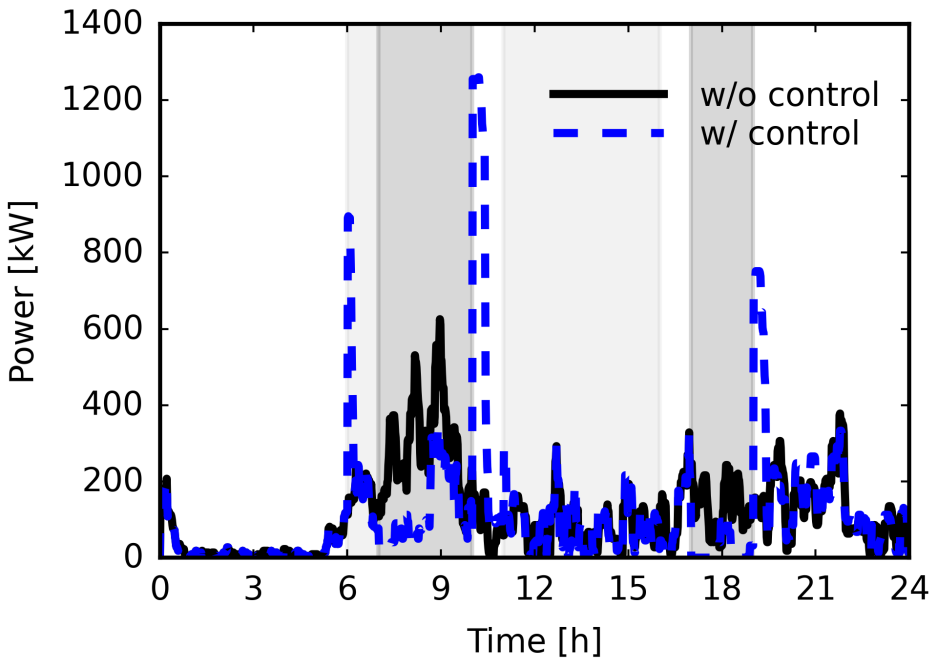

Figure 3.22: Aggregated power for all the simulated EWHs. The shed command postponed the heating power and reduced the peak power during the DR control period in the morning and evening, but also caused the rebound afterwards.

started at 6:00 and 11:00.

The shed event postponed the time for most EWHs to be turned On, as observed at 10:00 and 19:00 when the shed events ended. User comfort was maintained during the shed event as some EWHs were turned On when their energy take values were higher than the maximum level. The rebound effect was observed at approximately 9:00 and 18:00.

The impacts of DR events are demonstrated by the aggregated power for all the simulated EWHs (Fig. 3.22). The peak at 6:00 was caused by the load up event. The aggregated power was reduced from 7:00 to approximately 9:00 because of the shed event. The following rebound effect at 9:00 was caused by temperature recovering to maintain user comfort.

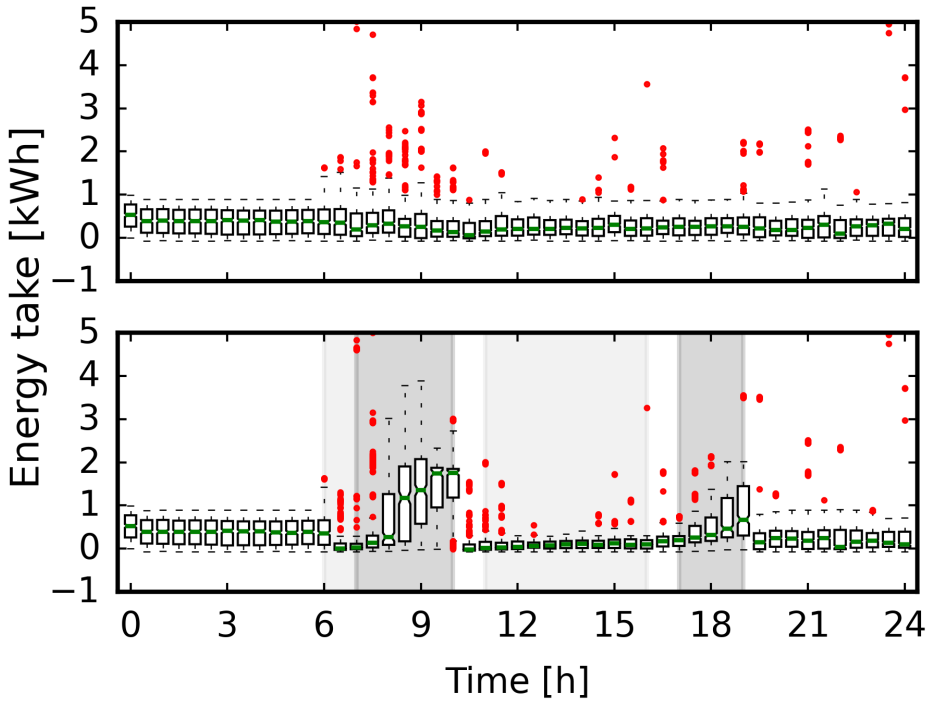

Figure 3.23: Energy take of the EWHs without control (top) and with CTA-2045 control. The shed command allowed more energy take while the load up did less.

When the shed event ended at 10:00, most EWHs were turned On which resulted in another peak. This was due to the insignificant effect of the early load up event that started at 11:00 to the aggregated power curve. The shed event in the evening reduced the power and also led to a peak afterwards. It is observed by comparing the two shed events that the longer the event, the larger the rebound peak afterwards.

The summary for the energy take of all EWHs shows the difference between normal operation and DR events (Fig. 3.23). For the case without DR (top), most of the EWHs had the energy take value between [0,1000Wh]. The outliers, which are represented by red dots, were caused by high hot water draw. Most of the outliers appeared in the morning and reflected the high water usage for residences at that time.

During the two load up events (Fig. 3.23 (bottom)), the boxes for energy take were shorter as the maximum energy take level was smaller (Table 3.3). During the two shed events, higher energy take values were allowed for all simulated EWHs. The minimum energy take values for shed events stayed at 0 instead of 1,800Wh as stated in Table 3.3 because some EWHs did not have hot water draw. Therefore, even when the minimum energy take level was high, some EWHs experienced an energy take of approximately 0 until there was hot water usage. This can be observed from 8:00 to 9:00 as the boxes were shifting above.

Starting from 9:00, the energy take for some EHWs were too high, and these EWHs were turned On to maintain user comfort. Therefore, at 9:30, the upper whisker was lower than that of 9:00. The 25% percentile and median at 9:30 were higher than those of 9:00, indicating that more EWHs had higher energy take. At 10:00, most EWHs had high energy take and the box moved upward, making the 0 energy take value an outlier. If the shed event had lasted longer, the box would keep moving upward and have the minimum and maximum energy take values as stated in Table 3.3. The shed event in the evening lasted for 2 hours and the forms of boxes behaved similarly to the first 2 hours of the morning shed event (7:00-9:00).

The aggregated energy take rose from approximately 20kWh to 510kWh from 7:00 to 9:00 and then remained at around 500kWh until the shed event ended at 10:00 (Fig. 3.24). The load up and shed events in the morning together postponed electricity usage of approximately 490kWh during the peak time. Theoretically, each EWH could have 0 energy take when the shed event starts and have 2,250Wh energy take when the shed event ends. Practically, the hot water draws were not identical

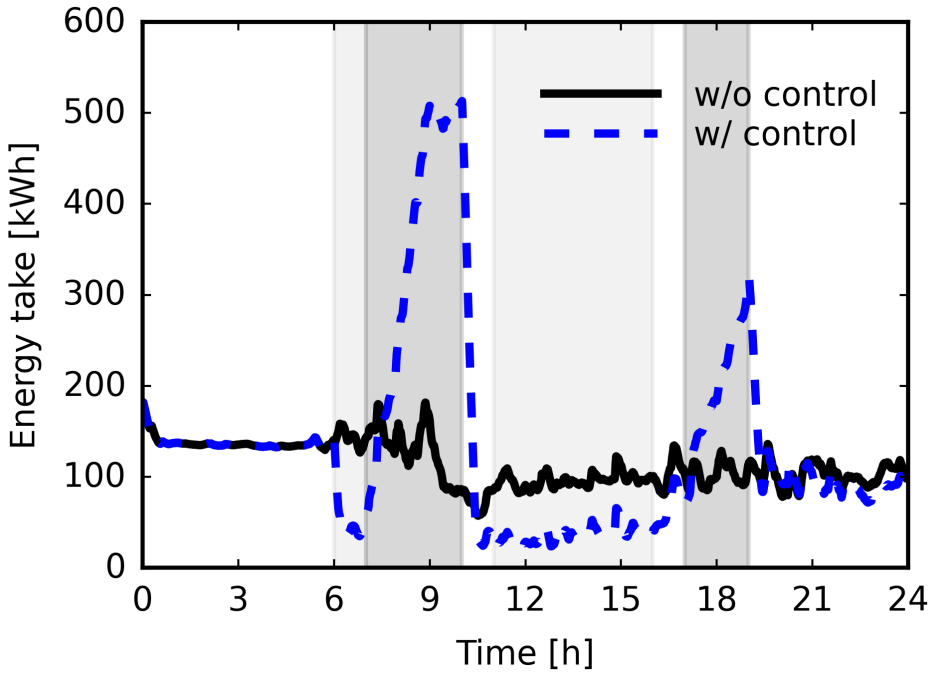

Figure 3.24: Aggregated energy take for all the simulated EWHs. The shed command in the morning and evening resulted in high energy take. When the load up command was implemented in the afternoon, energy take was kept at a low level.

and, therefore, the energy take values for EWHs could be different at a given time step. The simulated 353 EWHs were not able to have the aggregated energy take as 794kWh because, at any given time step, there were always some EWHs that did not reach the energy take of 2,250Wh and others that had more than 2,250kWh which were turned On. In this study, the average energy take an EWH can contribute was 1,388Wh maximum.

The load up event occurred in the afternoon and a lower aggregated energy take was observed with control. The load up command could be issued to the communities where the load PV generation is high. The shed event in the evening lasted for a short period of time during which the aggregated energy take increased up to approximately 310kWh. For both shed events in the morning and evening, the energy take decreased

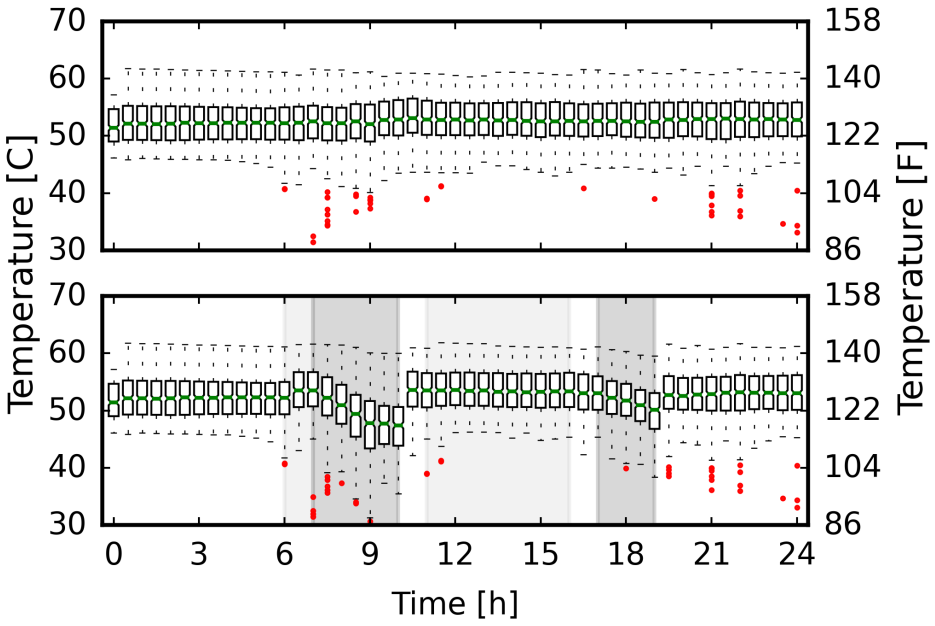

Figure 3.25: Water temperature in the tank for the EWHs without control (top) and with CTA-2045 control (bottom). The temperature was reduced during the shed event and was maintained high during the load up event in the afternoon.

very quickly after the DR event.

The water temperature in the tank for all EWHs was kept relatively stable during the normal operation event (Fig. 3.25 (top)). The minimum temperature decreased, and outliers with low temperature appeared from 7:00 to 9:00 due to high hot water usages. The two shed events resulted in lower water temperature. The water temperature increased significantly during the first load up event. The water temperatures for all EWHs were increased by the load up event in the afternoon, which can be observed clearly from the results at the aggregated level (Fig. 3.26).

In this study, user comfort was considered violated when the energy take value was more than 2,300Wh. The maximum energy take levels during shed event was 2,250Wh. The EWHs hvae 50 gallons, and the extra 50Wh allowed approximately

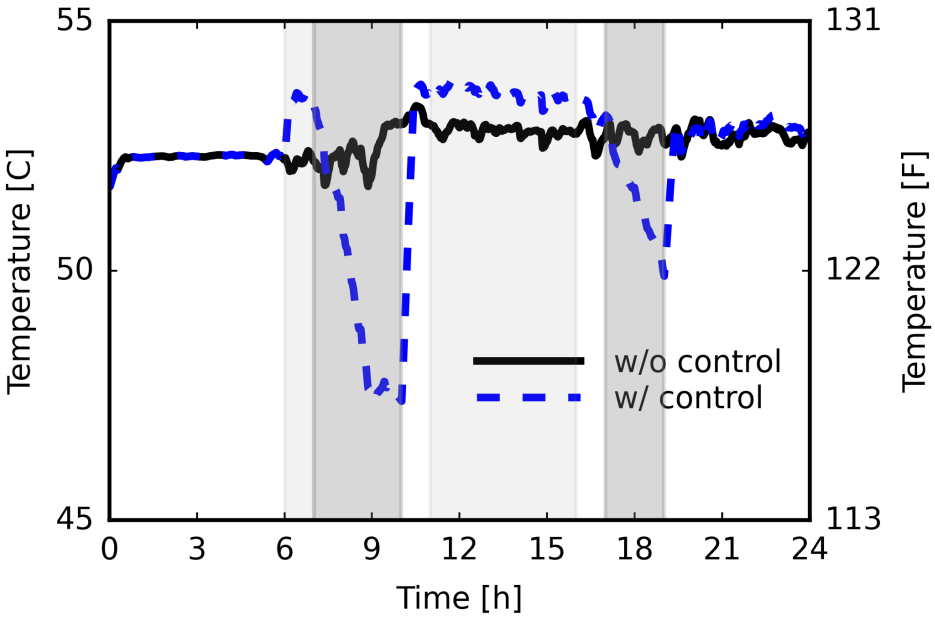

Figure 3.26: Average tank temperature for all simulated EWHs.

0.4F lower than the minimum user comfort value. For the case without DR response, 96 EWH had the violation for at least 1 minute, and, with DR control, the number was 171 (Fig. 3.27).

Further insight revealed that most EWHs had short periods of violation for the without control case, e.g., 72 EWHs violated for less than 15 minutes. With the DR control, 51 EWHs had violation minutes of less than 5. The DR control reduced the violation time for some EWHs because of the preheating process under the load up event starting from 6:00. The DR control also caused more EWHs to have more violation minutes due to the shed event. The total violation minutes for all the EWHs was calculated by adding up the violation minutes for each EWH. In total, the case without control had 1,500 violation minutes, and the case with control had 4,033. Given a total number of 353, each EWH experienced around 7 minutes of temperature that was lower than the minimum boundary on average.

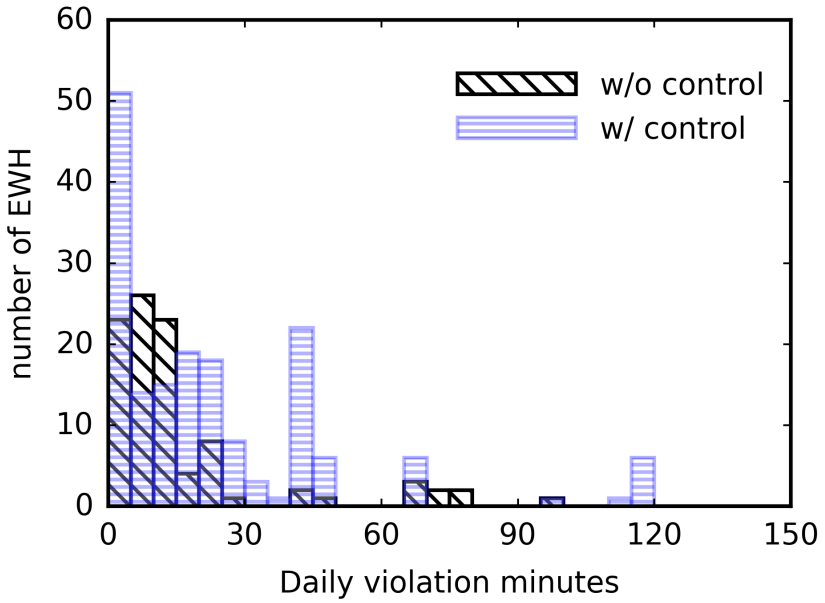

Figure 3.27: Summary of daily violation minutes for each EWH. Three EWHs had daily violation minutes with [40,50) without control, and this number was 18 with control. With DR control, the number of EWHs with more daily violation minutes increased.

3.4.2 Distribution Power System Operation

The total power demand for the simulated IEEE 123-bus was presented in Fig. 3.28. The results were acquired with the OpenDSS command `circuit.TotalPower`, and only the active power (kW) is presented. Peaks were observed at 6:00 when the load up event occurred and at 10:00 and 19:00 when the shed event ended, as has been explained in the previous section (Fig. 3.22). The peak power from 7:00–10:00 was reduced from 983kW to 706kW, a reduction of 28%.

The combined use of OpenDSS commands of `circuit.ActiveBus.puVmagAngle`, `circuit.SetActiveBus()`, and `circuit.AllBusNames` and returned 278 voltage values. If a bus has three phases, the voltages of Φ-1, Φ-2, and Φ-3 were recorded separately. The voltage for all the buses are presented in Fig. 3.29. All the voltage values

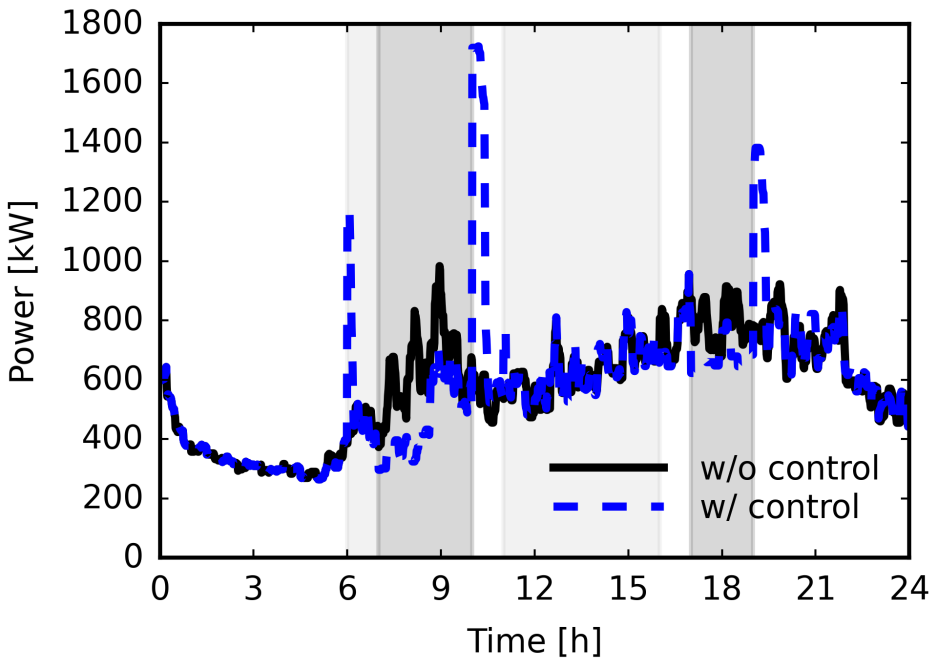

Figure 3.28: The aggregated residential load for all houses. The shed command postponed the peak power in the morning and evening for this distribution system.

were within the tolerance of 1±0.05 p.u., although large variations were observed at 6:00, 10:00, and 19:00.

For most of the cases, many of the bus voltages were higher than 1 p.u., as the simulated total residential loads were smaller than the spot loads in the original IEEE 123-bus cases. For example, node 2 had an original spot load of 20kW but was replaced by 2 residences, which could not reach such high power demand. Therefore, the voltage for the entire simulated power system was more than 1 p.u. for most of the time.

Bus voltages for selected hours were presented in Fig. 3.30 to show the impact of DR controls. The samples with the same marks for both cases were taken from Fig. 3.30. When the load up event occurred at 6:00, the voltage for most buses dropped as

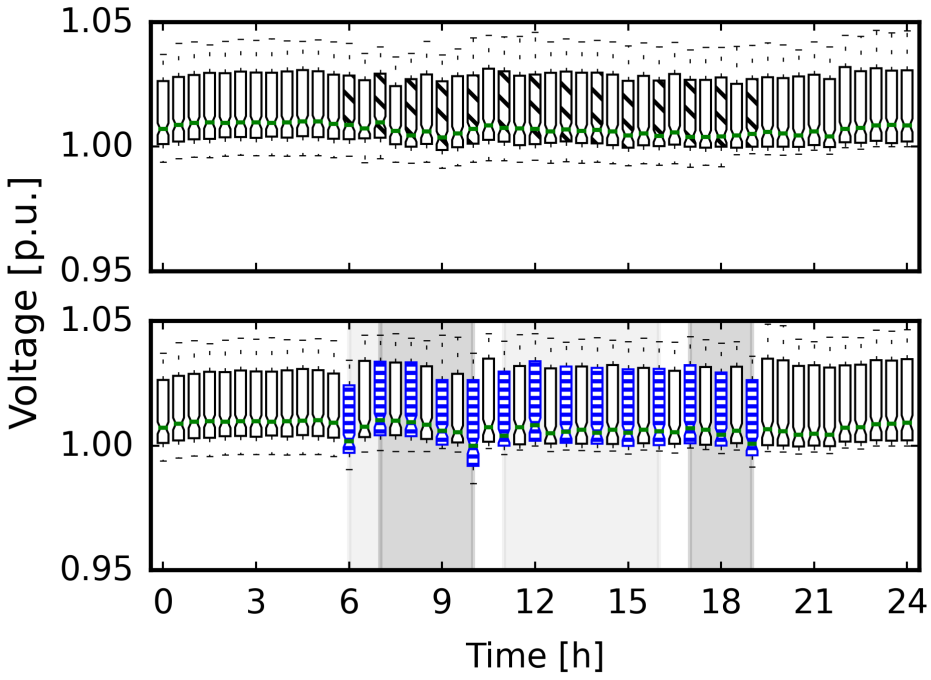

Figure 3.29: The voltages for all buses in the IEEE 123-bus feeder. The boxes during the DR period are marked and compared side-to-side.

power demand at most buses went high. Both the minimum, 25% percentile, median, 75% percentile, and maximum values for the with control case were lower.

The shed event occurred at 7:00, and the bus voltage went higher as power demand reduced. At 9:00, the 75% percentile values were lower, indicating the rebound for some EWHs, which were also observed in Figs. 3.21 and 3.22. The rebound effect was strong at 10:00 when the shed event ended and large power demand from EWHs brought the voltage down.

During the load up event starting at 11:00, most of the buses had lower voltages. The lower whisker was higher than the without control case due to the rebound effect at 10:00, which prevented some EWHs to be turned On at 11:00. The rebound effect at 10:00 and load event at 11:00 antedated the water heating process of most EWHs.

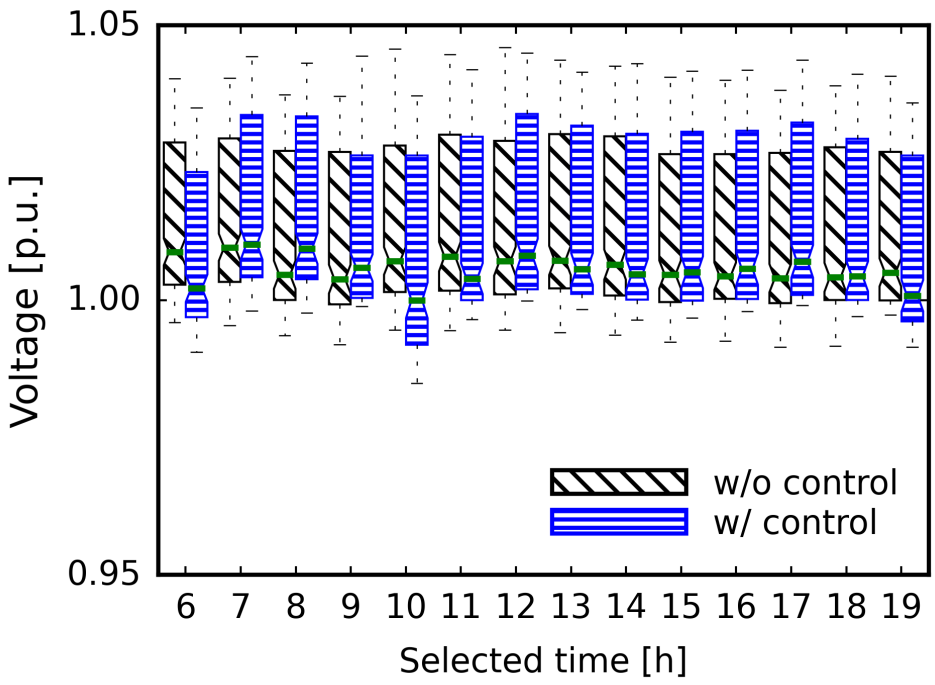

Figure 3.30: The side-to-side comparison of bus voltages with and without DR control. All the bus voltages were kept within the 5% tolerance during the DR events.

Therefore, at 12:00, less EWHs were On and the voltages on buses went higher with DR control. A similar cycle was observed at 13:00, 14:00 (antedated operation) and 15:00 (less EWHs were On) during the load up event. At 13:00 and 14:00, the median of voltages were lower, indicating more EWHs were On.

The voltages increased in general during the shed event in the evening from 17:00. Also observed is the rebound effect at 19:00 when the shed event ended. The DR controls shown above caused the violation of the voltages for all buses within the ±0.05p.u. tolerance.

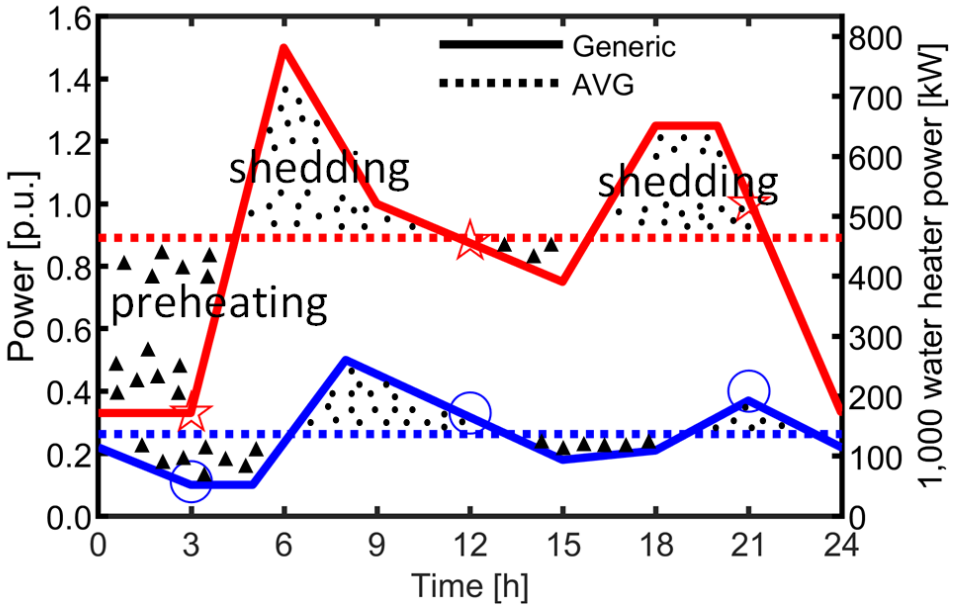

Figure 3.31: The illustration for shifting the water heater load to operate on the average power. The COP = 3.4 is calculated based on of the two average powers. With the reference to the average power, the EWH and HPWH could shift approximately 14% and 17% of their corresponding daily electricity usage, respectively.

3.5 Optimal DR Studies at Aggregated Level

3.5.1 Constant Power Operation Using Load Shifting

In the ideal case, the aggregated water heater loads can be kept constant by shifting the peaks, as illustrated in Fig. 3.31. The electricity used at peak load period, which is above the average power and marked with "•" can be shifted to the time when the power is low, as the areas marked with "▲". In this study, for the EWH, 3.1 p.u. of energy, which was 14% of daily electricity usage, could be shifted with the reference to the average power. For HPWH, the numbers are 1.1 p.u. and 17%.

By preheating and shedding, both EWH and HPWH can work on the constant powers, which are the average powers. It is assumed that both EWH and HPWH have

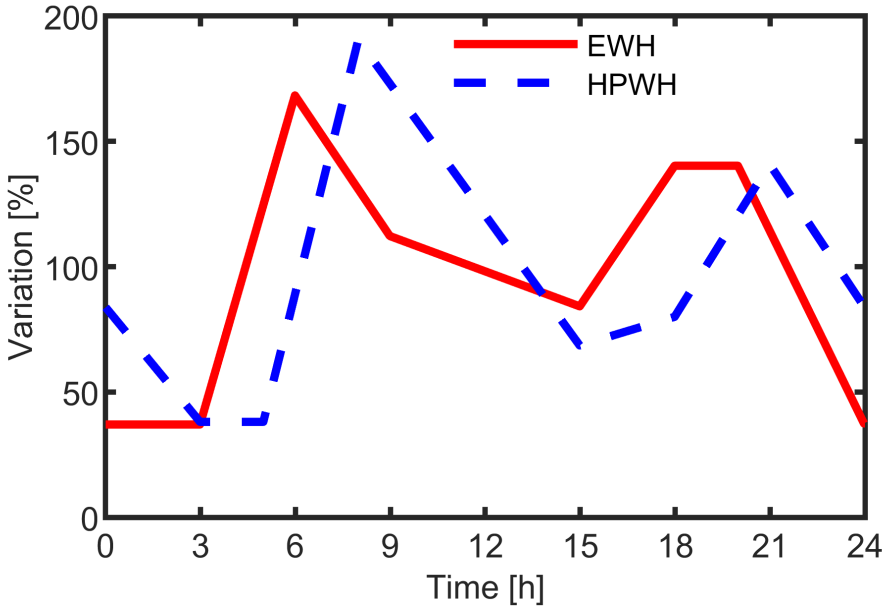

Figure 3.32: The relative values of EWH and HPWH generic load power compared with their corresponding average value. The HPWH has larger variation.

the same amount of input energy for water heating. Therefore, the portion between the two average powers is regarded as the COP for the aggregated HPWH, which is 3.4.

The absolute power of the aggregated HPWHs is lower in general when the numbers of EWHs and HPWHs are the same. However, further inspection reveals that the power profile of HPWHs has a larger variation with the reference to the average power (Fig. 3.32). In communities where HPWHs are widely installed, shifting the water heater loads can reduce the peak power demand significantly.

The water heater digital twins were used to calculate the average water temperature in the tank and monitor the user comfort. The hot water flow remains unchanged as the user behavior will not change. The preheating and shedding procedures change the hot water temperature in the tank. When the aggregated water heater powers

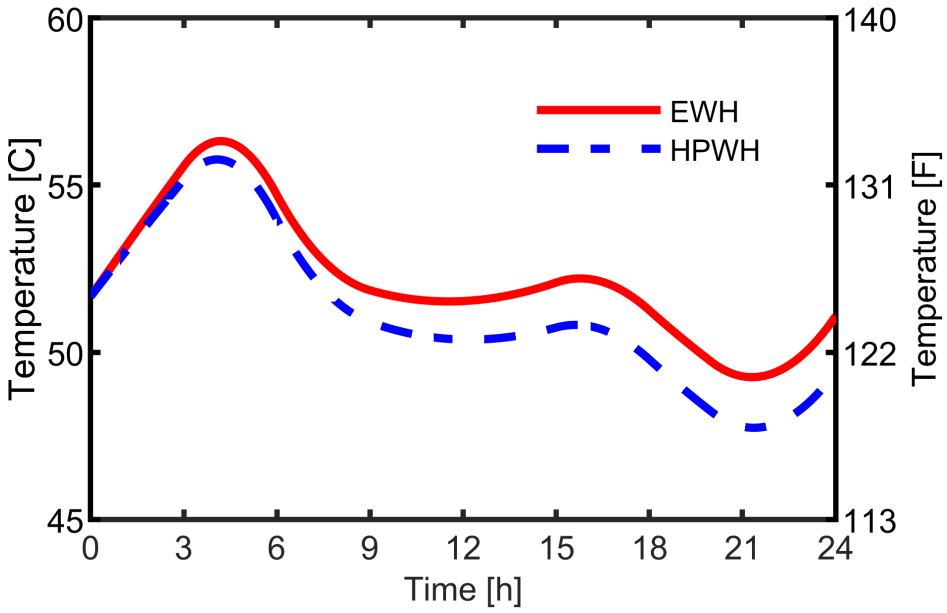

Figure 3.33: The average temperature for EWH and HPWH, which were calculated using the same water draw and the corresponding constant power. The input energy for EWH and HPWH were the same all the time. After the starting point, the HPWH always had lower tank temperature because of higher heat loss.

were constant, the average water temperatures in the tank were calculated according to (3.23) and presented in Fig. 3.33. For both EWHs and HPWHs, the tank temperatures were above the minimum required 115F when the aggregated heating power was constant. Due to the COP, the input energy for heating the water were the same for both EWH and HPWH at any moment even the HPWH used less electricity. The average tank temperature for HPWH was always lower because of higher standby losses to ambient. It is worth noting that even the HPWHs have higher standby losses to ambient, their overall efficiency is much higher than that of the EHWs due to the COP.

Measuring the temperature in the water tank requires sophisticated techniques as water with different temperature is stratified and is not mixed evenly. Water heaters

that are CTA-2045 ready can monitor the devices with the readable quantities related to energy. According to the Energy Star specification, the "energy content of the stored water" for water heater, E_W, is calculated as (3.2). The energy take between two time points is calculated as (3.4). In this chapter, the energy take at one time point was defined as the difference between the "energy content of the stored water" in that time point and that of the zero (0) time point.

The energy take for EWHs and HPWHs under constant power is shown in Fig. 3.34. The negative values in the early morning indicate the preheating procedure, during which energy was put into the water tank instead of being taken out. The energy take for HPWHs was higher due to higher heat loss. Because of the COP, the corresponding electricity for HPWHs had a much lower value, as presented in Fig. 3.34.

3.5.2 Load Shifting for Morning and Evening Peaks

The objective of DR is to shed the EWH load at critical time, and recover during the midday, as follows:

$$P_D(t) = \begin{cases} P_T, & \text{if } t \in T_D \\ P_O(t) + P_R(t), & \text{if } t \in T_R, \end{cases} \tag{3.27}$$

where P_D is the aggregated EWH load with DR; P_T, the target aggregated power; P_O, the original aggregated EWH load without DR; P_R, the shifted power; T_D, the set of time when DR is required; T_R, the set of time when the power is shifted to.

CTA-2045 provides energy take as an alternative to temperature control. The most useful value, i.e., the amount of energy that can be stored, is provided to the

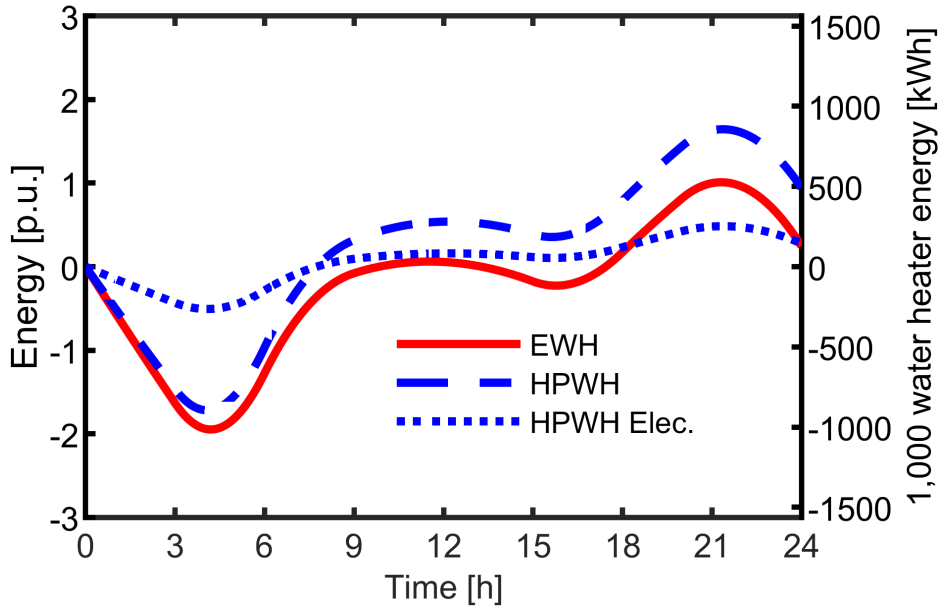

Figure 3.34: The energy take for EWHs and HPWHs for the same water draw and the corresponding average power. The energy take for HPWHs was more than that of EWHs when they had the same amount of input energy due to higher heat loss. The HPWHs use less electricity to heat the water because of their COP.

utility, and details of temperature control can be avoided. Adjusting the temperature bounds of the water heater can maximize the energy storage capability. However, for the concerns regarding safety and user comfort, the residences are not encouraged to change the set points, which are defined by the manufacturers with specific knowledge of tank geometry and sensor readings [67]. The case studies in this chapter represent the utility-controlled DR load type, instead of consumer-incentive DR control. Similar to industrial shedding, an extreme scenario was carried in this chapter to evaluate the potential of energy storage capacity of EWHs and HPWHs.

In this study, the generalized characteristics of residential PV was considered and the EWH and HPWH reserved the energy storage capacity for the afternoon. The aggregated power for an example DR with $T_D = [5:30, 7:00] \bigcup [18:00, 20:00]$,

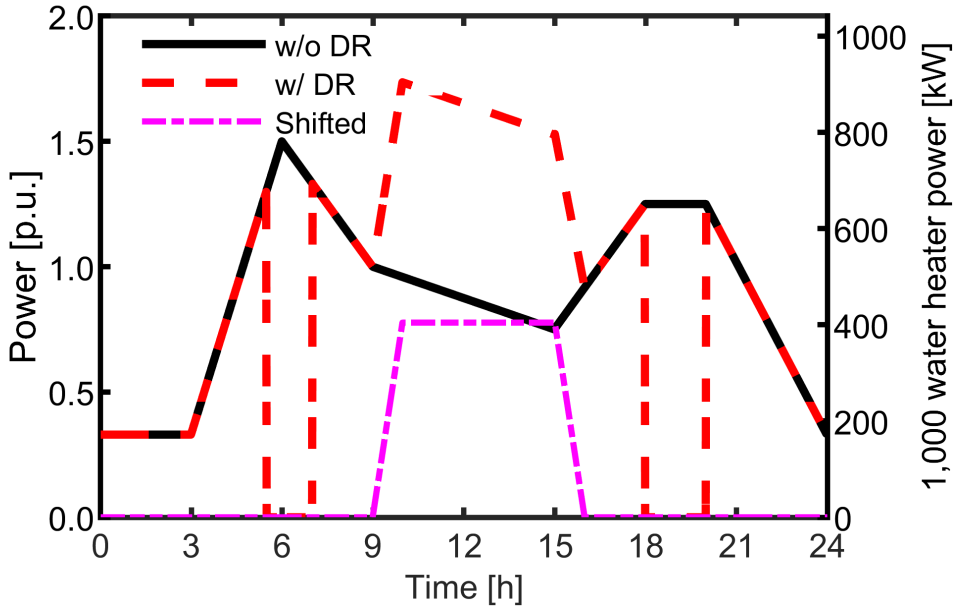

Figure 3.35: Example DR for aggregated EWH based on the generic load. This approach demonstrates how the peak demand of aggregated EWH load at the morning and evening peaks can be shifted to midday, when solar generation is relatively high.

$T_R = [9:00, 16:00]$ and $P_T = 0$ for EWH is shown in Fig. 3.35. In this extreme example case, the loads at morning and evening peaks were entirely shifted to the afternoon. The same shedding periods were selected for HPWH for comparison and results are shown in Fig. 3.36.

The electricity usage for both EHW and HPWH are shown in Fig. 3.37 and 3.38, respectively. For both EWH and HPWH, during the shedding periods, the electricity usage remained unchanged. In the DR case, the electricity usage increased faster due to the shifted load starting from 9am. For both with and without DR case, the total electricity usage was the same at the end of the day.

The aggregated power profiles for EWH and HPWH under DR control are shown together in Fig. 3.39. The fixed hot water flow from Fig. 3.19 was used for the DR study for both EWH and HPWH. During the shedding period in the morning, which

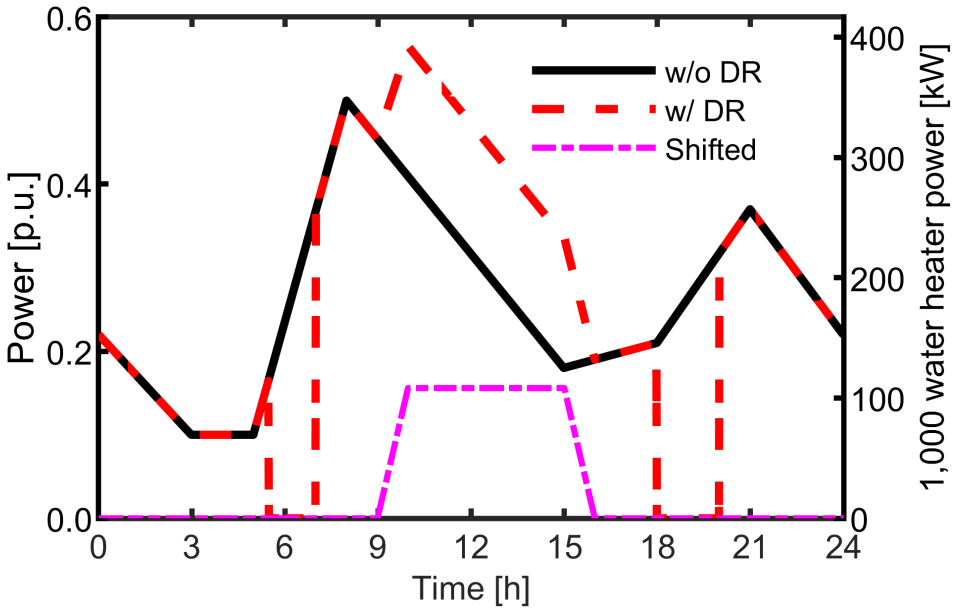

Figure 3.36: Example DR for aggregated HPWH based on the generic load. The shedding periods for the HPWH were selected as the same as that of the EWH case for comparison.

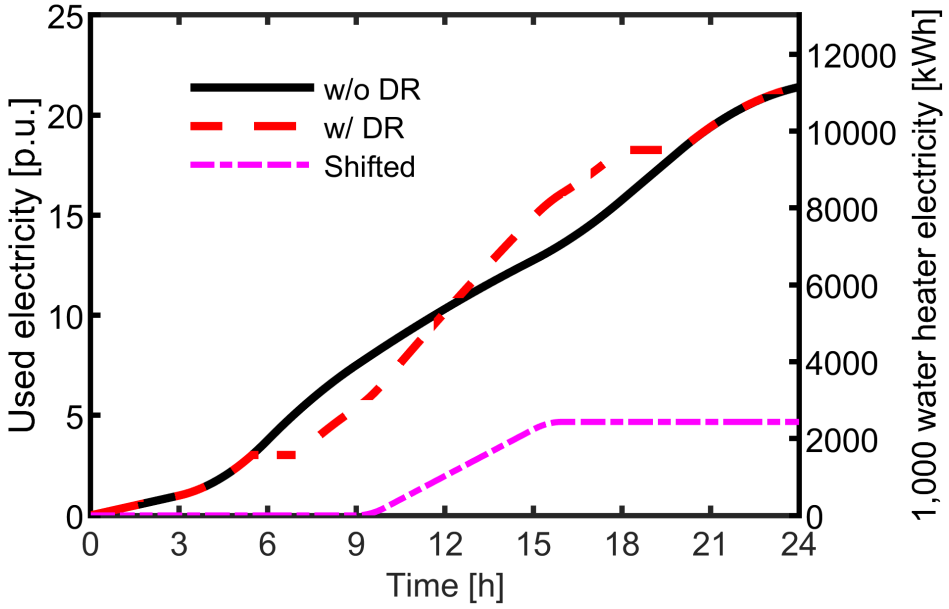

Figure 3.37: Accumulated electricity usage of the aggregated EWH. Both cases used the same amount of total electricity at the end of the day, which was 21.4 p.u. In the DR case, the electricity usage remained unchanged during the morning and evening peak shedding period. The electricity usage for the DR case increased fast in the afternoon due to the shifted electricity.

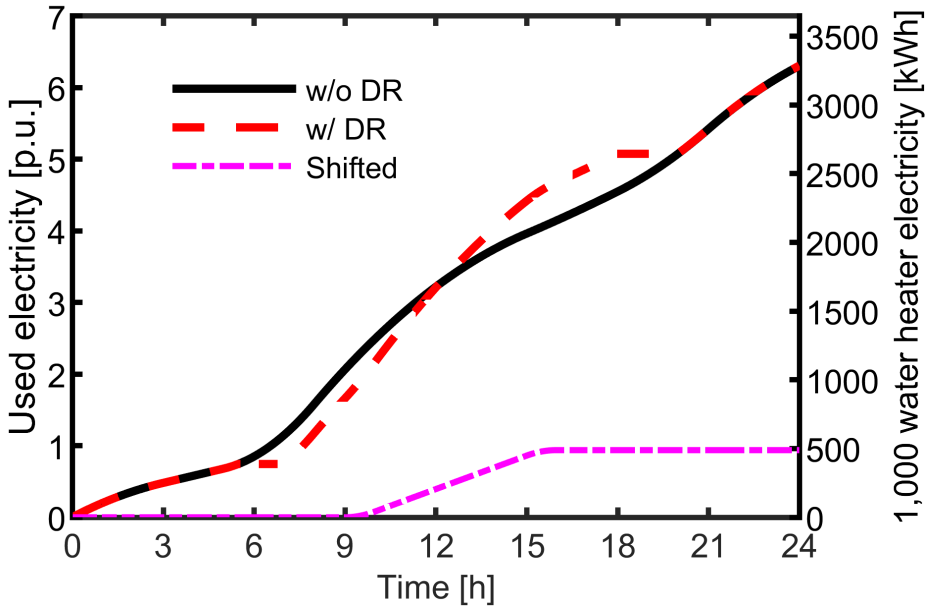

Figure 3.38: Accumulated electricity usage of the HPWHs. During the morning and evening peak shedding period, the used electricity remained unchanged in the DR case. More electricity was used in the afternoon due to the load shifting. Both cases used the same amount of electricity at the end of the day, which was 6.3 p.u.

stands for the maximum load reduction case scenario, the water temperature in the tank dropped significantly, as shown in Fig. 3.40. The water temperature for HPWH dropped even below the minimum 115F under the extreme shedding case. A practical home energy management would put the customer comfort as priority and avoid the tank temperature being too low. The high water temperature in the afternoon was feasible due to the implementation of mixing valve technology.

The corresponding energy take is shown in Fig. 3.41 for the DR case. For both EWHs and HPWHs, the shedding in the morning led to high energy take, leaving large reserved energy capacity for absorbing the surplus PV generation. The energy take went negative in the afternoon, indicating that the water was heated by the shifted load. The peak-to-peak values of the energy take in this example were 4.8

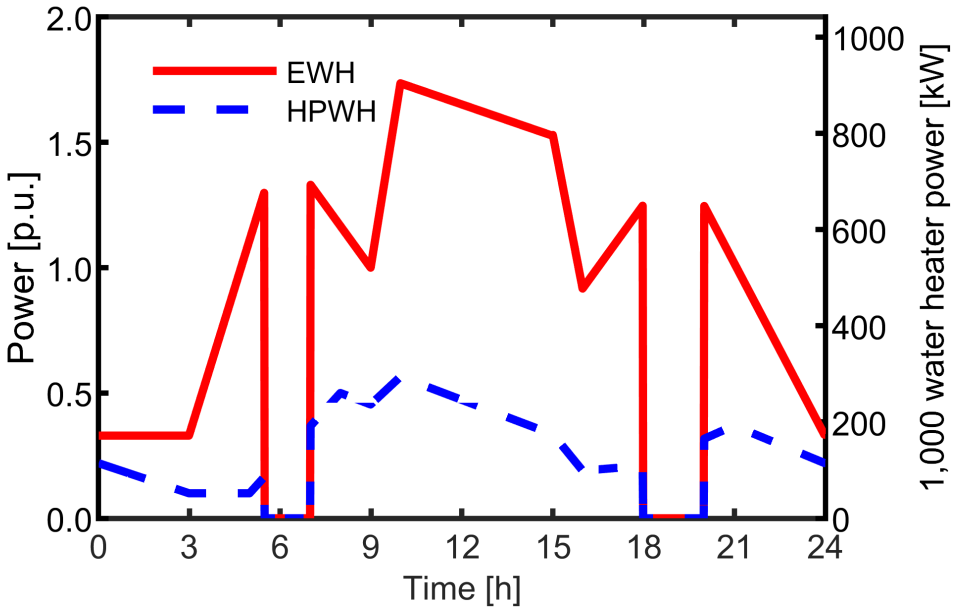

Figure 3.39: The aggregated power for EWH and HPWH with DR control. The morning and evening peaks for both EWH and HPWH were shifted to the afternoon when the PV had surplus generation.

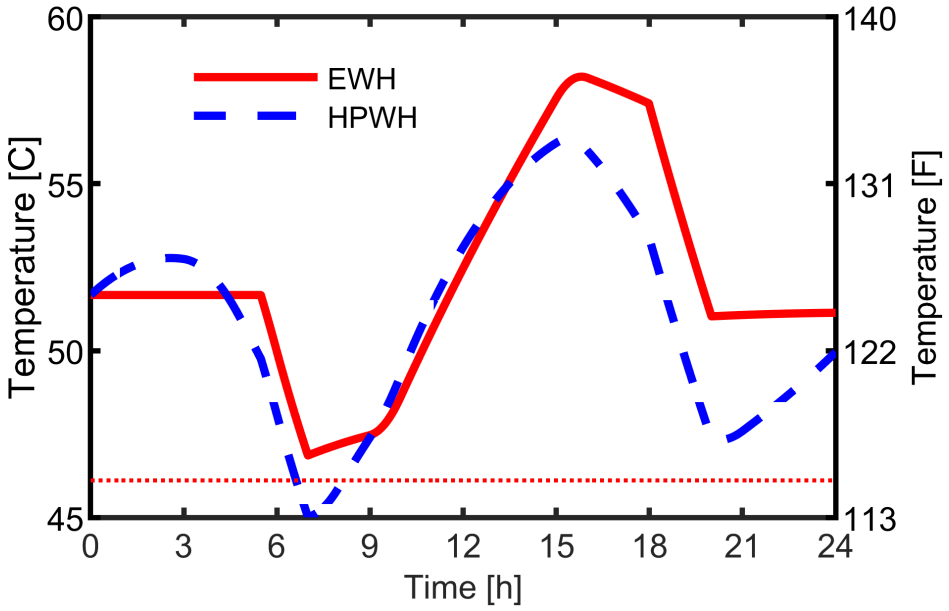

Figure 3.40: The average hot water temperature in the tank for both EWH and HPWH with DR control. The example shows a significant reduction in tank temperature in the early hours for the extreme condition when all the water heaters were turned Off. The recovery around midday means the water heaters can be used as storage for surplus PV generation.

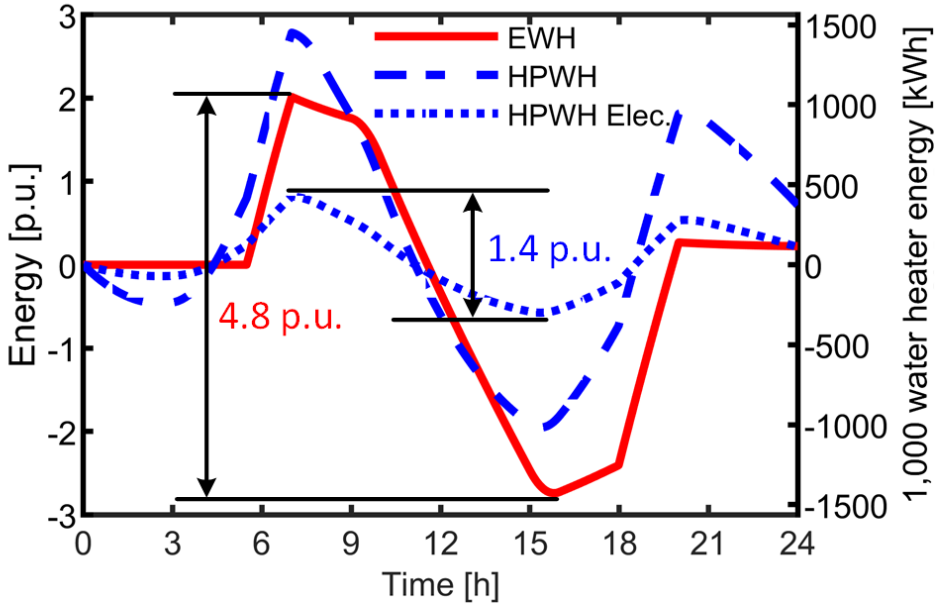

Figure 3.41: The energy take for both EWHs and HPWHs with DR control. The energy take was high during the shedding periods because there was no energy input. In the afternoon, the energy take was negative, indicating the preheating process and higher water temperature in the tank. The corresponding electricity usage for HPWHs was lower due to the COP. The reserved capacities for both EWHs and HPWHs were approximately 22% of the corresponding daily electricity usage.

p.u. and 1.4 p.u., for EWH and HPWH, respectively. Given that the daily electricity usage for EWHs and HPWHs are 21.4 and 6.3, the reserved electric energy capacity for both EWHs and HPWHs were approximately 22% of their daily electricity usage. For a community with 1,000 EWHs, a total 2,500kWh energy can be stored in the water heaters in the example DR case. If the water heaters are all HPWHs, the number is approximately 730kWh.

3.6 Conclusion

The multi-physical models for EWH and HPWH were created with the ability to calculate the water heating power, hot water flow, water temperature in the tank,

and energy take for any number of water heaters. A generalized approach to energy storage that enables all such systems and devices, not only batteries but also EWHs and, in principal, HVAC systems, to be controlled with the same variables, namely "energy capacity" and "energy take". Such controls comply with the specifications of Energy Star and CTA-2045, which can ensure a platform for industrial and utility adoption. It was found that the example BESS and EWH are comparable when considering their energy content as generalized energy storage with occupant safety from high water temperatures guaranteed through a mixing valve solution.

A distribution system with 353 residences was simulated using the IEEE 123-bus feeder with experimental user data and realistic hot water flow data from the California Building Energy Code Compliance (CBECC). DR complying to CTA-2045 specifications was implemented to all the EWHs. Peak power during the shed event in the morning was reduced by 28%. With the defined energy take levels in this study, the average energy take value was 1,388Wh at maximum. With the selected hot water draw profiles and number of different house types, each residence had 7 minutes more time during which user comfort requirements were not maintained. These results were achieved while keeping the variation of the bus voltages within 1±0.05 tolerance throughout the power system.

The proposed aggregated generic curves for residential water heaters, which use a minimal amount of data points, are the first of its kind to the best of the authors' knowledge. The aggregated generic curves for EWH and HPWH were obtained based on large-scale projects. The experimental data for EWH generic curve was collected

from approximately 800 users during a period of two years by the industrial collaborator, A. O. Smith. The experimental data for HPWH generic curve was provided by the BPA from the project involving 300 heat pump CTA-2045 enabled water heaters in the pacific northwest.

The peak power for the aggregated EWH load was approximately 3 times that of the HPWH and changing all EWH to HPWH reduces the daily electricity usage by approximately 70%. Case study results show that when referring to the average power, approximately 14% daily electricity usage for EWH could be shifted. The HPWH still maintained the opportunity to shift approximately 17% of the daily electricity usage. The EWH could reserve the energy storage capacity equal to 22% of its daily electricity usage in the case study. Changing to HPWHs reduces the electric storage capacity because HPWHs use less electricity than EHWs in general. However, HPWHs still reserved capacity equal to 22% of their daily electricity usage when the peaks were shifted to the afternoon.

Chapter 4

Virtual Power Plant Operation for Large Residential Communities including HVAC and Energy Storage

4.1 Introduction and Problem Formulation

The smart home concept facilitates the participation of all power generation entities and is an enabling idea for future power system sustainability. Futuristic smart homes both integrate information technology and provide opportunities for incorporating other innovative technologies, such as solar photovoltaic (PV), smart devices, and energy storage. With such technological advancements, smart homes can enhance energy efficiency, and improve both stability and reliability by allowing owners to regulate electricity usage [35–37]. They can also change the operations of utilities by minimizing both energy usage and peak demand in residences[38–41].

Smart homes reduce energy usage by reducing heating, ventilation, and air-conditioning (HVAC) demand via improved building insulation and usage of intelligent control techniques to automatically turn Off idle devices [157–160]. Furthermore, smart

homes have the authority to control the appliances according to the utility commands [161]. Such load control capability is increasingly important as local solar PV penetration grows and progressively more smart homes begin to act as distributed energy resources (DERs) by participating in the energy market [162–164].

Some technical challenges are associated with the high penetration of PV in residences, one of which is the "duck curve". This phenomenon occurs when the net power demand fluctuates with a large deviation within a short period, typically during the hours between the afternoon and the evening [4]. For ensuring local voltage support, it is necessary to maintain a minimum generation of electricity by utility plants. Hence, the reliability of the power system is compromised when the generation of power is minimized during the mid-day to allow high PV generation [61]. To match with the fast increasing power demand in the evening, high-cost high-ramp rate generators are required when PV generation becomes unavailable [62].

Ancillary services, such as those described in [84], are provided in order to enhance the capabilities of the electric power system. The addition of energy storage can alleviate the "duck curve" through load shaving, peak shifting, and self-consumption of the local PV generation. Smart homes can be used as virtual energy storage by utilizing various thermal components, such as the HVAC systems and electric water heater (EWH), for circumventing peak demand [85]. Residences can support the ancillary services through energy flexibility, which depends on factors including the capacity of the HVAC system [86]. Aggregated HVAC systems can be employed to improve power quality and efficiency in demand response (DR) [87]. At the aggregated level, HVAC systems may be controlled sequentially to reduce the peak demand while

maintaining the user comfort [85].

EWHs are also capable of providing ancillary services due to the large thermal mass of the water tank, as well as their presence in most households [65, 66]. The EWH can preheat the water to a much higher temperature while assuring the safety with the help of mixing valve technology [165]. Most EWH manufacturers provide the CTA-2045 modules in their new products or offer refurbishments to enable real-time communication and control [68, 69]. In previous research, EWHs were used to regulate the frequency in an electric power distribution system [166]. Another research study showed that the aggregated EWH load can be controlled to contribute to shifting the system peak load [70]. Communities with large penetration of controllable EWH have, in principle, the potential for providing ancillary services.

HVAC systems use the highest percentage of energy within typical residences and dominate the house energy usage and contribute the most to the peak power demand at the aggregated level [167]. To accommodate for large fluctuations in demand over the course of a day, expensive infrastructure must be installed to meet the maximum demand. Utilizing HVAC systems as DR devices has great opportunity to yield significant energy savings, especially at an aggregated level. A grey-box resistance-capacitance (RC) model provides accurate results for the indoor temperature with proper values for R and C [168, 169]. Aggregated modeling for a community of air conditioning loads has been proven effective for the study of large-scale DR implementation [15]. Commercial HVAC system modeling employs statistical methods that are also highly accurate [16].

The DR studies with residential-level HVAC models, however, are more recent and

have yet to reach this degree of confidence due to the strong link among HVAC energy use, random user behavior, and external weather conditions. The effect of weather induces more variation in energy and is more difficult to capture at the residential level. Current research proposes various methods to develop residential HVAC energy models, such as power-temperature modeling through disaggregation of smart meter data [170], or employing whole building energy simulators like EnergyPlus [171], or eQUEST [93].

To ensure adequate thermal comfort, the HVAC control follows Standard 55 of the American Society of Heating, Refrigerating and Air-Conditioning Engineers (ASHRAE), in terms of external and internal temperature, relative humidity, individual metabolic rate, etc. [17]. The ASHRAE Standards quantify the comfort of the space using a numerical scale called the Predicted Mean Vote (PMV) that was derived from survey results where participants ranked their comfort from -3, very cold, to 3, very hot. This allows for an association between a range of environmental conditions to a comfortable status within a home that can be calculated as a PMV between -0.5 and 0.5, which may be used to control heating and cooling systems without affecting thermal comfort.

HVAC systems are widely perceived as solely energy-consuming in the power grid. This view is being re-assessed in the field of home energy management (HEM) as recent research from the Oak Ridge National Laboratory (ORNL) demonstrates that the HVAC system can be regarded as an equivalent energy storage device and be conveniently controlled by a similar charging/discharging procedure [12]. For example, a commercial building with multiple zones can be modeled to operate as an equivalent

energy storage device and can be controlled by adjusting zonal airflow rates [13]. As claimed in [14], the round trip efficiency of the HVAC-based equivalent energy storage can be near 100%.

A research gap remains as most HVAC system models require parameters that are challenging to acquire [172]. It becomes increasingly difficult for aggregated HVAC load modeling considering additional parameters for the multiple buildings. Some alternative methods for aggregated HVAC load modeling may only monitor the average room temperature for multiple buildings, ignoring the thermal comfort of individual users [97, 173].

In this chapter, smart homes were operated as DERs in a distribution system for peak reduction and the alleviation of the "duck curve". The long term total load profile for the residential community was forecasted considering the trends of increasing percentages of smart homes and the PV penetration. It was demonstrated that with an appropriate HEM system, the "duck curve" at the power system level can be alleviated even when PV penetration is fairly high.

The smart homes successfully operated as DERs and the experimental data was available from the Smart Energy Technologies (SET) project in Glasgow, KY. The similar VPP operation for the distribution power system was realized by batteries and EWHs, respectively. Controlling the EWHs could achieve different peak reduction targets while guaranteeing the user comfort. The minimum participation rates for EWH are calculated and compared with that of the BESS.

The problems addressed in this chapter include the VPP control using residences as DERs and the development of aggregated HVAC power at large scale. Each of the

problems are defined in the subchapters: the VPP control using residences as DERs in section 4.2, and development of aggregated HVAC power at large scale in section 4.4.

In this chapter, the comparability between the HVAC system and a typical battery BESS was studied and demonstrated. A centralized sequential DR control method for the reduction of the ramping rate and peak power was elaborated in this work. The HVAC system was controlled by changing the thermostat set point, which was justified to ensure human comfort according to ASHRAE standards. Cases for different hot days, and for one day with different residence participation were studied.

This chapter is substantially based on the following journal papers:

- H. Gong, *et al.*, "Peak reduction and long term load forecasting for large residential communities including smart homes with energy storage," *IEEE Access*, Vol. 9, pp. 19 345–19 355, 2021.

- H. Gong, *et al.*, "Virtual power plant control for large residential communities using HVAC systems for energy storage," *IEEE Transactions on Industry Applications*, Vol. 58, No. 1, pp. 622-633, 2022.

4.2 Smart Homes as DERs for VPP

4.2.1 Technology Demonstrator and Analysis Framework

This study utilizes the experimental data from the Smart Energy Technologies (SET) project in Glasgow, KY, a city for which utility services are provided by the

Figure 4.1: Aerial view of Glasgow, KY, the location of the studied SET, along with pictures of smart devices for home energy management: thermostat, EWH and BESS, which are programmable and enabled by WiFi or Ethernet. The data acquired has a resolution of up to 1 minute and is available for both home owners and the utility.

municipal Electric Plant Board (EPB) in partnership with the Tennessee Valley Authority (TVA) [174]. Currently, this project is one of the largest rural field demonstrators in the US with high efficiency. The proposed software framework is implemented to model this entire advanced community that includes residential, business, and industrial sectors. The model incorporates a HEM system that allows regulating the residential EWH, HVAC, and BESS to reduce the peak demand and energy usage.

Building upgrades along with controllable and highly efficient devices are employed by the residential homes studied in this SET project (Fig. 4.1). According to the current data, over 300 homes out of around 5,000 from Glasgow, KY, are participating in the project. As a result, approximately 600,000 kWh of energy is saved annually. All the residences participating in this SET project receive measures to improve energy efficiency, such as efficient HVAC systems, better insulation, etc. Due to such improvements, energy usage is reduced in some of the SET homes, although

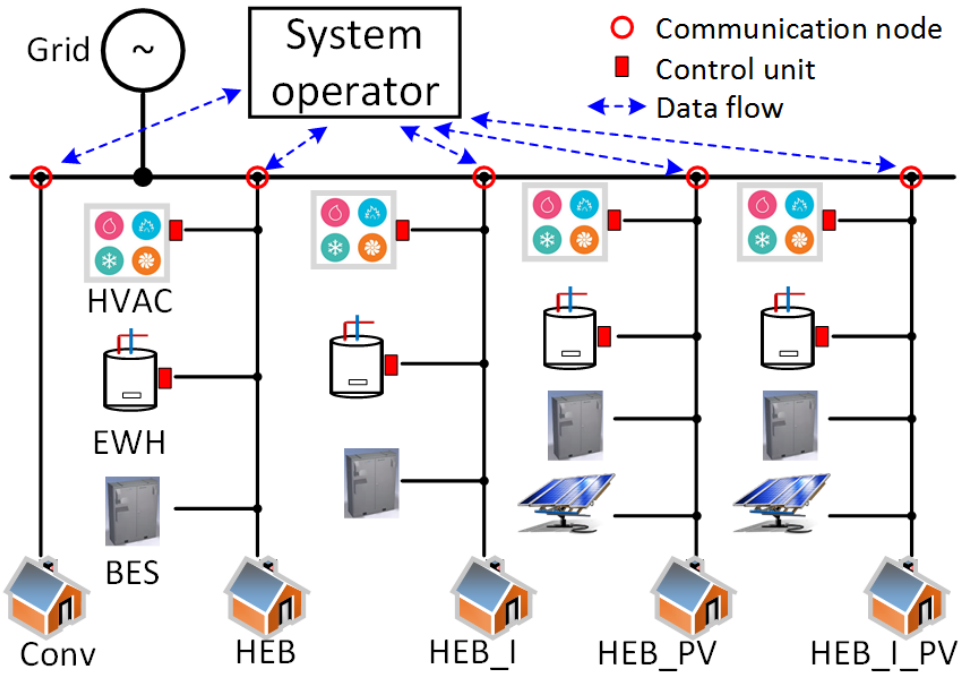

Figure 4.2: The proposed system model includes five types of SET homes, each type being representative of thousands of individual houses. In the study, the load data for the business and industrial sectors is provided by experimental measurements.

all of them are single-family houses with comparatively larger space. Furthermore, programmable WiFi-enabled thermostats, heat-pump EWH, and a residential BESS allow the SET homes to perform real-time HEM.

Although the total power demand of the Glasgow EPB service includes business, industrial, and residential sectors, the system modeling presented in this study mainly emphasizes the residential sector and the aggregated effects of regulating single SET homes. The residential community includes five types of houses: non-SET conventional homes, residences with **H**VAC, **E**WH, and **B**ESS control (HEB), the HEB house with improved **I**nsulation (HEB_I), and the HEB, HEB_I house with local solar **PV** panels (HEB_PV, HEB_I_PV), respectively, as illustrated in Fig. 4.2.

Apart from Non-SET conventional homes, the rest of the four types are SET

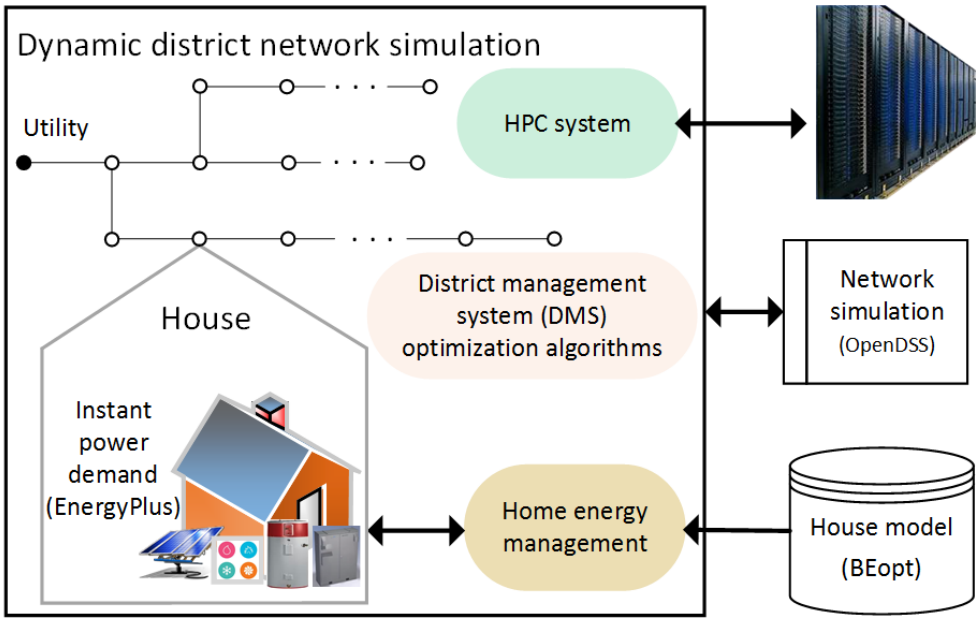

Figure 4.3: Schematic representation of the INSPIRE+D proposed simulation software framework, solely based on freeware, capable of running thousands of house energy models in parallel and concurrently performing power flow optimization.

homes. The residences in the SET project work as controllable loads with the integration of smart devices, bi-directional communications, and integrated management. It allows the houses to interact with the grid dynamically, and improves the coordination; leading to load shifting, peak demand reduction, and energy saving. The ultra smart home (USH) with the Solar Integration System (SIS) monitor the residential power flow and upload real-time data. The available data from 148 USHs includes the net power flow from the grid, the power and state-of-charge (SOC) of the BESS.

Another set of data with the daily power profile for more than 5,000 residences is provided by the utility. The data includes the electricity usage at 15-minute intervals for each individual home on example summer and winter days. The data serves as the baseline case, which presents typical power demand for the distribution system where most of the residences are conventional houses without PV. For the purpose

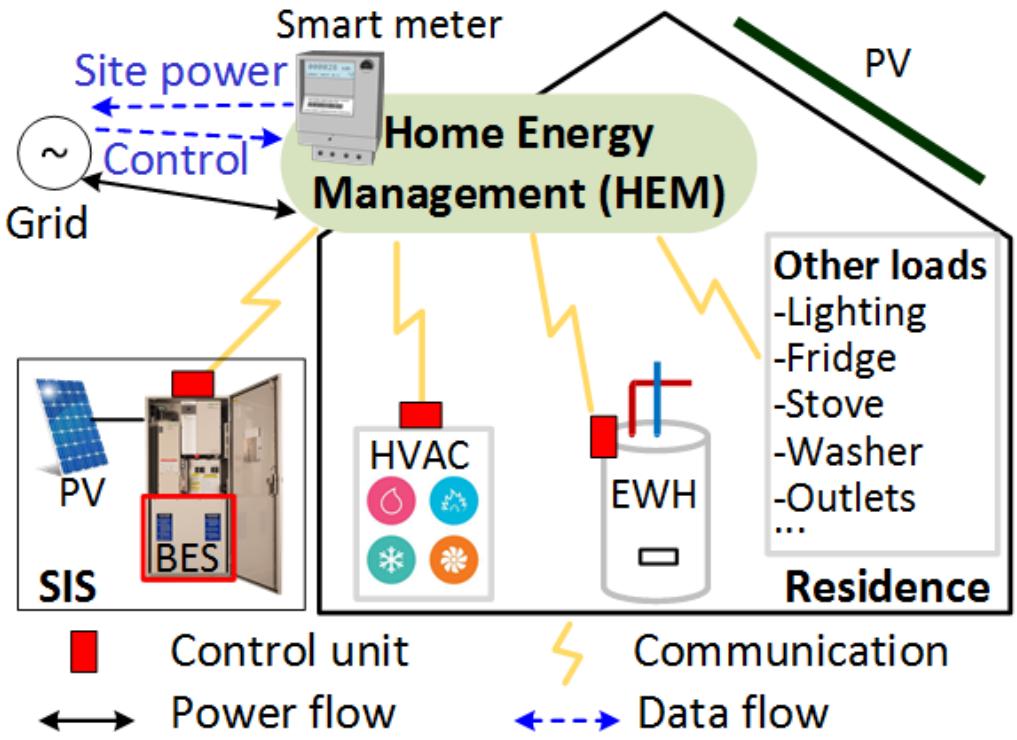

Figure 4.4: The proposed home energy management scheme for the SET homes. Solar PV and BESS are integrated into a Solar Integration System (SIS). HVAC and EWH load demands are controlled through temperature set points.

of the computational study, the solar PV system for each house is sized in order to meet the NZE requirements, i.e., the energy used over one year must be equal to the energy generated by the PV system.

The simulation for the power system formed by the SET community including over 5,000 homes is realized by an innovative, first of its kind, software framework '**I**ntegrated **N**etwork simulation for **S**mart **P**ower-flow **I**n **R**esidences using **E**nergyPlus and Open**D**SS' (INSPIRE+D), as shown in Fig. 4.3. INSPIRE+D incorporates freeware such as EnergyPlus, BEopt, OpenDSS, and Python, and is capable of both power flow analysis at the system level, and house energy modeling along with HEM at the single house level [11]. Its scalability allows the simulation of thousands

of different house models in parallel, utilizing a high-performance computing (HPC) system with thousands of cores.

4.2.2 Home Energy Management Design

The net load for a residence with HEM_I_PV is the result of the combined power for HVAC, EWH, other loads, BESS, and PV, as illustrated in Fig. 4.4. The net load for a HEM house at time t is calculated as:

$$P_H^t = P_E^t + P_{HVAC}^t + P_O^t + P_B^t - P_{PV}^t, \tag{4.1}$$

where P_H is the residential net power flow; P_E, P_{HVAC}, P_O, P_B and P_{PV} are the powers of the EWH, the HVAC system, other loads, the BESS and PV, respectively. It may be noted that for the BESS, positive and negative powers indicate charging and discharging, respectively.

The water tank temperature is limited as follows,

$$T_S^t - \Delta T_D \leq T_E^t \leq T_S^t, \tag{4.2}$$

where T_S is the set point of the EWH; ΔT_D, the dead band of the EWH, which is set to 18F, T_E^t the temperature of water in the EWH tank. T_E^t is updated automatically by the house energy model. The water heater power is decided by the nominal power and its status from the following,

$$P_E^t = P_{E,N} \cdot S_E^t, \tag{4.3}$$

where $P_{E,N}$ is the nominal power of the EWH. The status of EWH, S_E^t, is decided by the water temperature in the tank, set points and the dead band as per the following,

$$S_E^t = \begin{cases} 0 = Off, & T_E^t > T_S^t, \\ 1 = On, & T_E^t < T_S^t - \Delta T_D, \\ S_E^{t-1}, & other. \end{cases} \tag{4.4}$$

The set point, T_S^t, for the EWH determines the required On and Off switching and the resultant power flow according to (4.2) – (4.4).

The high specific heat capacity of water, negligible heat loss, and mixing valves enable advanced controls, e.g., postponed electric heating load while sustaining the comfort of the consumers [175]. The effect of the EWH controls are exemplified in Fig. 4.5 for three EWH working schemes and their corresponding tank temperatures. Peak power due to EWH operation occurs in the morning without adopting any control mechanism. To avoid this morning peak, EWH is controlled to operate in the early morning and at midnight in the HEB-type homes without any PV generation system. The residences that include PV shift the EWH load to the afternoon to absorb the surplus PV generation.

The HVAC power is represented as a function of the thermostat set point temperature change by the following,

$$P_{HVAC}^t = f(\Delta T_R^t). \tag{4.5}$$

Consumer comfort is taken into account by limiting the heating and cooling set points:

$$T_H^t \leq T_R^{t-1} + \Delta T_R^t \leq T_C^t, \tag{4.6}$$

where T_R, T_H, and T_C stand for the room temperature, set points for heating and

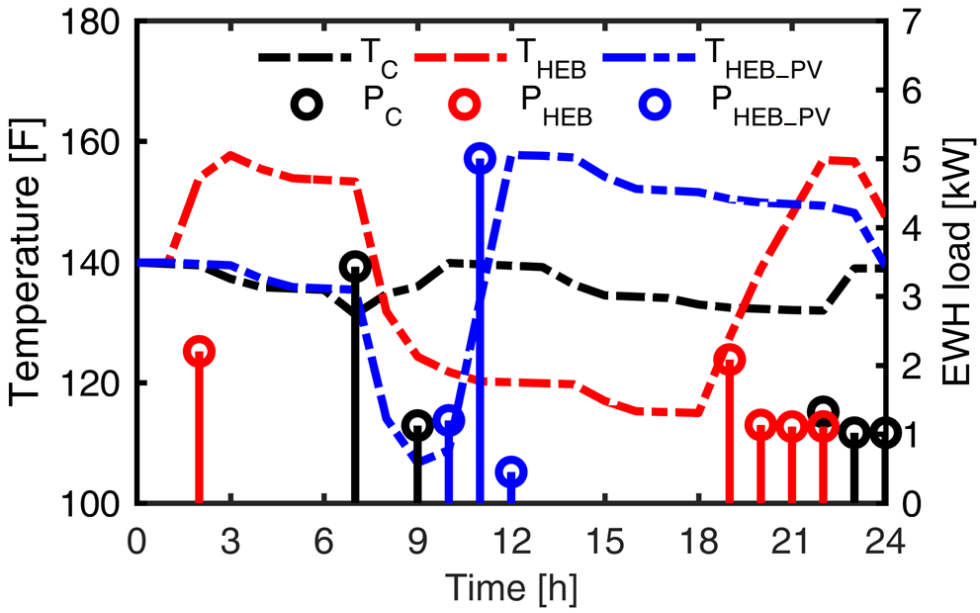

Figure 4.5: Water temperature in the tank and instantaneous power of EWH. HEB homes shift the EWH load to the morning and the evening. When equipped with solar PV, SET homes shift the EWH load to the afternoon to absorb surplus PV generation.

cooling, respectively. Previous research works show that the room temperature is influenced by factors including outdoor and ground temperatures, floor space, human activities and the heat radiation from indoor appliances [89].

The EnergyPlus software is employed to model the houses and quantify the results of the HVAC and EWH control. It may be noted that the user can over-ride the HEM controls if desired. The SET homes with the HEM system have lower HVAC loads on both the studied summer and winter days due to the improved insulation. The example control of HVAC in a winter day is presented in Fig. 4.6. By adjusting the mid-day temperature set point to a lower value, the HVAC power of the HEM house decreased significantly. In the afternoon when the SET house owner is away, the thermostat set point (T_S) is set low in order to reduce the HVAC load. T_S is changed

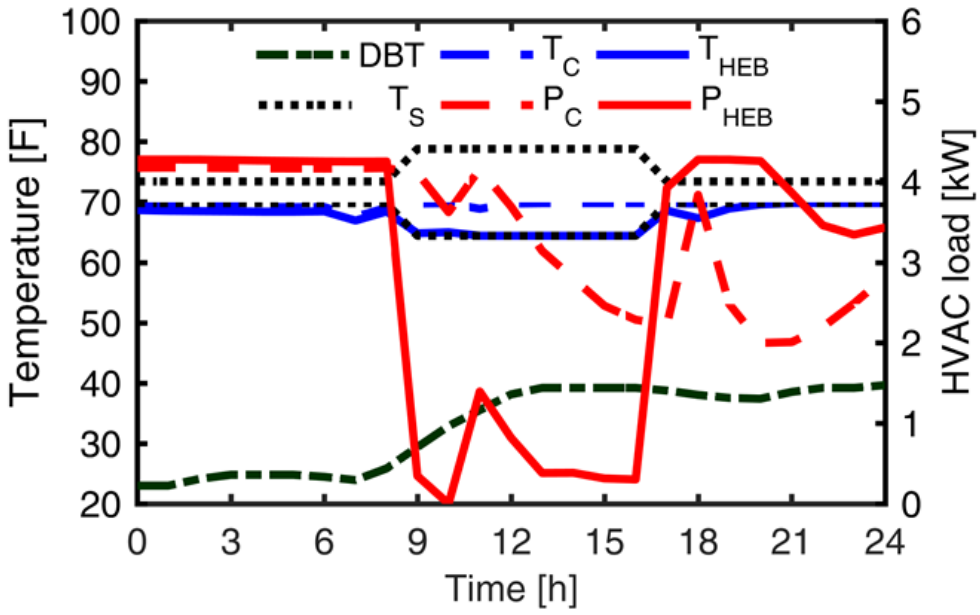

Figure 4.6: Simulated HVAC power demand for a typical home on an example winter day. A house of the conventional type (denoted by a suffix 'C') without HVAC control has higher HVAC power in the afternoon. In a HEB-type home, the capability of changing the heating set point (T_S), leads to lower HVAC power in the afternoon when the owner is away.

back at 17:00 before the house owner returns home.

The net power flow of the NZE house is thus defined as a function of the HVAC set points, water heater set point, and the BESS power, as below,

$$P_H^t = f(P_B^t, T_S^t, T_H^t, T_C^t). \tag{4.7}$$

Based on the previous equations (4.1)-(4.7), and substantially following the concepts described in [176], a HEM algorithm has been developed and implemented at residence level in order to meet the power limit set forth by the system operator utility via control signals during a DR event. Power in excess of the limit is firstly to be supplied, if available, by a BESS. Should such required supply exceed the maximum power of the BESS or should its state of charge be lower than admissible, appliances will be controlled to sequentially contribute to the power demand reduction, as briefly

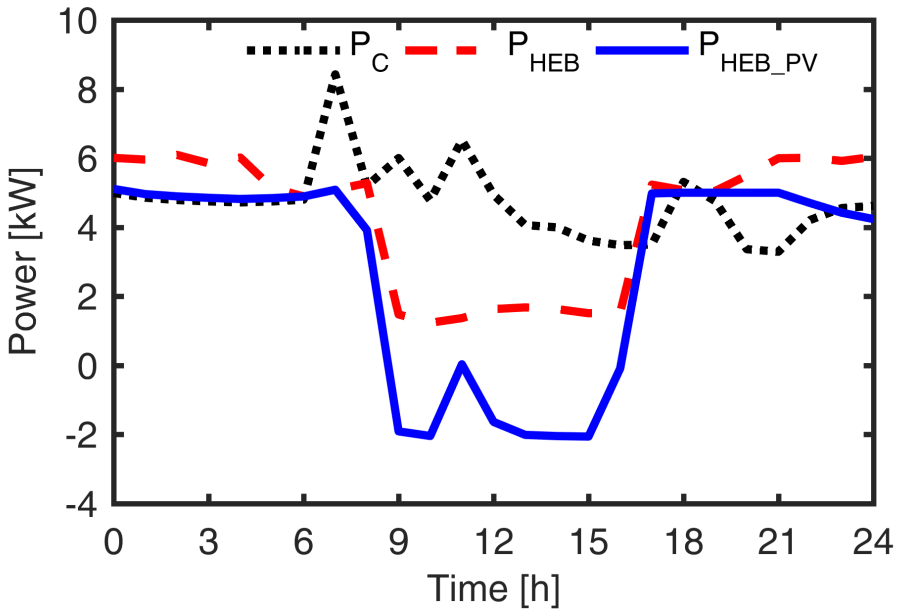

Figure 4.7: Simulated net power demand for a single-family house. The demands for HEB and HEB+PV houses are shaped by controlling the HVAC, EWH and BESS.

described in the following.

The energy used by the EWH will be reduced during DR by lowering the corresponding set point as exemplified in Fig. 4.5. In case the instantaneous power demand still exceeds the limit, the HVAC energy use is reduced by changing the set point for heating or cooling, depending on the season, as shown in Fig. 4.6. Changes may be performed incrementally until the utility-set upper power limit is met and making sure, as a priority, that the minimum user comfort requirements are met.

The controllability of BESS provides enhanced flexibility to the HEM system because the charging and the discharging operations do not impact the comfort of the residents. The example effect of the BESS control from Fig. 4.7 illustrate the HEM functions for smoothing the residential energy demand and reducing peak power.

Table 4.1: Case studies with different percentage distributions of house types in the community power system

Cases	Conv (%)	HEB (%)	HEB_I (%)	HEB_PV (%)	HEB_I_PV (%)
BL	>94	<3	<3	0	0
2	50	25	25	0	0
3	50	0	0	25	25
4	20	20	20	20	20
5	0	25	25	25	25

4.2.3 Long Term Impact of Technology Penetration

In Table 4.1, case studies based on different penetration of technologies, i.e., house types, are demonstrated. The experimental data provide the baseline case (BL) and stands for the current field situation where only around 300 out of approximately 5,000 homes are SET, and do not possess PV installations. In the second case, HEM control is not included. The net power flow curves of both the aggregated and the baseline case are similar, which validates the model. The improved insulation increases the efficiency of HEM_I homes, which causes a reduction in the total energy usage for case 2. Cases 2 to 5 present the gradual shift to futuristic high energy efficiency and distributed PV generation community. The simulation of the distribution power system for each case study was performed based on a modified IEEE 13-node test case, and solved by OpenDSS.

The case studies were performed on two preselected representative days in Glasgow, KY—1/19/2017 (Winter) and 7/20/2017 (Summer). It is shown in Fig. 4.8 (a) that the aggregated residential power demand peaks in the morning and the evening on the winter day. On this winter day, the residential load drops in the afternoon because of the solar irradiance, which brings heat into the room through walls and

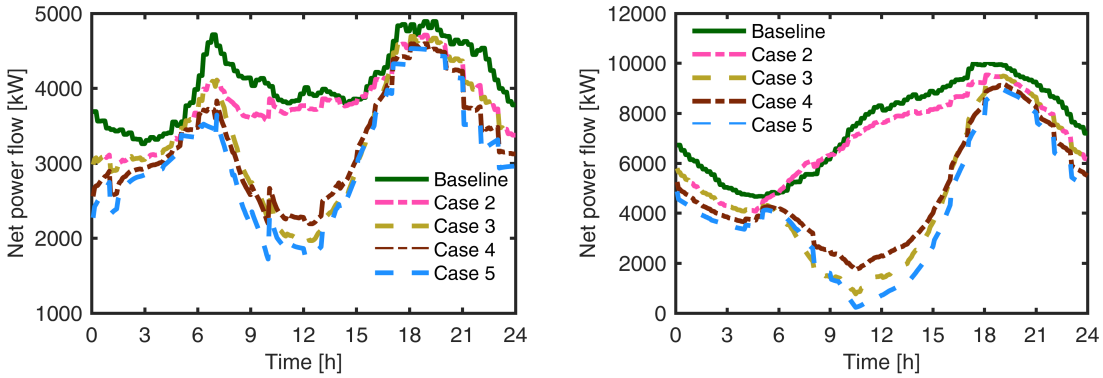

Figure 4.8: Aggregated residential net power flow without HEM for the studied (a) winter and (b) summer day, respectively. A high penetration of solar PV exacerbates the "duck curve".

windows. The net power flow decreases in the afternoon due to high PV penetration, leading to a prominent "duck curve" profile (Fig. 4.8 (a)).

The HEB_I type homes with improved insulation contribute to residential load reduction. From Fig. 4.8 (a), it can be seen that even when as few as 25% of the houses are of the HEB_I type, power reduces substantially. From Fig. 4.8 (b), a similarity can be observed for the studied summer day as well. The SET homes function like thermal and electrical energy storage systems with the proposed HEM control, which reduces the peak power flow in the morning and the evening in both cases as shown in 4.9 (a)). HEB_I homes featured in case 2, have lower energy usage compared with the baseline case, even though they do not accommodate any PV generation. Case 2 with 50% penetration of SET homes, allows the opportunity to shift the peaks and bring down the ramp rates due to the combined operation of the BESS, and the controllable HVAC and EWH loads. On the other hand, 50% penetration of SET homes having the energy storage capacity supported by controllable loads and BESS

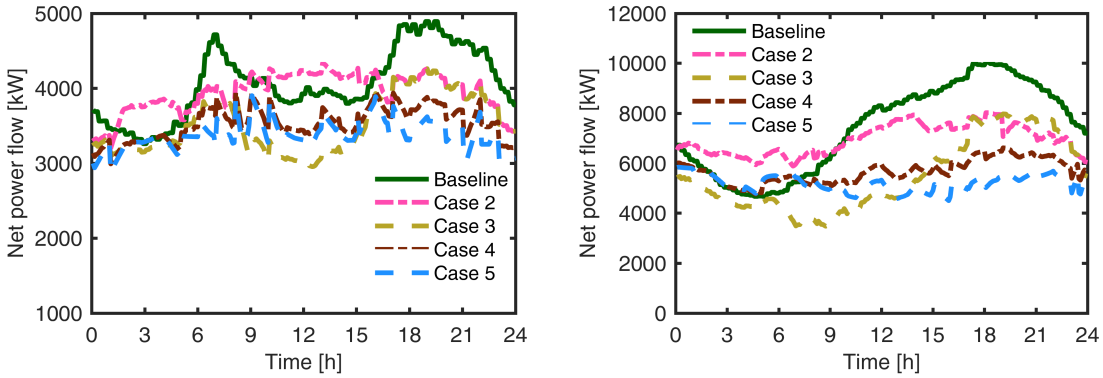

Figure 4.9: Aggregated residential net power flow with HEM for the studied (a) winter and (b) summer day, respectively. The proposed HEM reduces the peak demand and alleviates the "duck curve" effect.

is not sufficient for case 3 to absorb all the surplus PV generation and supply the total evening demand. Hence, case 3 demonstrates a significant "duck curve" effect. In case 4, the "duck curve" effect is alleviated to a certain extent due to the combined effects of a higher percentage of SET homes and reduced PV penetrations.

The PV generation from case 5 is similar to case 3, however, case 5 requires 100% SET homes in the power system. It is noteworthy that, the power usage, peak demand, and peak to peak value for case 5 features the lowest values. The study carried out on the summar day (7/20/2017) can also be explained by applying similar observations, as shown in Fig. 4.9 (b). The above results clarify that high PV penetration would not form any challenges for the utility grid with the usage of appropriate HEM systems.

4.3 Control for Batteries and EWHs for VPP Operation

4.3.1 Operation of Battery and EWH at Aggregated Level

The data from all 148 USHs on an example summer day includes the power and SOC of BESS, and the net power flow from the grid for each house at 1-hour time-steps. In Fig. 4.10, the BESS measured power plotted during an example day is adapted to the typical use of electricity in the Southeast region [177], and includes charging periods at night, when the load is typically low, and discharging periods in the afternoon, during typical high demand. The experimental SOC data presented in Fig. 4.11 shows a maximum of 94% for all BESSs. There is only one single data point that is below 20%. Therefore, in this work, the maximum and minimum SOC of all the BESSs are regarded as 94% and 20%, respectively.

The SOC of most BESSs remained at the maximum until around 2pm. Corresponding to the BESS discharging operation, the SOC dropped to the minimum at 6pm. The BESSs were fully charged late at night, completing the operation cycle for a typical summer day. Based on the measured power and SOC for the BESS, BESS energy capacities for all 148 USHs are calculated and the average is 16.2kWh. The measured net power flow from the grid for each USH house in Fig. 4.12 shows that during the typical peak hours in the afternoon, almost all the USHs achieved near zero power due to controlled battery discharge operation. Also observed is the high power in the early morning and late night. Thus, it can be concluded that the BESS operation has a great impact on the net power flow at the system level.

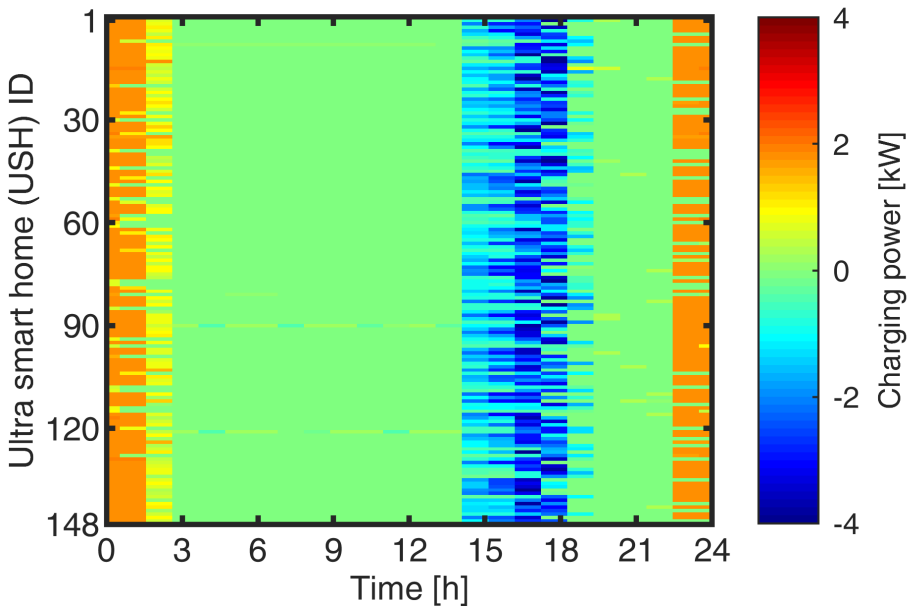

Figure 4.10: The BESS charging power for all the 148 ultra smart homes (USHs) on the example summer day. The negative value in the afternoon indicates the BESSs are discharging. BESSs were charged in the middle of the night.

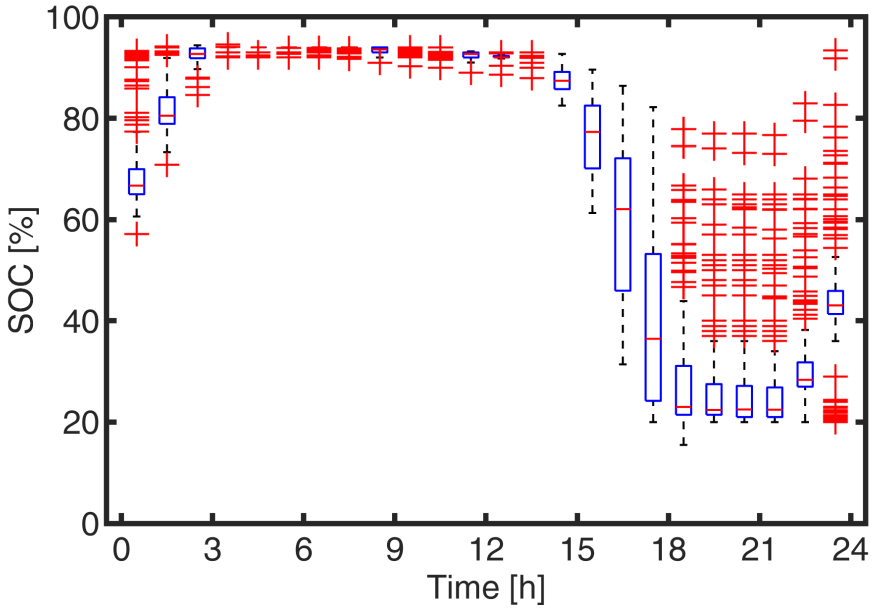

Figure 4.11: The SOC of BESSs from the 148 USHs on the example summer day. The measured data shows the SOC could be regarded within [20%, 94%]. The BESSs were charged in the middle of the night and maintained at the maximum SOC until around 2pm. The BESSs discharged for the afternoon peak and the low SOC remained until 9pm. The BESSs were charged afterwards for the next day.

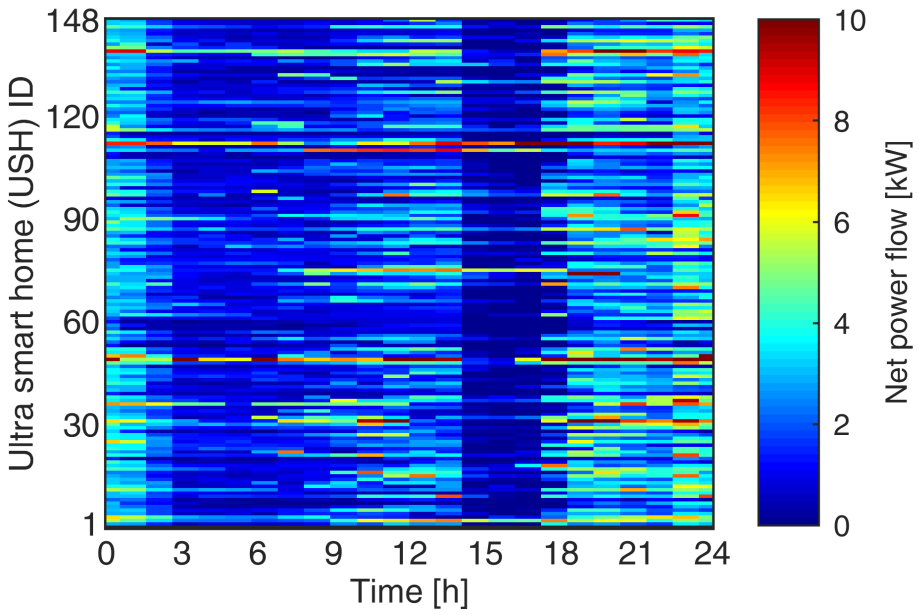

Figure 4.12: The net power from the grid for all the 148 USHs on the example summer day. The experimental data shows low net power at around 2pm–5pm. The power in the midnight was high due to BESS charging.

The measured net power and BESS charging power for each of the USHs were added together to produce corresponding aggregated curves, as shown in Fig. 4.13. The curve labeled as Ref loads USHs represents the difference between the net grid power and BESS charging.

A new load aggregated curve corresponding to resistive EWHs was calculated and later used in the study to replace the experimental heat pump water heater loads. The aggregated resistive EWH load typically has morning and evening peaks, with an average peak power of around 1.5kW [82]. The aggregated EWH power-time curve can be substantially defined by its major turning points for which the mathematical derivative, i.e., ramping rate, changes drastically. In the example shown in Fig. 4.14 these turning points occur at approx. 5, 7, 12, 15, 19 and 22 o'clock.

For example, a morning peak was exhibited around 7am, and a evening peak 7pm.

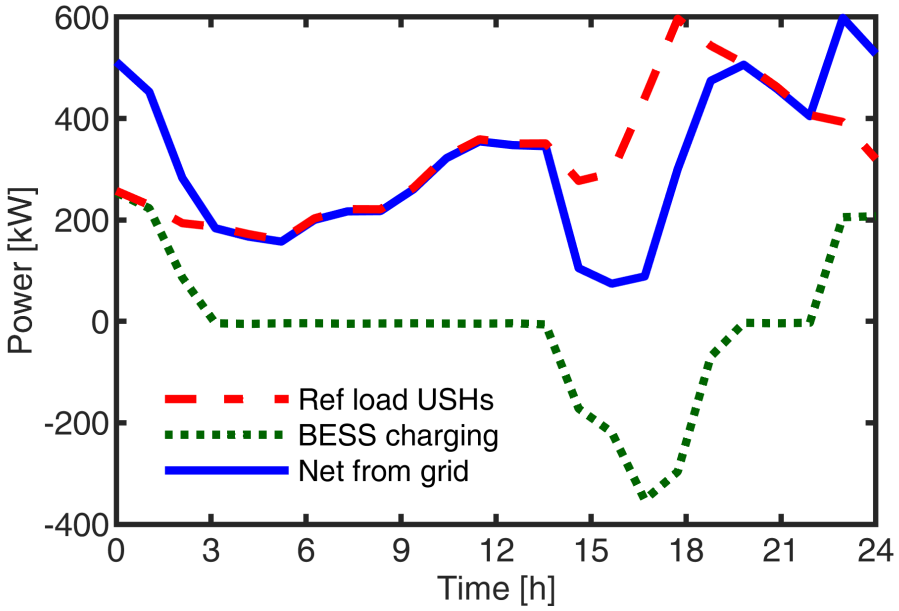

Figure 4.13: The aggregated power for all the 148 USHs based on the experimental data. The negative BESS charging power indicates the discharging operation at the peak hours. The aggregated net grid power at midnight was increased by the BESS charging.

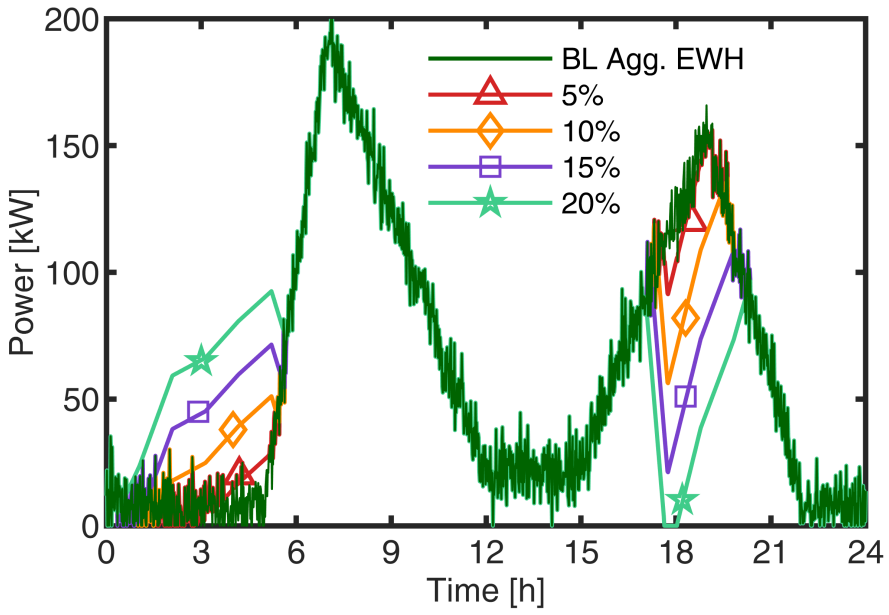

Figure 4.14: The power draw for EWH schemes including preheating and load shaving for different peak reduction targets labeled as percentage. The same amount of electricity for water heating was allocated at different times for the example day. The load shaving control was applied only to reduce the total evening peak.

The BL aggregated EWH curve from Fig. 4.14 stands for the aggregated EWH power for all 148 USHs without power shaving. A white noise with signal-to-noise ratio of 20 was added to the BL curve. This value is based on the typical results reported by previous studies [82], which considered the naturally random user behavior on 75 different water heaters, which is approximately half the number of the units considered in our study.

Mixing valve technology allows the water temperature in the tank to be as high as 145F, increasing the thermal capacity of the EWHs. The hot water at the EWH outlet is mixed with cold water in order to provide the user expected comfortable temperature. Four power shaving schemes were studied for different peak reduction targets and are shown in Fig. 4.14. The EWHs under all the schemes used the same amount of daily electricity and the same daily hot water draw. The peak shaving was realized by shifting the electricity used by EWH from the evening to the morning. It is worth noting that when the peak reduction target was 20%, the minimum aggregated EWH power was zero, meaning all EWHs were turned Off during the peak period. It is possible that the 20% peak reduction target was not achieved even when all EWHs were turned Off.

It was assumed that the average tank temperature for the BL case is 125F at all time. With known power $P(t)$ and tank temperature $\theta_T(t)$ from the BL case, the daily hot water draw $W(t)$ is calculated by solving (3.16). The same daily hot water draw is used to calculate the average tank temperature for different water heating schemes shown in Fig. 4.14. The results in Fig. 4.15 show that when the water was preheated to a higher temperature in the morning, the EWH had more standby loss

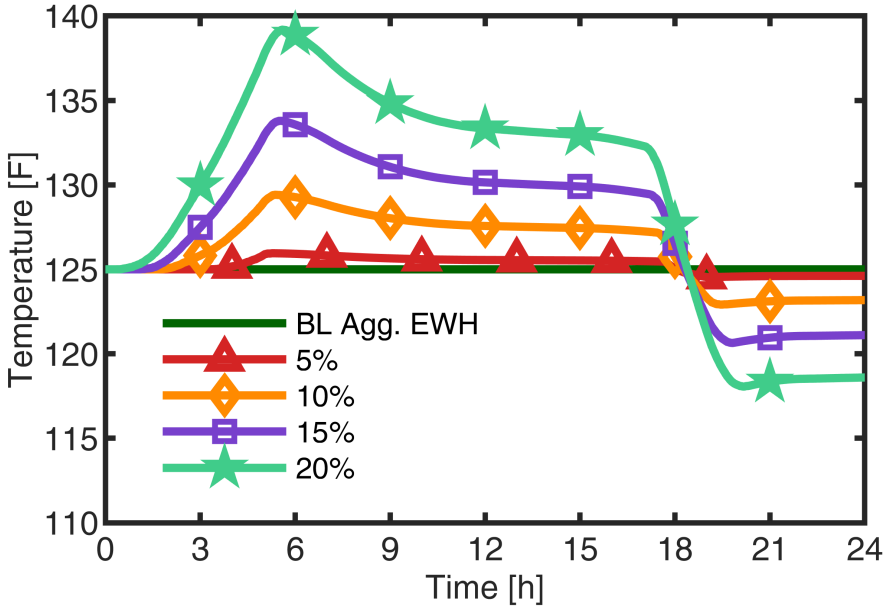

Figure 4.15: The average tank temperature of all the EWHs for different water heating schemes. Preheating in the morning led to higher temperature in the tank, resulting in more standby loss and lower tank temperature at the end of the day when the same amount of electricity was used for heating. Results show that the proposed heating schemes maintain the water temperature within the comfort and safety tolerances.

and lower temperature in the tank at the end of the day. Considering the benefits from peak reduction, the heat loss from preheating is worthwhile. In the case of 20% peak power reduction, the maximum average temperature reached approximately 140F, which can be realized through mixing valves. The lowest tank temperature for all the cases was 119F, which is satisfactory according to a study from the Department of Energy [178].

4.3.2 Reduction of Peak Power

In order to achieve higher peak power reduction, it is considered that all the heat pump EWH in the homes are replaced by equivalent resistive EWH. The Ref load USHs with the resistive EWH were calculated by subtracting the heat pump water

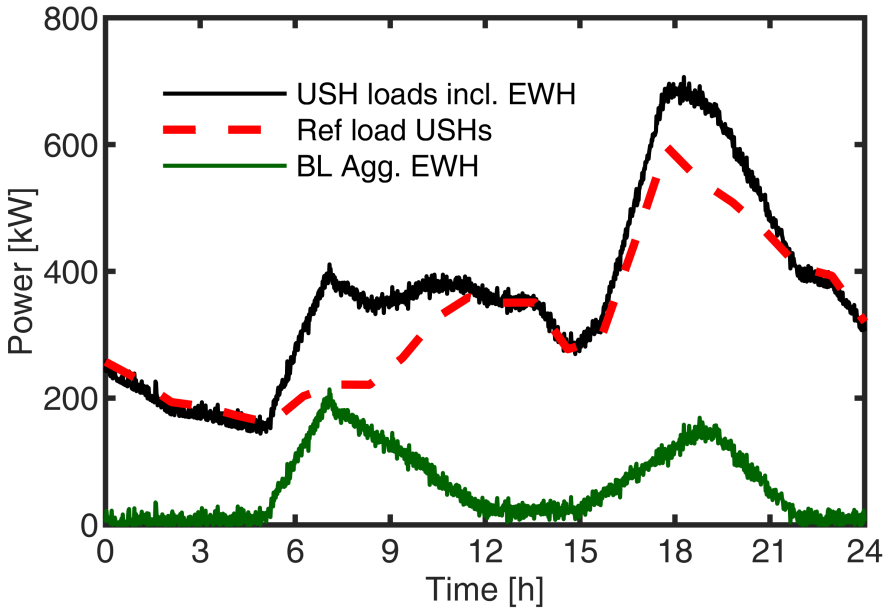

Figure 4.16: The aggregated EWH and residential loads. The experimental heat pump water heater load in the Ref load USHs curve was replaced by the BL aggregated EWH curve. The curve of USH loads with EWH stands for the aggregated residential loads where all USHs used purely resistive EWHs.

heater load from the measured load data (Fig. 4.16). The heat pump load was estimated as a constant value of 20kW. The USH loads with EWH which represent the aggregated load for a community where all houses have resistive EWH, were calculated by adding the estimated equivalent aggregated resistive EWH load to the Ref load USHs curve from Fig. 4.16.

The EWH power was shaved in the evening in order to reduce the peak demand, as shown in Fig. 4.17. The USH loads incl. EWH curve represents the baseline case where no peak reduction was applied. With peak reduction, the power in the evening was shifted to the morning. The aggregated water heating loads for different peak reduction targets were calculated in the previous section and presented in Fig. 4.14.

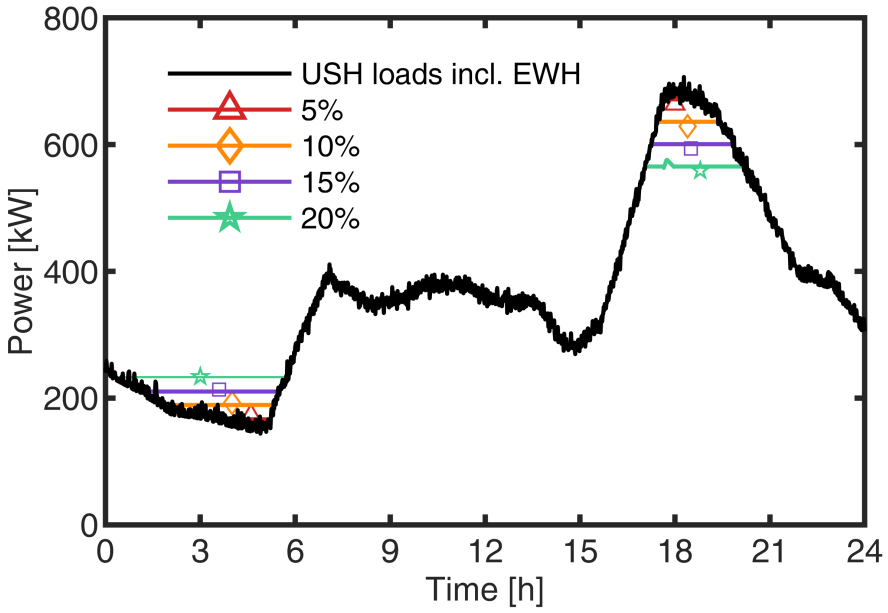

Figure 4.17: The aggregated total USH loads with different water heating schemes. Peak reduction was realized by shifting the water heating load in the evening to the early morning. It is worth noting that shaving the EWH loads reduced the peak demand by approximately 18% maximum in this example, missing the real target of 20%.

USHs can provide ancillary services by turning Off the EWHs. The minimum participating rate of EWH was estimated with the average EWH power of 1.5kW during the peak time. The minimum participation rates for USHs to turn Off EWH were 17%, 32%, 48%, 62%, for 5%, 10%, 15%, 20% peak reduction targets, respectively, as listed in Table 4.2. In the extreme case for 20% peak reduction target, even all the EWHs were turned Off at the critical hour, the power was only reduced by 18%, missing the 20% target. This is due to the fact that EWH can only shave its own power but can not supply other loads, unlike BESS. With all the EWHs turned off, further reduction in peak power is not feasible. Even with these limitations, EWH is still an attractive candidates for providing ancillary services due to its near ubiquity and low additional cost.

Table 4.2: The minimum requirement for USH participation

Peak reduction target (%)	Shaved power target (kW)	BESS PART. (%)	EWH PART. (%)
5	35	6	17
10	70	11	32
15	105	15	48
20	141	21	62

The same peak reduction was achieved by the BESS and results are shown in Fig. 4.18. All the BESSs were charged during the late night and early morning. When the load shaving control process started, all BESSs had the maximum SOC. In Fig. 4.18, only the discharging power is plotted. With the BESS controlled to provide ancillary services, both the maximum power and available energy were taken into consideration. The BESS power was estimated 4.8kW with the nominal voltage of 48Vdc and charging rate of 100A. The average BESS energy capacity was 16.2kWh and the SOC can vary from 94% to 20%. Therefore, the BESSs have the capability to provide approximately 12kWh energy on an average.

With the peak reduction target set to 5%, a total energy of 12kWh and a maximum power of 30kW were needed to be provided by the BESS. At least seven USHs were required to provide a peak power of 30kW, even one BESS would be enough to provide the required energy of 12kWh. The shaved energy during the peak hour were 12kWh, 49kWh, 114kWh, 210kWh for 5%, 10%, 15%, 20% peak reduction targets, respectively. Meanwhile, the shaved power levels were 35kW, 70kW, 105kW, 134kW for the same peak reduction targets. Therefore, the minimum participation rates of BESS were decided by the shaved power as 6%, 11%, 15%, 21% for the peak reduction targets, respectively, as listed in Table 4.2.

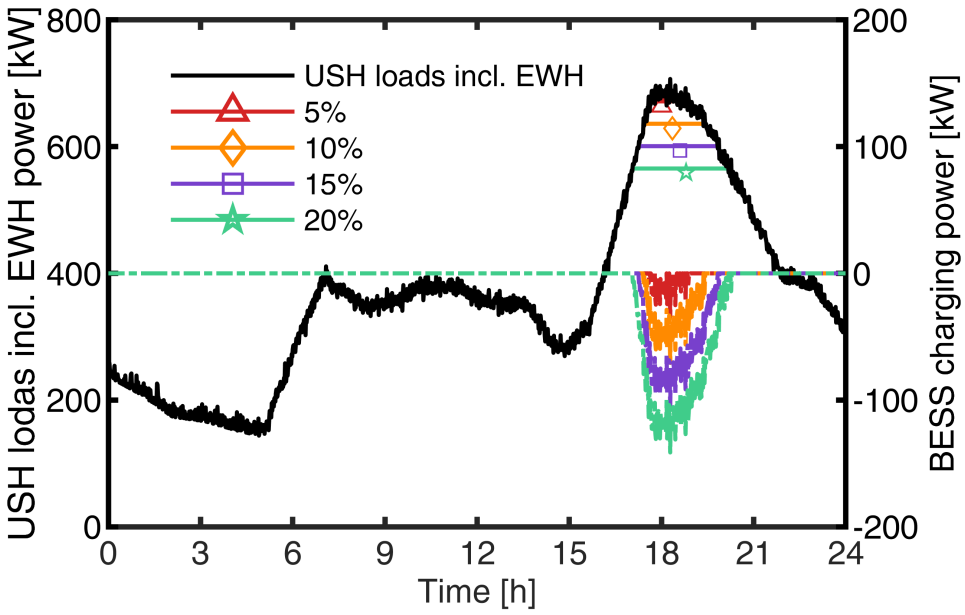

Figure 4.18: The aggregated total USH loads with peak reduction achieved by BESS. Only the discharge operation of BESS are shown.

It is shown that both BESS and EWH can provide ancillary services. Higher participation rates of EWH were required to realize the same peak reduction target. In this chapter, the maximum peak reduction achieved by the EWHs was 18% on the example summer day.

4.4 Modeling of HVAC Systems in Large Residential Communities

4.4.1 Experimental Results and Derivation of House Thermal Model Parameters

Beginning in 2008, TVA funded and managed a robotic house project with technical support from the ORNL. The robotic houses were constructed in a suburb of Knox County, TN in which the habitation of a family was physically emulated (Fig. 4.19).

Table 4.3: Parameters for the thermal model of the reference house

Parameter	Value
Thermal envelope area A_r	354 m^2
Coefficient of thermal resistance c_R	350 $^{\circ C \cdot m^2}/_{kW}$
Coefficient of thermal capacitance c_C	0.011 $^{kWh}/_{(^{\circ}C \cdot m^2)}$
Coefficient of heat transfer rate c_P	0.040 $^{kW}/_{m^2}$

This project developed an analytical base for energy optimization and new technology implementation at the individual house level. A different initiative, the SET project based in Glasgow, KY, provided a testbed for the optimization of power flow at the community level. In the TVA robotic house, energy usage for different components, including the HVAC, was measured on an hourly basis. The experimental data from SET had a 15-minute resolution.

The equivalent model that represents a typical residence, which was defined by parameters such as thermal envelope area, thermal resistance, thermal capacitance, and heat transfer rate, was derived from the TVA robotic house experimental data. The thermal envelope area is the only independent variable for the equivalent model. Other parameters for the equivalent thermal model were calculated using the thermal envelope area and coefficients, as follows:

$$R = \frac{c_R}{A_r}, \quad C = c_C \cdot A_r, \quad P_H = c_P \cdot A_r, \tag{4.8}$$

where R, is the thermal resistance; C, the thermal capacitance; and P_H, heat transfer rate. The other parameters are specified in Table 4.3.

The heat transfer function of the residential thermal model is described as follows:

(a)

(b)

(c)

(d)

Figure 4.19: The reference house (a). TVA robotic devices are controlled by computer programs to mimic realistic human behavior. Also shown is a shower emulator (b), automated dryer and washer (c), and a refrigerator with programmed arms (d) that activate according to automatic schedules.

$$C\frac{\mathrm{d}\theta_I(t)}{\mathrm{d}t} = \frac{1}{R}\Big(\theta_O(t) - \theta_I(t)\Big) - S(t)\cdot P_H, \tag{4.9}$$

where θ_I is the indoor temperature; θ_O, the outdoor temperature; S, the On/Off status of HVAC, defined as:

$$S(t) = \begin{cases} 0, & \text{if } S(t-1) = 1 \;\&\; \theta_I(t) \le \theta_L(t) \\ 1, & \text{if } S(t-1) = 0 \;\&\; \theta_I(t) \ge \theta_H(t) \\ S(t-1), & \text{otherwise,} \end{cases} \tag{4.10}$$

where θ_L and θ_H are the lower and upper band of the thermostat set point, of 70F and 74F, respectively for the TVA robotic house.

The data provided by the robotic house project has a resolution of 1-hour. Data from July of 2010 was used for the calculation of the parameters and the validation of the equivalent thermal model. The thermal resistance R was calculated assuming that the indoor temperature rate of change remained constant for every two consecutive hours, i.e., $d\theta_I(t) = 0$ in (4.9) through the whole month. Only hourly data for 12:00-16:00 of each day in July was used to estimate the coefficient of thermal resistance c_R, as during these times it is likely that the HVAC would be working, i.e., $S(t) = 1$ in (4.9). The calculated coefficient of the equivalent resistance based on the robotic house data is shown in Fig. 4.20. The solar heat gain as well as the latent and appliance heat gains were lumped together in the thermal resistance term.

The HVAC system for the reference house was modeled with fixed parameters (Table 4.3). The envelope area was calculated according to the floor plan. The coefficient of thermal resistance c_R was selected according to its relationship to outdoor

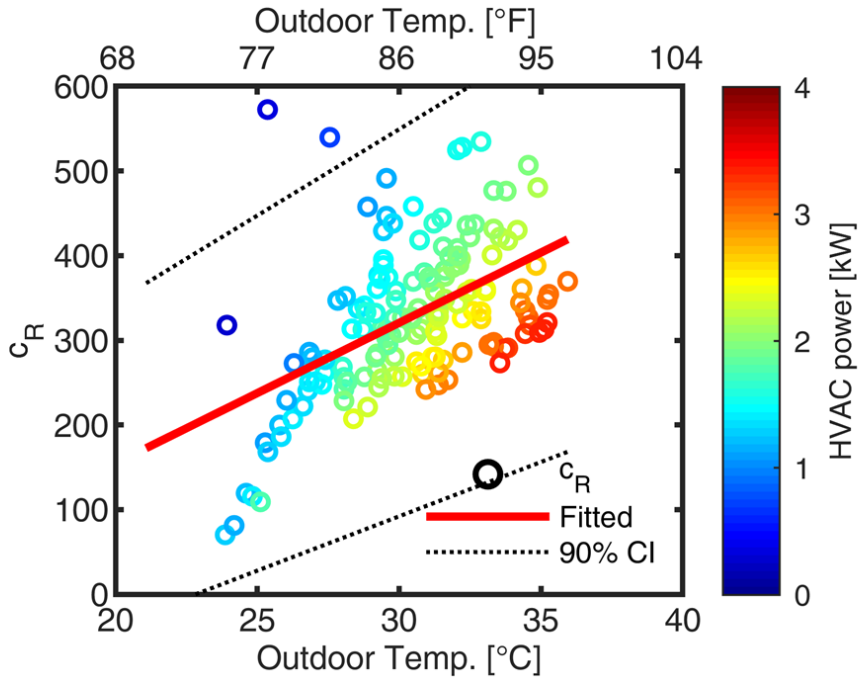

Figure 4.20: Analysis of the c_R equivalent thermal resistance coefficient for the reference house. Data corresponds to 5 hours during the time interval of direct interest for DR studies of each day in July 2010. Data was fitted with a 90% confidence interval, and only 2 points were outside the bounds.

temperature and justified with a confidence interval (Fig. 4.20). The c_C and c_P were adjusted based on the envelope area and recommended values [179]. With a cooling capacity of 4 tons and a Seasonal Energy Efficiency Ratio (SEER) of 13.5, the HVAC system had a constant input electrical power of approximately 3.6kW when it was On (Fig. 4.21). The developed HVAC model was simplified to have 1 stage process and only cooling is considered in the study.

For most of the days in Fig. 4.22, the outdoor temperature was high in the afternoon. The daily HVAC electricity usage for the experimental and simulated data are compared and presented in Fig. 4.23. Apart from the first few days and the last day when the outside temperature was relatively low, the simulation had highly satisfactory results.

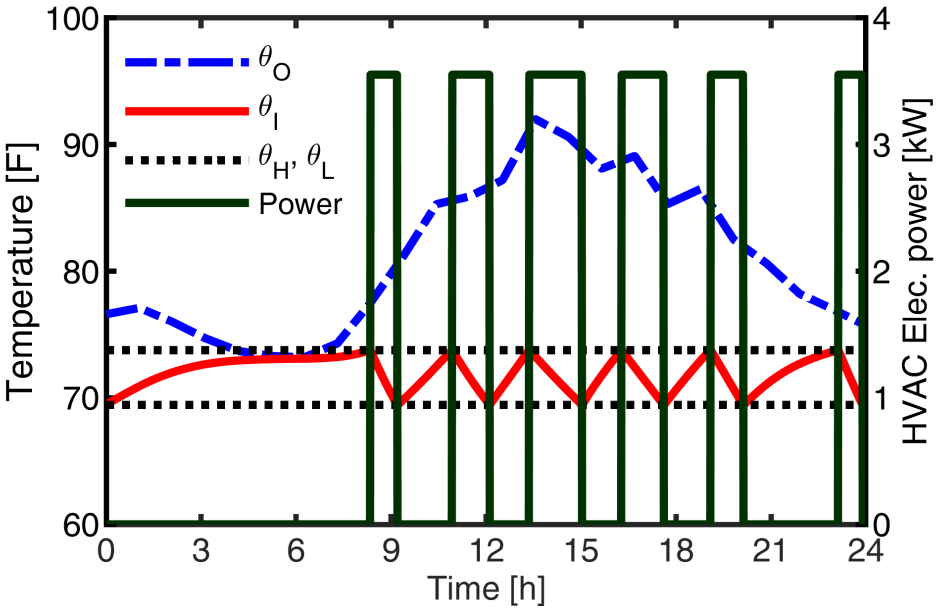

Figure 4.21: The daily simulation example of the HVAC system for the reference house. With a cooling capacity of 4 tons and a SEER of 13.5, the HVAC has approximately 3.6kW of constant electric power during operation.

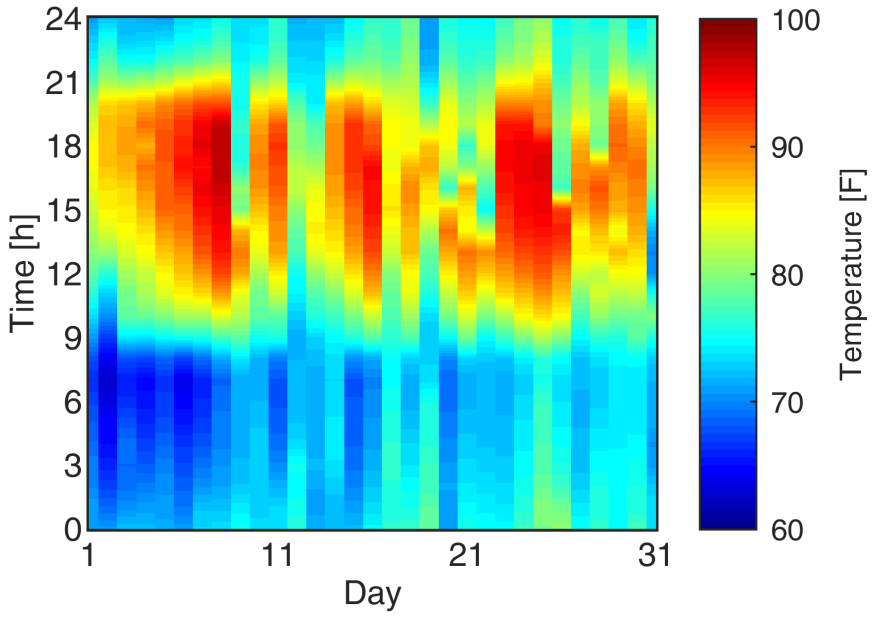

Figure 4.22: The outdoor temperature in July 2010 Knox County, TN. The temperature of this month was used for the calibration of the residential thermal model.

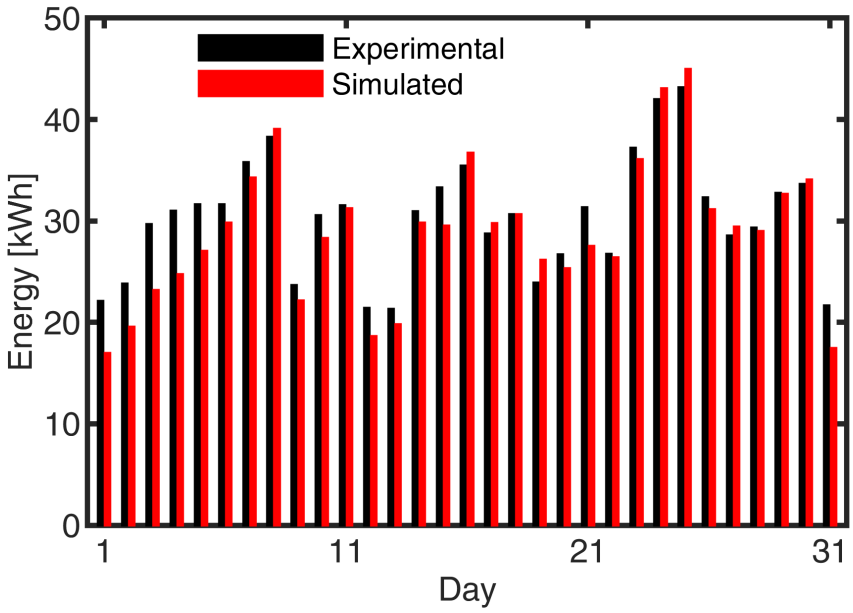

Figure 4.23: The daily HVAC electricity usage of the TVA robotic house in July, 2010. The simulation results were calculated using the proposed residential thermal model and parameters. The experimental data was retrieved from the robotic house project supported by TVA and ORNL.

Further study found that the proposed residential thermal model resulted in lower electricity daily usage for the HVAC when the outdoor temperature was both low and measured on an hourly basis. This occurred due to the cessation of HVAC operation during higher temperatures that were artificially reduced by the hourly temperature measurements. For example, if the thermostat set point was 75F and the outdoor temperature was 70F for half the hour and 80F for the other half, the experimental data would have the HVAC On for only the half hour. However, the averaged hourly based temperature data would be 75F, under which case the modeled HVAC would be Off the entire hour.

4.4.2 Modeling of Aggregated HVAC Load

Every single residence in this study was modeled separately based on (4.9) and

(4.10) with distinct sets of parameters. Each residential thermal model updates the indoor temperature dynamically considering the outside temperature, thermostat set points, and the DR signals. The aggregated HVAC power was calculated as:

$$P_A(t) = \frac{1}{SEER} \sum_{i=1}^{N} S^i(t) P_H^i, \tag{4.11}$$

where N is the total number of studied HVAC systems; P_H^i the heat transfer rate of house i in Btu/h.

The parameters of the thermal models across the community of residencies were selected to be either a specific constant value, normally distributed, or uniformly distributed (Table 4.4). The values for some parameters of the residential thermal models were the same for all considered houses, i.e., the coefficients c_C and c_P, and the lower limit set point θ_L. The upper limit set points θ_H of all the houses without DR control were randomly generated to represent different user preference, noted as uniform distribution $\mathcal{U}(74F, 78F)$. The initial indoor temperatures were randomly generated within the lower limit of thermostat set point, 70F, and the lowest of the upper limit set points, 74F, noted as uniform distribution $\mathcal{U}(70F, 74F)$. Therefore, the initial temperature for all residences were bounded to the lower and upper set points.

The distribution types and parameters related to the house construction, A_R and c_R, were selected so that the simulation results matched the experimental data from the SET project. The A_R and c_R for the considered HVAC system models were subject to normal distributions and noted as $\boldsymbol{A_R} \sim \mathcal{N}(354, 200^2)$ and $\boldsymbol{c_R} \sim \mathcal{N}(350, 280^2)$. The daily electricity usages for each of the 10,000 HVAC systems in the example case were

Table 4.4: Thermal model parameters distributed values for the large amount of residences considered

Parameter	Value (distribution)
Coefficient of thermal capacitance c_C	$0.011\ {}^{kWh}/_{(^\circ C \cdot m^2)}$
Coefficient of heat transfer rate c_P	$0.040\ {}^{kW}/_{m^2}$
Lower limit set point θ_L	70F
Upper limit set point θ_H	$\mathcal{U}(74F, 78F)$
Initial indoor temperature $\theta_I(0)$	$\mathcal{U}(70F, 74F)$
Thermal envelope area A_R	$\mathcal{N}(354, 200^2)$
Coefficient of thermal resistance c_R	$\mathcal{N}(350, 280^2)$

calculated and summarized into a histogram with a box size of 1kWh (Fig. 4.24). Both the experimental data and the simulation results were fitted to a nonparametric kernel-smoothing distribution and their probability density function (PDF) curves are presented in Fig. 4.24 as well. The comparison between the PDF curves of the simulated data and that of the experimental data demonstrates satisfactory results.

Algorithm 4.1 Calculate the energy storage capacity of the HVAC system

Set $\theta_O(t) = \theta_{O,F}$, $\theta_I(0) = \theta_{max}$, $m = 0$
while $\theta_I(m) > \theta_{min}$ **do**
    $m = m + 1$;
    $S(m) = 1$;
    calculated $\theta_I(m)$ in (4.9);
end
The energy capacity $E_C = P_H/COP \cdot \Delta t \cdot m$

The energy storage capacity for each of the 10,000 HVAC systems was decided by their distinct sets of thermal model parameters, as described previously, and was calculated separately using the methods introduced in Algorithm 4.1. The results were summarized into a histogram (Fig. 4.25) to represent the community. The average energy storage capacity for the 10,000 HVAC systems is approximately 11kWh. Given that the typical energy consumption for HVAC systems is calculated at around

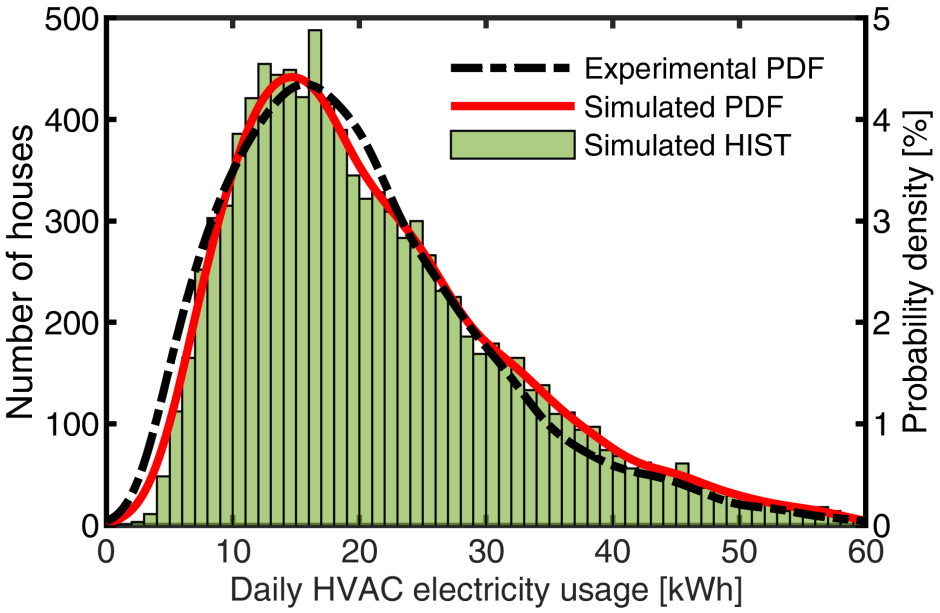

Figure 4.24: The distribution of daily HVAC electricity usage on a typical summer day for 10,000 houses in a large community case study. The experimental probability density function (PDF) is estimated based on daily residential electricity usage from the SET project on the same day. The average electricity usage is approximately 21kWh based on the simulation.

21kWh, the HVAC system as an energy storage device was charged/discharged approximately two rounds on the typical summer day in this study.

The simulated working status for the 10,000 participating HVAC systems without DR are shown in Fig. 4.26. In the early morning, even though the outdoor temperature was higher than the set point, not every HVAC turned On due to the thermal inertia of the house. At approximately 9:00, many HVACs started to turn On as the outdoor temperature increased quickly and the homes installation and shading could not prevent or slow heat transfer any longer.

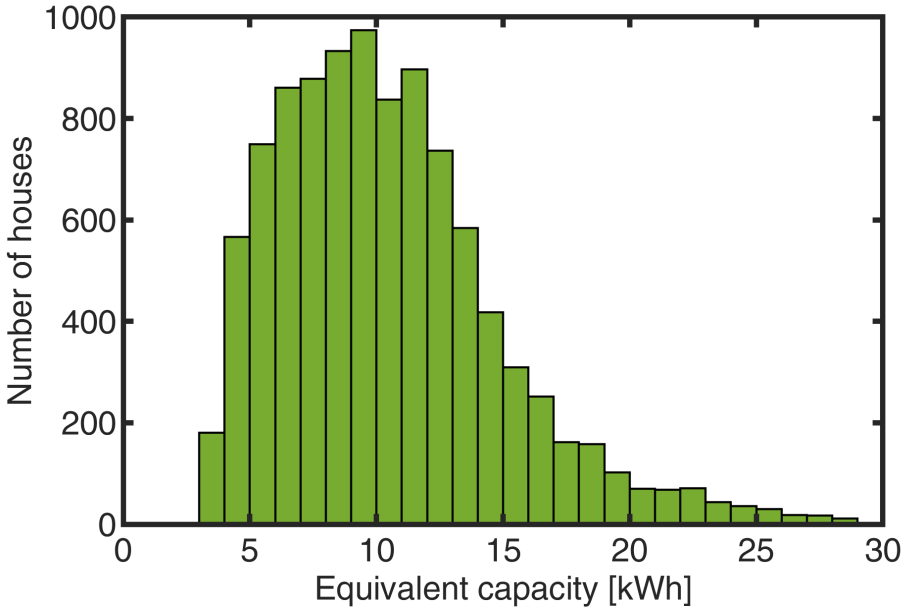

Figure 4.25: The distribution of the energy storage capacities of the HVAC systems for 10,000 houses in a large community case study. The energy storage capacity of each residence was calculated separately according to its own set of parameters. The average equivalent energy capacity of the HVAC systems is approximately 11kWh.

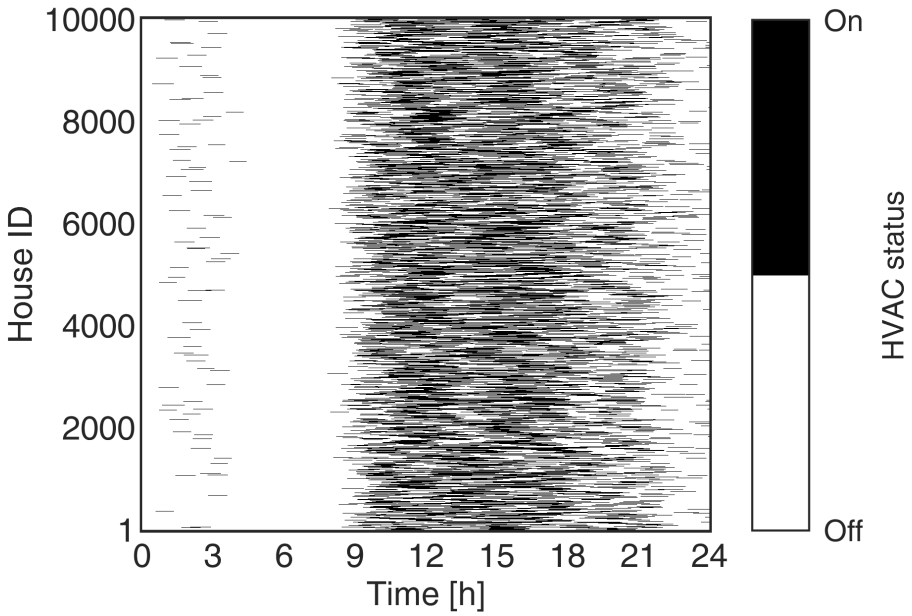

Figure 4.26: The working status for the simulation of 10,000 participating HVAC systems without DR. Most of the HVAC systems started turning on around 9:00 due to the increase in outdoor temperature.

4.5 VPP Control for Large Residential Communities using HVAC Systems as Equivalent Energy Storage

4.5.1 HVAC System as Equivalent Energy Storage

For uniform control of various devices and appliance in typical residences, the HVAC system may be described as equivalent energy storage, and its equivalent SOC is defined as:

$$SOC(t) = \frac{\theta_{max} - \theta_I(t)}{\theta_{max} - \theta_{min}}, \tag{4.12}$$

where the θ_{max} and θ_{min} are the maximum and minimum room temperature, respectively. In this study, the lower thermostat set point always has the same value as the minimum room temperature. The upper thermostat set point varies for different user preferences, and is set to the maximum room temperature only under the DR control.

The concept of equivalent SOC of the HVAC system is illustrated in Fig. 4.27. When the HVAC system is operating in the cooling mode, the maximum and minimum room temperature correspond to the equivalent SOC of 0% and 100%, respectively. The room temperature increases due to the higher outside temperature when the HVAC is Off, and this is the equivalent procedure of discharging the energy storage. When the HVAC is On, the room temperature decreases in most of the normal cases and correspondingly, the equivalent SOC increases.

The energy capacity of a HVAC system is defined as the **input electricity** needed

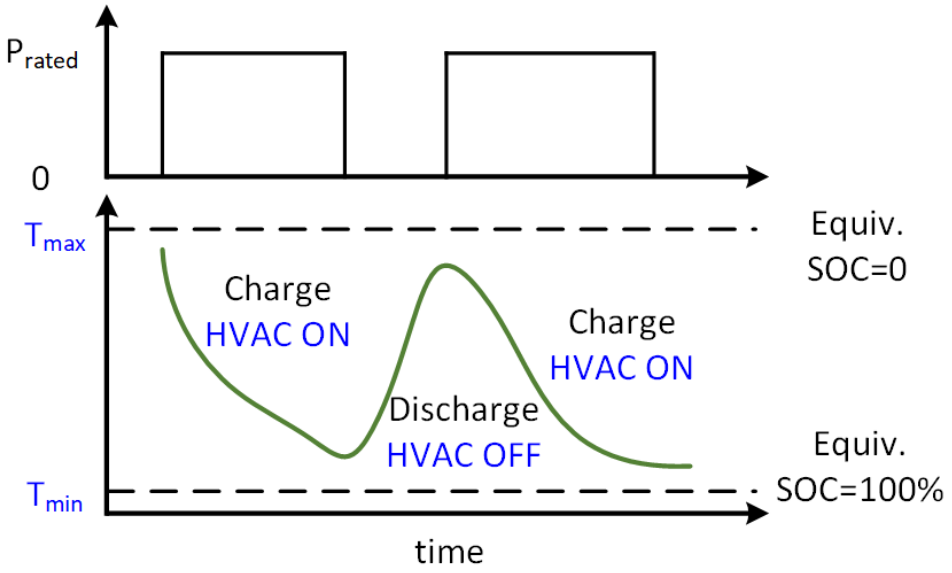

Figure 4.27: The HVAC system as energy storage when cooling. The maximum and minimum room temperature correspond to the equivalent SOC of 0% and 100%, respectively. When the HVAC is On, the room temperature decreases, as the equivalent of charging procedure of the BESS. On the contrary, the equivalent BESS "discharges" as the room temperature increases when the HVAC is Off.

to change the room temperature from the maximum to the minimum with a fixed outside temperature. The pseudocode for the calculation is shown in Algorithm. 4.1. The energy capacity of the HVAC system for each house is calculated with its own set of parameters.

In this study, the outside temperature $\theta_{O,F}$ for the calculation of the HVAC energy capacity is fixed to 86F, as this is the average outdoor temperature in Glasglow, KY during the month of July when this DR study takes place [180]. The lower thermostat set point is fixed to 70F for all the HVAC systems.

The maximum room temperature θ_{max}, was selected to be 81F as this is the highest indoor temperature that results in a comfortable PMV rating under typical conditions for July as calculated by the online CBE Thermal Comfort Tool that follows ASHRAE Standard 55 [181]. A typical relative humidity of 54%, clothing

level of 0.5 clo representing common indoor summer wear, an air speed of 0.1 m/s, and metabolic rate corresponding to sitting were used to verify that 81F results in a PMV rating of 0.46 PMV. This is classified as acceptable as it is less than 0.5 PMV, meaning that 90% of people on average would be comfortable according to the ASHRAE Standards. The operative temperature was assumed equal to the indoor temperature or slightly lower, indicating the occupant would either be by a neutral or cool surface such as an interior wall out of sunlight or piece of furniture.

First in the equivalent energy storage study, the initial room temperature is set to the maximum and the HVAC is kept On until the room temperature reaches the minimum. The required number of steps is recorded and used together with the heat transfer rate and the simulation resolution to calculate the energy capacity of the HVAC system. It is worth noting that the energy capacity is defined as the required **electricity**, therefore, the HVAC electric power, which is calculated as P_H/COP, is used for the calculation. The coefficient of performance (COP) and SEER are interchangeable.

The equivalent SOC of the HVAC system in the daily simulation example (Fig. 4.21) is shown in Fig. 4.28. In the morning, the HVAC was Off and the room temperature increased until around 8:00, and the equivalent SOC decreased accordingly. When the HVAC was On, the room temperature was decreased until it reached the lower thermostat set point. As a result, the equivalent SOC increased to 100%. The equivalent SOC did not drop below 60% in this example, indicating the potential to deepen "discharge" of the HVAC system through a control scheme.

The upper thermostat set point was set to the maximum room temperature during

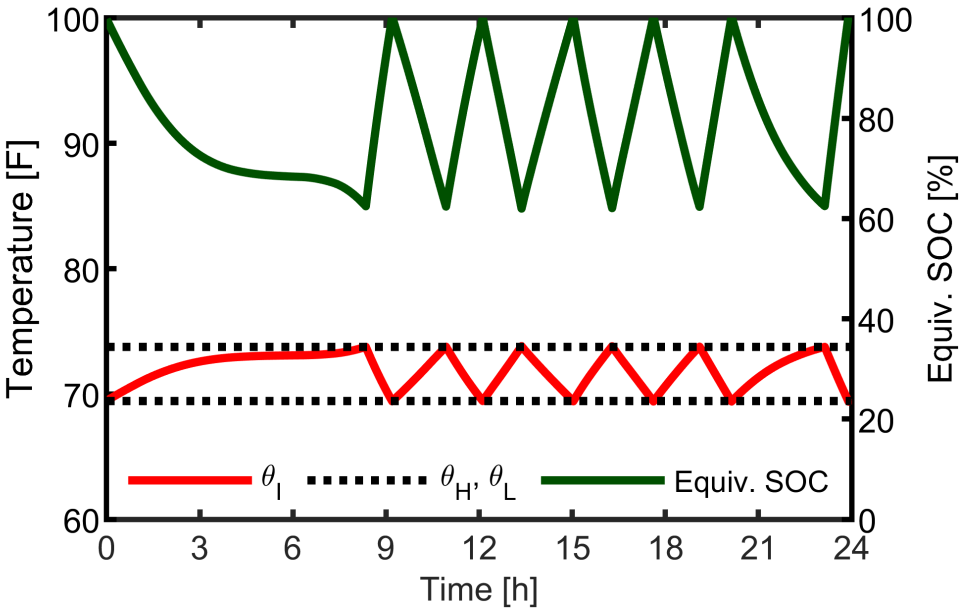

Figure 4.28: Illustration of the relationship between room temperature and equivalent SOC based on the results shown in Fig. 4.21. The equivalent SOC was 100% when the room temperature reached the lower thermostat set point. The lowest equivalent SOC could be as high as 60% with a fixed upper thermostat set point, indicating the potential of deeper "discharge".

11:00–16:00 for the DR control and the results are shown in Fig. 4.29. The equivalent SOC reached 0% as the room temperature became the maximum. The house could shed the HVAC power for a longer period of time by "discharging" the equivalent SOC to 0%.

4.5.2 Optimal Control of the HVAC Systems

Two objectives were considered for VPP controls. The first is to reduce the peak power in the afternoon during 12:00 to 16:00:

$$\text{Minimize } P_{max} = \max\Big(P_A(t)\Big),\ t \in [12:00, 16:00]. \tag{4.13}$$

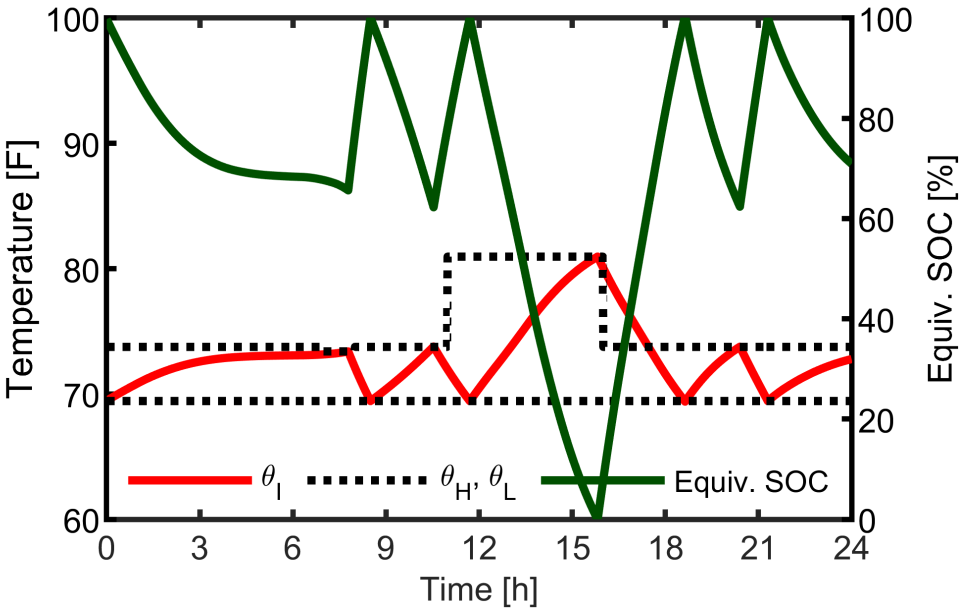

Figure 4.29: The room temperature and equivalent SOC for the HVAC system with the sequential DR control. The equivalent SOC of the HVAC system could reach 0% by changing the upper thermostat set point to the maximum room temperature.

The second is to reduce the ramping rate of the aggregated HVAC power for the entire day:

$$\text{Minimize} \quad \Delta P_{max} = \max\left(\frac{P_A(t+\Delta t) - P_A(t)}{\Delta t}\right), t \in [0:00, 24:00]. \quad (4.14)$$

The objectives are realized by central control system that could be operated by a utility and generates the DR signals for each residence according to one-day ahead weather forecasting data. The DR control signals for each house include the upper limit thermostat set point, $\theta_{H,DR}$. When the DR event occurs in this study, the upper limit thermostat set point of the committed residence was changed to $\theta_{H,DR} = 73$F for precooling and 81F for peak reduction.

In this study, residences committed to the DR control will not overwrite the signals from the utility, for three reasons. First, residences committed to DR control enjoy

financial rewards and are bounded by contract [92]. Second, under the DR control, the room temperature would still be kept comfortable for most of the users according to ASHRAE standards as described in the previous section. Third, the DR signals from the utility will only be implemented at each house for short durations of time.

Houses are divided into multiple groups, and each group has its own scheduled time to apply the DR control by changing the upper limit thermostat set point. The HVAC systems in the same group apply the DR control for the same period of time. The next group of HVAC systems apply the DR control after a fixed time gap. The behavior of HVAC systems during a DR event is described as follows:

$$\begin{cases} \boldsymbol{\theta_H^1}(t_1) = \theta_{H,DR},\ t_1 \in [T_S, T_E] \\ \boldsymbol{\theta_H^2}(t_2) = \theta_{H,DR},\ t_2 \in [T_S + \Delta T_S, T_E + \Delta T_E] \\ \ldots \\ \boldsymbol{\theta_H^{n+1}}(t_{n+1}) = \theta_{H,DR},\ t_n \in [T_S + n\Delta T_S, T_E + n\Delta T_E], \end{cases} \tag{4.15}$$

where n is the group number; $\boldsymbol{\theta_H^n}$, the upper limit thermostat set points for all houses in group n; T_S and T_E are the times when the 1st group starts and ends the DR, respectively; ΔT_S, ΔT_E are the time gap between two groups to start and end DR, respectively.

In the example case, the 10,000 houses committed to DR control were divided into 100 groups, and each of their upper limit thermostat set points are shown in Fig. 4.30. The horizontal stripes indicate different customer preferences for indoor temperature. Two DR events were applied by changing the upper limit thermostat set points as shown by the blue and red vertical lines. The first DR event occurred in the morning as the upper limit thermostat set points of the first group were reduced

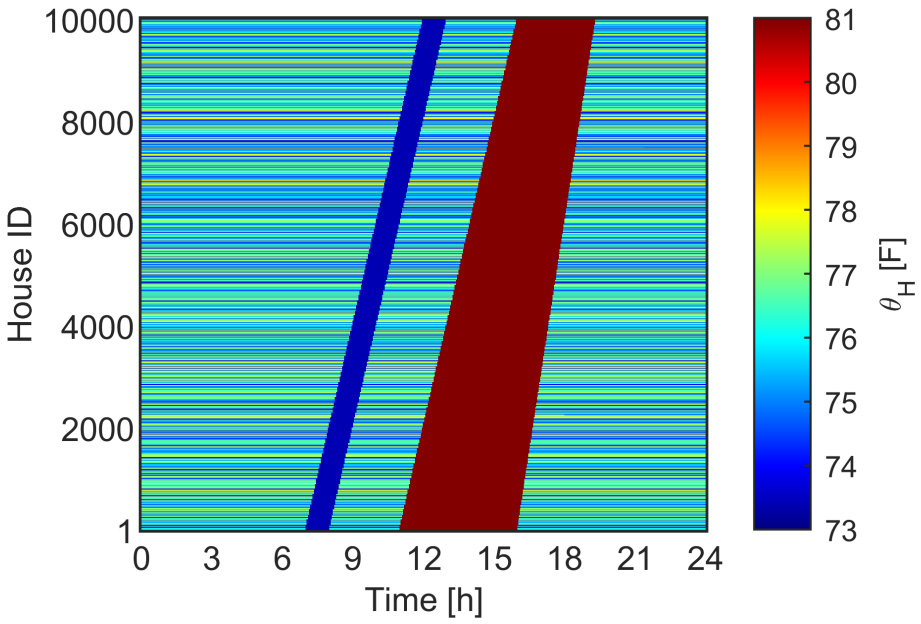

Figure 4.30: The upper limit thermostat set points for all the 10,000 HVAC systems within the proposed sequential DR control. The different set points indicate the various user preferences. The values were set to low in the morning for precooling, and set to high in the afternoon to reduce the peak, both in a sequential way.

to 73F from 7:00 to 8:00. Other groups followed sequentially by reducing their set points after a fixed time gap of 3 minutes between control adjustments, i.e., group two 7:03–8:03, group three 7:06–8:06, etc. Since there are 100 groups, the last batch of residences were precooled from 12:00–13:00.

The second DR event occurred in the afternoon for peak reduction between 12:00 and 16:00 (Fig. 4.30). Starting from 11:00, the first group of the HVAC systems increased the upper limit thermostat set point to 81F. Other groups increased their set points at a fixed time gap of 3 minutes, in a sequential way. The first group reverted to the original set points at 16:00 and other groups followed with a fixed time gap of 2 minutes, in the proposed staggered pattern. The time gaps to implement the DR control and to resume the original set point of the user are intentionally different

to demonstrate the flexibility of the proposed sequential control.

It is worth noting that the DR signal for precooling and peak reduction in this case overlapped between 11:00 and 13:00, for three reasons. First, the precooling was for the reduction of ramping rate. Therefore, if the duration of precooling DR is short, the ramping rate would be large as many HVAC systems are turned On in a short period of time. Second, if the precooling starts very early, the natural process of heat transferring from outside to the residence will start before the temperature outside has risen to an uncomfortable level, leading to unnecessary additional electricity usage. Third, the overlapping structure provides a buffer time to avoid sudden drops in the aggregated HVAC power.

4.5.3 Results and Analysis for VPP Operation

The time step for the simulations in this section is 1-minute. The simulation results were integrated to 15-minute resolution, which is the conventional time interval used by utilities in metering, to calculate the ramping rate. When 100% of the 10,000 residences participated in the DR control, the working status of the HVAC systems are shown in Fig. 4.31. The proposed sequential DR control resulted in three clear stripes of HVAC state changes, namely, the one starting at 7:00, the one at around noon, and the one starting at 16:00. The HVAC systems were turned On and Off in a sequential way in order to avoid sudden changes of the aggregated power when the thermostat set points were changed by the DR control.

The same 10,000 HVAC systems were simulated using the same outdoor temperature both with and without DR control. The outdoor temperature and average

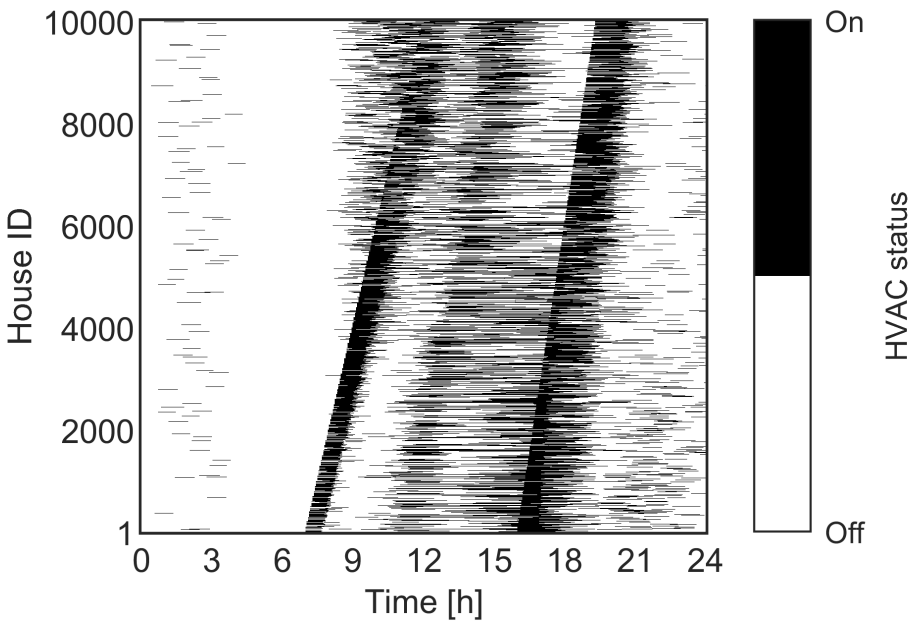

Figure 4.31: The working status for the simulation of 10,000 HVAC systems in a DR study with centralized controls. HVAC systems were turned On/Off in a sequential way, reducing the ramping rate and the peak load.

indoor temperatures for both cases are shown in Fig. 4.32. Also shown are the simulated indoor temperatures of individual houses with the DR control. In the study, the lower limit thermostat set point was fixed to 70F for all the houses. The upper limit thermostat set points for all the 10,000 houses were uniformly distributed in the range of [74F, 78F] in order to represent various user preferences.

When the DR signal arrived in the afternoon, the upper limit thermostat set points for the batch of houses under control were set to 81F. In Fig. 4.32, only the highest value of the upper limit thermostat set point from all the residences at each time step was plotted. For example, when there was no DR signals, the upper limit thermostat set points for all houses are between 74F and 78F ($\theta_H \in [74F, 78F]$). When there was DR signal for precooling in the morning, $\theta_H \in [73F, 78F]$, and where the DR signal was for peak reduction, $\theta_H \in [74F, 81F]$. The θ_H in the plot was 81F when there was

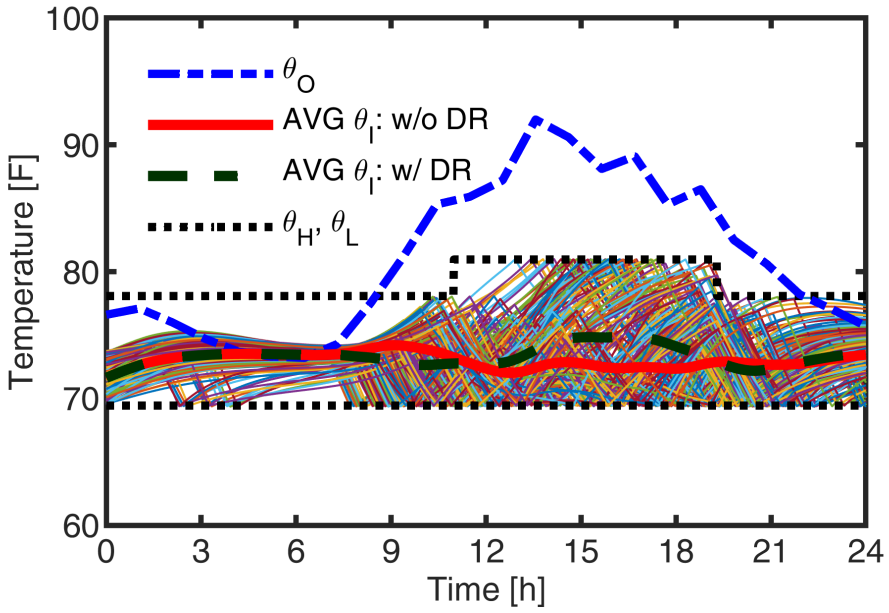

Figure 4.32: The outdoor temperature and average indoor temperatures of the 10,000 simulated HVAC systems. For the DR program, indoor temperature was allowed to be higher but still acceptable according to ASHRAE standards.

DR control for peak reduction in the afternoon, and 78F for other durations.

The selection of the maximum allowed indoor temperature, which is 81F for the illustrated example, is based on a combination of human comfort regulations, as per ASHRAE Standard 55-2017, and user behavior preferences, as expressed through enrollment in different DR schemes that trade comfort controls versus unitary electricity cost [17]. It should be noted that the average temperature for all homes does not exceed 75F at any time and that only very few homes, which selected a minimum electricity cost DR program option, reach the 81F maximum temperature after 17:00, and even then, only for a very short duration of time.

The indoor temperature of all 10,000 residences were presented with a sampling frequency of 30-minute in boxplot (Fig. 4.33). When the residences were precooled (bottom), their indoor temperatures were lower at around 9:00, which allowed more

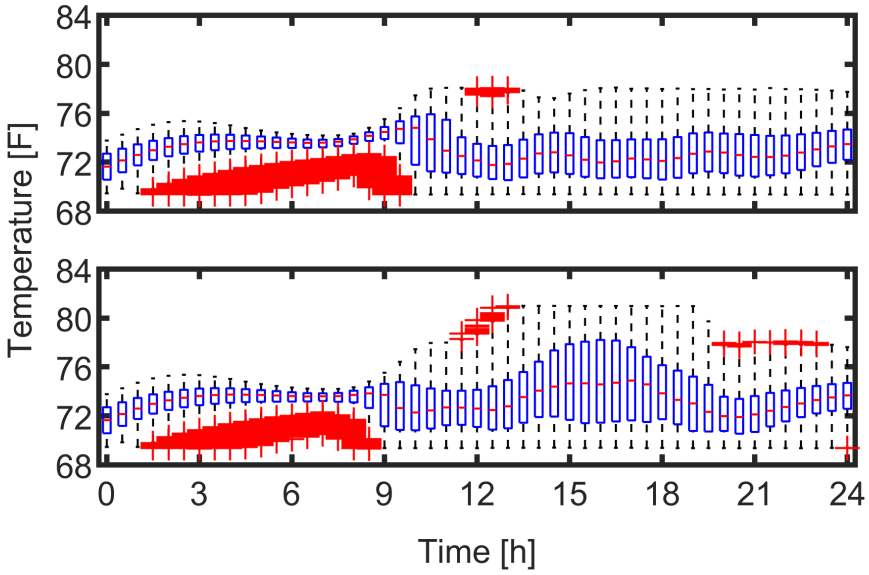

Figure 4.33: The indoor temperature variations of all 10,000 residences (top: without DR control, bottom: with DR control). The effect of precooling can be spotted around 9:00, and the effect of peak reduction can be observed in the afternoon.

HVAC systems to stay Off and reduced the ramping rate. In the afternoon, the maximum indoor temperature of some residences reached 81F under the DR control, which was the highest temperature still acceptable for most users under the conditions explained in the previous section. Even so, given any time point, the indoor temperature for 75% of the residences was no more than 78F, which appeared at 16:00.

The equivalent SOC for the houses without DR is shown in Fig. 4.34. The HVAC systems operated as energy storage devices were "discharged" at different levels due to the various upper limit thermostat set points. None of the houses were "discharged" thoroughly to 0% without DR control.

Some of the HVAC systems were thoroughly "discharged" to 0% at the critical

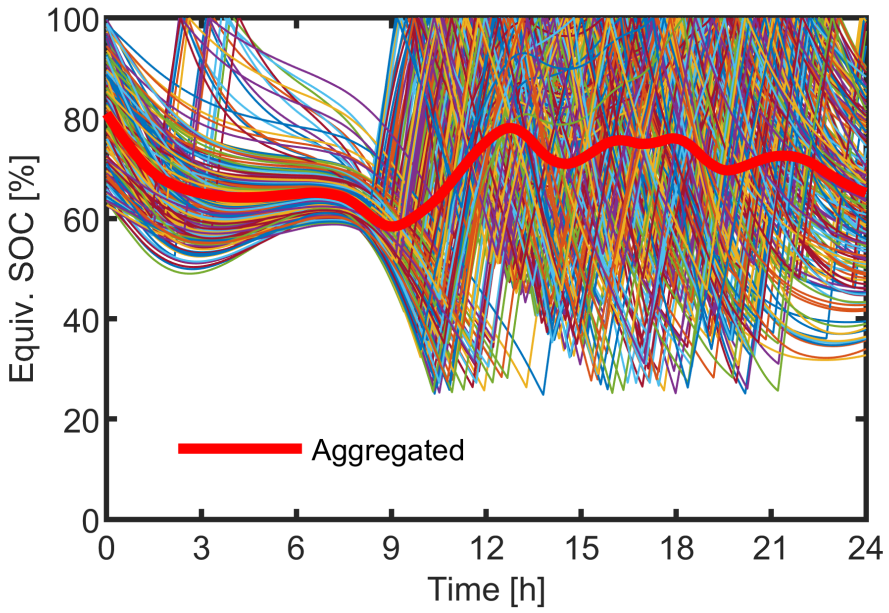

Figure 4.34: Simulation results of the equivalent SOC for the 10,000 HVAC systems studied without DR control. None of the houses were "discharged" thoroughly during the peak hour.

hours due to the DR control, as shown in Fig. 4.35. The sequential control implemented in this study avoided "discharging" all the HVAC systems to 0% at the same time, in order to avoid the large rebound ramping rate afterwards. The aggregated SOC started to decrease from 12:00, indicating the equivalent "discharging" process as use of stored energy. This demonstrates that the HVAC systems could operate comparably with the batteries.

The proposed sequential DR control strategy is exemplified by this study that successfully results in a very large reduction of the peak power from 12:00 to 16:00 through temporarily allowing higher temperatures inside the participating homes. The indoor temperatures in Fig. 4.32 were the results for 100% participation of 10,000 residences on an example summer day. The corresponding aggregated HVAC power and equivalent SOC are shown in Figs. 4.36 and 4.37 with different residence

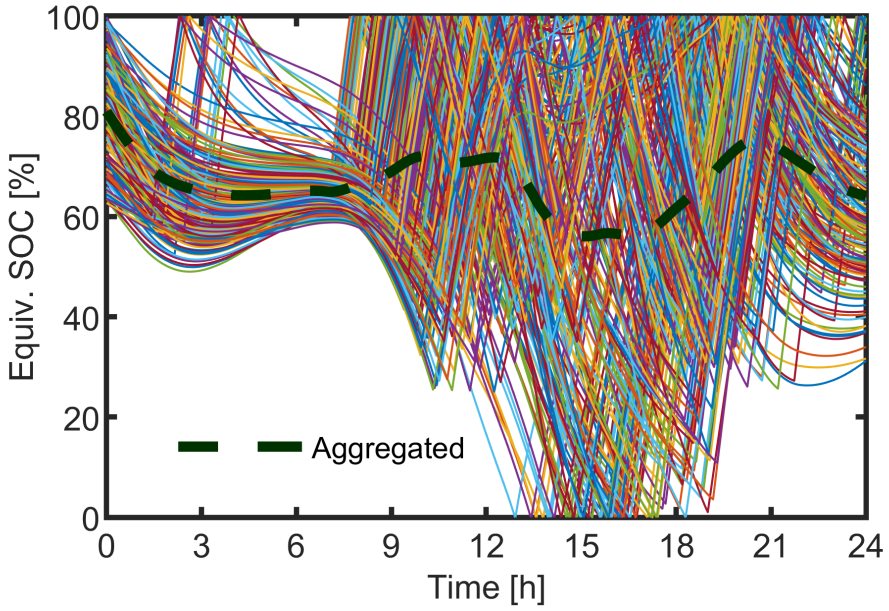

Figure 4.35: Simulation results of the equivalent SOC for the 10,000 HVAC systems with DR control. Houses were fully "discharged" as the equivalent SOC reached 0% at different period of time. The aggregated equivalent SOC did not reach 0% because not all the houses were fully "discharged" at the same time. The sequential DR control was implemented to avoid the large rebound ramping rate afterwards.

participation for the same day. The simulation results for different residence participation levels are summarized in Table 4.5 where it can be seen that the ramping rate and total daily electricity usage are decreased with more participation. The residences participating in the simulated DR program were selected based on their house ID in ascending sequence in this study.

The aggregated HVAC power from Fig. 4.36 shows that, under normal operation

Table 4.5: Summary of simulation results for different residence participation

Participation [%]	P_{max} [MW]	ΔP_{max} [MW/15-min]	Daily Elec. [MWh]
0 (w/o DR)	21.3	36.2	213
25	20.1	31.6	211
50	18.9	29.7	208
75	18.1	25.3	206
100	16.8	23.4	203

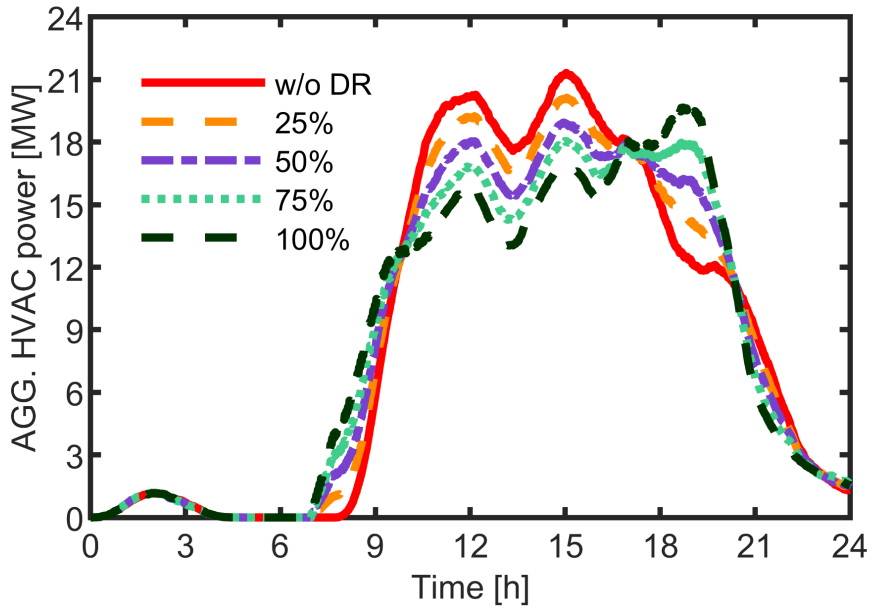

Figure 4.36: Simulation results of aggregated HVAC power for the 10,000 houses studied on 7/14 with different residence participation. The legends stand for the residence participation in DR control. Detailed simulation results are summarized in Table 4.5.

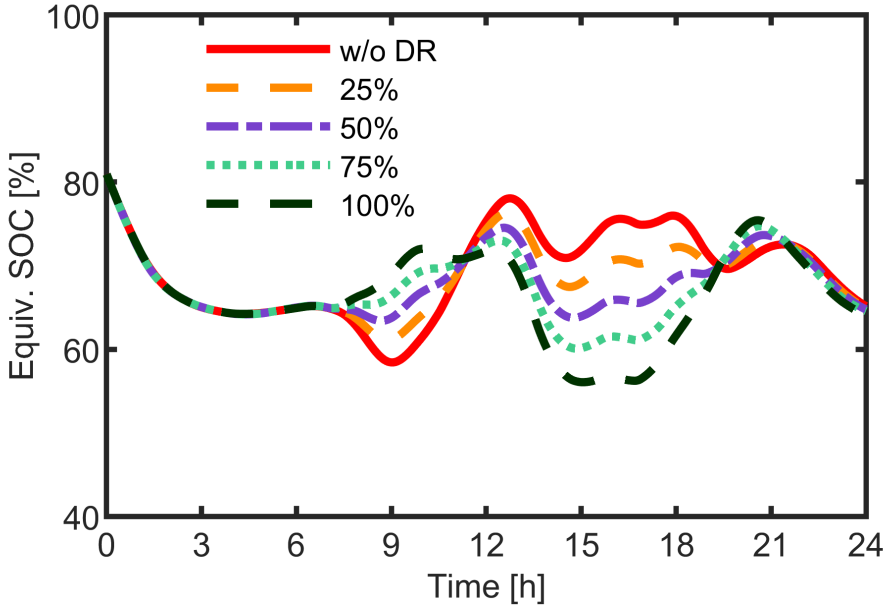

Figure 4.37: Simulation results of the aggregated equivalent SOC for the 10,000 HVAC systems studied on 7/14 with different residence participation.

without DR controls, the ramping rate around 8:00 was large due to many HVAC systems starting around the same time, and the peak power from 12:00 to 16:00 was high due to high outdoor temperature. The ramping rate, peak power in the afternoon, and the total daily HVAC electricity were reduced under the proposed sequential control, even with low residence participation. When the participation rate is high, e.g., 100%, the peak power period for the DR case was shifted to a later time as a consequence of indoor temperature recovery, and in addition, the ramping rate was greatly reduced.

The aggregated equivalent SOC of the 10,000 HVAC systems shown in Fig. 4.37 demonstrates the effectiveness of the proposed sequential DR control scheme, which provided benefit to the utility as described while still resulting in a near 65% aggregated equivalent SOC as was the same as on the day before DR was applied. Another important note is that the total energy storage capacity for the 10,000 residences was fixed because the energy capacity of each HVAC system was fixed, as explained in Section 4.5.1. The equivalent precharging process, which started from 7:00, avoided significant power draw at 12:00 and large ramping rate starting from 9:00. The peak power in the afternoon from 12:00 to 16:00 was reduced by the equivalent discharging process. The proposed sequential DR control managed to postpone the equivalent charging process to 18:00.

The outside temperature is stochastic and, therefore, the DR control scheme for the simulation of aggregated HVAC power as an energy storage resource was repeated on two additional different hot days in the summer (Fig. 4.38). In this study, the proposed sequential control was demonstrated in the hot days because the fuel for

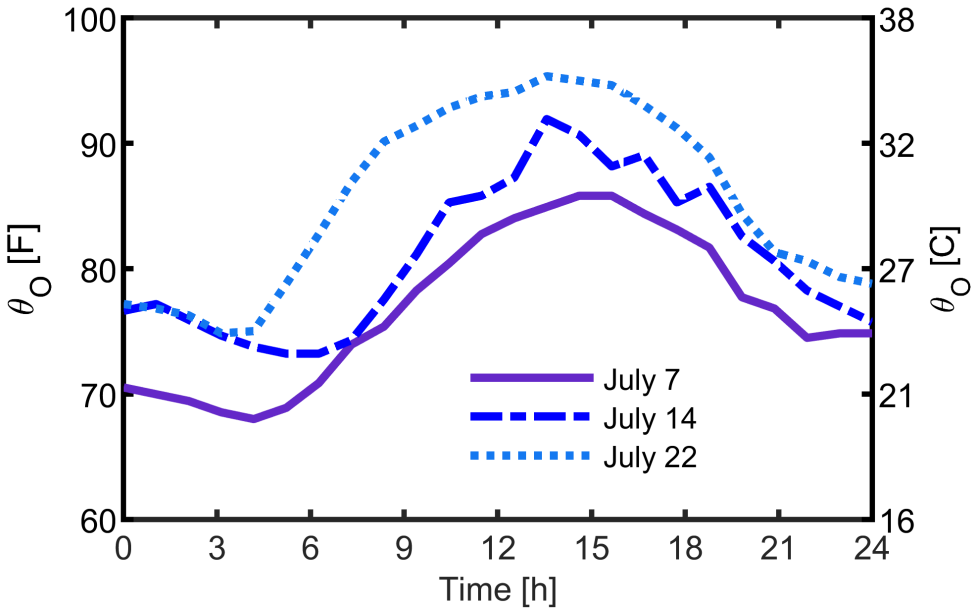

Figure 4.38: Outside temperature of example days selected from the experimental data from Glasgow, KY, in the year of 2017. The proposed sequential control was tested on the days with high outside temperatures when the HVAC systems tend to have high cooling power demand.

space cooling is 100% electricity, and the peak reduction is only needed when the HVAC systems have high power. The proposed sequential control was not shown for cold days as some of the residences might use fuels other than electricity for heating [182]. Therefore, the results of the sequential control for cooling are directly related to the number of residences participating in the DR control, while for heating, the portion of electricity-heating houses must be considered.

The simulation results for different summer days are presented in Fig. 4.39 and summarized in Table 4.6. In this comparison, the DR control participation was considered 100%. The case study for w/o DR and 100% participation in Fig. 4.36 and Table 4.5 is referred as "Day: 7/14" (middle).

The case "Day: 7/7" (top) represents a slightly cooler summer day. The proposed

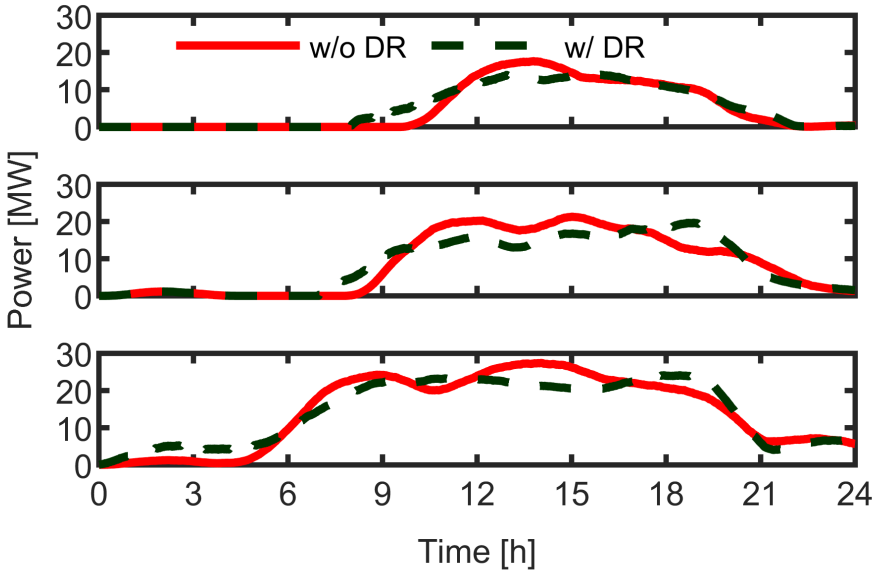

Figure 4.39: Simulation results of aggregated HVAC power for the 10,000 houses studied on different hot days (top to bottom: 7/7, 7/14, 7/22). The ramping rate in the morning, as well as the peak power in the afternoon from 12:00 to 16:00 were reduced. Detailed simulation results are summarized in Table 4.6.

sequential control reduced the already low ramping rate by precooling and peak power by turning On the HVAC systems in batches during a longer time span. The total daily electricity usage was increased by 2% under the proposed DR control due to the precooling. This happened because lower temperature in the morning resulted in more heat transferring into the houses.

The case "Day: 7/22" (bottom) represents a very hot day when the ramping rate and peak power of the aggregated HVAC power without DR control were high. The proposed sequential control reduced the maximum ramping rate by 35% and the peak power during 12:00 to 16:00 by 16% while the total daily electricity maintained nearly the same.

The aggregated equivalent SOC of the 10,000 residences for the three different days

Table 4.6: Summary of simulation results for different days

Day	Participation [%]	P_{max} [MW]	ΔP_{max} [MW/15-min]	Daily Elec. [MWh]
7/7	0 (w/o DR)	17.7	30.7	125
	100%	14.2	17.9	128
7/14	0 (w/o DR)	21.3	36.2	213
	100%	16.8	23.4	203
7/22	0 (w/o DR)	27.4	34.4	349
	100%	23.0	22.3	347

are shown in Fig. 4.40. For the 7/7 case (top), the equivalent SOC was maintained higher starting from 9:00 because of the precooling to avoid high ramping rate for "charging" starting from around 10:30. For the 7/14 case (middle), the precooling started from around 7:30, avoiding high ramping rate starting from around 9:00. For the 7/22 case (bottom), the precooling moved the equivalent "charging" process from 6:00 to early morning, reducing the ramping rate. For all the cases, the lower equivalent SOCs in the afternoon demonstrate the HVAC system can "discharge" as energy storage to reduce the peak power.

4.6 Conclusion

One of the largest rural field demonstrators for smart energy technologies, which is situated in Glasgow, KY, US, was analyzed in this chapter. The community comprises more than 5,000 residential homes with 300+ smart homes along with additional business and industrial sectors. The simulated and the experimental data obtained from the case studies presented in this chapter demonstrate the declining trend of total power demand with the long-term growth of high PV penetration in smart homes. Smart homes operated as DERs with an aim to reduce residential peak demand

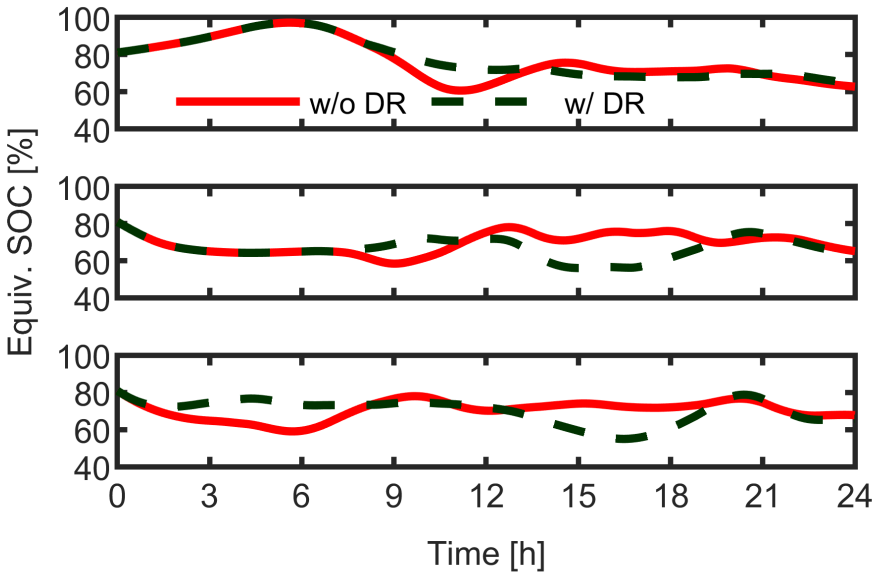

Figure 4.40: Simulation results of the aggregated equivalent SOC for the 10,000 HVAC systems on different hot days (top to bottom: 7/7, 7/14, 7/22). With the DR control, the equivalent precharging process in the morning reduced the ramping rate. The HVAC systems as energy storage discharged deeper in the afternoon under DR control and reduced the peak power.

by carrying out a combined optimal control of the EWH and HVAC set points in coordination with BESS. The aggregated residential load in long term is predicted in this chapter based on different penetrations of smart homes in a community.

The capability of EWH to provide ancillary services was studied based on the experimental data from 148 smart homes, including the net power flow from the grid, power and SOC of BESS for each house. The EWHs achieved peak reduction at the aggregated level by shaving the water heating load while maintaining the tank temperature at acceptable levels. The minimum participation rates of EWH and BESS were calculated and compared.

The example building model and its equivalent circuit parameter values were validated against the field measured data. Also proposed was an aggregation technique

for the modeling of HVAC systems in large communities that is based on the robotic house project managed by the Tennessee Valley Authority (TVA). An equivalent energy storage model for HVAC systems was developed, and it was demonstrated that HVAC systems can be controlled by a charging/discharging procedure similar to a typical battery at both individual and aggregated levels. A VPP sequential control scheme that temporarily allows higher indoor temperatures up to values that are still considered acceptable for typical preferences and standard regulations of user comfort was applied. The results based on 10,000 HVAC systems show that, on a very hot summer day, when the DR participation was 100%, the peak power in the afternoon and the ramping rate were reduced by approximately 16% and 35%, respectively while the daily energy usage was almost the same.

Chapter 5

Modeling of EVs in Charging (G2V), V2H, and V2G Operation

5.1 Introduction and Problem Formulation

The increasing penetration of electric vehicles (EVs) in residential communities has created a phenomenon known as the "dragon curve". Many EVs begin charging at around the same time in the evening as house owners return home. Rooftop photovoltaic (PV) for residences can provide electricity to charge these EVs, but the mismatch between high PV generation and EV charging times results in an even more severe "duck curve" at the distribution power system level. Time-of-Use (ToU) rates are one of the efforts that helps to guide the behaviors of house electricity usage [144]. For an individual house, a residential energy storage system (RESS) is essential to realize the response for different price signals.

The data from the National Travel Household Survey (NHTS), which was most recently updated in 2017, has been used in the past for the modeling of EV charging power [183]. Even though the random nature of human behavior dominates the individual EV performance, the aggregated EV charging load is subject to probability

distributions according to the data. Previous research has modeled the aggregated EV charging load based on EV arrival time, arrival state-of-charge (SOC), and charging finish time [184, 185].

The distribution power system can be modeled by software such as GridLAB-D, OpenDSS or MATPOWER. GridLAB-D provides an integrated power system model that includes the residences. Each residence can be further defined with details for an inverter, a PV system, an EV, or a RESS [186]. The power system can be modeled by OpenDSS at the community distribution level and with EnergyPlus at the residential level. Efforts have been made to realize the dynamic communication between OpenDSS and multiple EnergyPlus threadings [11].

EV batteries provide large energy storage [187], enabling vehicle-to-vehicle (V2G) services which interact with the power system to provide ancillary services with respect to peak power reduction and power reserve. With V2G service, the virtual power plant (VPP) framework was enabled in a power system to smooth wind power output [188]. EVs increased the resilience for microgrid with its own renewable generation and different types of loads [189]. The V2G service could also provide reactive power compensations, which in [190] potentially reduced the electric power losses up to 95%.

The CTA-2045 specifies the communications with residential devices and provides a standard interface for signals to facilitate home energy management (HEM). The CTA-2045 standards has been used for the uniform control of residential battery, electric water heater, heating, ventilation, and air conditioning (HVAC) systems, and EVs. Laboratory evaluations for V2G operation was reported in [191] by the

Electric Power Research Institute (EPRI) to address the compatibility and capability of the system. The travel behavior of the American public is published in the NHTS [183]. The details in personal and household travel were reported including the daily mileage, travel purpose, arrival home time, etc.

In the rapidly evolving electric power system, wherein new renewable and distributed energy resources are being connected and fossil fuel based generators are being retired at a growing rate, it is increasingly more important to ensure a continued and reliable supply of electricity. For example, approximately 8,000 MW may need to be imported to avoid blackouts in California by filling in gaps caused by renewable energy generation variability and increased power demand. Another major threat to energy supply reliability are large natural disasters, such as, in recent years, wide-spread wild fires [18]. In 2020, there were more than 8 thousand fires in California alone resulting in almost 1.5 million burnt out acres and significant power system damage [19]. In a winter storm in 2021, approximately 2 million homes suffered power outages in Texas which substantially increased electricity demand due to record-breaking low temperatures [20]. Worse still, about 34,000 MW of renewable wind generation capability within Texas was lost during this storm as freezing temperatures forced power plants offline in quick succession [21]. It is very important to ensure power system reliability through whatever means possible under such conditions to protect residents from environmental health risks.

Residences equipped with rooftop solar PV panels and battery energy storage systems (BESS) turn into prosumers with generation capability to supply their own

on-site demand [192]. The increasing trend of independent PV producers is representative of the possibility of decentralized power generation and distribution [193]. Solar PV panels can achieve the best performance when its material is suitable for the external condition as measured by matrices including energy payback time (EPBT), energy production factor (EPF) and life cycle conversion efficiency (LCCE) [194]. The thermal and chemical treatment based end-of-life (EOL) method reduces the cost for recycling PV system waste material making PV generation even greener [195]. Solar PV systems may be considered a reliable distributed energy resource (DER) only when it is coordinated with BESS [196]. In-home BESS can store variable renewable generated energy allowing it to be used whenever needed by the user but often have a limited energy capacity due to its hefty initial investment [197]. When advanced thermal management is implemented, BESS can charge and discharge with large power while maintaining operational safety [198].

The growing trend of EV provides the potential to boost the energy capacity of residential energy storage systems (ESS) [199]. Hence, research towards the development of smart energy management in residential houses using home ESS and EV battery systems is in progress [22, 23]. Residences with EV can help to improve the load factor in communities, reducing costs related to the maintenance of transformers, feeders, etc. [24] A previous study using data from the NHTS found that most cars commute around 20 miles daily, resulting in 90% of SOC remaining on average for EVs when they return home [25].

Recent research shows that EV batteries can operate as a voltage source or offline uninterruptible power supply (UPS) for a home in an outage [98, 99]. A well managed

energy storage system with BESS and EV support could provide good performance during both transient and steady-state operation, considering the voltage waveform and current harmonics distortion [100]. Different operation modes of EV in smart homes have been proposed and explored, and it was shown that depending on the usage preferences of the user, EV batteries can act as a power source to feed residential appliances during a power outage [98]. When energy not supplied (ENS) or system average interruption duration index (SAIDI) is taken into consideration, the participation of a EV connected to the home improved resilience the most [101].

The vehicle-to-home (V2H) capability of EV realizes the outage management and cost reduction for a smart home [102, 103]. EV systems can potentially adopt the same method introduced in [104] allowing the battery system to switch between input PV energy harvesting mode and output V2H mode for emergency situations. V2H functionality also improves power system resilience factors including load restoration, reactive power supply, and peak reduction, etc. [105–109]. Bidirectional wireless power transfer will further facilitate V2H applications by enabling higher power transfer and easing the barrier to entry for the consumer [110].

Depending on the user preferences and applications of the EV, the additional energy storage can expand the residential ESS, but may not be available at the residence when the outage occurs. For example, according to recent reports, the very large 90kWh battery installed on the most recent EV model of the Ford F-150 truck can be controlled to supply up to 10 days of electricity for a connected home [26]. Other factors including user behavior regarding residential load, the capacity of the residential ESS, renewable energy generation, etc., should all be taken into

consideration for systematically quantifying building resilience.

The problems addressed in this chapter include the development of total EV charging power, optimal control of V2G and G2V operation, and building resilience. Each of the problems are defined in the subchapters: the development of total EV charging power in section 5.2, optimal control of V2G and G2V operation in section 5.3, and building resilience in section 5.4.

In this chapter, the aggregated EV charging power was modeled based on the NHTS 2017 data, considering the arrival home time and daily mileage. The optimal charging scheme for BESSs and EVs was proposed for the best financial benefits. EVs was connected to the IEEE 123-bus feeder system and DR signals complying to CTA-2045 were applied.

The metrics for building resilience was quantified considering different time occurrences for power outages. The building resilience for residences with varying electricity usage, PV generation capability, and BESS capacities was analyzed in order to provide a reference for all types of house owners. This chapter focuses on minute-based simulations of power flow and energy use with building resilience studied by monitoring the energy balance on the demand and supply sides. The quantification of building residence provides utilities with a basis for better planning of rolling blackouts and power restoration, and guide house owners when sizing their localized residential power system.

This chapter is substantially based on the following papers:

- H. Gong, *et al.*, "Optimization of aggregated EV power in residential communities with smart homes," *2020 IEEE Transportation Electrification Conference*

& Expo (ITEC), pp. 779–782, 2020.

- H. Gong, *et al.*, "V2G Operations for Community as VPP Complying to CTA-2045 Standards Based on Stochastic EV Power Modeling," *2022 IEEE Transportation Electrification Conference & Expo (ITEC), (Submitted in Jan, 2022).*

- H. Gong, *et al.*, "Improving the power outage resilience of buildings with solar PV through the use of battery systems and EV energy storage," *Energies*, Vol. 14, No. 18, p. 5749, 2021.

5.2 Optimal EV Charging at Aggregated Level

5.2.1 Modeling of EV Charging Power Based on NHTS 2017 Data

The proposed system comprises of residences with PV systems, RESSs, and EVs (Fig. 5.1). The residential load can be generated by GridLAB-D. Solar power can be calculated based on given weather data. It should be noted that the residential load might be negative due to the generators in the smart homes. This will reverse the direction of power flow.

The factors to impact the total EV charging loads in the distribution system were simplified to three variables: charging finish time, arrival time, and arrival SOC. In this study, the charging finish time was set to 6:00 in the morning. The arrival time and arrival SOC were estimated from the NHTS 2017 data [183].

The arrival time is categorized into 15-minute intervals from the NHTS 2017 data. Its probability density function (PDF) was estimated using the kernel density

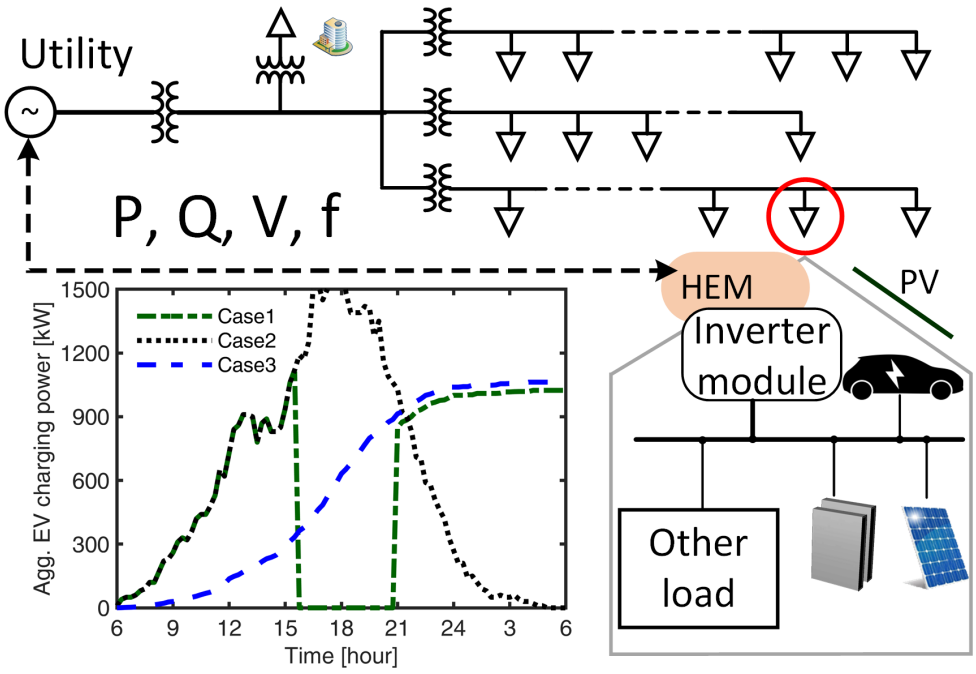

Figure 5.1: The scheme for the distribution system modeling. Residences with PVs, EVs, and RESSs were considered. Other loads and PV data were obtained with measured data from local utilities.

estimation (KDE). With this, the distribution of arrival times for 1,000 EVs was generated (Fig. 5.2). The KDE function is defined as follows:

$$\widehat{f}(t;h) = \frac{1}{N}\sum_{i=1}^{N} K(t-t_i;h), \tag{5.1}$$

where $\widehat{f}(t;h)$ is the estimated KDE; K, the kernel function, which is triangular in the study. The bandwidth was set to 0.2 in the study.

The daily driving distance from the NHTS 2017 data was used to estimate the arrival SOC for the EVs. The distribution of daily driving distance less than 120 miles was shown (Fig. 5.3). The distribution was fit as a lognormal distribution [200], as follows:

$$f(d) = \frac{1}{d\sigma\sqrt{2\pi}} exp\left(-\frac{(\ln d-\mu)^2}{2\sigma^2}\right), \tag{5.2}$$

where d is the driving distance, the mean of lognormal distribution μ=3; and the

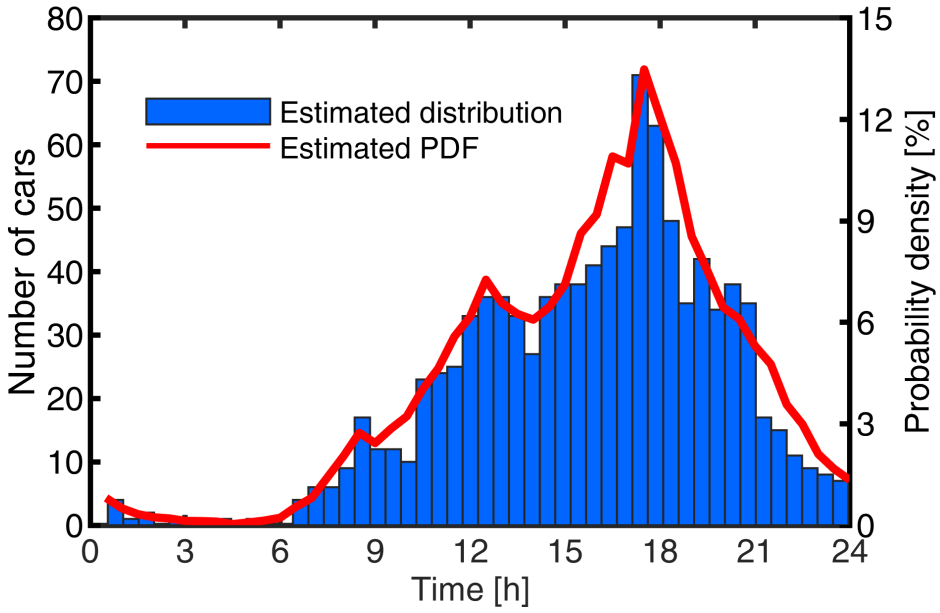

Figure 5.2: Distribution of EV arrival home time. The PDF was calculated by the KDE based on NHTS 2017 data. The histogram is the estimated distribution for 1,000 EVs.

deviation σ=1.12 in the study.

The PDF of arrival SOC for EVs is related to the daily driving distance and was described as follows:

$$f(SOC_i^a) = (1 - \frac{d}{d_M}) \times 100\%, \tag{5.3}$$

where d_M is the maximum driving distance allowed by the EV battery energy capacity. In the study, The effective cost per mile was set to 0.46 [201]. Assuming that each EV battery energy capacity is 90kWh, the d_M used in the study was 196 miles. The estimated PDF and distribution of arrival SOC for 1,000 EVs are shown (Fig. 5.4).

The individual EV power was calculated with the arrival time, arrival SOC, and charging finish time. The energy required for an EV is subject to the following:

$$\int_{t_{a,i}}^{t_{f,i}} P_{E,i}^t dt = E_i - E_i \times SOC_{a,i}, \tag{5.4}$$

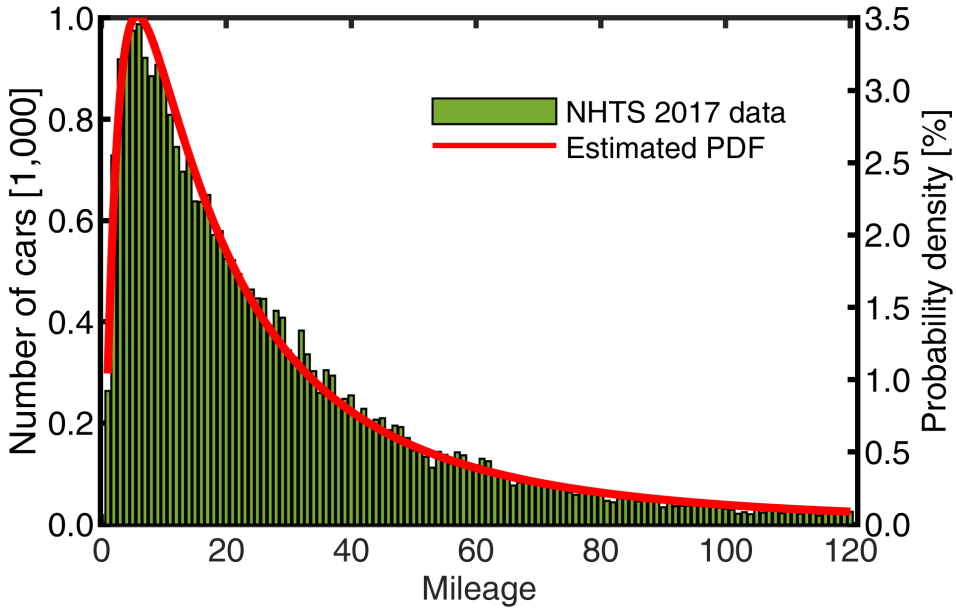

Figure 5.3: Distribution of daily mileage for EVs based on NHTS 2017 data. Daily driving distances of more than 120 miles are excluded in the study. The PDF for the distribution is described as a lognormal function.

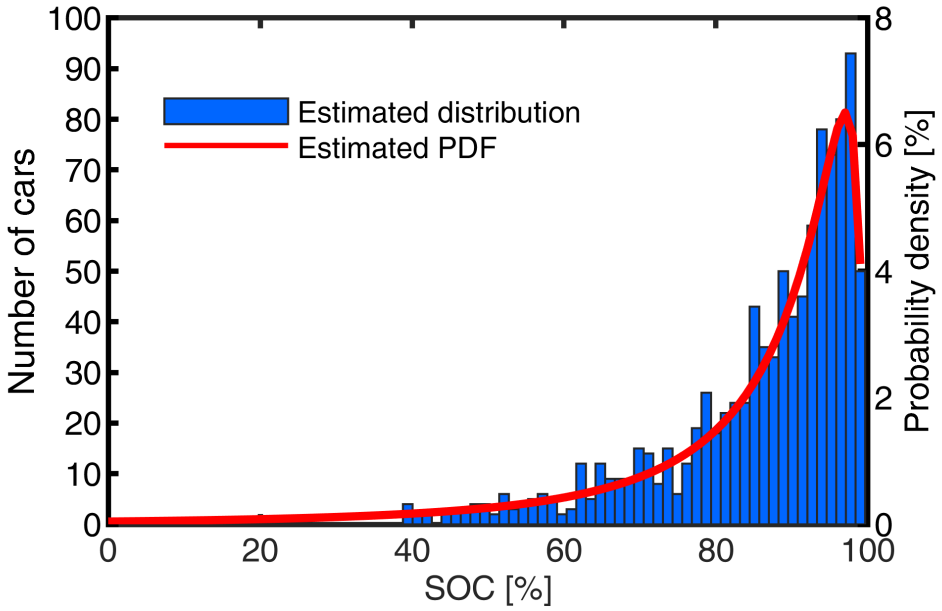

Figure 5.4: Distribution of SOCs for EVs when they arrive home. The PDF was calculated based on the KDE of daily mileage. The histogram is the estimated distribution for 1,000 EVs.

where $t_{a,i}$, the arrival time subject to (5.1); $t_{f,i}$, charging finish time which was fixed to 6:00 in the morning; $P^t_{E,i}$, EV charging power of house i at time t; E_i, the EV battery energy capacity; $SOC_{a,i}$, arrival SOC subject to (5.3).

5.2.2 EV and BESS Scheduling

The main objective for the study is to minimize the daily utility charge for electricity usage of the entire distribution system, described as follows:

$$Min \quad \sum_{1}^{n} UC^t, \tag{5.5}$$

where UC^t is the utility charge for the entire distribution power system at time step t.

The utility charge at time step t is calculated as:

$$UC^t = \int (E^t_b \cdot r^t_b - E^t_s \cdot r^t_s) dt, \tag{5.6}$$

where E^t_b is energy purchased from the utility at time t; r^t_b, utility charge rate at time t; E^t_s, energy sold to the utility at time t; r^t_s, the rate utility pays to buy back energy at time t.

The constrains include the power balance of the community:

$$P^t_G = P^t_{PV} + P^t_E + P^t_{RESS} + P^t_R, \tag{5.7}$$

where P^t_G is the power purchased from the grid; P^t_{PV}, the PV generation; P^t_E, the charging power of EVs; P^t_{RESS}, the charging power of RESSs; P_R, other residential power usage.

The energy capacity for RESSs is described as:

$$20\% \leqslant SOC^t_{RESS} \leqslant 100\%. \tag{5.8}$$

The EV and RESS power values are defined as independent variables with their ranges given as follows:

$$P_{E,i}^{t} \leqslant P_{E,i,max}, \tag{5.9}$$

$$|P_{RESS}^{t}| \leqslant N \cdot P_{RESS,max}, \tag{5.10}$$

where $P_{E,i,max}$, the maximum charging power of EV in house i; N, house numbers; $P_{RESS,max}$, the rated power for an individual RESS.

The ToU electricity rate indicates that most EVs arrive home during the peak charging period [144]. Therefore, the charging of EVs must avoid the high ToU rates to minimize utility charges. EVs that were available when there was surplus PV generation were charged with maximum power to consume the local solar power. EVs were charged with minimum power after the high ToU period. The EV scheduling is described as follows:

$$P_{E,i}^{t} = \begin{cases} P_{E,i,max}, & 1 \leq t \leq ToU_s \\ 0, & ToU_s \leq t \leq ToU_e \\ P_{E,i,min}, & t \leq n, \end{cases} \tag{5.11}$$

where ToU_s, ToU_e stand for high ToU start and end time, respectively; $P_{E,i,min}$ is the minimum power required to charge EV at house i to 100% at the last time step. The individual EV charging power is shown (Fig. 5.5). In this aggregated study, the location of the EV during charging and discharging is not specified, for example, at midday, the EV maybe assumed to be in an office parking and connected to a public charger. EVs were charged to 100% SOC at 6:00 the next morning (Fig. 5.6).

The RESS of the distribution system was considered as a large battery. It started with a SOC of 50%, was charged to 100% before high ToU period, discharged to 20%

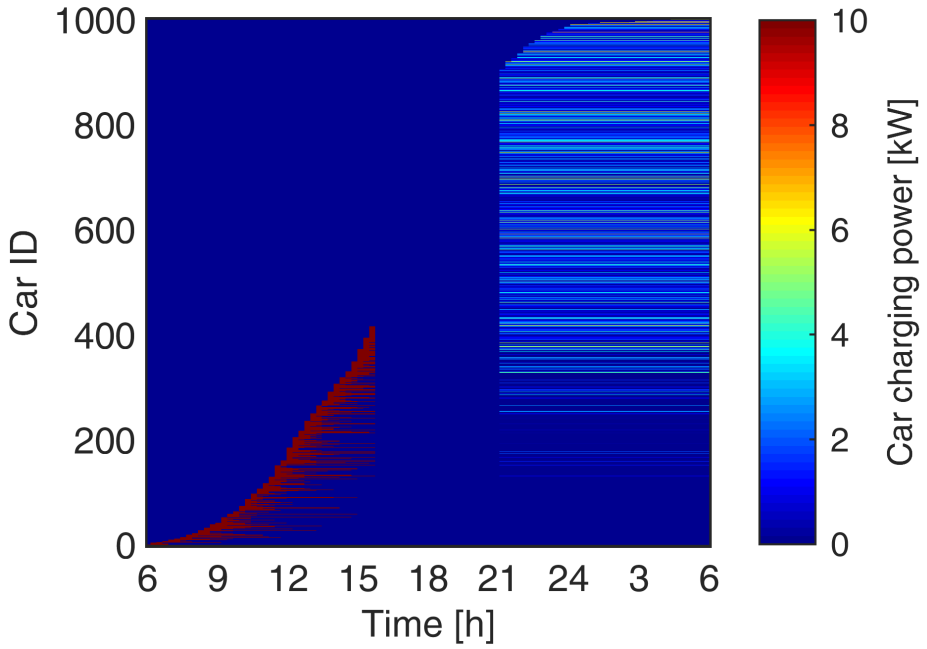

Figure 5.5: The charging power for all EVs in the distribution system. The EVs were charged at maximum and minimum power before and after the high ToU time, respectively. During the high ToU time, no EVs were charged.

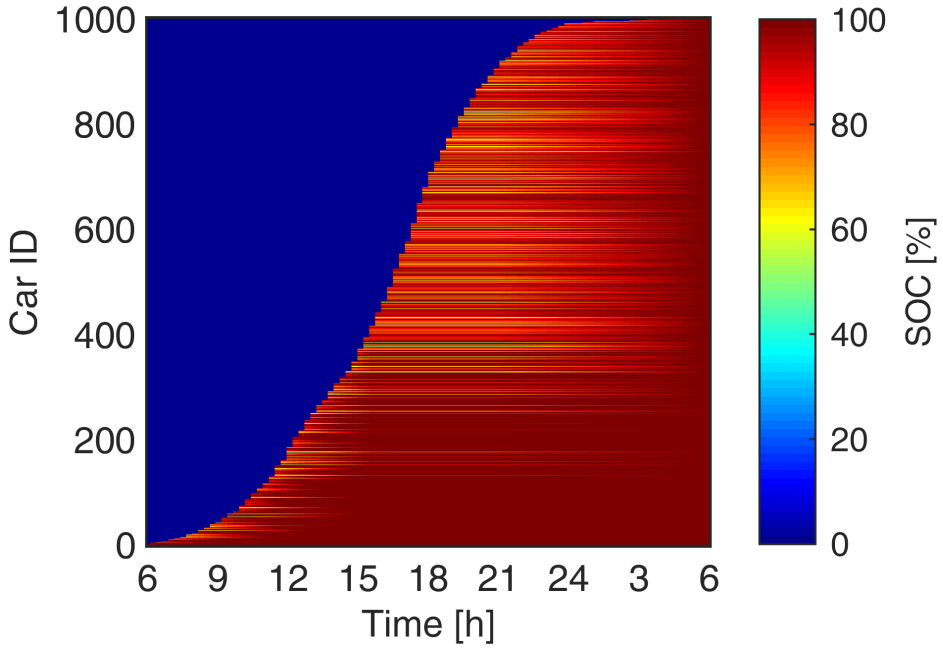

Figure 5.6: The SOCs for all EVs in the distribution system. The SOCs were regarded as 0 before EVs arrived home. EVs were guaranteed 100% SOC at 6:00 the next day.

during the high ToU period, and recharged to 50% afterwards, as follows:

$$\begin{cases} \int_{1}^{ToU_s} P_{RESS}^{t} dt = 50\%, & 1 \le t \le ToU_s \\ \int_{ToU_s}^{ToU_e} P_{RESS}^{t} dt = -80\%, & ToU_s \le t \le ToU_e \\ \int_{ToU_e}^{n} P_{RESS}^{t} dt = 30\%, & t \le n. \end{cases} \tag{5.12}$$

5.2.3 Case Studies

The residential community being studied had 1,000 houses, each of which with a single EV. The residential load was from one typical summer day in Glasgow, KY and averaged to represent 1,000 homes [85]. The PV data is from LG&E KU and was scaled to the ratings of 5kW for each house [202]. The RESS is rated 9.8kWh/5kW and started with a SOC of 50%. The EV SOCs and arrival time are subject to the distribution (Fig. 5.4 and Fig. 5.2). The EVs were not allowed to discharge in the study. The resolution for the study was 1-minute.

The aggregated power of EVs, RESSs, and net metered power for the residential distribution system on the example summer day are shown (Fig. 5.7). In this case all of the houses had a PV system and a RESS. The EVs were only charged when the ToU is not high (Fig. 5.5).

The RESSs were charged when the PV generation was high and discharged during the high ToU period. After high ToU period, the RESSs were charged to 50%. The proposed schedule reduced the electricity usage during the high ToU time, therefore, it reduced the total utility charge for the entire community. The entire residential community also served as a virtual power plant (VPP) for coordination of EVs and RESSs. As a VPP, the system managed to keep net metered power stable for a long period of time.

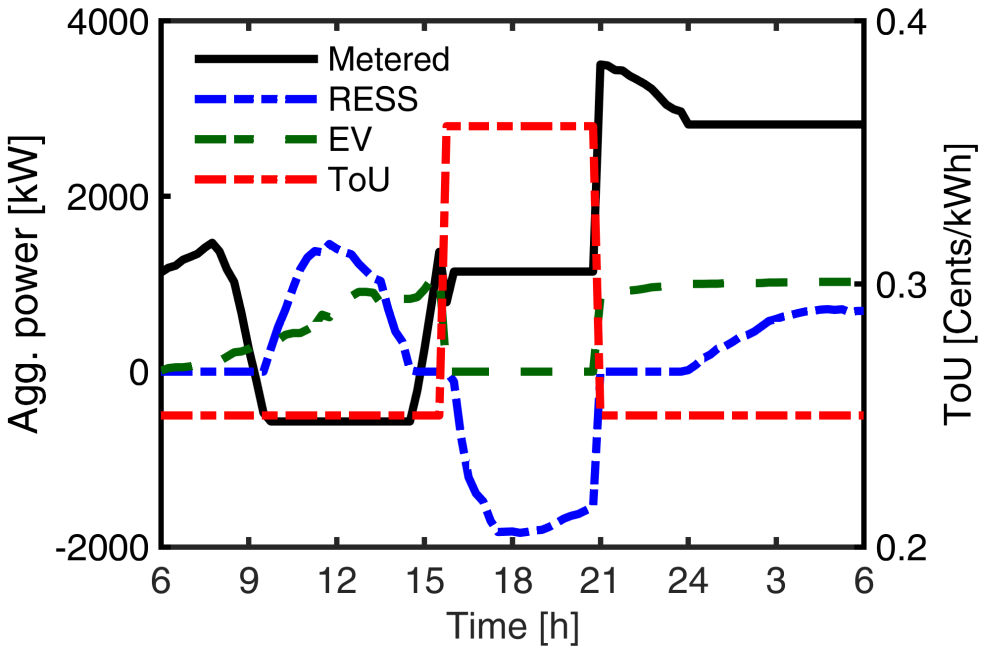

Figure 5.7: The aggregated power at distribution level. The EV curve was decided by the charging schedule. The RESS was first charged when the PV generation is high, discharged during high ToU period, and was charged to 50% afterwards. The metered curve shows that the community sold less electricity to the utility when PV generation was high and reduced usage during the high ToU period.

Simulation results for residential communities with different penetrations of EVs and RESSs are shown (Fig. 5.8). The 0% curve represents the baseline case without PVs or RESSs where the optimal scheduling of EVs avoided the high ToU. With the increase in PV penetration, solar generation became higher. In the case of 100%, houses had to sell electricity back to the utility in the afternoon.

Higher RESS penetration means larger total capacity. Therefore, the higher the penetration, the lower the aggregated net metered power during the high ToU period, and the lower the utility charge. The averaged total cost per house for 0%–100% are \$17, \$15, \$13, \$11, \$10, respectively. The 100% penetration has the advantage of peak reduction during high ToU time. The high solar generation also means that

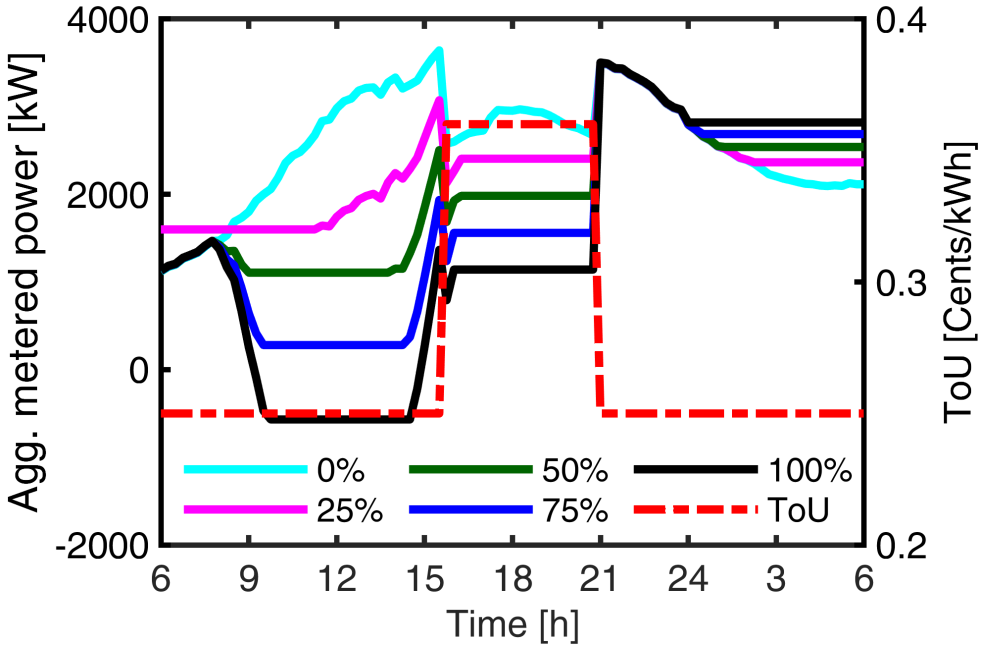

Figure 5.8: Metered powers for different penetrations of EVs and RESSs under optimal schedules. Percentage shows the penetration of residences with a PV system and RESS. The 0% case stands for the baseline. Higher penetration leads to more PV generation in the afternoon and lower electricity usage during the high ToU period.

residences must sell electricity back to the grid at a low price. Charging of RESSs after high ToU time did not increase the peak demand.

5.3 V2G Operations for Community as VPP Complying to CTA-2045 Standards

5.3.1 CTA-2045 Concept and EV Operations

The CTA-2045 can be applied to EV service equipment (EVSE) for the compatibility with other smart devices which can be used for HEM [191]. For a level-2 charger, the EV power is defined by the current as the voltage is fixed at 240V under ideal condition. The current for EV charging can be changed to respond to control

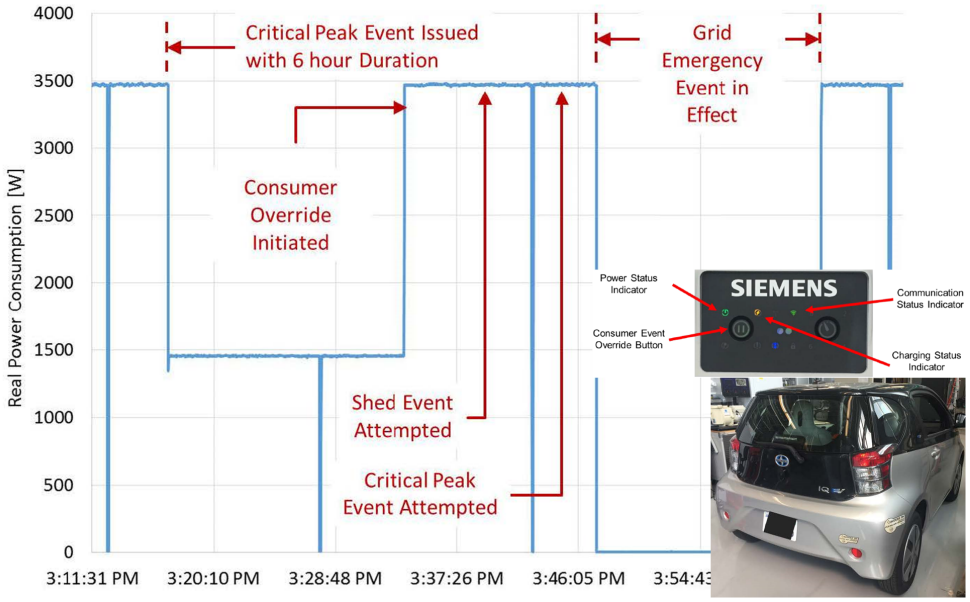

Figure 5.9: The performance test results for CTA-2045 EV supply equipment published by Electric Power Research Institute (EPRI)[191]. Shown are the EV for testing, visual indicators and controls on EVSE, and results for different control signals.

signals from the grid. The example results from the EPRI report (Fig. 5.9) show the EV power responding to different control signals, which typically include normal operation, shed, critical peak, grid emergency, and variable. In this chapter, the V2G control was enabled by adding the control signal with negative current.

Knowledge of the availability for EV battery energy is essential to plan for V2G service. At the community level, the aggregated behavior for EV owners is highly predictable as the randomness of individuals is averaged out. The data from the NHTS provides daily information for vehicles of hundreds of thousands households, including the arrival home time and daily driving mileage [183]. The Gaussian Kernel Density Estimator was used for the estimation of the distribution of arrival home time and arrival SOC, as presented in Section 5.2.1.

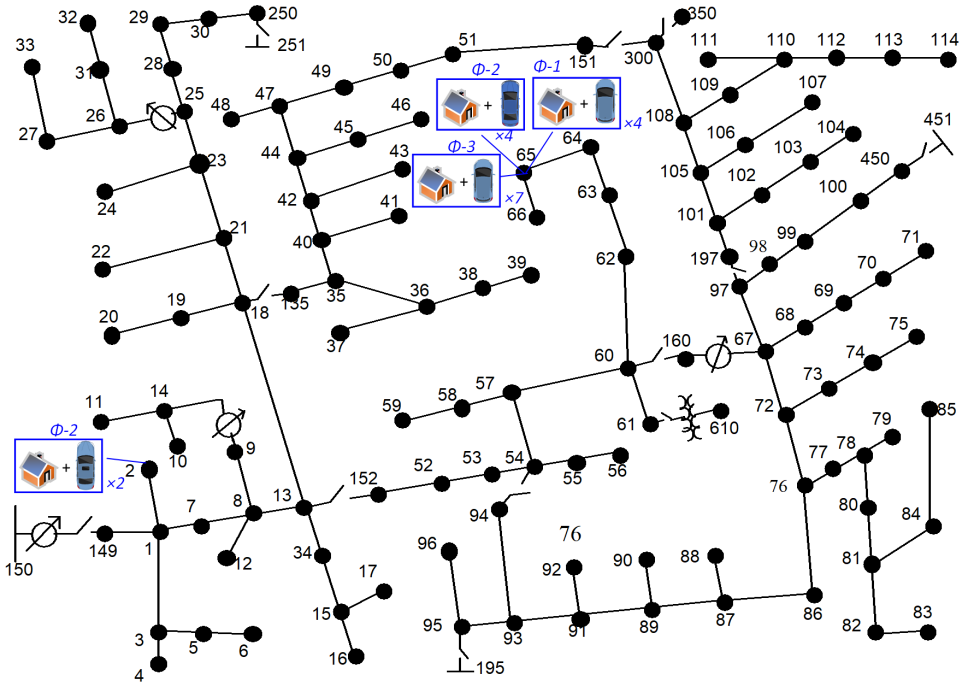

Figure 5.10: A total of 353 residences were randomly generated with the newly procedure described and connected together with associated EV as spot loads to a modified IEEE 123-bus feeder test case.

5.3.2 DR Program and Distribution Power System

The power distribution system for a community with EVs was modeled using the IEEE 123-bus feeder test (Fig. 5.10). For each phase of all the nodes, every 10KW was replaced by a residence including the corresponding EV. For example, phase-2 of bus-2 has active power of 20kW, therefore, two residences were connected to phase-2 of bus-2. Based on the test case values [118], a total number of 353 residences were connected. All the 353 residences have their distinctive load data, which was from the smart energy technologies (SET) project [22]. For all the buses, the power factor was fixed to 0.95 in the study.

All available EVs with more than 50% participated the DR event and worked on V2G mode, with a current of -50A, i.e., discharging power of 12kW. Two cases were

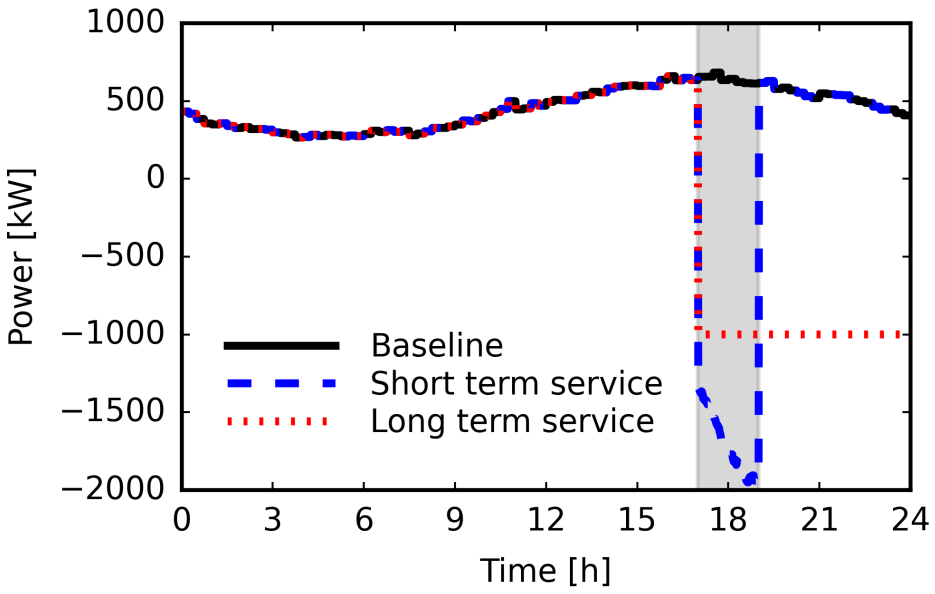

Figure 5.11: A purposefully exaggerated case scenario in which the EVs with SOC excess of 50% provide V2G resulting in a negative net power flow with absolute value much larger than the typical residential load.

shown in Fig. 5.11 for long and short term V2G services. For the short term service, the example DR signals were from 17:00 to 19:00 and all the available EVs were discharging at 12kW . At the beginning, all the available EVs supplied approximately 2,000kW to the grid. The discharging power increased as more EV arrived home. For the long term service case, the total power flow at the distribution system level was kept constant.

Details for the short term service including SOC for all EVs, available energy in the power system, and bus voltages were analyzed. No SOC was recorded before the first EV arrived home. During the DR period for short term service, the average SOC decreased, and increased afterwards as EVs with higher SOC arrived. Therefore, even without charging, the average SOC for all EVs increased after the DR period. EVs with low SOC could be charged during the work day when public charging is

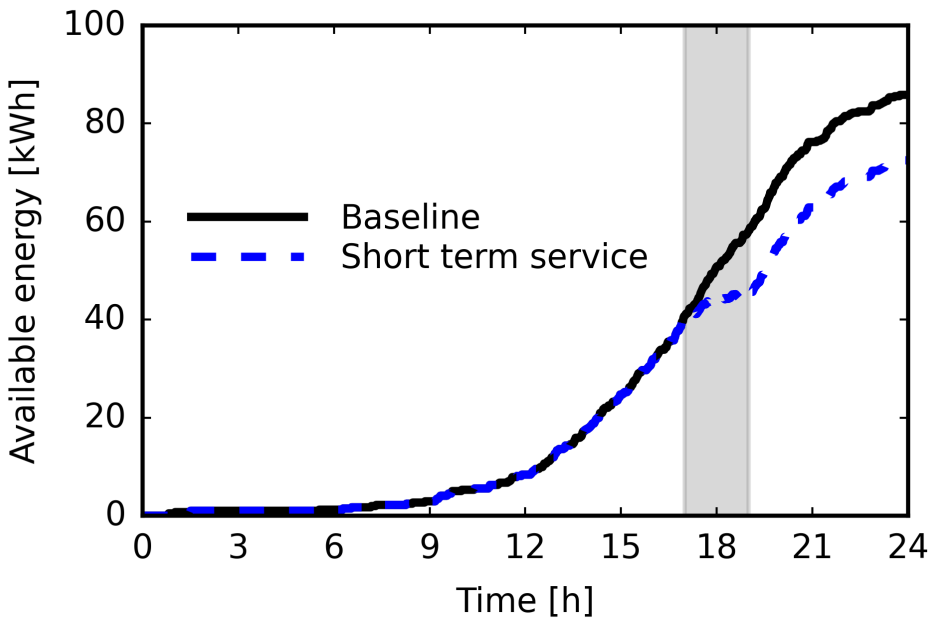

Figure 5.12: The total available energy from EV batteries, which increased as more EVs arrived home. The available energy still increased even when the EVs were discharging under control.

available, or at home when no DR events happen. The total available energy from all EV batteries increased during the example day as more EV arrived home, even during the DR period (Fig. 5.12).

5.3.3 Case Studies

The preliminary results of the short term service were analyzed. In the extreme scenario of this chapter, EVs provided large negative net power flow with absolute value much larger than the typical residential load (Fig. 5.11). The voltage on all buses were within the variation tolerance of 5% for the entire simulated day (Fig. 5.13). The comparison for the bus voltages during the DR period of the short term service is presented in Fig. 5.14. The reverse large power flow caused by EVs resulted in larger variation as expected.

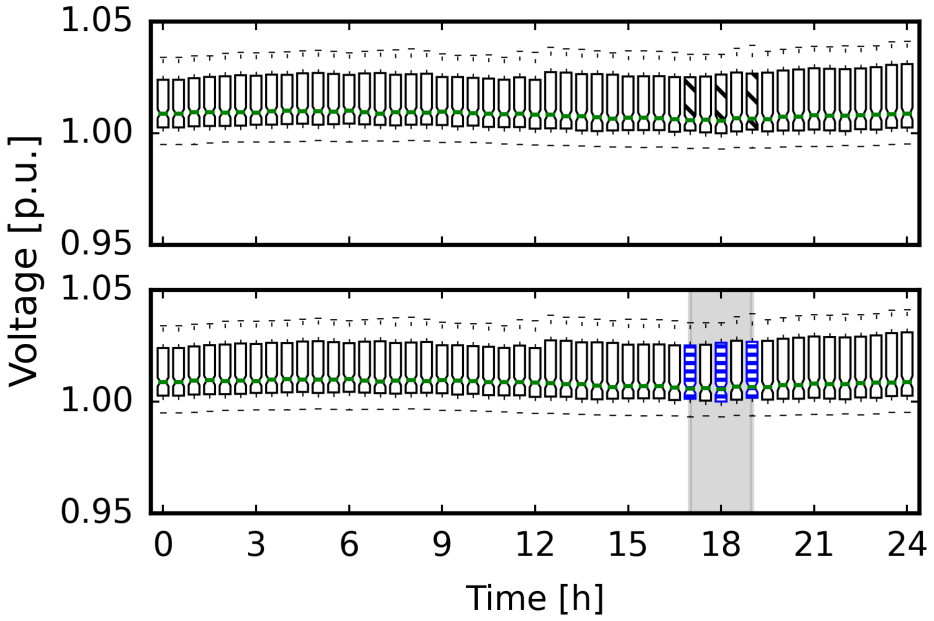

Figure 5.13: The voltage for all buses on the simulated day for top: without DR, bottom: with DR. Samples were taken for every 30 minutes. There were virtually no violation for the simulated daily case.

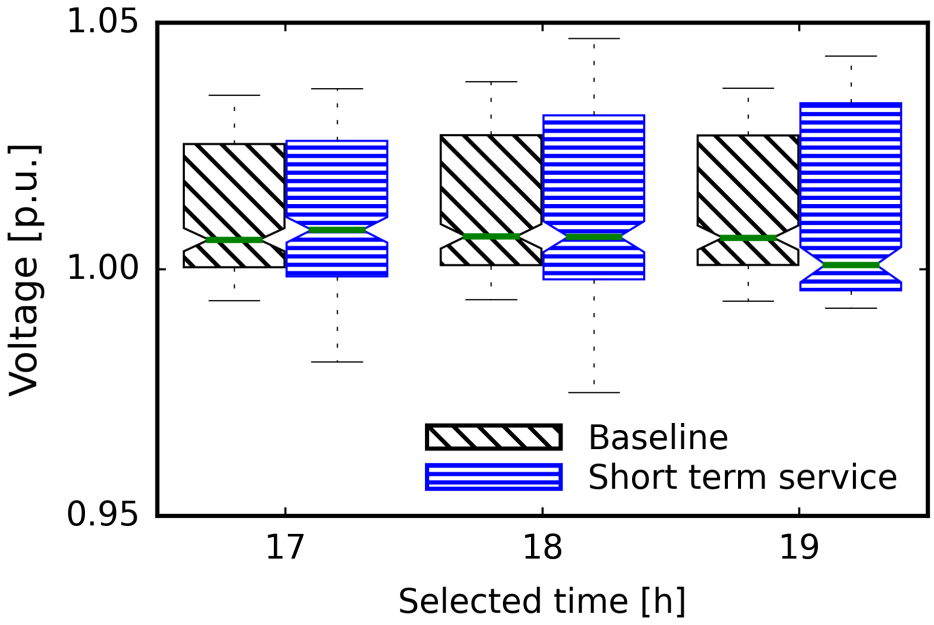

Figure 5.14: The voltages for all buses in the power system for selected hours. The high reserved power flow from EV discharging caused more voltage variation. Virtual no violation was observed as all voltages values are within the 5% tolerance.

With the coordination among EVs, the entire community can operate as a VPP, providing constant power for a long period of time, as the long term service case in Fig. 5.11. To achieve this, when the DR started at 17:00, the aggregated EV power needed to provide approximately -1,800kW, which was possible as the maximum power available by all EVs was approximately 2,000kW More details for the long term service will be presented in future study. The details will include the control of EVs, the monitoring of SOC, available energy, and bus voltage.

5.4 Improving the Power Outage Resilience of Buildings with Solar PV through the Use of Battery Systems and EV Energy Storage

5.4.1 Energy Model for the Reference House

The main parameters for the reference house considered in the study are summarized in Table 5.1. The use of batteries for power flow and energy studies are based on results from the EnergyPlus software and the INSPIRE+D co-simulation framework [11]. The framework realizes the dynamic communication between the power system simulator and the building model, based on a prototype EnergyPlus model released originally by the Pacific Northwest National Laboratory (PNNL) [203]. The weather data for the studied Burbank area in California Climate Zone 9 was publicly available as a typical meteorological year (TMY) [204]. The California climate Zone 9 is very mild and has reduced HVAC energy usage, represents a best scenario that has been selected as part of an industry-led government-sponsored research program case

Table 5.1: Main specifications for the electricity usage model of the reference house

Parameters	Value
Conditioned area	223 m^2 (2,401 ft^2)
House type	4-bedroom, 3.5-bathroom
Location	Burbank, CA, Zone 9
PV rating/annual generation	7.2kW/11,316kWh
Annual electricity usage w/o EWH	13,628kWh
Annual electricity usage of EWH	4,233kWh
EWH rated electric power	5kW
BESS energy capacity/maximum power	11kWh/5kW
Initial BESS SOC	100%
Minimum BESS SOC	20%
EV battery energy capacity/maximum power	90kWh/10kW
EV battery SOC when EV arrives home	90%
Minimum EV battery SOC	20%

study. The outputs of the EnergyPlus model include energy usage and generation with a 5-minute resolution and detailed usage for appliances including HVAC, water heater, etc.

In the schematic representation and graphs from Fig. 5.15, the dark blue area in the middle of the annual electricity usage graph corresponds to power flow from the house to the grid caused by surplus PV generation. Variations in the blue area was caused by the pool pump, which operates during 9:00–15:00. The yellow strip at around 21:30 stands for evening demand peaks of power flow into the house.

The electric water heater (EWH) was modeled and its typical high and relatively short power draw corresponds to the red dots in Fig. 5.15. The electricity usage and power profile of the EWH are determined by the water draws, quantified according to the California Building Energy Code Compliance for Residence (CBECC-Res) [80]. The rated electric power of EWH is 5kW, and the calculated annual electricity usage of the EWH is 4,233kWh.

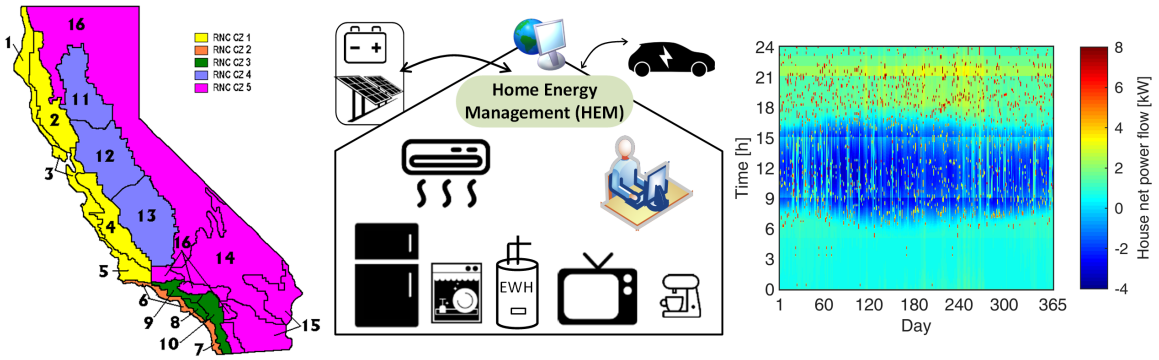

Figure 5.15: Illustrations for the example reference home: location in California zone climate 9 (left); HEM, PV, battery, EV, and appliances diagram including major energy users HVAC system and EWH (center); and power flow during a year (right). The negative power flow during daytime is due to surplus solar PV generation. The very high power draw marked with red dots and occurring mostly in the evening and at night is due to the EWH.

The stationary BESS introduced to the home is a Li-ion battery rated as 11kWh/5kW in the following studies, and is assumed to have 100% SOC when the power outage occurs. The EV battery is rated as 90kWh for the reference house. The most recent level 2 charger allows the EV to be charged/discharged at a maximum power of 10kW with a lower limit of 20% for the EV battery [205]. The EV is scheduled to leave home at 6 am and return at 6 pm every day with an SOC of 90%, given the fact that most daily driving mileages are less than 20 [25].

The example topology published in patent [206] includes inverters for connections to EV and other components (Fig. 5.16). Such a multifunctional system can ensure V2H operation, providing support during grid power outages and increased resilience. Residential power system components are represented as nodes or individual elements that interact with a central power management system connected to the cloud for long-distance control and capable of multi-function operation. The central system includes a smart power integrated connected to power grid, BESS , PV cell and

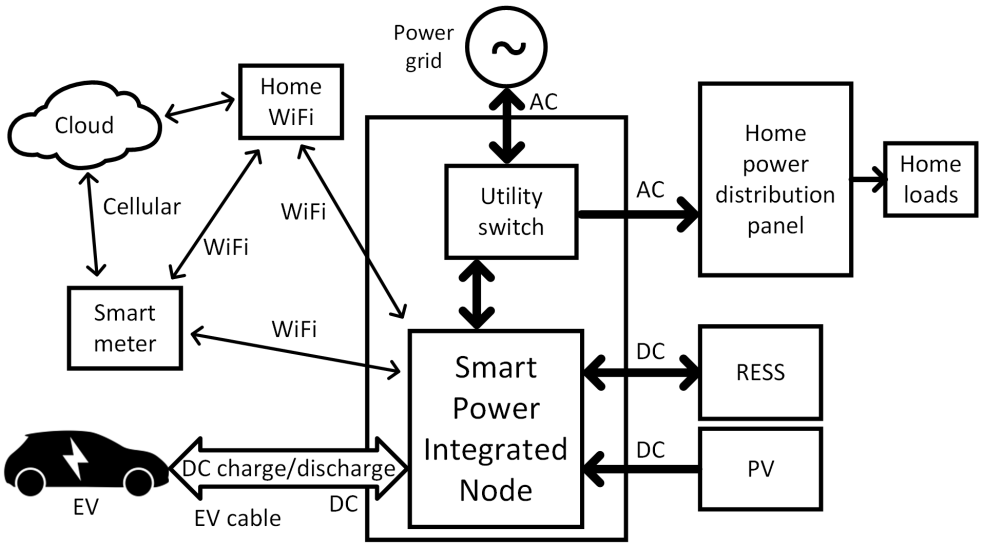

Figure 5.16: Example of a residential power and energy management system, based on the concept described in a US patent [206]. Such a multifunctional system can ensure V2H operation, providing support during grid power outages and increased resilience.

EV. Communication can be realized via Ethernet, WiFi, cellular connection, or any available communication protocol. The smart power integrated node (SPIN) provides DC charge and discharge capability to EV via an EV cable in this embodiment. The SPIN may incorporate functionalities such as service setup, display & control, and is capable of receiving transit information from remote server or user interfaces. The operating procedure defined by the user is employed by its many DC/DC, DC/AC switching components.

5.4.2 Method for Calculating the Self-sustainment Duration for a Reference House

Power outages or blackouts may occur at any time throughout the entire year, and in such conditions, the house loses electricity supply from the grid. In the following studies, residential loads are supplied by the BESS and PV generation when the

blackout occurs, and the resulting performance is analyzed for the following 24 hours. The total electricity provided by the BESS after the power outage occurs is defined as:

$$E_{B,t} = \sum_{i=0}^{t} P_{B,i} \cdot \Delta t, \tag{5.13}$$

where i is the simulated time step, with $i = 0$ indicating the time origin when the power outage occurs; and $P_{B,i}$, represents the power of BESS. During a power outage, the BESS supplies the total house demand to provide full building resilience. Therefore,

$$P_{B,i} = P_{H,i}, \tag{5.14}$$

where $P_{H,i}$ is the net power flow of the residence. When $P_{H,i}$ is larger than the maximum power rating of the BESS, the residential load has to be curtailed.

The self-sustainment performance is measured as the duration when the BESS can supply the residential loads. At one instance, e.g., time step s, when the power outage occurs, the BESS was discharged down to the minimum acceptable SOC. The self-sustainment operation duration T_s for this instance is defined as:

$$\exists i = T_s : E_{B,i} \leq E_C \wedge E_{B,i+1} \geq E_C, \tag{5.15}$$

where E_C, the maximum available energy of the residential ESS:

$$E_C = \eta_B \cdot E_{C,B}, \tag{5.16}$$

where η_B is 80% in the study, as the maximum SOC for BESS is 100% and minimum is 20%; $E_{C,B}$, the rated energy capacity of BESS. When the SOC is 100%, the surplus PV generation is curtailed. After calculating the following 24 hours for step s, the same procedure is applied to step $s+1$, and up to the last time step s_{max}. Every time

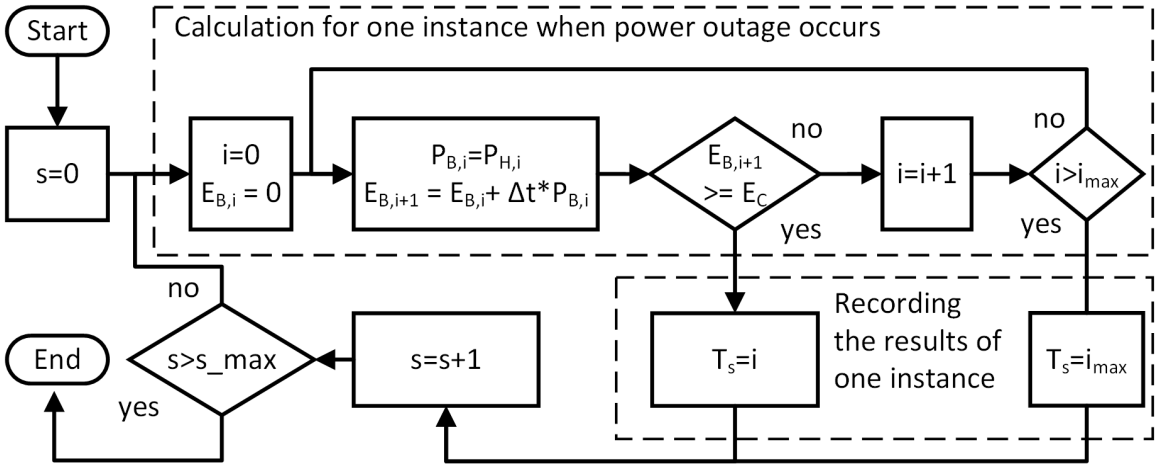

Figure 5.17: Systematic procedure for the evaluation of building resilience. Simulation is performed for each time step, corresponding to instances for which power outage occurs. The self-sustainment duration is calculated for each instance.

step has its own corresponding self-sustainment operation duration T_s. The procedure for calculating the self-sustainment operation duration is illustrated in Fig. 5.17.

The constraints are the maximum BESS power:

$$|P_{B,i}| \leq P_{max}. \tag{5.17}$$

Residential power must be curtailed if it is too high during a outage. On the other hand, the PV generation input needs to be curtailed if the negative net power flow is too high.

Simulation results in Fig. 5.18 show that the time of the power outage has a great impact on the self-sustainment duration from the reference house. When the power outage occurred at the midnight as shown on the left, the reference house self-sustained approximately 17 hours (Fig. 5.18 (a)). The BESS SOC in this case dropped in the early morning, increased in the midday, and decreased in the evening until it was 20%. This happened because the BESS was charged by the surplus

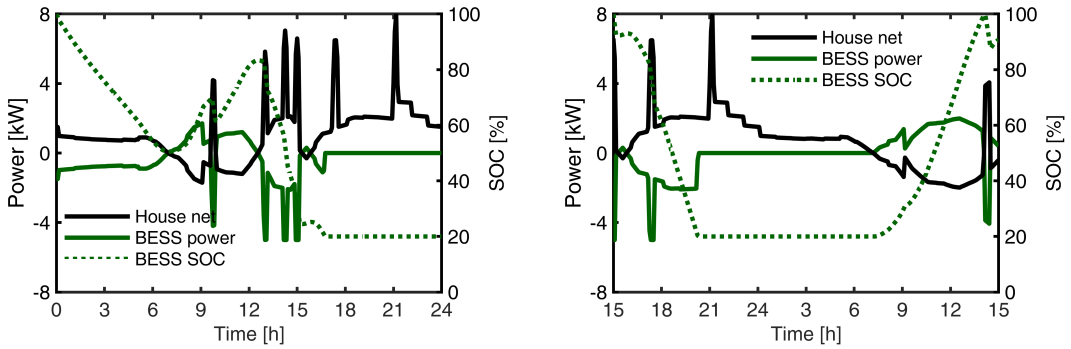

Figure 5.18: An example of the daily self-sustain case for the reference house when the power outage occurs at (a) midnight and (b) 3 pm. The BESS covers the residential load in the morning and was charged by surplus solar PV generation throughout the day. As PV power rapidly declined and no longer met the residential load, the BESS discharged until falling to the minimum SOC of 20%. The reference house tends to self-sustain longer when the power outage occurs in the early morning because the BESS could be charged by PV generation during the daytime hours.

PV generation in the midday and discharged to power the loads for the rest of the time. On the same example day, however, when the power outage occurred at 3 pm, the house self-sustained for approximately 5 hours, as shown in Fig. 5.18 (b). The house self-sustained a significantly shorter amount of time because the BESS was not charged for that day when PV generation faded away in the evening.

With the simulation time step of 5-minutes, there are $12 \times 24 \times 365 = 105,120$ instances throughout the entire year when the power outage could occur. Correspondingly, there are 105,120 calculated self-sustained operation durations which are represented as different colors in Fig. 5.19, with each cell indicating a 5-minute increment. The two instances in Fig. 5.18 are represented in the corresponding colors for the 17 and 5 hours for their two cells. Self-sustained operation duration trended towards being longer if the power outage occurred in the early morning because the BESS was charged in the midday by surplus solar PV generation. The self-sustained

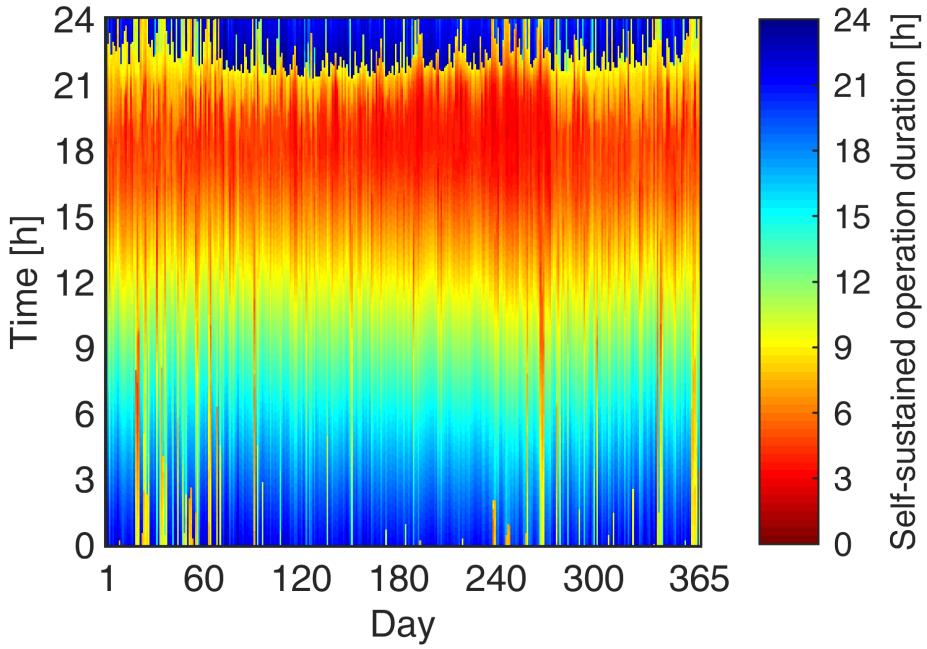

Figure 5.19: Self-sustained operation duration of the reference house for power outages occurring at different times. All 105,120 instances of varying days and times for power outages were calculated throughout the year. The self-sustained operation duration is longer if the power outage occurs in the morning because the BESS could be charged during the day with surplus solar PV generation.

operation duration around 6 pm was short because of both the evening residential load peak and lower solar PV generation.

The simulation results of self-sustained operation duration for the entire year were summarized with an interval of 1-hour in Fig. 5.20. If the self-sustained operation duration of the house falls into the interval of $(t_1, t_1 + 1]$, it can self-sustain any hours within $[0, t_1]$. The building resilience is defined by the cumulative probability curve presented in Fig. 5.21, which indicates that after a power outage occurrence, the reference house will self-sustain virtually at 100% load for up to 3 hours, and has a 50% probability of self-sustainment up to 10 hours.

The cumulative curve, which stands for the building resilience, was fitted and

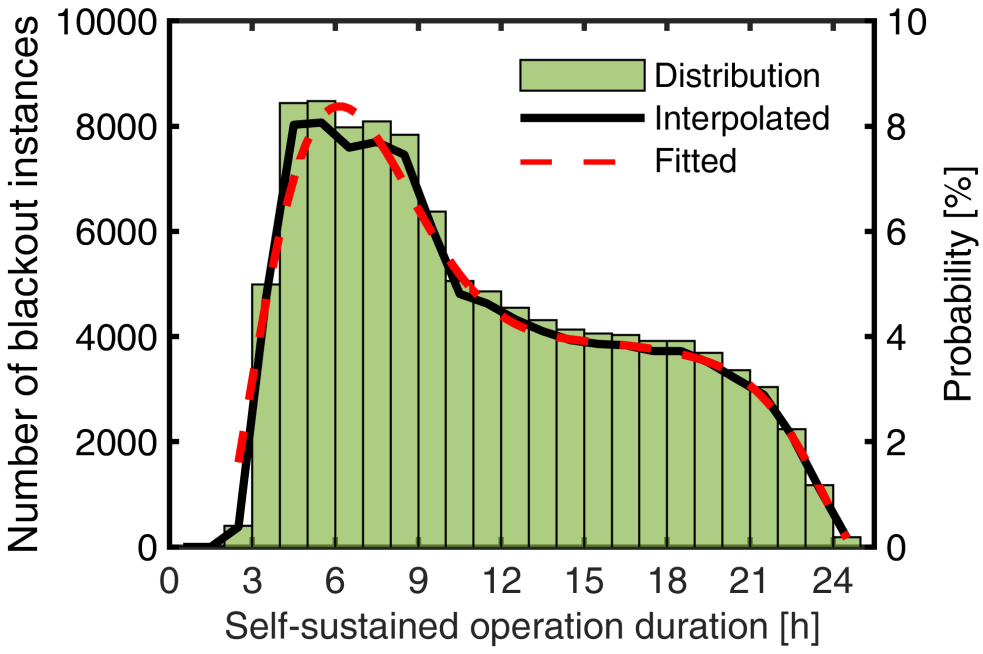

Figure 5.20: The distribution of residence self-sustained operation duration for all 105,120 instances. All instances were binned into duration categories with a time interval of 1-hour.

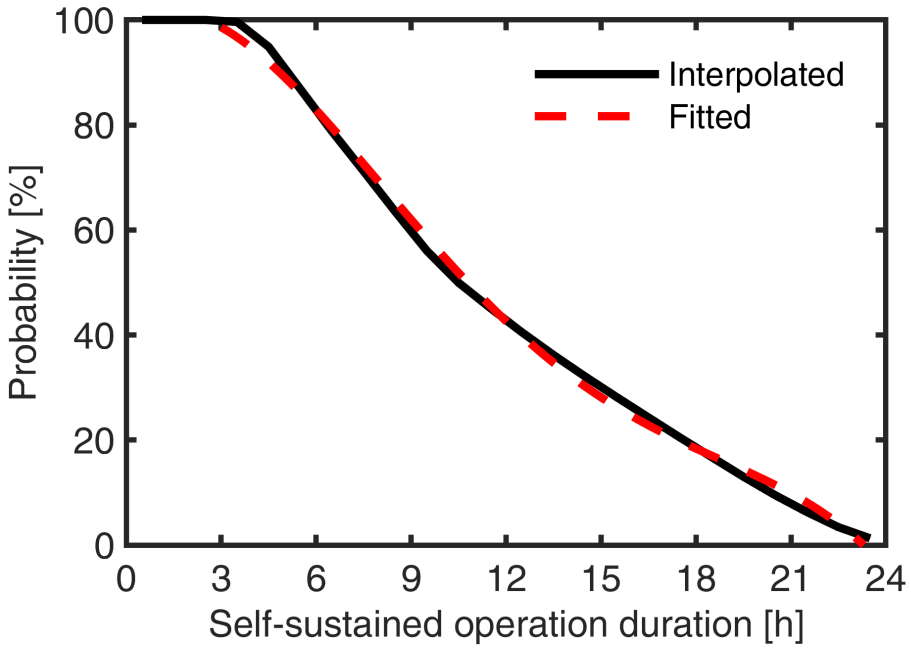

Figure 5.21: The cumulative probability curve, which defines the building resilience for self-sustained operation duration of the reference house. Regardless of the timing of the power outage inception, the reference house will self-sustain virtually at 100% load for up to 3 hours, and has a 50% probability of self-sustainment up to 10 hours.

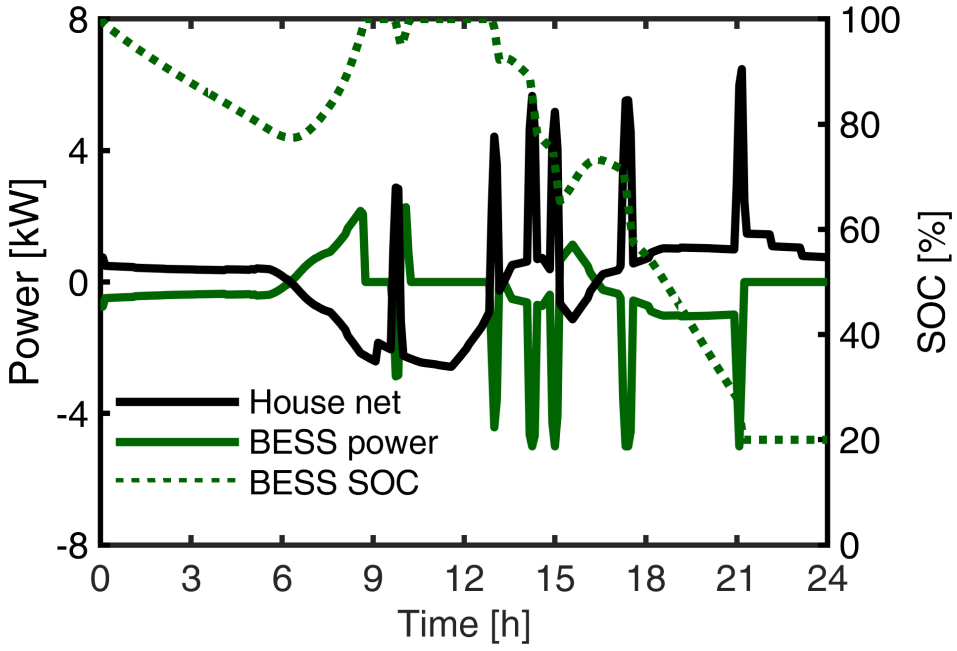

Figure 5.22: An example of a self-sustained case with residential load, except for the electric water heater, curtailed to 50% of the reference value. The self-sustainment duration was 21 hours, 4 hours longer than the reference house because of the lower electricity usage.

represented explicitly with a 4^{th} order polynomial equation, as follows:

$$f(t) = \begin{cases} 100, & t \in [0, 3) \\ p_1 t^4 + p_2 t^3 + p_3 t^2 + p_4 t + p_5, & t \in [3, 24], \end{cases} \tag{5.18}$$

where the coefficients for the reference example are p=[-0.0017, 0.0934, -1.5743, 3.7379, 99.1833].

5.4.3 Study for Different Home Load and BESS Energy Capacities

Curtailing the load can reduce the electricity usage and prolong the self-sustained operation in a power outage. The load in Fig. 5.22 was reduced to 50% after the power outage occurred at the midnight. Reducing the load in this scenario enabled

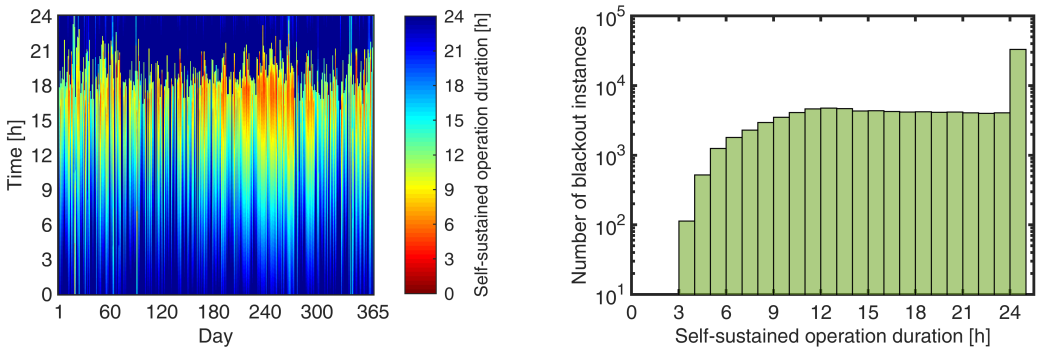

(a) (b)

Figure 5.23: Self-sustained operation duration of the house with 50% of the reference residential load presented as a (a) heat map and (b) distribution. The likelihood of the house self-sustaining for more than 24 hours is approximately 31%.

the house to self-sustain for approximately 21 hours, 4 hours more than the reference house at the same instance, as shown in Fig. 5.18 (a).

Curtailing the residential load increased the self-sustained hours for all 105,120 instances throughout the entire year (Fig. 5.23 (a)). The house load, except for EWH power, was curtailed to 50% while other parameters had the same values from Table 5.1. The distribution with 1-hour interval bins in Fig. 5.23 (b) shows the probability to self-sustain more than 24 hours was increased to approximately 31% when the residential load was curtailed to 50%. Meanwhile, the reference house without load curtailment has a near 0% chance to self-sustain for more than 24 hours (Fig. 5.21).

A BESS with larger capacity could store more surplus energy from solar PV generation and sustain the house for a longer time when a power outage occurs. When the house was connected to a BESS with a capacity of 27kWh, the self-sustained operation duration was prolonged to 22 hours, as shown in Fig. 5.24, 5 hours more than the reference house case in Fig. 5.18 (a).

Larger BESS capacity increased the self-sustained operation duration for all 105,120

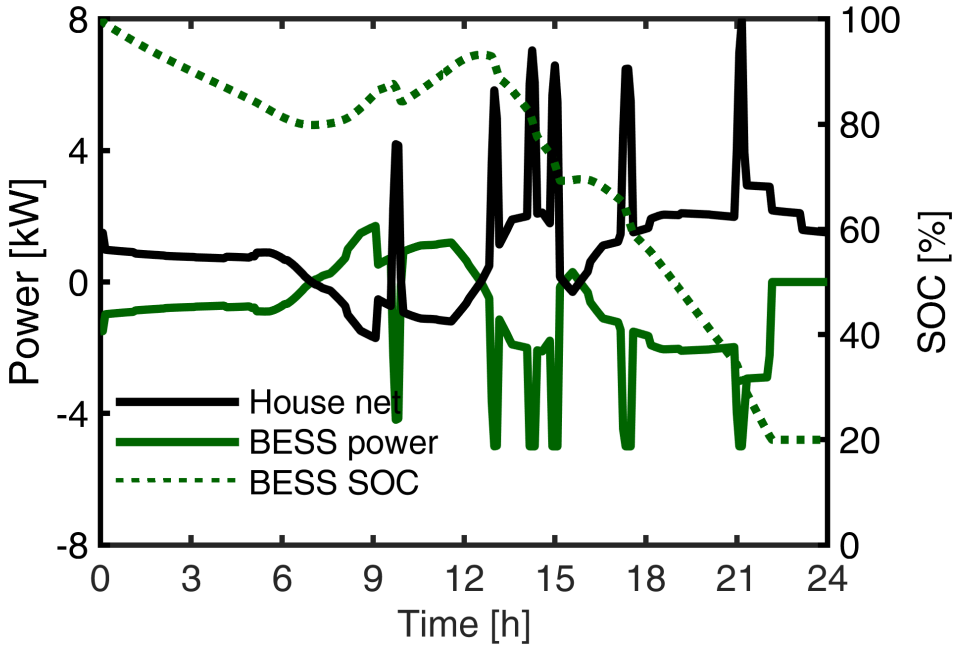

Figure 5.24: An example of self-sustained operation for a house with an increased BESS rating of 27kWh. In this case, the self-sustained operation of approximately 22 hours was 5 hours longer than the reference case.

instances throughout the entire year (Fig. 5.25 (a)). When the reference house was equipped with a BESS rated at 27kWh, it could self-sustain at least 24 hours for approximately 72% of all instances (Fig. 5.25 (b)). The self-sustained operation duration was extended in general with larger BESS capacity, as cases with longer time intervals increased compared to the reference house case shown in Fig. 5.20.

The effect of combining partial load and BESS capacity modifications on self-sustained operation duration were studied and for each combination, only the probability of self-sustaining for at least 24 hours was recorded. For example, the combination of 50% load percentage and 11kWh BESS resulted in a 31% likelihood of self-sustaining for at least 24 hours, as shown in Fig. 5.23. The simulation results for other combinations were summarized in Fig. 5.26. The load percentages from 50% to

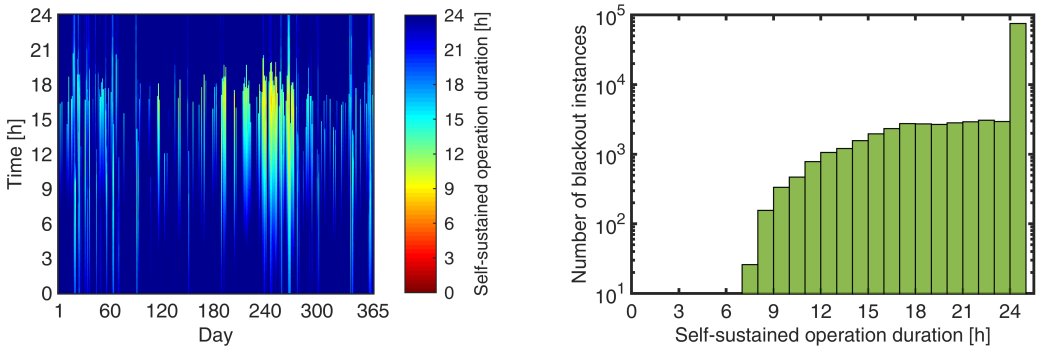

(a) (b)

Figure 5.25: Self-sustained operation duration of the house with a BESS rating of 27kWh is presented as a (a) heatmap, and (b) distribution. The probability that the house can self-sustain for more than 24 hours is approximately 72%.

300% covered are representative of the power profiles of residences with different user behaviors and house types. BESS capacities studied were between the range of 10 to 60kWh. The colors represent the probabilities for residences with combinations of different load percentages and BESS capacities to self-sustain for more than 24 hours.

In Fig. 5.26, the horizontal trend indicates the case for different residential loads with a fixed BESS. The case studies for curtailing the reference house from Fig. 5.23 can be referred as the BESS=11kWh horizontally. When the residential load of the reference house curtailed from 100% to 50%, the probability to self-sustain more than 24 hours was increased from virtually 0% to 31%, as shown in Fig. 5.23. For a BESS capacity larger than 40kWh, the probability for a house with 100% residential load to self-sustain more than 24 hours is almost 95%. With a larger BESS of 60kWh, the probability for the house to self-sustain at least 24 hours is more than 90% even when the load is 150%.

In Fig. 5.26, the vertical trend indicates that for a fixed load percentage, the probability of the residence self-sustaining for more than 24 hours increased, in line

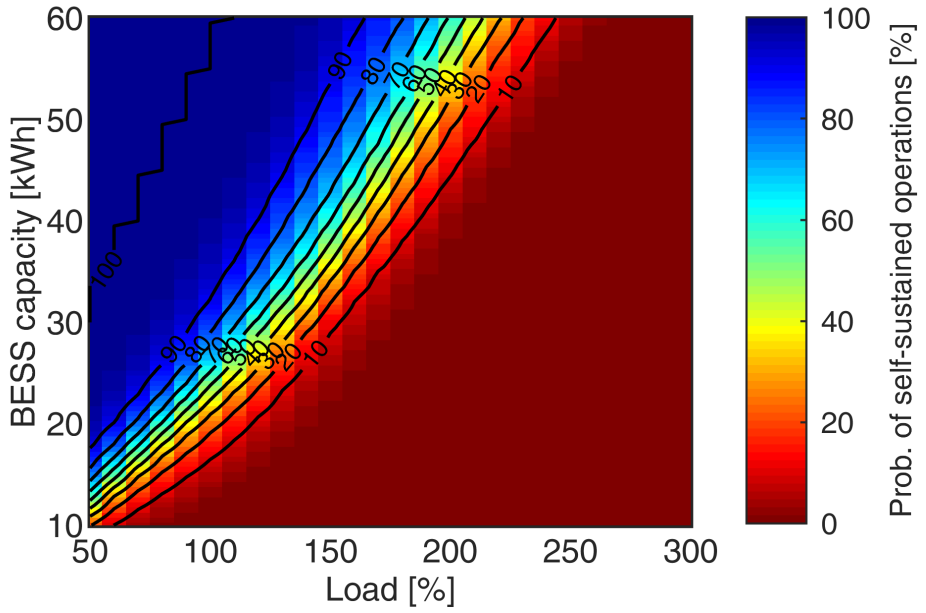

Figure 5.26: Results of a case study examining varying combinations of BESS capacities and home load percentages in self-sustainment duration of 24 hours or greater.

with the expectations, as the BESS capacity increased. The case study for increasing the BESS capacity to 27kWh from Fig. 5.25 can be referred to as the Load = 100% case vertically. When the BESS capacity was increased from 11kWh to 27kWh, the probability for the house to self-sustain for more than 24 hours increases from virtually 0% to 72%. For a house load percentage of less than 250%, increasing the BESS capacity significantly increases the residence self-sustainment duration.

5.4.4 EV Participation

The reference EV battery considered in the study is rated 90kWh/10kW with the returning SOC of 90%, as summarized in Table 5.1. Within this study, the EV is scheduled to leave and return home at 6 am and 6 pm, respectively. The EV can interface with the HEMS and supply residential loads when the EV is at home. When supplying power to the home, the total capacity of the residential ESS is expanded

and the total energy capacity defined in (5.15) becomes:

$$E_C = \eta_B \cdot E_{C,B} + \eta_E \cdot E_{C,E} \cdot B_E, \tag{5.19}$$

where η_E is 80%. the maximum range of the EV battery SOC (20%–100%); $E_{C,E}$, the energy capacity of the EV battery; B_E, Boolean results for 1 represent EV at home, 0 otherwise.

Two types of EV discharging scenarios considering whether or not the BESS was charged by the EV battery were explored in this study. In the first scenario, the EV was discharged to supply the residential load when it arrived home and the BESS stopped discharging, as shown in Fig. 5.27 (a). As a result, the BESS SOC remained the same until the EV left home at 6 am the next morning. In the second scenario, the EV supplied the residential load and charged the BESS (Fig. 5.27 (b)). In this case, the BESS was left with 100% SOC when EV left home. The residence can self-sustain for more than 24 hours under both EV discharging scenarios compared to self-sustaining approximately 5 hours in the reference case without EV discharging, as shown in Fig. 5.18 (b).

Load percentage and BESS capacity effects on self-sustainment were studied and results are shown in Fig. 5.28. For both EV discharging scenarios, the probability to self-sustain more than 24 hours was increased to more than 90% for the reference house, which can be located as (Load=100%, BESS capacity=11kWh) in the heatmap shown in Fig. 5.28. Enabling EV to interface with HEMS increases house resilience significantly compared with the case shown in Fig. 5.26. Furthermore, self-sustainment duration increased when the BESS was able to be charged directly by

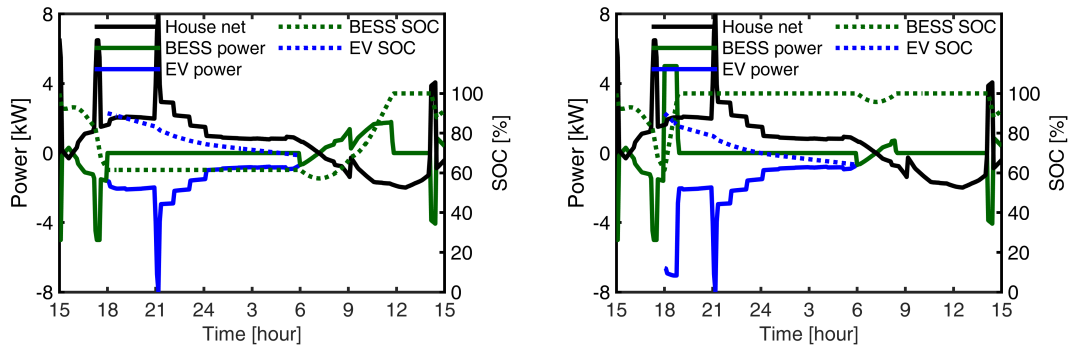

Figure 5.27: An example of a self-sustained case for the reference house with EV contributing to (a) supply the residential load only, (b) supply the residential load and charge the BESS. Assuming that the EV arrived home every day at 6 pm with a SOC of 90% and left home at 6 am the next day.

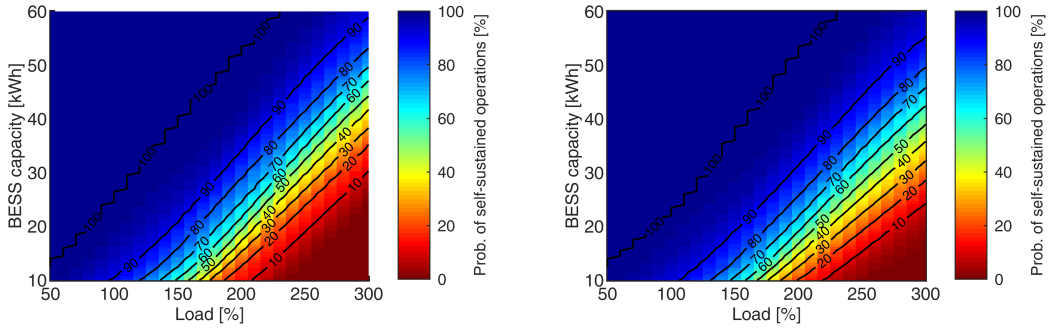

Figure 5.28: Case study for combinations of different load percentage and BESS capacities with an EV participating to (a) supply the residential load only, (b) supply the residential load and charge the BESS.

the EV battery, especially when the load percentage is high. For example, when the BESS capacity is 11kWh and load percentage is 150%, the results for the two EV discharge scenarios are between [50%, 60%] and [60%, 70%], respectively.

In some extreme power outages, such as those caused by extended wildfire, the power supply may only be restored after a few days. In such cases, the EV is expected to stay home and $B_E = 1$ in (5.19). The battery can be incorporated to expand the

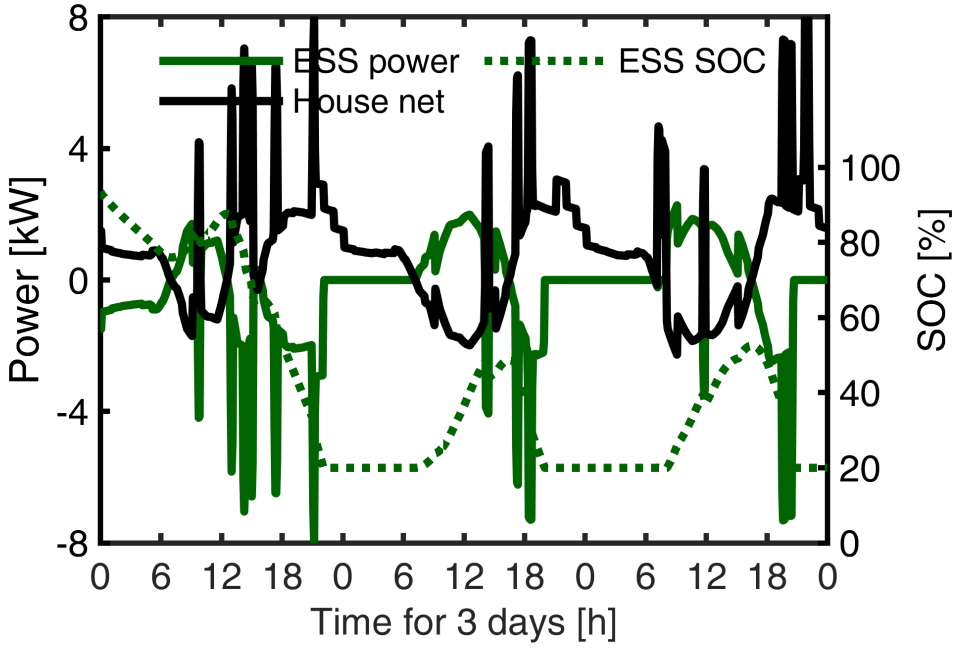

Figure 5.29: An example self-sustain case for the house with the EV staying at home. Shown is the case with an EV battery rated at 20kWh. The capacity of the energy storage system (ESS) was expanded dramatically by incorporating the EV battery.

residential ESS capacity, which is defined according to (5.19) as:

$$E_C = \eta_B E_{C,B} + \eta_E E_{C,E}. \tag{5.20}$$

The simulation results from Fig. 5.29 show that when the EV battery rated 20kWh was incorporated in the ESS, self-sustained operation duration was increased to approximately 20 hours. Introduction of the EV battery increased the total RESS capacity significantly, and since the duration of self-sustainment drastically increased, all instances with an interconnected EV were analyzed for 72 hours following an outage.

The results for all 105,120 instances are shown in Fig. 5.30. When the EV with a battery of 20kWh stayed at home, the house could self-sustain longer in general and at least 72 hours for approximately 10% of the instances (Fig. 5.30 (b)).

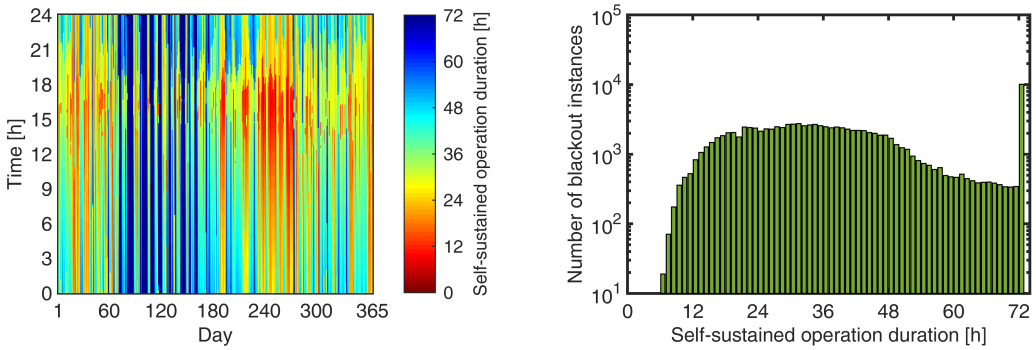

(a) (b)

Figure 5.30: The self-sustained operation duration of the house with an EV at home for the duration of 72 hours presented as a (a) heatmap, and (b) distribution. The EV battery was rated 20kWh in this case. The probability that house can self-sustain for at least 72 hours is approximately 10%.

With a 20kWh EV battery staying at home during the outage, building resilience of the residence improves significantly. The probability of the residence self-sustaining for at least 12 hours is almost 100%, as shown in the cumulative probability curve in Fig. 5.31. In this example, the probability that the house could self-sustain at least 24, 48, and 72 hours are approximately 80%, 26%, and 10%, respectively. The cumulative distribution of building resilience for varying scenarios was fitted and represented explicitly with a 4^{th} order polynomial equation, as follows:

$$f(t) = \begin{cases} 100, & t \in [0, 12) \\ p_1 t^4 + p_2 t^3 + p_3 t^2 + p_4 t + p_5, & t \in [12, 72], \end{cases} \tag{5.21}$$

where the coefficients are p=[-0.0000097, 0.0022765, -0.1557, 1.8578, 95.7078]. It is essential to keep the resolution of the first two coefficients 7-decimal to maintain the accuracy.

The effect of different EV battery ratings were studied and results are shown in Fig. 5.32. All parameters apart from the EV energy capacity are kept the same as the reference house (Table 5.1). The probability shown in Fig. 5.31 is represented

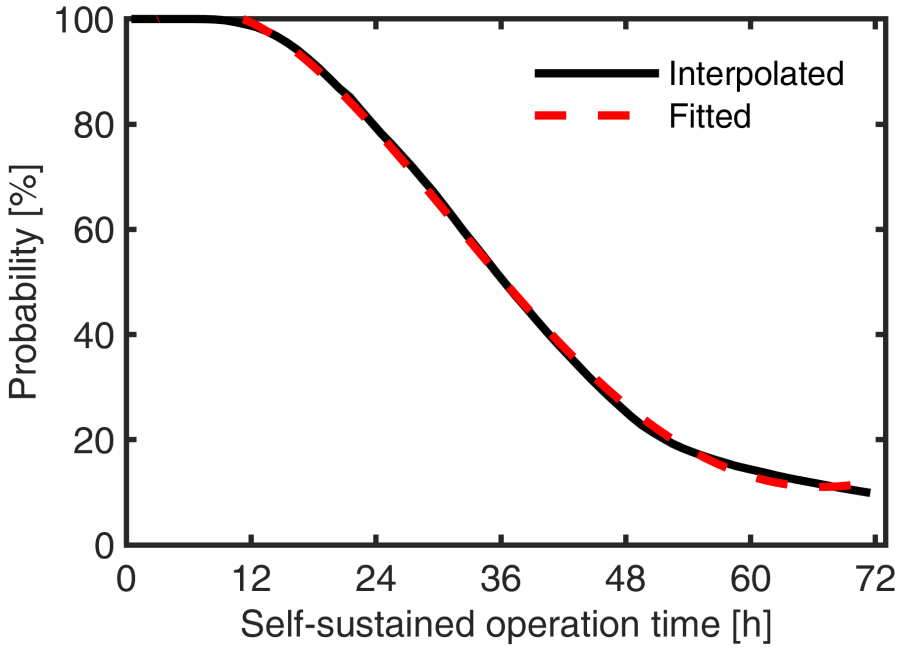

Figure 5.31: The cumulative distribution for the self-sustained operation duration of the house withan EV at home rated for 20kWh. Building resilience was analyzed over a duration of 72 hours.

by the case of fixing the x-axis at 20kWh. At this value, the colors show that there exists approximately 80%, 26%, and 10% probability for self-sustainment duration of 24, 48, and 72 hours, respectively. EV battery capacities of 30kWh, 60kWh, and 90kWh give the residence a 100% probability to self-sustain approximately 12, 30, and 45 hours, respectively. The probabilities for residence with EV battery capacities of 30kWh, 60kWh, and 90kWh to meet a given duration target, e.g., 48 hours, are approximately 60%, 92%, and 98%, respectively.

5.4.5 Discussion

In this chapter, the resilience of a building was quantified as the probability to self-sustain for a specified duration of time following a power outage, which can occur at any time throughout an entire year. Factors including the electricity usage of the

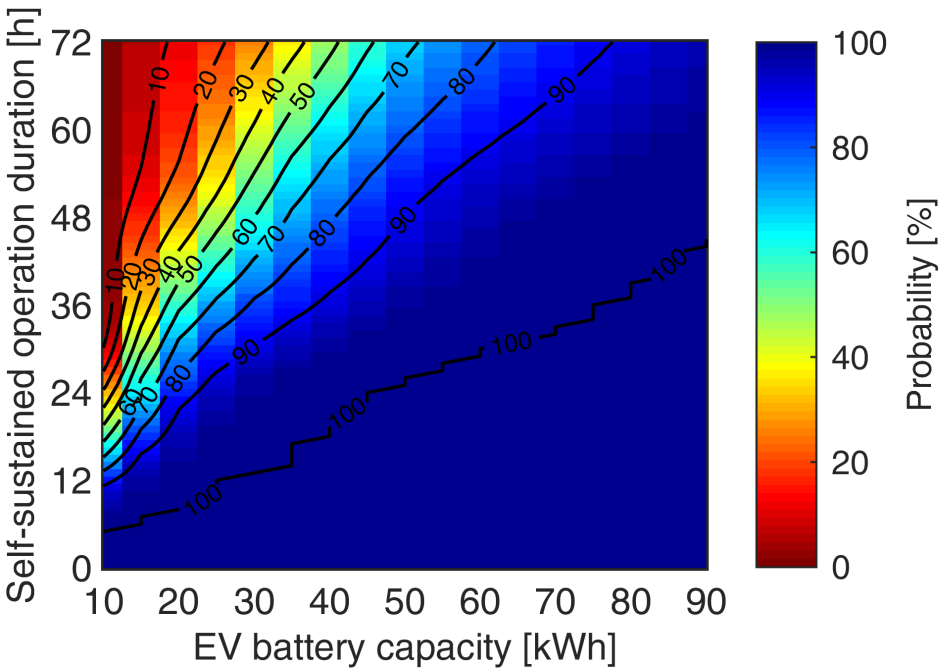

Figure 5.32: Building resilience heatmap for the house with an EV staying at home and providing additional energy storage. The effect of different EV capacities on building resilience was evaluated.

house, renewable generation, the capacity of the residential energy storage system (ESS), and the availability of a EV with its associated battery have been studied. The results show that the reference house considered could self-sustain up to 3 hours in almost all instances.

The probabilities for a house to self-sustain for at least 24 hours were summarized for combinations of different home loads, which range from 50% to 300%, and BESS capacities, which range from 10kWh to 60kWh. For a residence with a fixed BESS capacity, of 40kWh, the quantified results, which are the probabilities for the house to self-sustain for at least 24 hours are 100%, 95%, and 60%, for home load percentages of 50%, 100%, and 150%, respectively. For the example residence with 100% full load, the quantified results, which are the probabilities for the house to self-sustain for at

least 24 hours are 0%, 25%, and 95%, for BESS capacity of 11kWh, 20kWh, and 40kWh, respectively. The quantified results provides the utility and house owners with the basis for planning rolling blackout, power restoration, and for sizing the residential ESS.

This chapter explored the possibility of utilizing an EV during a power outage by incorporating its charged battery into the residential ESS. Considering fixed times for the EV departure from and return to the residence, building resilience increased for all cases even when the EV is away and not available in the daytime. The probability of a reference house with a BESS of 11kWh, home load percentage of 100%, and a EV battery of 90kWh to self-sustain for at least 24 hours is approximately 90% in such cases. When the house owner opts to keep the EV at home all the time during an extreme power outage, building resilience increased significantly even without load curtailment. The results show that incorporating the EV battery into residential ESS substantially increases self-sustainment duration. With EV battery capacities of 20kWh, 50kWh, and 90kWh, the probability for the house to self-sustain 24 hours is, 85%, 100%, and 100%, respectively. With the same capacities, the probability to self-sustain for 48 hours is, 30%, 90%, and 98%, respectively.

The effect of different PV ratings was studied with PV rating being changed from 5kW to 10kW with increments of 0.1kW. Results show that, with the ratings considered and all other parameters fixed, this has a negligible impact on building resilience as minor changes in self-sustained duration were noted. This indicates that the capacity of the BESS and that of an additional EV battery system provided have some of the largest impact on improving building resilience.

5.5 Conclusion

The distribution of arrival time and daily driving mileage were estimated according to NHTS 2017 data. The arrival SOCs for EVs were calculated based on the daily driving mileage. An EV charging schedule was proposed in which the high ToU period was avoided to achieve the most financial benefits and a 100% SOC was guaranteed at 6:00 in the morning on the next day.

The influences of different penetrations for RESSs and PVs on the aggregated power and daily utility charge were studied. Simulation results show that the coordination of RESSs and EVs resulted in the reduction of daily utility charge. The entire residential community can work as a VPP under the proposed schedule for RESSs and EVs.

A power distribution system for a example community was modeled with residences having EVs to provide V2G services complying to the CTA-2045 standards. Without dedicated controls, the spike in the reverse power flow from EV to grid may be significant, resulting in potential overload in the main feeder transformer. Even Under this extreme studies, voltage regulation is not reported as a major issue as virtually no violation was observed. The energy capacity of EVs is extremely large, substantially exceeding the load of the community, and could provide community long time support for load shifting, in this case through the entire night. In future work, the control for EVs will be proposed and verified to make the entire community a virtual power plant to have constant net power flow for a long time.

A procedure was developed to quantify the building resilience considering the load

percentage, capacity of BESS and EV battery. A reference house from California, with an annual electricity usage of 13,628kWh and a BESS with capacity of 11kWh, was used as the baseline for developing the building resilience model. The probability for the reference house to self-sustain for more than 3, 10, and 24 hours was found to be 100%, 50% and 0%, respectively. For the reference house, when the BESS capacity was increased, for example, to 40kWh, the probability for the house to self-sustain for at least 24 hours increased to 95%. When the load of the reference house was reduced, for example, to 50%, while other parameters were kept the same, the probability of self-sustaining for 24 hours increased to 31%. When an EV with a battery capacity of 90kWh was incorporated in the HEM system, the probability for the reference house to self-sustain at least 24 hours increased to 90%. If this same EV was parked at home all the time, the probability to self-sustain 24 hours was 100%, and the likelihood of self-sustaining for 48 hours increased to 98%. When the EV battery capacity was 20kWh, the results for 24 and 48 hours were 85% and 30%, respectively.

Chapter 6

Forecast of Community Total Electric Load and HVAC Component Disaggregation through a New LSTM-based Machine Learning Method

6.1 Introduction

According to the Energy Information Agency, the residential sector accounted for 22% of the total U.S. energy portfolio [207]. In residential communities, which are the focus of this chapter, heating, ventilation, and air-conditioning (HVAC) systems are the largest energy users and major contributors to the peak power [34, 167, 208]. For perspective, the approximately 45% of the residential sector energy use from HVAC systems [209], represents 10% of the total U.S. grid's demand. The accurate

estimation and forecast of the total and electric power components provides utilities with planning and control opportunities for optimal energy generation and use, and for avoiding large demand fluctuations.

Together with the specific thermal inertia of the building, an HVAC system may support temporary demand response (DR) controls and a provide distributed energy resource, including virtual energy storage capacity, without affecting occupancy thermal comfort [88, 96]. Previous research shows that HVAC systems in a residential community may be controlled by a similar charging and discharging procedures as electric batteries [64]. More recently, transactive energy approaches were proposed for automated HVAC controls and enabled the reduction of total electricity cost, while maintaining user comfort [210]. Another application of HVAC controls, based on Stackelberg game theory, contributed to reducing the mismatch between residential energy usage and renewable generation by more than 40% in a best case scenario [90].

Provided that the data for the total residential load is available, the HVAC power may be identified, in principle, based on the observation that it is the component most sensitive to outdoor weather conditions. An example previous study into HVAC load disaggregation at the individual residence level was conducted using 30 minute data representative of smart meter data for 85 homes [211] utilizing daily average outdoor temperature. The authors propose an hourly linear regression based method including subtraction of average baseload profiles per season, that is found to have an error of approximately 8% across different buildings. Recent work by our group of authors, based on systematic experimental data from a individual residence, smart home, reported good results for total forecasts and isolation of baseload and HVAC power

components, by characterizing weather conditions through both outside temperature and irradiance [212].

Other previous work into individual residence HVAC load disaggregation includes a random forest machine learning model training procedure and pipeline optimization with detailed automated feature selection considering weather, calendar based, pattern-based, statistical, etc [213]. The model was tuned using the 182 homes and tested on 10 all from the Pecan Street experimental database with an overall R^2 of 0.905 over eight days. Additionally, an hourly Multi-sequence Non-homogeneous Factorial Hidden Markov Model (MN-FHMM) performed with an average error of 22% with a dataset of over 100 homes. A common factor between this model and an additional one described in [214], is that temperature was used as the only weather input. In practice, the effect of the solar irradiance on the building heating maybe significant, as previously discussed for a computational and experimental study of smart "robotic" homes [94]. One set of authors combined both multiple weather parameters including solar irradiance with frequency components ascertained from Fourier Series Analysis of high resolution minutely data to disaggregate both heating and lighting loads [215], but this resolution data is not wide spread and efforts into smart meter disaggregation are further needed.

Fewer studies into aggregated HVAC load separation of entire distribution circuits including hundreds to thousands of homes were found. The linear regression based method from individual homes in [211] was replicated by the authors in [216] at the aggregate level of a residential community of 400 homes with verification against a Gridlab-D model of the community. Also at the community level, the authors of

[217] improved another traditional multiple regression method using time of year, weather data, holidays, and varying cut off temperatures to calculate total hourly load with an error of approximately 5% and disaggregate heating and cooling portions from over 80,000 residencies and 8,000 commercial buildings located in Canada. The authors call for further validation of the method and approach to hourly temperature selection points for heating and cooling as ground truth sub metering HVAC data is not available at this wide scale, which is explored further in our chapter.

The current chapter brings additional novel contributions specific to community-level applications addressing a research gap in HVAC load analysis. Specifically, a procedure for identification of an outside temperature range for which the HVAC systems across the community do not operate from hourly "V-curves" of total power to outdoor temperature. Key temperatures from the identified range are used in a novel two-step machine learning (ML) method employing long short-term memory (LSTM) algorithms for the HVAC separation. Under zero irradiance and identified key TmHVAC temperature conditions, the baseload is estimated by the LSTM model and used to disaggregate of the HVAC power component.

The chapter is organized in multiple sections with the next one being devoted to the problem formulation and the introduction of the experimental big data and its preliminary analysis for a representative residential community with all electric air conditioning in the summer and mixed natural gas and electricity heating supply in the winter. The proposed method for forecast and disaggregation is presented, together with a pseudo-code algorithm and flowchart, and example results, in the third section. A fourth section further analyzes case study results, selection of parameters,

and demonstrates low for errors for the the total power forecast. A comparison with conventional linear-regression results is presented in the fifth section, indicating the advantages of the proposed method both in term of automated analysis and improved accuracy. The sixth section includes discussions on the validity of the separation method based on statistics and human behavioural patterns for the baseload and fundamental physics for the influence of outdoor weather conditions. Finally, the conclusions summarize the main findings, original contributions and advantages of the proposed ML method.

This chapter is substantially based on the following paper:

- H. Gong, *et al.*, "Community level total load forecast and HVAC disaggregation through a new LSTM method," *Energies*, 15p, 2021, *(Submitted in Dec, 2021)*

6.2 Problem Formulation and Experimental Data

A main objective of the study described in this chapter is to use systematically-collected historic data for electric power and weather conditions, i.e., outside temperature and solar irradiance, to produce a day-ahead forecast of the total electric load demand at community level and to separate, i.e., disaggregate, out of it the power component corresponding to the HVAC heating and cooling systems. The newly developed algorithms are based on ML models, which are of the black-box data-driven type, and therefore require "big data" consisting of very large time series.

A real-life case study for a representative suburban community from Kentucky, which is also relevant for a wider region of the US, is considered throughout the

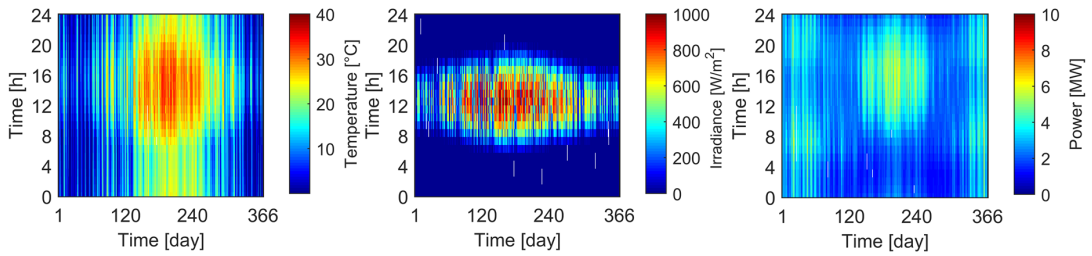

Figure 6.1: The 2020 experimental data for weather and total electric power for the community considered in the study. All 1810 buildings employ electric air-conditioners for cooling during the summer, but only 53% of them are using electric heat pumps for heating during the winter.

chapter. The electric power experimental data for the four years, 2017 to 2020, inclusive, as measured at the main circuit feeder of the Liberty Rd. area served by the Louisville Gas and Electric and Kentucky Utilities (LG&E and KU) distribution system in Lexington, KY, has been collected with a one minute time resolution. The weather data is provided with five minute resolution by the National Oceanic and Atmospheric Administration (NOAA) (Fig. 6.1.)

Within this aggregated community there are 1810 buildings, mostly houses used as family homes and residences. Space cooling in the summer is provided for all buildings via HVAC air conditioners. For heating in the winter, 966 of the buildings employ electric heat pump HVAC systems, and the rest use natural gas furnaces. This equipment deployment, together with the weather conditions, contribute to explaining the electric power pattern and the peak usage illustrated in Fig. 6.1c, which is in line with expectations for communities with dual heating supply/fuel.

The daily load demand for the total electricity used by the analyzed combined community measured at the main feeder in years 2017-2019 circuit has specific seasonal profiles, depicted as box plots in Fig. 6.2). The minimum, 25^{th}, 50^{th} also known

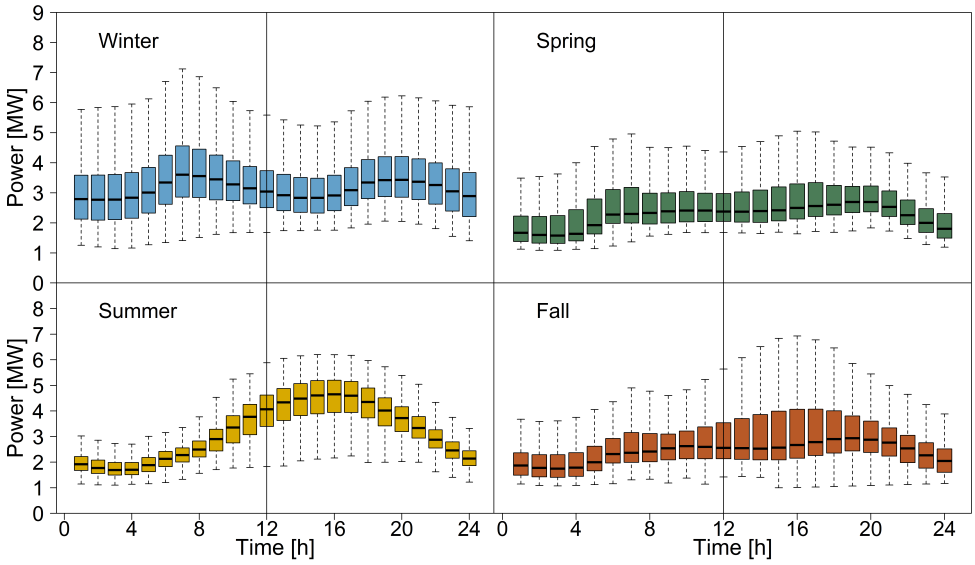

Figure 6.2: Hourly box plots show the distribution of the measured total electric power in 2017-2019 for the example residential community considered in the study across an entire day for all four seasons. The expected impact of season on total electricity used is illustrated, hence inclusion of weather parameters in modeling.

as the median, 75^{th} percentiles and the maximum power usage are shown as the bottom of the dotted line, edge of the lower box, middle black line, edge of the top box, and top of the dotted line. The distributions shown per hour of the day change with the season. The magnitude of the maximum load and time of day at which it occurs are particularly affected with the median maximum usage for the summer falling in the afternoon at approx. 4.5MW. In comparison, the winter is bimodal with the maximum load across the day happening in the early morning with outliers reaching to more than 7MW, due to extreme instances of cold.

Such variations are common and are typically considered through categorical variables in quantile regression models such as the Vanilla Benchmark Model [218]:

$$y(t) = \beta_0 + \beta_1 M_t + \beta_2 W_t + \beta_3 H_t + \beta_4 W_t H_t + f(T_t) \tag{6.1}$$

where t is the time variable [min], $y(t)$ the load [min], M_t denotes the month [1-12], W_t the week [1-4], H_t the hour within the day [1-24], and $f(T_t)$ is another quantile regression function relating the temperature [C or F] at t to the categorical time of year variables. This model was originally employed as the basis for global forecasting competitions [219], and has been later improved to include the regency effect, i.e., the impact of temperatures at previous times [113].

These established relationships between time of year, weather, temperatures at previous time increments, and the total load have been further studied and identified in other chapter relating to HVAC load separation and forecast. For example, an aggregated residential total load forecast that considers the time of year through one hot encoding, the day of the week, and previous sequences of energy usage was reported in [114].

Another study, by a different group of authors, identified a time lag between an outdoor temperature increase and the resulting larger HVAC load, corresponding to the previously mentioned regency effect [220]. This referenced study included the influence of solar heat gains from sunlight in the HVAC model. For such reasons, the authors of this chapter have selected sequence inputs of the previous load power, outdoor temperature, and solar irradiance, as well as future weather inputs to forecast the day-ahead future load for use in a HVAC disaggregation case study. The data has also been split to include summer and winter months as separate datasets in order to account for the categorical time of year influence.

By accounting for the influence of previous and future weather in the model, the patterned portion of the load can be calculated with high confidence because the

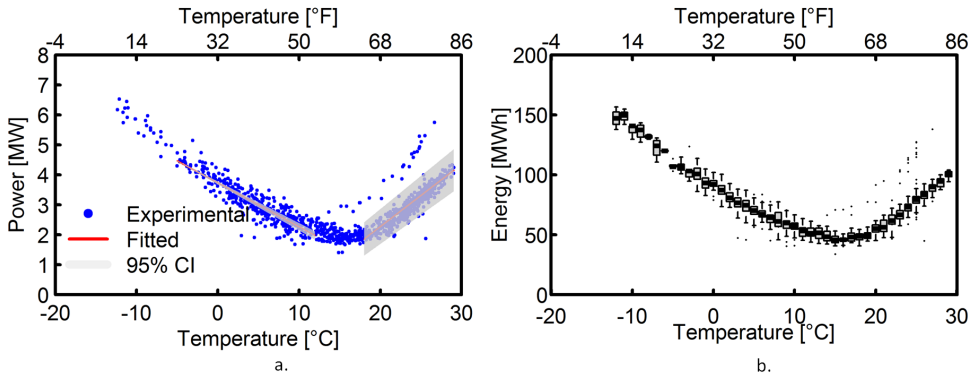

Figure 6.3: Daily V-curves for power (a) and energy (b) with linear regression, confidence interval, and box plot example representations for the studied community.

community level HVAC disaggregation conducted in this chapter has less uncertainty from weather variability. The impact of stochastic human-behavior based portions of the total load is minimized at the community level as the randomness of individual schedules and decisions are smoothed. The aggregate effect on human behavior is seen in large scale experimental studies of community level wide air-conditioning, lighting, dishwasher, and clothes washer/dryer loads utilized by U.S. Department of Energy Building America Program and the National Renewable Energy Laboratory (NREL) [221]. This know phenomenon was used by our group in [222] to produce equivalent aggregated water heater models for community-wide Virtual Power Plant (VPP) control studies.

For analysis of key features or inputs used in our case study, the total power and weather data has been averaged on a daily basis and also integrated to calculate energy. The graphical results shown in Fig. 6.3 are typically referred to a daily "V-curve". The spread of data, which is influenced not only by temperature, but also by irradiance and other factors, is exemplified through the 95% confidence interval for power in cooling mode and a box plot representation for energy. It should be noted

that extremely high or low values for the hourly temperature maybe averaged out in the daily calculations, and may contribute to the relatively low number of outliers for power and energy. The proposed hourly model described in the following section accounts for these extreme temperatures by forecasting for each hour of the following day using the key weather parameters identified in this section.

6.3 Proposed Method for Forecast and Disaggregation

The proposed method, which is described in this section, is a combination of multi-step machine learning algorithms based on big data sets, and of a physical engineering observation of the weather conditions under which the operation of the HVAC system is not required, i.e., stand by, and hence its corresponding component electric power draw is substantially zero. To quantify these conditions, as accurately as possible, the "V curve" has been derived using the extensive hourly data rather than the traditional daily averages (Fig. 6.4a).

In line with expectations, the data spread in this case is larger than for the daily values, but the V-profile is still similar with two edges for heating and cooling, respectively, and an in-between region in which the total electric power is minimum, as it substantially covers only the "baseload", i.e., the sum of all other load components, apart from the HVAC. Such conditions may occur, for example, at night, when the irradiance is zero and the outside temperature is close to the set point for the indoor temperature, which has a typical 20°C value, or during the day in the so

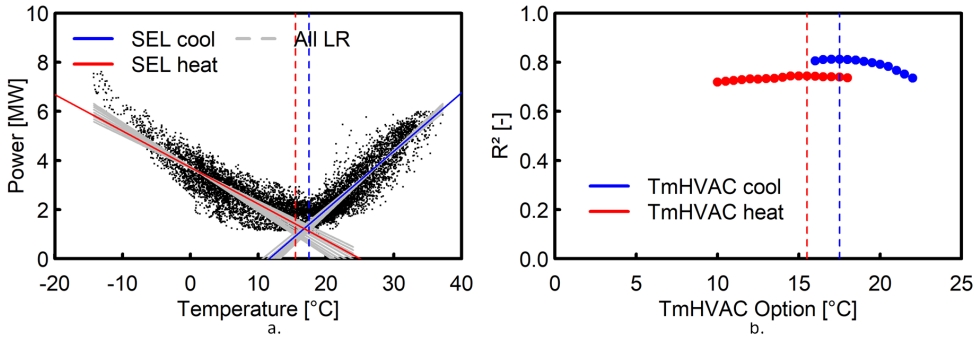

Figure 6.4: Hourly V-curve for electric power together with linear data fits corresponding to different values for the outdoor temperature key indicator, TmHVAC, for cooling and heating, respectively (a). Parametric study for the R-square goodness of the linear fit as a function of the considered TmHVAC.

called "shoulder months" of spring and fall when due to the combined effect of mild temperature, irradiance, and building thermal insulation there is no need for heating nor cooling.

As a first step of the method, two outdoor temperature key indicators, denoted by TmHAVC, one for heating and one for cooling, are introduced to identify the minimum and the maximum temperature, respectively, for which the HVAC systems are on stand-by and not using virtually any electricity. The proposed mathematical procedure to select the TmHVAC points is described in Algorithm 6.1. A wide range from 10 to 18°C was considered for the TmHVAC heating point, and 16 to 22°C was studied for the TmHVAC cooling point. Within these ranges, the hourly data was divided into subsets, and linear fitting was performed as illustrated in grey in Fig. 6.4a. The temperatures corresponding to the highest values for the coefficient of determination, or the R^2 goodness of the fit, which for the example community study are 15.5 to 17.5°C, are shown in Fig. 6.4b and may be recommended for further use. As it will be later discussed, the selection of TmHVAC may also consider the

data spread, for example at very low temperatures due to gas heating for part of the community, and the need to achieve a better fit particularly at high loads, in order to ensure that the demand is fully met under extreme conditions.

Algorithm 6.1 Mathematical process for TmHVAC temperature selection.

Prepare year of total power and outdoor temperature data
Select range of potential cooling TmHVAC options, e.g., 16-22 C
Select range of potential heating TmHVAC options, e.g., 10-18 C
Iterate for each TmHVAC cooling option

- Select temperatures above the TmHVAC cooling option and the corresponding total powers
- Fit the curve by linear or polynomial regression
- Calculate the coefficient of determination (R^2)

Repeat iteration procedure with temperatures below the TmHVAC heating options
Select TmHVAC cooling and heating points with the highest R^2 value

In the second step of the method, a ML black box model based on a sequence-to-sequence encoder-decoder LSTM algorithm of the type previously introduced by the authors for home-level applications [212] was adapted for community-level studies and employed for the forecast of the total electric power load. This ML model was trained using hourly integrated power and weather data for the example community over the winter and summer for three years, 2017 to 2019.

The input data, ML gate, was structured in series of consecutive 72 hours, i.e., 3 full days, and an additional 24 hours array for the day-ahead weather forecast. The weather factors were simplified to the two most important: outdoor temperature and solar irradiance. It is assumed that the houses are tightly sealed and wind driven infiltration is not a major factor. The results, ML gate, are represented by 24 hours of total electric power forecast. The model was tested over the year with the most

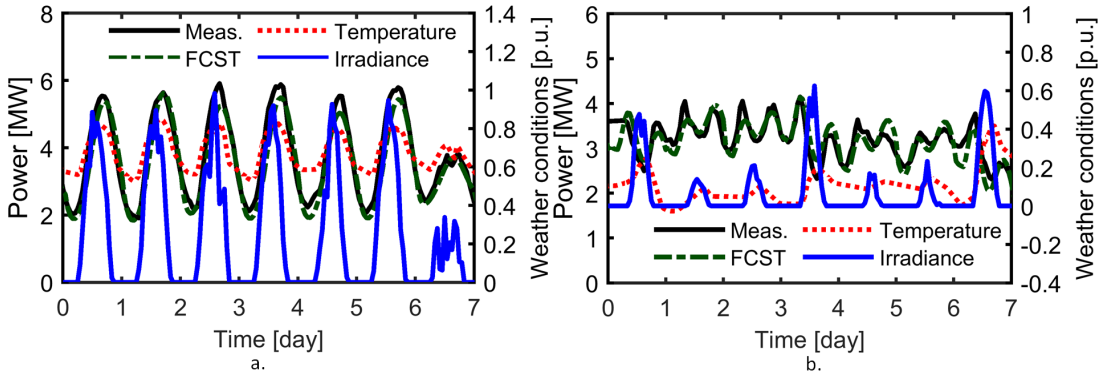

Figure 6.5: Total load measured and forecasted for 2020 example weeks starting on June 4th (a) and January 27th (b). Also plotted and illustrative of the correlation are the weather conditions, which are specified in the p.u.system with a reference outdoor temperature of 40°C and a solar irradiance of 1000W/m^2, which is used throughout the chapter unless specified otherwise.

recently available data, which is 2020, by providing instead of a weather forecast the actual data.

The comparison between the forecasted and the measured total electric power was satisfactory, as illustrated by the example summer and winter weekly profiles included in Fig. 6.5. The last day in the week shown has a decreased load caused by extremely low irradiance. The model accounts for changes in weather conditions and resulting impact on total power demand across the community and was able to predict the reduced load. Utilities would benefit from the proposed day-ahead forecast to schedule generation needed on days outside of typical weather such as very hot summer days and very cold winter days. It is also important to note that the specific neighborhood selected has a near constant occupancy level as construction is completed and no new houses are to be added. Scaling to account for a 1.25% growth rate could be applied to the final forecasted result from the proposed model to account for the increase in population but was not considered for this case study.

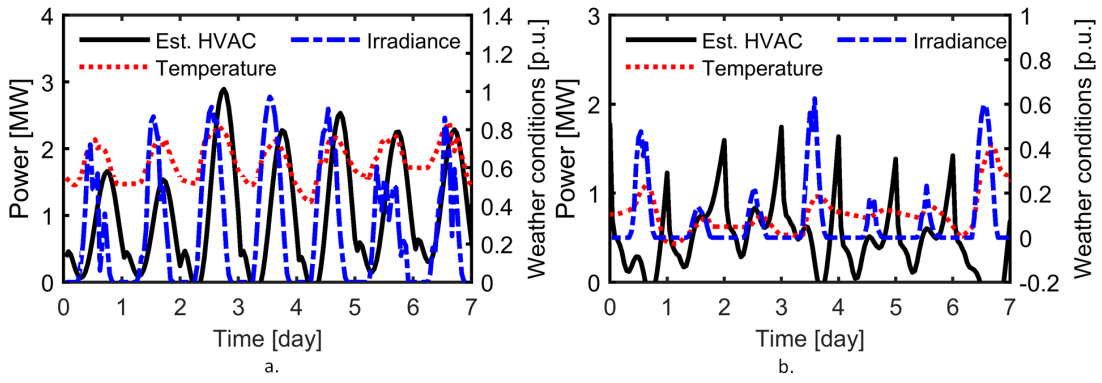

Figure 6.6: HVAC electric power component dissagregated as the difference between the total forecasted power from Fig. 6.5 and the estimated baseload power from Fig. 6.7 for summer (a) and winter (b).

In a third step of the method, the previously established and trained LSTM model that employs 72 hour data series, was employed/tested, in an innovative engineering type approach, with constant TmHVAC values, selected for the cooling and heating season, respectively, and with zero irradiance. The electric power results constitute the estimated baseload for the community and correspond to the situation in which the HVAC systems are on stand-by and hence not using virtually any electricity.

In the fourth and final step of the method, the HVAC load component is disaggregated, i.e., separated, through the subtraction of the estimated baseload from the total electric power. The results for the previously considered example weeks are shown in Fig. 6.6. During the summer, the effect of the thermal inertia of the buildings, all of which operate electrically powered HVAC air-conditioners, is noticeable and provides reassurance that the proposed ML method is consistent with the expected physics-based behaviour.

The overall procedure is summarized through the combined pseudo-code for the following Algorithm 6.2 and the flowchart from Fig. 6.8. Also included in this figure

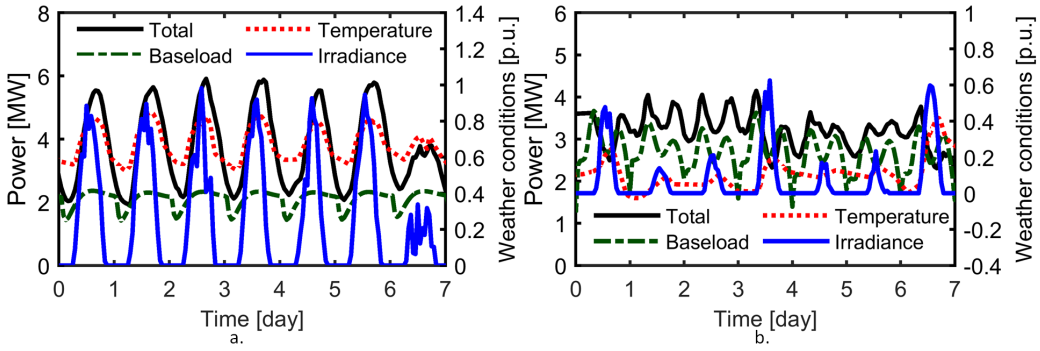

Figure 6.7: Baseload power estimated for summer (a) and winter (b) example weeks plotted for reference together with the total measured power and the weather conditions from Fig. 6.5. The difference between the two powers provides the component corresponding to the HVAC load.

are the 2020 test year results for forecasted total power and baseload and HVAC components, showing that during the summer the baseload maintained a fairly repetitive load profile and the HVAC variations are dependent of weather conditions. Unless specified otherwise, the values used for TmHVAC throughout the chapter study are 12 and 18°C for heating and cooling respectively, for rationale later explained in a discussion section.

Algorithm 6.2 Total and baseload forecast and disaggregation of the HVAC power component.

Prepare the data for training the LSTM model

- Input gate: Total power for previous 3 days, weather data for previous 3 days, and weather data for the next day
- Output gate: Total power for the next day

Train the LSTM model
Forecast the total power using the LSTM model
Estimate the baseload power component using the LSTM model

- Input: weather data for the next day is replaced by TmHVAC and zero irradiance

Estimate the HVAC power component.

6.4 Case Study

6.4.1 Results

The overall winter seasonal results obtained by applying the method to the studied community are plotted in heatmap format in Fig. 6.9 similarly to the results provided for the summer in Fig. 6.8b. A specific winter pattern of bi-modal daily peaks in the morning and evening, which corresponds to weather conditions and typical human behaviour aggregated at community level is noticeable. For this community, in the winter the contribution of the base load is expected to be more substantial, especially when considering that approximately half of the buildings are heated with natural gas furnaces. The summer daily specific profile, has only one typical peak in the late afternoons into the evenings, when all buildings are electrically air conditioned and most people are expected to be at home.

The overall performance of the LSTM model was analyzed and quantified separately for the summer and winter (Fig. 6.10). The residual for the summer results has a mean of -137kW and a standard deviation of 361kW. The corresponding values for the winter results are 33kW and 302kW, respectively. The mean residual percentage errors are 2.3 and 0.5% of the maximum forecasted community load, which is 5.965 and 6.051MW, in the summer and winter, respectively. The Mean Absolute Percent Error (MAPE) across the entire test periods is 9.5% for the summer and 7.3% for the winter. Based on the trends observed and on the error analysis, the LSTM model for the community total electric power forecast can be considered as satisfactory.

The proposed LSTM model is satisfactory as its MAPE is comparable with other

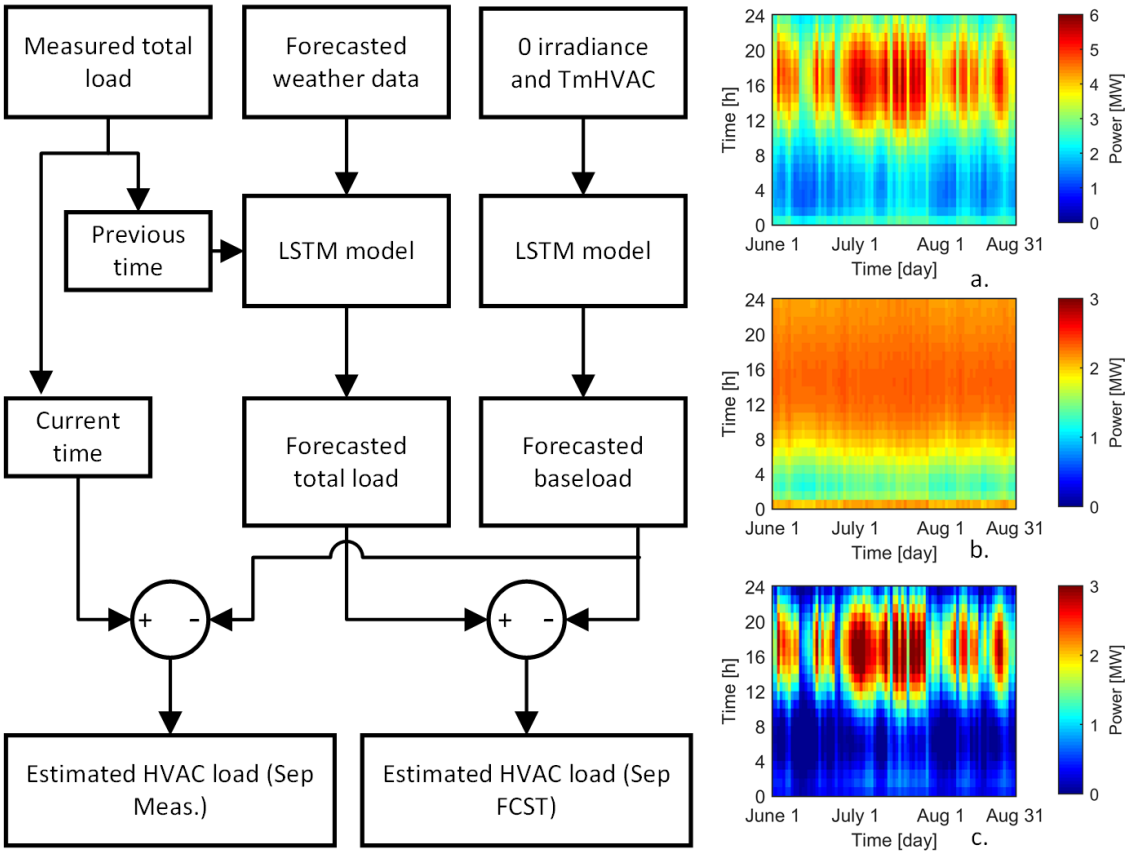

Figure 6.8: Flow chart of the proposed LSTM-based method for forecasting and dissagregation. Also included are the total (a), baseload (b), and separated/dissagregated HVAC power component (c) for the example community during the 2020 summer.

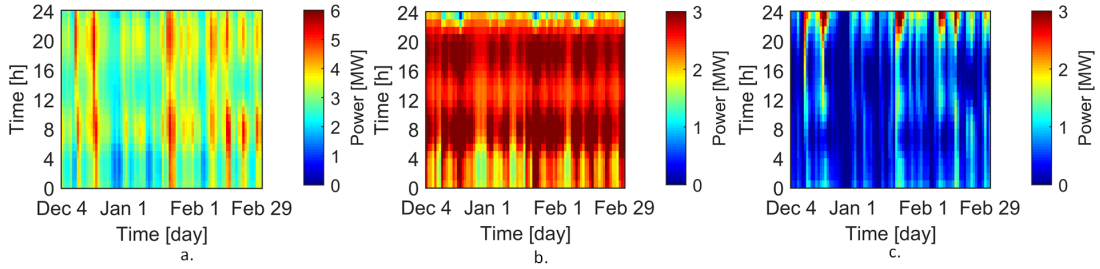

Figure 6.9: Winter case study for 2019/2020 for forecasted total power (a), estimated baseload (b), and disaggregated HVAC component separated thorugh the difference between total and baseload (c).

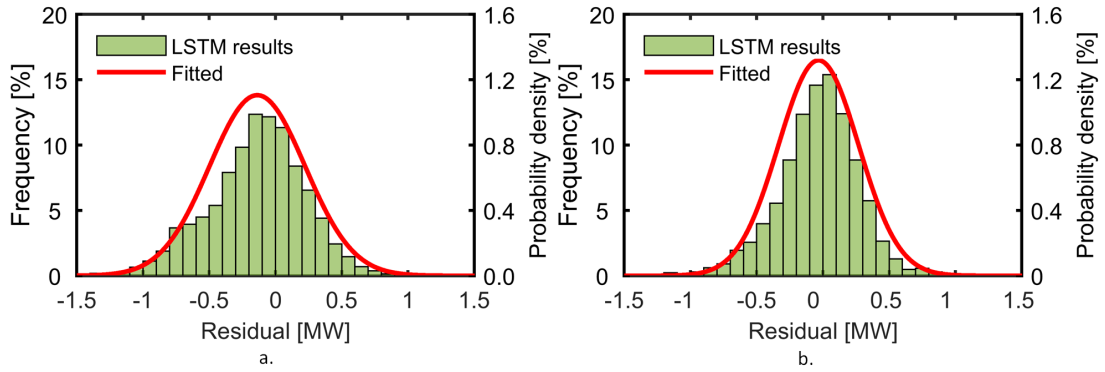

Figure 6.10: Distribution of errors for the total electric power load forecasts in the summer (a) and winter (b) with a box size of 100kW. The mean residual is -137kW with a standard deviation of 361 kW in the summer and 33kW with a standard deviation of 302kW in the winter, which represent small fractions of the forecasted maximum load of approximately 6MW.

recent studies on day-ahead hourly forecasts at the aggregate level on residential distribution circuits such as about 8% in [114] and 11% [223]. Improvement to the state of the art forecasting accuracy at the distribution level would assist in generation purchasing and reduce use of expensive fast responding generation scheduled by utilities only as needed during the day. It is important to note that as machine learning models improve the proposed 2-step HVAC disaggegation method in this chapter, can be still be utilized as the engineering insight utilizing TmHVAC values as a general input to a trained model for baseload forecasts is universal.

The TmHVAC key outdoor temperature indicator was introduced and defined with respect to Fig. 6.4. The results for the total power forecast are independent of TmHVAC, but the separation of baseload and HVAC component is not. For the example community in the winter, the selection of TmHAVC, as the minimum temperature above which the HVAC system is assumed to be in standy-by zero electric power mode, is challenging because approximately half of the buildings employ natural

gas furnaces. In this case, a value of 12°C was preferred for TmHVAC on additional considerations including those related to the parametric linear study depicted in Fig. 6.4, in order to obtain a better fit for very low temperatures and high total electric loads, and ultimately ensure that the demand is meet under critical conditions.

Further reassurance for the selection is provided by the analysis of the energy for the HVAC community component as a percentage of the total. The daily values have been calculated through the time integration of profiles such as those illustrated in Figs. 6.5, 6.7, and 6.6, and for this example week the HVAC energy from the total ranges in between 8 and 24%. When considering the fact that half of the houses do not use electricity for heating, the results at individual residence level may be considered as consistent with reports based on larger-scale surveys [167]. Another approach, which may be considered for the future, when large numbers of smart meters are expected to be deployed in the field at individual house level, would be to statically determine TmHVAC for the community based on experimental big data.

For the summer, a parametric study was conducted considering TmHVAC values between 16 and 20°C and the disaggregated results for the HVAC load component for an example day are plotted in Fig. 6.11. The daily profiles for HVAC and for its complementary estimated baseload maintain their specific curve shapes but the peak values may change. The in-between value of 18°C, is recommended not only as a trade off. Furthermore, this value is well supported by the correlation study from Fig. 6.4 and also on the basis of considering regional specifics for the building thermal insulation, and relatively high likelihood of simultaneous occurrence of mild temperature and high solar irradiance that may contribute to natural heating.

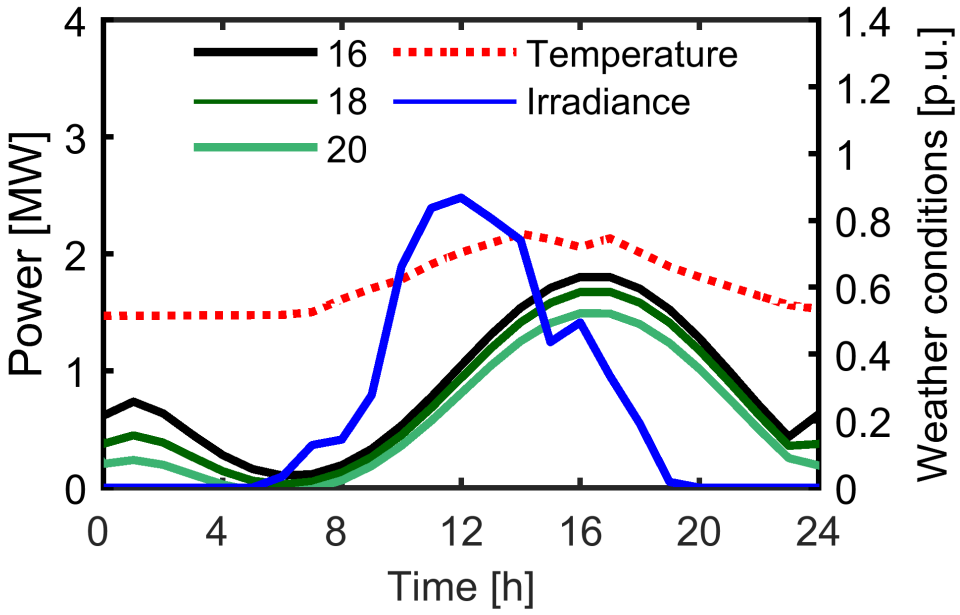

Figure 6.11: Parametric study for TmHAVC influence on the HAVC disaggregated electric power component on an example summer day example. Temperature and irradiance are reported in p.u. with reference to base values of 40 deg C and 1000 W/m^2.

6.4.2 Comparison with Conventional Approaches

Traditional models for load forecast are based on linear regression (LR), e.g., [218]. Such an LR model, typically referred to as power per cooling degree, was implemented and employed for a summer study of our example community based on the optimal linear data fit for the total electric power previously discussed in Section 6.2 and shown in Fig. 6.3. The LR results from Fig. 6.12a were purposefully selected to illustrate a fortunate situation of satisfactory agreement between measurements and forecast throughout the week with the notable exception of the second day.

A systematic overall analysis of the LR results shows that the good agreement may be rather occasional because there is wide spread of the residual over the entire power range, pointing out to the disadvantages in terms of accuracy of traditional

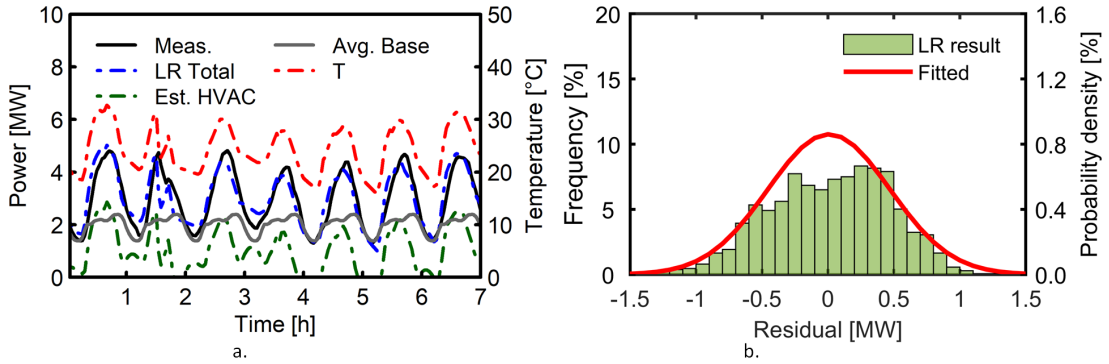

Figure 6.12: Example week following June 20, 2020 using a conventional linear regression (LR) model for the relationship between outdoor temperature and total electric power (a). The error distribution of LR model for total power is widely spread out, unlike the corresponding results for the newly proposed LSTM-based method shown in Fig. 6.10a.

analysis versus the newly proposed ML method based on LSTM-type ML algorithms (see Fig. 6.12b and Fig. 6.10b).Yet another advantage of the ML method is that it is fully automated on a numerical computer and virtually eliminates the reliance on the analyst experience, as it is typically the case for LR studies.

A baseload profile, detailed for 24-hours and invariable from day to day, was estimated also based on the hourly V-curve for power. The temperature range for which the HVAC system is considered to be on stand by at zero power was approximated as 12 to 18°C. Due to the fact that there are not enough data points within this temperature range during the daytime in the months of June to August in 2017, 2018, and 2019, the data set has been extended to include the month of May, under the assumption that human behaviour is comparable in late spring and summer. The average value of the resultant baseload compares satisfactorily with the corresponding value from the proposed LSTM-based method and has rather similar profile variation. This provides additional confidence in the new ML method. It further means that

the errors noted for the LR estimation of total power are passed on to the HVAC power component disaggregated through difference, and that the new ML method is advantageous in this respect as well.

6.4.3 Discussion

The baseload forecasted and the HVAC power component disaggregated with the proposed ML method can be, in principle, experimentally validated against measurements. While for the total electric power such validation was performed at aggregated community level as part of the study, as previously discussed, for the power components, the process requires information at individual building power supply level. Although dedicated intrusive load monitoring (ILM) equipment and methods are available [34], the cost and the effort associated with the field deployment for equipment specific instrumentation within thousands of buildings is currently prohibitive and limits verification of the proposed approach. More specifics into the current state of energy monitoring in the United States are included in Section 1.

Steps towards the validation of the community level components for baseload and HVAC power are described in the following by comparing calculations with data trends from experiments and alternative models that are already established. In a previous section of the chapter, such a comparison has been already discussed with favorable conclusions versus the summer baseload estimated using more traditional LR methods.

Additional satisfactory verification of this summer typical baseload was conducted. In principle, a day with a constant temperature of 18°C, equal to the recommended

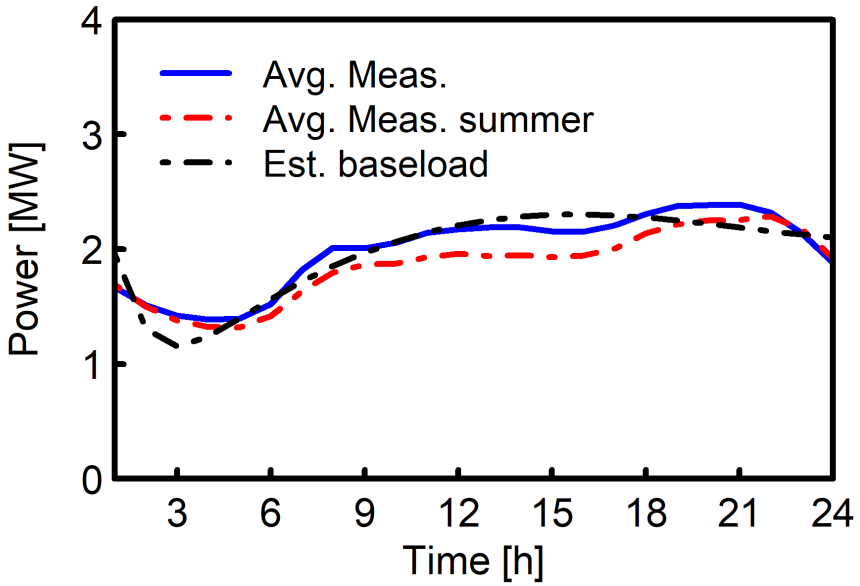

Figure 6.13: Baseload hourly profiles for summer days estimated with the proposed method and based on the experimental total load at approx. 18°C considering data for May to August (Avg. Meas. summer) and for all months (Avg. Meas.) during 2017-2019.

TmHVAC for cooling, would provide the experimental baseload as the HVAC will be in stand-by zero-power mode. In reality, such a full day does not exist as the temperature varies and tends to be substantially higher in the afternoon. Instead, synthetic data for a summer day of constant temperature was produced for each hour by averaging the power data within one degree range of the specified 18°C with the averages plotted in Fig. 6.13 considering suitable data from the extended summer of May to August, inclusive, or throughout the entire year, respectively.

The HVAC electric power component disaggregated with the proposed ML method follows weather variations, as expected based on fundamental physics rules. For example, in Fig. 6.6a the latency of HVAC power with respect to temperature, due to building thermal inertia, is clearly illustrated. Furthermore, within this example

summer week, the daily integration of the total electric power and its components, yields the percentage of the HVAC energy from the total to be in between 30 and 46%, such values being consistent with reports based on larger-scale surveys [167].

Yet another verification that the new method aligns well with sound scientific fundamentals is through favorable comparison of the results with those provided by models scaled up from representative buildings. One such medium-size 3-bedroom house of the conventional type, equipped with a standard SEER 13 HVAC system, and considered representative for the region, has been developed as part of another experimental project with support from Tennessee Valley Authority (TVA) [224]. The house has been modeled with the widely used EnergyPlus software [94].

The representative building physics-based white box model includes details of the HVAC system, and physical parameters, such as surface area, windows, wall thickness, roofing, thermal insulation, etc, and the results include HVAC electric power. This can be scaled up to community level using, for example, the advanced techniques proposed in [97]. For simplicity, in the current study the scaling has been performed through direct multiplication with the total number of 1810 buildings from the community. For an example day of June 7, 2020, the p.u. results with a 3.35MW base are plotted in Fig. 6.14 together with the HVAC power component disaggregated with the proposed ML method indicating satisfactory agreement and providing further confidence in the new method.

The proposed ML method is well suited for short-term day-ahead forecasts, which enables utilities to optimize generation dispatch plans in advance of load, an thus lowest cost units can be prioritized and insufficient capacity day to day could be

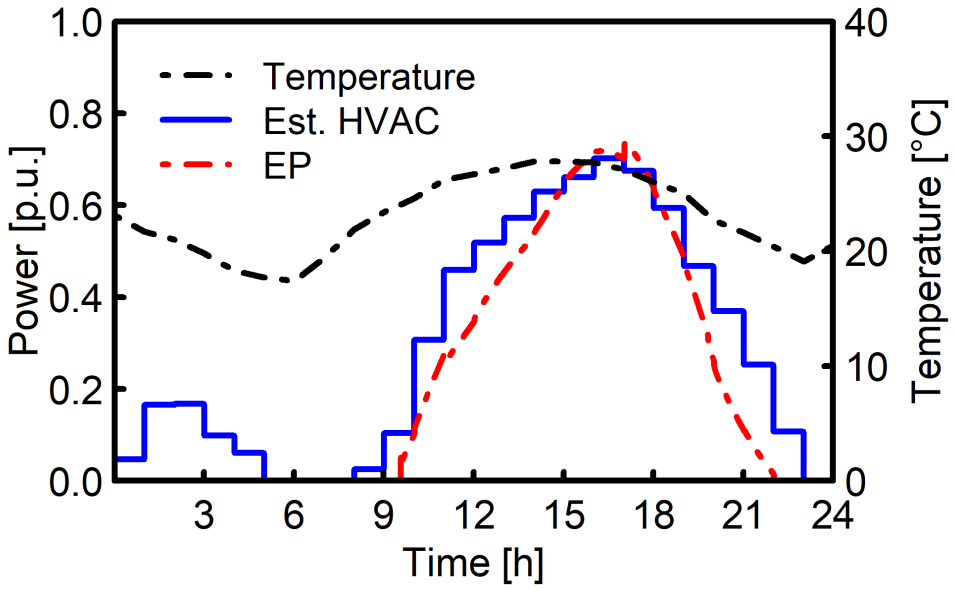

Figure 6.14: Example day variations for the HVAC power component at community level disaggregated with the proposed ML method and scaled up from an EnergyPlus model of a representative house.

avoided. Additionally, because the proposed scheme disaggregates the HVAC power component, it can support detailed studies to further the economic benefit to utilities by estimating the effect, and cost reductions, of smart HVAC load management and demand curtailment of HVAC, which can reduce further capacity needs, distribution and transmission system upgrades, as well as facilitate the incorporation of additional intermittent renewable resources by syncing HVAC loads with the available of renewable power.

For the summer, the detailed HVAC based studies may include establishing the available energy and optimal timing for DR programs, during which large groups of individual HVAC air-conditioners are controlled on and off as an aggregated VPP in order to shift and possibly reduce the peak electric load [96]. For the winter, they may include extremely low temperature condition and the accurate prediction of the

HVAC and total power load, in order to make sure that available generation may fully meet the demand and hence reliably ensure the thermal comfort through all the buildings in the community.

Studies for long-term HVAC technology evolution and field deployment may also be supported. As HVAC systems with higher Seasonal Energy Efficiency Ratio (SEER) may be gradually introduced for more efficient summer air conditioning, reduced cost of energy use, and to comply with new industry requirements, e.g., [225], the corresponding HVAC load component is expected to reduce. The associated forecasted profile can then be combined with the estimated baseload to derive the predicted total load requirements, which is useful for planning purposes. The approximate half-and-half split in between winter heating with natural gas furnaces and electric heat pumps for the community analyzed, provides a good basis for long-term future studies in which new HVAC systems are deployed based on the evolution of technology, fuel type availability and cost, and possibly new environmental regulations, e.g. [226]. The improved HVAC specific forecasts and long-term development studies could allow utilities to better estimate capacity expansion needs and could lead to prevention of economic loss due construction of excess generation capacity. It could also lead to retirement of unnecessary or under-used generation facilities.

6.5 Conclusions

The ML-based method proposed in this chapter addresses at the community level the timely topic of day-ahead forecast with a view at enabling optimal energy controls and utility planning. A first advantage of the method is that it only requires

minimal historic hourly information, represented by the total power as measured at a main distribution line, which includes the summation of all loads on the branch, as well as weather characteristics for outdoor temperature and solar irradiance that are typically available from public databases. The method is shown to be superior to traditional linear-regression approaches in terms of combined automated operation and higher accuracy. This has been demonstrated for total power through satisfactory comparison and an MAPE error below 10% with respect to experimental data from a suburban community in Kentucky representative for a wider US region.

Another advantage of the proposed method is that it separates the baseload and the HVAC components out of the total power. This is possible through the introduction of new key temperature indicators corresponding to the stand-by zero-power operation for the HVAC systems for summer cooling and winter heating and an innovative additional run of the trained LSTM model with such constant temperature and zero irradiance. The validity of the components estimation and disaggregation is supported by favorable findings, in line with expectations based on fundamental physics, statistics, and human behavioral patterns. Furthermore, the economic benefits of the proposed 2-step HVAC disaggregation model include lower costs for generation planning, use of more intermittent renewable generation resources, and cost benefit assessment of HVAC load management and controls.

Chapter 7

Conclusion

In this final chapter, the conclusions and contributions of the dissertation are summarized. Future research is recommended with a view at possible further progress in the subject area.

7.1 Summary and Conclusions

A new co-simulation framework, named INSPIR+D, was developed for the modeling of electric power distribution systems, individual buildings, and smart devices. A modified IEEE 123-bus test system with 353 homes was proposed as representative for a typical residential community with loads based on simulated and measured data. Simulation results include bus voltages and power flow throughout the circuit.

The energy usage models for buildings were developed and validated based on the California Building Energy Code Compliance Residential (CBECC-Res) Standards, and experimental data from southern Kentucky, within the co-simulation framework. A proposed hybrid energy storage system employed batteries and water heaters to alleviate example cases of the "duck curve" phenomenon that is caused by non-coincident solar generation and load demand. A methodology for the sizing of the residential

power balance system was proposed based on multi-objective differential evolution. The objectives include the energy capacity and power ratings of the battery energy storage system (BESS), and the fluctuation of the net metered power. Results show that the same grid power flow can be achieved with a 30% smaller battery through the use of the proposed hybrid energy storage system.

Aggregated generic curves for electric water heater (EWH) and heat pump water heater (HPWH) using a minimal amount of data points were obtained from large-scale field demonstrators. The experimental data was artificially aggregated in time and space and results showed that the aggregated HPWH load had its daily power peak appear later than that of EWHs in both the morning and evening. The study illustrates that changing all EWH to HPWH would reduce the daily electricity usage by approximately 70%.

For this study, the potential of EWH and HPWH as energy storage was evaluated. When referring to the average power, approximately 14% daily electricity usage for EWH could be shifted. The simulation indicated that the HPWH has the capability to shift approximately 17% of the daily electricity usage. Both EWH and HPWH could reserve the energy storage capacity equal to 22% of its daily electricity usage in the case study.

Digital twin models for EWH and HPWH were created with the ability to calculate the water heating power, hot water flow, water temperature in the tank, and energy take for individual and multiple water heaters. A generalized approach to energy storage that enables EWH, HPWH, and heating, ventilation, and air conditioning (HVAC) systems, to be controlled with the same variables, namely "energy

capacity" and "energy take" was proposed. A total of 353 EWHs were simulated to represent a realistic community user behavior based on hot water draw from CBECC-Res data. Simulation results show that when all the residences from the subdivision react to the same DR signal at the same time, the total power at the main distribution feeder changed drastically, but the voltages for all buses were maintained within an acceptable range of 1±0.05.

Virtual power plant (VPP) operation for a residential community was proposed by controlling the smart homes as distributed energy resources (DER). Generalized energy storage (GES) definitions were developed and provided so that they may be applied in a uniform control method for batteries, EVs, HVAC systems, and EWHs in smart homes. The long term aggregated residential load was predicted based on different penetrations of smart homes in a community. Battery and EWH as energy storage devices were compared and results show that EWHs with approximately 3 times the participation rates achieved the same peak reduction targets.

An equivalent energy storage model for HVAC was developed and a charging/discharging procedure similar to a typical battery at both individual and aggregated levels was applied. An aggregation technique for the modeling of HVAC systems in large communities that was based on the robotic houses built and monitored by the Tennessee Valley Authority (TVA) was proposed. The VPP operation was realized by sequential control, which temporarily allows higher indoor temperatures up to values that were still acceptable for typical preferences and standard regulations of human comfort. The results based on 10,000 HVAC systems show that, on a very hot summer day, when the DR participation was 100%, the peak power in the afternoon and the

ramping rate were reduced by approximately 16% and 35%, respectively, while the daily energy usage was almost the same.

A Kernel Density Estimation technique was developed and applied for the modeling of aggregated EV charging power, based on the arrival time and daily driving mileage from the National Household Travel Survey (NHTS) 2017 data. EVs were charged with control signals complying to the CTA-2045 standards. An EV charging schedule was proposed in which the high time-of-use (ToU) period was avoided and a 100% SOC was guaranteed at 6:00 in the morning on the next day. Another case shows that the energy capacity of EVs is extremely large, substantial exceeding the load of the community, therefore, can enable the entire residential community to operate as a VPP under control.

A procedure was developed to quantify the building resilience considering the PV generation, load percentage, capacity of BESS and EV battery. The probability for the reference house to self-sustain for more than 3, 10, and 24 hours was found to be 100%, 50% and 0%, respectively. When an EV with a battery capacity of 90kWh was incorporated in the home energy management system, the probability for the reference house to self-sustain at least 24 hours increased to 90%. If this same EV was parked at home all the time, the probability to self-sustain 24 hours was 100%, and the likelihood of self-sustaining for 48 hours increased to 98%. When the EV battery capacity was 20kWh, the results for 24 and 48 hours were 85% and 30%, respectively.

An ML-based method addressing the timely topic of day-ahead forecast with a view at enabling optimal energy controls and utility planning at the community level

was proposed and employed. The method is highly advantages in that it only requires minimal historic hourly information, represented by the total power as measured at a main distribution line, which includes the summation of all loads on the branch, as well as weather characteristics for outdoor temperature and solar irradiance that are typically available from public databases. Another significant advantage of the proposed method is that it separates the baseload and the HVAC components out of the total power, representing a significant novel contribution.

The method is shown to be superior to traditional linear-regression approaches in terms of combined automated operation and higher accuracy. This has been demonstrated for total power through satisfactory comparison and an MAPE error below 10% with respect to experimental data from a suburban community in Kentucky representative for a wider US region. New key temperature indicators corresponding to the stand-by zero-power operation for the HVAC systems and an innovative additional run of the trained LSTM model with such constant temperature and zero irradiance were introduced. The validity of the components estimation and disaggregation was supported by favorable findings, in line with expectations based on fundamental physics, statistics, and human behavioral patterns. Furthermore, the economic benefits of the proposed 2-step HVAC disaggregation model include lower costs for generation planning, use of more intermittent renewable generation resources, and cost benefit assessment of HVAC load management and controls.

7.2 Original Contributions

The major contributions of the Ph.D. dissertation research include:

1. Newly developed co-simulation framework for dynamic modeling and control for power system and building energy. Further development of the EPRI DER testbed to include model-in-the-loop capabilities for EWH and HVAC systems. (Chapter 2)

2. An innovative hybrid energy storage system comprising of BESS and EWH, systematically sized using a specific differential evolution method. (Chapter 2)

3. First of the kind, generic load curves for EWH and HPWH at aggregated level. A novel method to evaluate the energy storage capacity of water heaters and scale results to thousands of units. (Chapter 3)

4. A virtual electric power plant with optimal coordinated controls for HVAC, EWH, and BESS, considering smart homes occupant comfort and ambient temperature, a feature typically absent from other prior-art techniques. (Chapter 4)

5. A newly developed aggregation technique for HVAC loads in large communities with results validated against field measured data from TVA robotic houses and the SET project, one of US' largest rural smart grid demonstrators. (Chapter 4)

6. Statistical KDE model for the aggregated EV charging power developed based on the latest National Household Travel Survey data. (Chapter 5)

7. Proposed metrics for the quantification of building resilience with case studies for EV battery support in V2H and V2G mode. (Chapter 5)

8. A new generalized approach for energy storage modeling suitable for EWH, HVAC, BESS, and EV and the latest CTA-2045 concepts. Demonstrative case studies on a large di stribution circuit include ancillary services for energy storage and power flow. (Chapters 3, 4, 5)

9. A new machine learning LSTM model for the forecast of total power and disaggregation of the HVAC and baseload components. (Chapter 6)

7.3 Recommendations for Future Research

Based on the results of this Ph.D. dissertation and recent research, possible further work may include the following;

1. An extension of the building modeling capabilities to include reactive power should be considered. At current work, a constant power factor of 0.95 was assumed to all building loads in the study for the simulation of distribution power system. Further studies may investigate the relationship between the power factor and building active power loads, considering the contributions of typical appliances.

2. The mixing valve technology allows water temperature in the tank to be high, potentially increasing the energy storage capacity of water heater. Once the water temperature is already very high, the EWH might not need to further heat the water for a very long duration. Further research could examine the scenarios where water temperature is allowed to be very high for weekly and longer time frame.

3. Further studies of the aggregated EV charging power may consider the relationship between EV departure time and EV arrival time for each vehicle. The conditional probability of EV departure time given the arrival time may be calculated, in order to improve the estimation of EV charging power, and the potential of V2G services. Other distributions, e.g., joint Gauss, and exponential may also be employed.

4. The typical meteorological year (TMY) data, which summarizes historic average and might miss the extreme conditions, was used for the building energy modeling and evaluation of building resilience. Future work should consider using the multiple years of actual weather data or the weather year for energy calculations (WYEC) data set.

References

[1] K. Peterson, P. Torcellini, R. Grant, C. Taylor, S. Punjabi, and R. Diamond, "A common definition for zero energy buildings," *Prepared for the US Department of Energy by The National Institute of Building Sciences, US Department of Energy*, 2015.

[2] (2019, Aug.) Zero Net Energy, California Public Utilities Commission. [Online]. Available: http://www.cpuc.ca.gov/ZNE/

[3] (2019, Aug.) Nearly zero-energy buildings - EU Commission. [Online]. Available: https://ec.europa.eu/energy/en/topics/energy-efficiency/buildings/nearly-zero-energy-buildings

[4] P. Denholm, M. O'Connell, G. Brinkman, and J. Jorgenson, "Overgeneration from solar energy in california. a field guide to the duck chart," National Renewable Energy Lab.(NREL), Golden, CO (United States), Tech. Rep., 2015.

[5] A. Sangwongwanich, Y. Yang, and F. Blaabjerg, "High-performance constant power generation in grid-connected pv systems," *IEEE Transactions on Power Electronics*, vol. 31, no. 3, pp. 1822–1825, 2016.

[6] G. Mokhtari, G. Nourbakhsh, and A. Gosh, "Optimal sizing of combined pv-energy storage for a grid-connected residential building," *Advances in Energy Engineering*, vol. 1, no. 3, pp. 53–65, 2013.

[7] X. Jin, J. Maguire, and D. Christensen, "Economic sizing of batteries for the smart home," 2018.

[8] T. Simpkins, K. Anderson, D. Cutler, and D. Olis, "Optimal sizing of a solar-plus-storage system for utility bill savings and resiliency benefits," in *Innovative Smart Grid Technologies Conference (ISGT), 2016 IEEE Power & Energy Society*. IEEE, 2016, pp. 1–6.

[9] N. Carew, B. Larson, L. Piepmeier, and M. Logsdon, "Heat pump water heater electric load shifting: A modeling study," *Ecotope, Inc., Seattle*, 2018.

[10] "Residential Water Heater Training," http://university.hotwater.com/wp-content/uploads/sites/2/2015/02/un-branded-Residential-Training-Manual-1-5-16.pdf, accessed: 2020-10-27.

[11] H. Gong, V. Rallabandi, D. M. Ionel, D. Colliver, S. Duerr, and C. Ababei, "Dynamic modeling and optimal design for net zero energy houses including hybrid electric and thermal energy storage," *IEEE Transactions on Industry Applications*, vol. 56, no. 4, pp. 4102–4113, 2020.

[12] J. Dong, M. Starke, B. Cui, J. Munk, E. Tsybina, C. Winstead, Y. S. Xue, M. Olama, and T. Kuruganti, "Battery equivalent model for residential hvac," in *2020 IEEE Power & Energy Society General Meeting (PESGM)*. IEEE, 2020, pp. 1–5.

[13] J. Wang, S. Huang, D. Wu, and N. Lu, "Operating a commercial building hvac load as a virtual battery through airflow control," *IEEE Transactions on Sustainable Energy*, vol. 12, no. 1, pp. 158–168, 2020.

[14] N. S. Raman and P. Barooah, "On the round-trip efficiency of an hvac-based virtual battery," *IEEE Transactions on Smart Grid*, vol. 11, no. 1, pp. 403–410, 2019.

[15] W. Zhang, J. Lian, C. Chang, and K. Kalsi, "Aggregated modeling and control of air conditioning loads for demand response," *IEEE Transactions on Power Systems*, vol. 28, no. 4, pp. 4655–4664, 2013.

[16] G. Goddard, J. Klose, and S. Backhaus, "Model development and identification for fast demand response in commercial hvac systems," *IEEE Transactions on Smart Grid*, vol. 5, no. 4, pp. 2084–2092, 2014.

[17] American National Standards Institute and American Society of Heating, Refrigerating and Air-Conditioning Engineers, ANSI/ASHRAE *Standard 55-2017 Thermal environmental conditions for human occupancy*. American Society of Heating, Refrigerating and Air-Conditioning Engineers (ASHRAE), 2017.

[18] E. Erickson, R. Slobodin, M. Poshtan, T. Taufik, and J. Callenes, "Using power infrastructures for wildfire detection in California," in *2020 IEEE Power & Energy Society Innovative Smart Grid Technologies Conference (ISGT)*. IEEE, 2020, pp. 1–5.

[19] "California Fire Statistics," https://www.fire.ca.gov/stats-events/, accessed: 2021-04-09.

[20] J. Prohov (WFAA), "Millions of texans without electricity during winter storm, rotating power outages could now last for 'hours'," https://www.kcentv.com/article/weather/live-updates-winter-storm-north-texas-dallas-fort-worth-february-15-2021/287-6f6cca9f-f093-481e-9d1e-4b3c4c91c64d, accessed: 2021-04-09.

[21] "Frozen wind turbines contribute to rolling power blackouts across Texas," https://www.cnn.com/2021/02/15/us/power-outages-texas-monday/index.html, accessed: 2021-04-09.

[22] H. Gong, V. Rallabandi, M. L. McIntyre, E. Hossain, and D. M. Ionel, "Peak reduction and long term load forecasting for large residential communities including smart homes with energy storage," *IEEE Access*, vol. 9, pp. 19 345–19 355, 2021.

[23] X. Hou, J. Wang, T. Huang, T. Wang, and P. Wang, "Smart home energy management optimization method considering energy storage and electric vehicle," *IEEE Access*, vol. 7, pp. 144 010–144 020, 2019.

[24] F. V. Cerna, M. Pourakbari-Kasmaei, L. S. Pinheiro, E. Naderi, M. Lehtonen, and J. Contreras, "Intelligent energy management in a prosumer community considering the load factor enhancement," *Energies*, vol. 14, no. 12, p. 3624, 2021.

[25] H. Gong and D. M. Ionel, "Optimization of aggregated ev power in residential communities with smart homes," in *2020 IEEE Transportation Electrification Conference & Expo (ITEC)*. IEEE, 2020, pp. 779–782.

[26] "The Electric Ford f-150 Can Power Your Entire House for Three Days on a Single Charge," https://www.thedrive.com/tech/40695/the-electric-ford-f-150-can-power-your-entire-house-for-three-days-on-a-single-charge, accessed: 2021-05-25.

[27] "CTA standard: Modular communications interface for energy management," Consumer Technology Association (CTA), Tech. Rep., 2020.

[28] X. C. Katherine Dayem, "Standardized Communications for Demand Response: An Overview of the CTA-2045 Standard and Early Field Demonstrations," National Rural Electric Cooperative Association (NRECA), Tech. Rep., 2018.

[29] "Energy Star water heaters - test method to validate demand response," https://www.energystar.gov/products/spec/residential_water_heaters_specification_version_3_0_pd, accessed: 2021-08-12.

[30] C.Thomas, "Performance test results: CTA-2045 water heater," Electric Power Research Institute (EPRI), Tech. Rep. 3002011760, 2017.

[31] "CTA-2045 water heater demonstration report including a business case for cta-2045 market transformation," Bonneville Power Administration (BPA), Tech. Rep. BPA Technology Innovation Project 336, 2018.

[32] Glick et al, "Assessment of Demand Response and Advanced Metering," https://www.ferc.gov/media/

2021-assessment-demand-response-and-advanced-metering#, December 2021.

[33] "L532/l534 load control switches. an advanced load control solution for managing peak demand," https://www.landisgyr.com/product/l532-l534-load-control-switches/?download=276174&filename=/webfoo/wp-content/uploads/2021/07/2021.06-L532-L534-Load-Control-Switches.pdf, 2021.

[34] X. Yuan, P. Han, Y. Duan, R. E. Alden, V. Rallabandi, and D. M. Ionel, "Residential electrical load monitoring and modeling–state of the art and future trends for smart homes and grids," *Electric Power Components and Systems*, vol. 48, no. 11, pp. 1125–1143, 2020.

[35] F. Blaabjerg and D. M. Ionel, *Renewable energy devices and systems with simulations in matlab® and ansys®*. CRC Press, 2017.

[36] M. Stoyanova, Y. Nikoloudakis, S. Panagiotakis, E. Pallis, and E. K. Markakis, "A survey on the internet of things (iot) forensics: Challenges, approaches, and open issues," *IEEE Communications Surveys Tutorials*, vol. 22, no. 2, pp. 1191–1221, 2020.

[37] M. Masera, E. F. Bompard, F. Profumo, and N. Hadjsaid, "Smart (electricity) grids for smart cities: Assessing roles and societal impacts," *Proceedings of the IEEE*, vol. 106, no. 4, pp. 613–625, 2018.

[38] U. Zafar, S. Bayhan, and A. Sanfilippo, "Home energy management system concepts, configurations, and technologies for the smart grid," *IEEE Access*, vol. 8, pp. 119 271–119 286, 2020.

[39] F. Luo, G. Ranzi, C. Wan, Z. Xu, and Z. Y. Dong, "A multistage home energy management system with residential photovoltaic penetration," *IEEE Transactions on Industrial Informatics*, vol. 15, no. 1, pp. 116–126, 2019.

[40] F. Y. Melhem, O. Grunder, Z. Hammoudan, and N. Moubayed, "Energy management in electrical smart grid environment using robust optimization algorithm," *IEEE Transactions on Industry Applications*, vol. 54, no. 3, pp. 2714–2726, 2018.

[41] S. Aznavi, P. Fajri, A. Asrari, and F. Harirchi, "Realistic and intelligent management of connected storage devices in future smart homes considering energy price tag," *IEEE Transactions on Industry Applications*, vol. 56, no. 2, pp. 1679–1689, 2020.

[42] T. Alquthami and A. S. Meliopoulos, "Smart house management and control without customer inconvenience," *IEEE Transactions on Smart Grid*, vol. 9, no. 4, pp. 2553–2562, 2018.

[43] M. Shafie-Khah and P. Siano, "A stochastic home energy management system considering satisfaction cost and response fatigue," *IEEE Transactions on Industrial Informatics*, vol. 14, no. 2, pp. 629–638, 2018.

[44] S. A. U. Nambi, R. V. Prasad, and A. R. Lua, "Decentralized energy demand regulation in smart homes," *IEEE Transactions on Green Communications and Networking*, vol. 1, no. 3, pp. 372–380, 2017.

[45] H. T. Nguyen, D. T. Nguyen, and L. B. Le, "Energy management for households with solar assisted thermal load considering renewable energy and price uncertainty," *IEEE Transactions on Smart Grid*, vol. 6, no. 1, pp. 301–314, 2015.

[46] S. Althaher, P. Mancarella, and J. Mutale, "Automated demand response from home energy management system under dynamic pricing and power and comfort constraints," *IEEE Transactions on Smart Grid*, vol. 6, no. 4, pp. 1874–1883, 2015.

[47] C. O. Adika and L. Wang, "Autonomous appliance scheduling for household energy management," *IEEE transactions on smart grid*, vol. 5, no. 2, pp. 673–682, 2014.

[48] S. Zhou, Z. Wu, J. Li, and X.-p. Zhang, "Real-time energy control approach for smart home energy management system," *Electric Power Components and Systems*, vol. 42, no. 3-4, pp. 315–326, 2014.

[49] B. Moradzadeh and K. Tomsovic, "Two-stage residential energy management considering network operational constraints," *IEEE Transactions on Smart Grid*, vol. 4, no. 4, pp. 2339–2346, 2013.

[50] J. Dickert and P. Schegner, "A time series probabilistic synthetic load curve model for residential customers," in *PowerTech, 2011 IEEE Trondheim*. IEEE, 2011, pp. 1–6.

[51] Z. Zhao, W. C. Lee, Y. Shin, and K.-B. Song, "An optimal power scheduling method for demand response in home energy management system," *IEEE Transactions on Smart Grid*, vol. 4, no. 3, pp. 1391–1400, 2013.

[52] P. Radecki and B. Hencey, "Online model estimation for predictive thermal control of buildings," *IEEE Transactions on Control Systems Technology*, vol. 25, no. 4, pp. 1414–1422, 2017.

[53] D. Sturzenegger, D. Gyalistras, M. Morari, and R. S. Smith, "Model predictive climate control of a swiss office building: Implementation, results, and cost–benefit analysis," *IEEE Transactions on Control Systems Technology*, vol. 24, no. 1, pp. 1–12, 2016.

[54] S. Vaghefi, M. Jafari, J. Zhu, J. Brouwer, and Y. Lu, "A hybrid physics-based and data driven approach to optimal control of building cooling/heating systems," *IEEE Transactions on Automation Science and Engineering*, vol. 13, no. 2, pp. 600–610, 2016.

[55] M. N. Sheha and K. M. Powell, "Dynamic real-time optimization of air-conditioning systems in residential houses with a battery energy storage under different electricity pricing structures," in *13th International Symposium on Process Systems Engineering (PSE 2018)*, ser. Computer Aided Chemical

Engineering, M. R. Eden, M. G. Ierapetritou, and G. P. Towler, Eds. Elsevier, 2018, vol. 44, pp. 2527 – 2532.

[56] D. Zhang, S. Li, M. Sun, and Z. O'Neill, "An optimal and learning-based demand response and home energy management system," *IEEE Transactions on Smart Grid*, vol. 7, no. 4, pp. 1790–1801, 2016.

[57] S. Li, D. Zhang, A. B. Roget, and Z. O'Neill, "Integrating home energy simulation and dynamic electricity price for demand response study," *IEEE Transactions on Smart Grid*, vol. 5, no. 2, pp. 779–788, 2014.

[58] J. D. Rhodes, W. H. Gorman, C. R. Upshaw, and M. E. Webber, "Using beopt (energyplus) with energy audits and surveys to predict actual residential energy usage," *Energy and Buildings*, vol. 86, pp. 808–816, 2015.

[59] E. Wilson, C. Engebrecht-Metzger, S. Horowitz, and R. Hendron, "2014 building america house simulation protocols," National Renewable Energy Lab.(NREL), Golden, CO (United States), Tech. Rep., 2014.

[60] J. Van Roy, B. Verbruggen, and J. Driesen, "Ideas for tomorrow: New tools for integrated building and district modeling," *IEEE Power and Energy Magazine*, vol. 11, no. 5, pp. 75–81, 2013.

[61] R. H. Schulte and F. C. Fletcher, "100conundrum," *The Electricity Journal*, vol. 32, no. 2, pp. 31 – 36, 2019.

[62] D. Watson and M. Rodgers, "Utility-scale storage providing peak power to displace on-island diesel generation," *Journal of Energy Storage*, vol. 22, pp. 80–87, 2019.

[63] S. Ahmad Hamidi, D. M. Ionel, and A. Nasiri, "Modeling and management of batteries and ultracapacitors for renewable energy support in electric power systems–an overview," *Electric Power Components and Systems*, vol. 43, no. 12, pp. 1434–1452, 2015.

[64] D. Madjidian, M. Roozbehani, and M. A. Dahleh, "Battery capacity of deferrable energy demand," in *2016 IEEE 55th Conference on Decision and Control (CDC)*. IEEE, 2016, pp. 4220–4225.

[65] T. Peirelinck, C. Hermans, F. Spiessens, and G. Deconinck, "Domain randomization for demand response of an electric water heater," *IEEE Transactions on Smart Grid*, pp. 1–1, 2020.

[66] "Eia residential energy consumption survey (recs)," https://www.eia.gov/consumption/residential/data/2015/#waterheating, accessed: 2020-11-28.

[67] "American Council for an Energy-Efficient Economy (ACEEE): Hot Water Forum," https://www.aceee.org/2021-hot-water-forum, accessed: 2021-08-12.

[68] "Bpa regional study of cta-2045 enabled water heaters," https://www.bpa.gov/EE/Technology/demand-response/Pages/CTA2045-DataShare.aspx, accessed: 2020-11-28.

[69] "Filed test results of the consumer technology association's cta-2045 demand response standard," https://www.peakload.org/assets/35thConf/A4CTA2045PanelSession.pdf, accessed: 2020-11-28.

[70] T. Clarke, T. Slay, C. Eustis, and R. B. Bass, "Aggregation of residential water heaters for peak shifting and frequency response services," *IEEE Open Access Journal of Power and Energy*, vol. 7, pp. 22–30, 2019.

[71] A. Doğan and M. Alçı, "Real-time demand response of thermostatic load with active control," *Electrical Engineering*, vol. 100, no. 4, pp. 2649–2658, 2018.

[72] M. A. Z. Alvarez, K. Agbossou, A. Cardenas, S. Kelouwani, and L. Boulon, "Demand response strategy applied to residential electric water heaters using dynamic programming and k-means clustering," *IEEE Transactions on Sustainable Energy*, vol. 11, no. 1, pp. 524–533, 2019.

[73] T. Peirelinck, C. Hermans, F. Spiessens, and G. Deconinck, "Domain randomization for demand response of an electric water heater," *IEEE Transactions on Smart Grid*, vol. 12, no. 2, pp. 1370–1379, 2020.

[74] O. E. Bosaletsi and W. Cronje, "Decentralized control scheme applied to domestic electric water heaters to minimize frequency deviations: Initial results." in *2021 Southern African Universities Power Engineering Conference/Robotics and Mechatronics/Pattern Recognition Association of South Africa (SAUPEC/RobMech/PRASA)*. IEEE, 2021, pp. 1–6.

[75] J. Wang, H. Zhang, Y. Zhou, J. Sun, and D. Wang, "Evaluation of the potential regulation capacity of water heater loads," in *2013 5th International Conference on Power Electronics Systems and Applications (PESA)*. IEEE, 2013, pp. 1–5.

[76] G. C. Heffner, C. A. Goldman, and M. M. Moezzi, "Innovative approaches to verifying demand response of water heater load control," *IEEE Transactions on Power Delivery*, vol. 21, no. 1, pp. 388–397, 2005.

[77] J. Kondoh, N. Lu, and D. J. Hammerstrom, "An evaluation of the water heater load potential for providing regulation service," in *2011 IEEE Power and Energy Society General Meeting*. IEEE, 2011, pp. 1–8.

[78] V. Lakshmanan, H. Sæle, and M. Z. Degefa, "Electric water heater flexibility potential and activation impact in system operator perspective–norwegian scenario case study," *Energy*, p. 121490, 2021.

[79] N. Kruis, P. Bruce Wilcox, J. Lutz, and C. Barnaby, "Development of realistic water draw profiles for california residential water heating energy estimation," in *Proceedings of the 15th IBPSA Conference San Francisco, CA, USA, Aug. 7–9*, 2017.

[80] "CBECC-Res Compliance Software Project," http://www.bwilcox.com/BEES/cbecc2019.html, accessed: 2020-08-04.

[81] Q. Shi, C.-F. Chen, A. Mammoli, and F. Li, "Estimating the profile of incentive-based demand response (IBDR) by integrating technical models and social-behavioral factors," *IEEE Transactions on Smart Grid*, vol. 11, no. 1, pp. 171–183, 2019.

[82] B. Cui, J. Joe, J. Munk, J. Sun, and T. Kuruganti, "Load flexibility analysis of residential hvac and water heating and commercial refrigeration," Oak Ridge National Lab.(ORNL), Oak Ridge, TN (United States), Tech. Rep., 2019.

[83] H. Gong, O. M. Akeyo, T. Rooney, B. Branecky, and D. M. Ionel, "Aggregated generic load curve for residential electric water heaters," in *2021 IEEE Power & Energy Society General Meeting (PESGM)*. IEEE, 2021, pp. 1–5.

[84] "Electricity Ancillary Services Primer," http://nescoe.com/wp-content/uploads/2017/11/AnxSvcPrimer_Sep2017.pdf, accessed: 2020-11-28.

[85] H. Gong, V. Rallabandi, M. L. McIntyre, and D. M. Ionel, "On the optimal energy controls for large scale residential communities including smart homes," in *2019 IEEE Energy Conversion Congress and Exposition (ECCE)*, Baltimore, MD, USA, 2019, pp. 503–507.

[86] R. El Geneidy and B. Howard, "Contracted energy flexibility characteristics of communities: Analysis of a control strategy for demand response," *Applied Energy*, vol. 263, p. 114600, 2020.

[87] X.-D. Chen, L. Li, M.-L. Tseng, K. Tan, and M. H. Ali, "Improving power quality efficient in demand response: Aggregated heating, ventilation and air-conditioning systems," *Journal of Cleaner Production*, p. 122178, 2020.

[88] H. Gong, E. S. Jones, R. E. Alden, A. G. Frye, D. Colliver, and D. M. Ionel, "Demand response of hvacs in large residential communities based on experimental developments," in *2020 IEEE Energy Conversion Congress and Exposition (ECCE)*. IEEE, 2020, pp. 4545–4548.

[89] J. H. Yoon, R. Baldick, and A. Novoselac, "Dynamic demand response controller based on real-time retail price for residential buildings," *IEEE Transactions on Smart Grid*, vol. 5, no. 1, pp. 121–129, 2014.

[90] M. Tavakkoli, S. Fattaheian-Dehkordi, M. Pourakbari-Kasmaei, M. Liski, and M. Lehtonen, "Bonus-based demand response using stackelberg game approach for residential end-users equipped with hvac system," *IEEE Transactions on Sustainable Energy*, vol. 12, no. 1, pp. 234–249, 2021.

[91] A. Taşcıkaraoğlu, N. G. Paterakis, O. Erdinç, and J. P. Catalao, "Combining the flexibility from shared energy storage systems and dlc-based demand response of hvac units for distribution system operation enhancement," *IEEE Transactions on Sustainable Energy*, vol. 10, no. 1, pp. 137–148, 2018.

[92] X. Xu, C.-f. Chen, X. Zhu, and Q. Hu, "Promoting acceptance of direct load control programs in the United States: Financial incentive versus control option," *Energy*, vol. 147, pp. 1278–1287, 2018.

[93] M. Cai, S. Ramdaspalli, M. Pipattanasomporn, S. Rahman, A. Malekpour, and S. R. Kothandaraman, "Impact of hvac set point adjustment on energy savings and peak load reductions in buildings," in *2018 IEEE International Smart Cities Conference (ISC2)*, 2018, pp. 1–6.

[94] E. S. Jones, R. E. Alden, H. Gong, A. G. Frye, D. Colliver, and D. M. Ionel, "The effect of high efficiency building technologies and pv generation on the energy profiles for typical us residences," in *2020 9th International Conference on Renewable Energy Research and Application (ICRERA)*. IEEE, 2020, pp. 471–476.

[95] A. Bagnasco, S. Massucco, M. Saviozzi, F. Silvestro, and A. Vinci, "Design and validation of a detailed building thermal model considering occupancy and temperature sensors," in *2018 IEEE 4th International Forum on Research and Technology for Society and Industry (RTSI)*. IEEE, 2018, pp. 1–6.

[96] H. Gong, E. S. Jones, R. Alden, A. G. Frye, D. Colliver, and D. M. Ionel, "Virtual power plant control for large residential communities using hvac systems for energy storage," *IEEE Transactions on Industry Applications*, pp. 1–1, 2021.

[97] H. Gong, E. S. Jones, and D. M. Ionel, "An aggregated and equivalent home model for power system studies with examples of building insulation and hvac control improvements," in *2020 IEEE Power & Energy Society General Meeting (PESGM)*. IEEE, 2020, pp. 1–4.

[98] V. Monteiro, J. Pinto, and J. L. Afonso, "Operation modes for the electric vehicle in smart grids and smart homes: Present and proposed modes," *IEEE Transactions on Vehicular Technology*, vol. 65, no. 3, pp. 1007–1020, 2015.

[99] H. Shin and R. Baldick, "Plug-in electric vehicle to home (v2h) operation under a grid outage," *IEEE transactions on smart grid*, vol. 8, no. 4, pp. 2032–2041, 2016.

[100] V. Monteiro, T. J. Sousa, C. Couto, J. S. Martins, A. A. N. Melendez, and J. L. Afonso, "A novel multi-objective off-board ev charging station for smart homes," in *IECON 2018-44th Annual Conference of the IEEE Industrial Electronics Society*. IEEE, 2018, pp. 1983–1988.

[101] N. Z. Xu, K. W. Chan, C. Y. Chung, and M. Niu, "Enhancing adequacy of isolated systems with electric vehicle-based emergency strategy," *IEEE Transactions on Intelligent Transportation Systems*, vol. 21, no. 8, pp. 3469–3475, 2019.

[102] M. Rastegar and M. Fotuhi-Firuzabad, "Outage management in residential demand response programs," *IEEE transactions on smart grid*, vol. 6, no. 3, pp. 1453–1462, 2014.

[103] A. Alahyari, M. Fotuhi-Firuzabad, and M. Rastegar, "Incorporating customer reliability cost in pev charge scheduling schemes considering vehicle-to-home capability," *IEEE Transactions on Vehicular Technology*, vol. 64, no. 7, pp. 2783–2791, 2014.

[104] Y.-C. Hsu, S.-C. Kao, C.-Y. Ho, P.-H. Jhou, M.-Z. Lu, and C.-M. Liaw, "On an electric scooter with g2v/v2h/v2g and energy harvesting functions," *IEEE Transactions on Power Electronics*, vol. 33, no. 8, pp. 6910–6925, 2017.

[105] M. Panteli, C. Pickering, S. Wilkinson, R. Dawson, and P. Mancarella, "Power system resilience to extreme weather: fragility modeling, probabilistic impact assessment, and adaptation measures," *IEEE Transactions on Power Systems*, vol. 32, no. 5, pp. 3747–3757, 2016.

[106] E. B. Watson and A. H. Etemadi, "Modeling electrical grid resilience under hurricane wind conditions with increased solar and wind power generation," *IEEE Transactions on Power Systems*, vol. 35, no. 2, pp. 929–937, 2019.

[107] A. Sangswang and M. Konghirun, "Optimal strategies in home energy management system integrating solar power, energy storage, and vehicle-to-grid for grid support and energy efficiency," *IEEE Transactions on Industry Applications*, vol. 56, no. 5, pp. 5716–5728, 2020.

[108] P. Jamborsalamati, M. Hossain, S. Taghizadeh, G. Konstantinou, M. Manbachi, and P. Dehghanian, "Enhancing power grid resilience through an iec61850-based ev-assisted load restoration," *IEEE Transactions on Industrial Informatics*, vol. 16, no. 3, pp. 1799–1810, 2019.

[109] E. Hossain, S. Roy, N. Mohammad, N. Nawar, and D. R. Dipta, "Metrics and enhancement strategies for grid resilience and reliability during natural disasters," *Applied Energy*, vol. 290, p. 116709, 2021. [Online]. Available: https://www.sciencedirect.com/science/article/pii/S0306261921002294

[110] M. Bertoluzzo, S. Giacomuzzi, and A. Kumar, "Design of a bidirectional wireless power transfer system for vehicle-to-home applications," *Vehicles*, vol. 3, no. 3, pp. 406–425, 2021.

[111] A. Bracale, P. Caramia, P. De Falco, and T. Hong, "Multivariate quantile regression for short-term probabilistic load forecasting," *IEEE Transactions on Power Systems*, vol. 35, no. 1, pp. 628–638, 2019.

[112] T. Hossen, A. S. Nair, R. A. Chinnathambi, and P. Ranganathan, "Residential load forecasting using deep neural networks (dnn)," in *2018 North American Power Symposium (NAPS)*. IEEE, 2018, pp. 1–5.

[113] B. Liu, J. Nowotarski, T. Hong, and R. Weron, "Probabilistic load forecasting via quantile regression averaging on sister forecasts," *IEEE Transactions on Smart Grid*, vol. 8, no. 2, pp. 730–737, 2017.

[114] W. Kong, Z. Y. Dong, Y. Jia, D. J. Hill, Y. Xu, and Y. Zhang, "Short-term residential load forecasting based on lstm recurrent neural network," *IEEE Transactions on Smart Grid*, vol. 10, no. 1, pp. 841–851, 2019.

[115] X. Wang, T. Zhao, H. Liu, and R. He, "Power consumption predicting and anomaly detection based on long short-term memory neural network," in *2019 IEEE 4th international conference on cloud computing and big data analysis (ICCCBDA)*. IEEE, 2019, pp. 487–491.

[116] H. Jain, B. A. Bhatti, T. Wu, B. Mather, and R. Broadwater, "Integrated transmission-and-distribution system modeling of power systems: State-of-the-art and future research diretions," *Energies*, vol. 14, no. 1, p. 12, 2021.

[117] K. P. Schneider, B. A. Mather, B. C. Pal, C.-W. Ten, G. J. Shirek, H. Zhu, J. C. Fuller, J. L. R. Pereira, L. F. Ochoa, L. R. de Araujo, R. C. Dugan, S. Matthias, S. Paudyal, T. E. McDermott, and W. Kersting, "Analytic considerations and design basis for the ieee distribution test feeders," *IEEE Transactions on Power Systems*, vol. 33, no. 3, pp. 3181–3188, 2018.

[118] "IEEE PES Test Feeder: 123-BUS Feeder," https://cmte.ieee.org/pes-testfeeders/resources/, accessed: 2022-4-20.

[119] S. Duerr, C. Ababei, and D. M. Ionel, "Smartbuilds: An energy and power simulation framework for buildings and districts," *IEEE Transactions on Industry Applications*, vol. 53, no. 1, pp. 402–410, 2017.

[120] J. Anandan, "EPRI's DER integration testbed and toolkit," Electric Power Research Institute (EPRI), Tech. Rep. 3002016138, 2019.

[121] B. Ealey, "Overview of EPRI's DER simulation tool for emulating smart solar inverters and energy storage systems on communication networks," Electric Power Research Institute (EPRI), Tech. Rep. 3002013622, 2018.

[122] A. Bandyopadhyay, J. P. Conger, and M. E. Webber, "Energetic potential for demand response in detached single family homes in austin, tx," in *2019 IEEE Texas Power and Energy Conference (TPEC)*, 2019, pp. 1–6.

[123] X. Kou, F. Li, J. Dong, M. Starke, J. Munk, T. Kuruganti, and H. Zandi, "A distributed energy management approach for residential demand response," in *2019 3rd International Conference on Smart Grid and Smart Cities (ICSGSC)*, 2019, pp. 170–175.

[124] A. Pratt, M. Ruth, D. Krishnamurthy, B. Sparn, M. Lunacek, W. Jones, S. Mittal, H. Wu, and J. Marks, "Hardware-in-the-loop simulation of a distribution system with air conditioners under model predictive control," in *2017 IEEE Power & Energy Society General Meeting*. IEEE, 2017, pp. 1–5.

[125] J. Lian, Y. Tang, J. Fuller, K. Kalsi, and N. Wang, "Behind-the-meter transactive control approach for home energy management system," in *2018 IEEE Power Energy Society General Meeting (PESGM)*, 2018, pp. 1–5.

[126] S. Walker, T. Labeodan, W. Maassen, and W. Zeiler, "A review study of the current research on energy hub for energy positive neighborhoods," *Energy Procedia*, vol. 122, pp. 727–732, 2017.

[127] G. Mavromatidis, K. Orehounig, and J. Carmeliet, "Evaluation of photovoltaic integration potential in a village," *Solar Energy*, vol. 121, pp. 152–168, 2015.

[128] M. Zeraati, M. E. H. Golshan, and J. Guerrero, "Distributed control of battery energy storage systems for voltage regulation in distribution networks with high pv penetration," *IEEE Transactions on Smart Grid*, 2016.

[129] B. Zhang, Q. Yan, and M. Kezunovic, "Placement of ev charging stations integrated with pv generation and battery storage," in *2017 Twelfth International Conference on Ecological Vehicles and Renewable Energies (EVER)*. IEEE, 2017, pp. 1–7.

[130] S. Xiao, M. B. Shadmand, and R. S. Balog, "Model predictive control of multi-string pv systems with battery back-up in a community dc microgrid," in *2017 IEEE Applied Power Electronics Conference and Exposition (APEC)*. IEEE, 2017, pp. 1284–1290.

[131] S. Xiao and R. S. Balog, "An improved hierarchy and autonomous control for dc microgrid based on both model predictive and distributed droop control," in *2018 IEEE Applied Power Electronics Conference and Exposition (APEC)*. IEEE, 2018, pp. 3319–3325.

[132] X. Wang and F. Blaabjerg, "Harmonic stability in power electronic-based power systems: Concept, modeling, and analysis," *IEEE Transactions on Smart Grid*, vol. 10, no. 3, pp. 2858–2870, 2018.

[133] G. Sulligoi, A. Vicenzutti, V. Arcidiacono, and Y. Khersonsky, "Voltage stability in large marine-integrated electrical and electronic power systems," *IEEE Transactions on industry applications*, vol. 52, no. 4, pp. 3584–3594, 2016.

[134] Z. Wu, S. Zhou, J. Li, and X.-P. Zhang, "Real-time scheduling of residential appliances via conditional risk-at-value," *IEEE Transactions on Smart Grid*, vol. 5, no. 3, pp. 1282–1291, 2014.

[135] K. Al-Jabery, Z. Xu, W. Yu, D. C. Wunsch, J. Xiong, and Y. Shi, "Demand-side management of domestic electric water heaters using approximate dynamic programming," *IEEE Transactions on Computer-Aided Design of Integrated Circuits and Systems*, vol. 36, no. 5, pp. 775–788, 2016.

[136] S. Shao, M. Pipattanasomporn, and S. Rahman, "Development of physical-based demand response-enabled residential load models," *IEEE Transactions on power systems*, vol. 28, no. 2, pp. 607–614, 2012.

[137] K. Kurohane, T. Senjyu, A. Yona, N. Urasaki, T. Goya, and T. Funabashi, "A hybrid smart ac/dc power system," *IEEE Transactions on Smart Grid*, vol. 1, no. 2, pp. 199–204, Sep. 2010.

[138] Z. M. Haider, K. K. Mehmood, S. U. Khan, M. O. Khan, A. Wadood, and S.-B. Rhee, "Optimal management of a distribution feeder during contingency and overload conditions by harnessing the flexibility of smart loads," *IEEE Access*, vol. 9, pp. 40 124–40 139, 2021.

[139] H. Hao, C. D. Corbin, K. Kalsi, and R. G. Pratt, "Transactive control of commercial buildings for demand response," *IEEE Transactions on Power Systems*, vol. 32, no. 1, pp. 774–783, 2017.

[140] N. Tansangwom and W. Pora, "Development of smart water heater complied with mqtt and echonet lite protocols," in *2018 IEEE International Conference on Consumer Electronics - Asia (ICCE-Asia)*, 2018, pp. 206–212.

[141] M. Pipattanasomporn, M. Kuzlu, S. Rahman, and Y. Teklu, "Load profiles of selected major household appliances and their demand response opportunities," *IEEE Transactions on Smart Grid*, vol. 5, no. 2, pp. 742–750, 2013.

[142] "United states census bureau: Numer of housing unites," https://data.census.gov/cedsci/table?q=bedrooms&tid=ACSDT1Y2018.B25041&vintage=2018&hidePreview=true&g=400C100US45640&moe=false&tp=false, accessed: 2022-4-20.

[143] (2019, Aug.) Tesla Powerwall. [Online]. Available: https://www.tesla.com/powerwall

[144] "Time-Of-Use (TOU) Rate Plans, Southern California Edison," https://www.sce.com/residential/rates/Time-Of-Use-Residential-Rate-Plans, accessed: 2022-4-20.

[145] "Net Surplus Compensation Rate, Southern California Edison,"

https://www.sce.com/regulatory/tariff-books/rates-pricing-choices/net-surplus-compensation, accessed: 2022-4-20.

[146] W. H. Kersting, "Radial distribution test feeders," in *2001 IEEE Power Engineering Society Winter Meeting. Conference Proceedings (Cat. No. 01CH37194)*, vol. 2. IEEE, 2001, pp. 908–912.

[147] Y. Liu, P. V. Etingov, S. Kundu, Z. Hou, Q. Huang, H. Zhou, M. Ghosal, D. P. James, J. Zhang, Y. Xie *et al.*, "Open-source high-fidelity aggregate composite load models of emerging load behaviors for large-sale analysis," Pacific Northwest National Lab.(PNNL), Richland, WA (United States), Tech. Rep., 2020.

[148] C. C. Hiller, "Comparing water heater vs. hot water distribution system energy losses," *ASHRAE transactions*, vol. 111, p. 407, 2005.

[149] F. Sossan, A. M. Kosek, S. Martinenas, M. Marinelli, and H. Bindner, "Scheduling of domestic water heater power demand for maximizing pv self-consumption using model predictive control," in *IEEE PES ISGT Europe 2013*, 2013, pp. 1–5.

[150] A. Magerko, A. Huque, T. Hubert, A. Cortes, and R. May, "Enabling behind-the-meter distributed energy resources to provide grid services," in *2019 IEEE 46th Photovoltaic Specialists Conference (PVSC)*. IEEE, 2019, pp. 2064–2071.

[151] "Energy Smart Electric Water Heater Controller: Installation, Operation and Troubleshoooting Instructions," https://www.lowes.com/pdf/Energy_Smart_Electric_Water_Heater_Controller.pdf, accessed: 2021-08-12.

[152] "Reginal study of cta-2045 enabled water heaters," https://www.bpa.gov/EE/Technology/demand-response/Pages/CTA2045-DataShare.aspx, accessed: 2021-06-24.

[153] "Energy Plus Documentation: Engineering Reference," https://energyplus.

net/assets/nrel_custom/pdfs/pdfs_v9.5.0/EngineeringReference.pdf, accessed: 2021-09-08.

[154] V. R. Salcido, Y. Chen, Y. Xie, and Z. T. Taylor, "Energy Savings Analysis: 2021 IECC for Residential Buildings," Pacific Northwest National Laboratory (PNNL), Tech. Rep., 2021.

[155] "Ecotope Research: HPWHsim," https://github.com/EcotopeResearch/HPWHsim, accessed: 2021-09-08.

[156] H. Gong, E. S. Jones, A. H. M. Jakaria, A. Huque, A. Renjit, and D. M. Ionel, "Generalized energy storage model-in-the-loop suitable for energy star and cta-2045 control types," in *2021 IEEE Energy Conversion Congress and Exposition (ECCE)*. IEEE, 2021, pp. 1–5.

[157] H. Zandi and E. McKee, "Rl-hems: Reinforcement learning based home energy management system for hvac energy optimization," *ASHRAE Transactions*, vol. 126, pp. 421–429, 2020.

[158] M. Javadi, A. E. Nezhad, K. Firouzi, F. Besanjideh, M. Gough, M. Lotfi, A. Anvari-Moghadam, and J. P. S. Catalão, "Optimal operation of home energy management systems in the presence of the inverter-based heating, ventilation and air conditioning system," in *2020 IEEE International Conference on Environment and Electrical Engineering and 2020 IEEE Industrial and Commercial Power Systems Europe (EEEIC / I CPS Europe)*, 2020, pp. 1–6.

[159] M. Alavy, T. Li, and J. A. Siegel, "Energy use in residential buildings: Analyses of high-efficiency filters and hvac fans," *Energy and Buildings*, vol. 209, p. 109697, 2020.

[160] R. Z. Homod, K. S. Gaeid, S. M. Dawood, A. Hatami, and K. S. Sahari, "Evaluation of energy-saving potential for optimal time response of hvac control system in smart buildings," *Applied Energy*, vol. 271, p. 115255, 2020.

[161] S. Khemakhem, M. Rekik, and L. Krichen, "Optimal appliances scheduling for demand response strategy in smart home," in *2017 18th International Conference on Sciences and Techniques of Automatic Control and Computer Engineering (STA)*, 2017, pp. 546–550.

[162] Y. Wang, X. Ai, Z. Tan, L. Yan, and S. Liu, "Interactive dispatch modes and bidding strategy of multiple virtual power plants based on demand response and game theory," *IEEE Transactions on Smart Grid*, vol. 7, no. 1, pp. 510–519, 2015.

[163] G. Brusco, G. Barone, A. Burgio, D. Menniti, A. Pinnarelli, L. Scarcello, and N. Sorrentino, "A smartbox as a low-cost home automation solution for prosumers with a battery storage system in a demand response program," in *2016 IEEE 16th International Conference on Environment and Electrical Engineering (EEEIC)*, 2016, pp. 1–6.

[164] L. Bhamidi and S. Sivasubramani, "Optimal sizing of smart home renewable energy resources and battery under prosumer-based energy management," *IEEE Systems Journal*, pp. 1–9, 2020.

[165] M. T. Beyerle and J. D. Nelson, "Water heater with integral thermal mixing valve assembly and method," Feb. 23 2016, uS Patent 9,268,342.

[166] Y. Qi, D. Wang, X. Wang, H. Jia, T. Pu, N. Chen, and K. Liu, "Frequency control ancillary service provided by efficient power plants integrated in queuing-controlled domestic water heaters," *Energies*, vol. 10, no. 4, p. 559, 2017.

[167] "Residential energy consumption survey (RECS)," https://www.eia.gov/consumption/residential/index.php, accessed: 2020-06-29.

[168] M. Hu, F. Xiao, and L. Wang, "Investigation of demand response potentials of residential air conditioners in smart grids using grey-box room thermal model," *Applied energy*, vol. 207, pp. 324–335, 2017.

[169] M. Hu and F. Xiao, "Price-responsive model-based optimal demand response control of inverter air conditioners using genetic algorithm," *Applied energy*, vol. 219, pp. 151–164, 2018.

[170] X. Zhang, M. Cai, M. Pipattanasomporn, and S. Rahman, "A power disaggregation approach to identify power-temperature models of hvac units," in *2018 IEEE International Smart Cities Conference (ISC2)*, 2018, pp. 1–6.

[171] D. T. Vedullapalli, R. Hadidi, and B. Schroeder, "Optimal demand response in a building by battery and hvac scheduling using model predictive control," in *2019 IEEE/IAS 55th Industrial and Commercial Power Systems Technical Conference (I CPS)*, 2019, pp. 1–6.

[172] B. Cui, J. Dong, J. D. Munk, N. Mao, and T. Kuruganti, "A simplified regression building thermal modelling method for detached two-floor house in us," Oak Ridge National Lab.(ORNL), Oak Ridge, TN (United States), Tech. Rep., 2018.

[173] X. Chen, Q. Hu, Q. Shi, X. Quan, Z. Wu, and F. Li, "Residential hvac aggregation based on risk-averse multi-armed bandit learning for secondary frequency regulation," *Journal of Modern Power Systems and Clean Energy*, vol. 8, no. 6, pp. 1160–1167, 2020.

[174] "TVA Smart Community," https://www.tva.com/environment/environmental-stewardship/epa-mitigation-projects/smart-communities, accessed: 2020-11-28.

[175] H. Gong, V. Rallabandi, D. M. Ionel, D. Colliver, S. Duerr, and C. Ababei, "Net zero energy houses with dispatchable solar pv power supported by electric water heater and battery energy storage," in *2018 IEEE Energy Conversion Congress and Exposition (ECCE)*. IEEE, 2018, pp. 2498–2503.

[176] M. Pipattanasomporn, M. Kuzlu, and S. Rahman, "An algorithm for intelligent home energy management and demand response analysis," *IEEE Transactions on Smart Grid*, vol. 3, no. 4, pp. 2166–2173, 2012.

[177] "Hourly electricity consumption varies throughout the day and across seasons," https://www.eia.gov/todayinenergy/detail.php?id=42915, accessed: 2020-11-28.

[178] "Savings project: Lower water heating temperature," https://www.energy.gov/energysaver/services/do-it-yourself-energy-savings-projects/savings-project-lower-water-heating, accessed: 2020-11-28.

[179] D. S. Callaway, "Tapping the energy storage potential in electric loads to deliver load following and regulation, with application to wind energy," *Energy Conversion and Management*, vol. 50, no. 5, pp. 1389–1400, 2009.

[180] Weather Spark, "Average Weather in July in Glasglow Kentucky, United States," https://weatherspark.com/m/15163/7/Average-Weather-in-July-in-Glasgow-Kentucky-United-States#Sections-Temperature, accessed: 2021-04-15.

[181] F. Tartarini, S. Schiavon, T. Cheung, and T. Hoyt, "CBE thermal comfort tool: Online tool for thermal comfort calculations and visualizations," *SoftwareX*, vol. 12, p. 100563, 2020.

[182] U.S. Energy Information Administration (EIA), "Residential Energy Consumption Survey (RECS)," https://www.eia.gov/consumption/residential/data/2015/hc/php/hc6.1.php, accessed: 2021-07-28.

[183] "National Travel Household Survey," https://nhts.ornl.gov/, accessed: 2020-5-13.

[184] K. Park, S. Yoon, and E. Hwang, "Flexible charging coordination for plug-in electric vehicles based on uniform stochastic charging demand and time-of-use tariff," in *2019 IEEE Transportation Electrification Conference and Expo (ITEC)*. IEEE, 2019, pp. 1–4.

[185] B. Khaki, Y.-W. Chung, C. Chu, and R. Gadh, "Probabilistic electric vehicle

load management in distribution grids," in *2019 IEEE Transportation Electrification Conference and Expo (ITEC)*. IEEE, 2019, pp. 1–6.

[186] T. Markel, A. Meintz, K. Hardy, B. Chen, T. Bohn, J. Smart, D. Scoffield, R. Hovsapian, S. Saxena, J. MacDonald *et al.*, "Multi-lab EV smart grid integration requirements study. providing guidance on technology development and demonstration," National Renewable Energy Lab.(NREL), Golden, CO (United States), Tech. Rep., 2015.

[187] "Useable battery capacity of full electric vehicles," https://ev-database.org/cheatsheet/useable-battery-capacity-electric-car, accessed: 2022-01-24.

[188] W. Wang, P. Chen, D. Zeng, and J. Liu, "Electric vehicle fleet integration in a virtual power plant with large-scale wind power," *IEEE Transactions on Industry Applications*, vol. 56, no. 5, pp. 5924–5931, 2020.

[189] A. J. Hasan, L. F. Enriquez-Contreras, J. Yusuf, M. J. Barth, and S. Ula, "Demonstration of microgrid resiliency with v2g operation," in *2021 IEEE Transportation Electrification Conference & Expo (ITEC)*. IEEE, 2021, pp. 243–248.

[190] U. C. Chukwu and S. M. Mahajan, "The prospects of v2g for reactive power compensation in electric distribution networks," in *2019 IEEE Power & Energy Society General Meeting (PESGM)*. IEEE, 2019, pp. 1–5.

[191] C. Thomas, "Performance test results: Cta-2045 electric vehicle supply equipment," ELECTRIC POWER RESEARCH INSTITUTE (EPRI), Palo Alto, California (United States), Tech. Rep. 3002011757, 2017.

[192] M. Afzalan and F. Jazizadeh, "Quantification of demand-supply balancing capacity among prosumers and consumers: Community self-sufficiency assessment for energy trading," *Energies*, vol. 14, no. 14, p. 4318, 2021.

[193] "U.S Energy Information Administration–Electricity," https://www.eia.gov/electricity/data/state/, accessed: 2021-04-09.

[194] P. Rajput, M. Malvoni, N. Manoj Kumar, O. Sastry, and A. Jayakumar, "Operational performance and degradation influenced life cycle environmental–economic metrics of mc-si, a-si and hit photovoltaic arrays in hot semi-arid climates," *Sustainability*, vol. 12, no. 3, p. 1075, 2020.

[195] P. Gangwar, N. M. Kumar, A. K. Singh, A. Jayakumar, and M. Mathew, "Solar photovoltaic tree and its end-of-life management using thermal and chemical treatments for material recovery," *Case Studies in Thermal Engineering*, vol. 14, p. 100474, 2019.

[196] E. Chatterji and M. D. Bazilian, "Battery storage for resilient homes," *IEEE Access*, vol. 8, pp. 184 497–184 511, 2020.

[197] Independent Statistics & Analysis, "Battery Storage in the United States: An Update on Market Trends," U.S. Department of Energy (DOE), Tech. Rep., 2020.

[198] A. Bhattacharjee, R. K. Mohanty, and A. Ghosh, "Design of an optimized thermal management system for li-ion batteries under different discharging conditions," *Energies*, vol. 13, no. 21, p. 5695, 2020.

[199] "California Auto Outlooks," https://www.cncda.org/news/, accessed: 2021-04-09.

[200] Q. Liang, L. Lin, B. Zhou, and W. Zhao, "Modeling of pev charging load based on trip chain theory and the impact of pev on distribution networks," in *2018 International Conference on Power System Technology (POWERCON)*. IEEE, 2018, pp. 1789–1794.

[201] S. Shafiee, M. Fotuhi-Firuzabad, and M. Rastegar, "Investigating the impacts of plug-in hybrid electric vehicles on power distribution systems," *IEEE Transactions on Smart Grid*, vol. 4, no. 3, pp. 1351–1360, 2013.

[202] "Live Solar Generation Data," https://lge-ku.com/live-solar-generation, accessed: 2020-08-04.

[203] "Building Energy Codes Program–Residential Prototype Building Models," https://www.energycodes.gov/development/residential/iecc_models, accessed: 2021-04-09.

[204] "Burbank-Glendale-Passadena Bob Hope AP 722880 (TMY3)," https://energyplus.net/weather-location/north_and_central_america_wmo_region_4/USA/CA/USA_CA_Burbank-Glendale-Passadena.Bob.Hope.AP.722880_TMY3, accessed: 2021-04-09.

[205] "FlexPower–Discover SPIN," http://flxpwr.com/, accessed: 2021-04-09.

[206] "Multifunction power management system," https://uspto.report/patent/grant/11,011,913, accessed: 2021-06-29.

[207] United States Energy Information Administration (EIA), "Use of energy explained, monthly energy review, table 2.1," https://www.eia.gov/energyexplained/use-of-energy/, 2021.

[208] H. C. Anderson, A. Al Hadi, E. S. Jones, and D. M. Ionel, "Power factor and reactive power in us residences–survey and energyplus modeling," in *2021 10th International Conference on Renewable Energy Research and Application (ICRERA)*. IEEE, 2021, pp. 418–422.

[209] U. S. Energy Information Administration (EIA), "Residential energy consumption survey," https://www.eia.gov/energyexplained/use-of-energy/homes.php, 2015.

[210] B. Liu, M. Akcakaya, and T. E. Mcdermott, "Automated control of transactive hvacs in energy distribution systems," *IEEE Transactions on Smart Grid*, vol. 12, no. 3, pp. 2462–2471, 2020.

[211] M. Liang, Y. Meng, N. Lu, D. Lubkeman, and A. Kling, "Hvac load disaggregation using low-resolution smart meter data," in *2019 IEEE Power Energy Society Innovative Smart Grid Technologies Conference (ISGT)*, 2019, pp. 1–5.

[212] R. Alden, H. Gong, E. S. Jones, C. Ababei, and D. M. Ionel, "Artificial intelligence method for the forecast and separation of total and hvac loads with application to energy management of smart and nze homes," *IEEE Access*, 2021.

[213] B. Najafi, L. Di Narzo, F. Rinaldi, and R. Arghandeh, "Machine learning based disaggregation of air-conditioning loads using smart meter data," *IET Generation, Transmission & Distribution*, vol. 14, no. 21, pp. 4755–4762, 2020.

[214] A. Aswani, N. Master, J. Taneja, V. Smith, A. Krioukov, D. Culler, and C. Tomlin, "Identifying models of hvac systems using semiparametric regression," in *2012 American Control Conference (ACC)*, 2012, pp. 3675–3680.

[215] M. Zou, S. Zhu, J. Gu, L. M. Korunovic, and S. Z. Djokic, "Heating and lighting load disaggregation using frequency components and convolutional bidirectional long short-term memory method," *Energies*, vol. 14, no. 16, 2021. [Online]. Available: https://www.mdpi.com/1996-1073/14/16/4831

[216] A. Abbas and B. Chowdhury, "A data-driven approach for providing frequency regulation with aggregated residential hvac units," in *2019 North American Power Symposium (NAPS)*. IEEE, 2019, pp. 1–6.

[217] N. MacMackin, L. Miller, and R. Carriveau, "Modeling and disaggregating hourly effects of weather on sectoral electricity demand," *Energy*, vol. 188, 2019-12.

[218] T. Hong, *Short term electric load forecasting*. North Carolina State University, 2010.

[219] T. Hong, P. Pinson, S. Fan, H. Zareipour, A. Troccoli, and R. J. Hyndman, "Probabilistic energy forecasting: Global energy forecasting competition 2014 and beyond," *International Journal of Forecasting*, vol. 32, no. 3, pp. 896–913, 2016. [Online]. Available: https://www.sciencedirect.com/science/article/pii/S0169207016000133

[220] H. Liang and J. Ma, "Separation of residential space cooling usage from smart meter data," *IEEE Transactions on Smart Grid*, vol. 11, no. 4, pp. 3107–3118, 2020.

[221] R. Hendron and C. Engebrecht, "Building america research benchmark definition," National Renewable Energy Laboratory, Technical Report NREL/TP-550-47246, December 2009.

[222] H. Gong, T. Rooney, O. M. Akeyo, B. T. Branecky, and D. M. Ionel, "Equivalent electric and heat-pump water heater models for aggregated community-level demand response virtual power plant controls," *IEEE Access*, vol. 9, pp. 141 233–141 244, 2021.

[223] A. Bellahsen and H. Dagdougui, "Aggregated short-term load forecasting for heterogeneous buildings using machine learning with peak estimation," *Energy and buildings.*, vol. 237, 2021-04.

[224] Boudreaux et al, "Final Review of the Campbell Creek Demonstration Showcased by Tennessee Valley Authority," Oak Ridge National Laboratory, Oak Ridg, Tennessee 37831-6283, Tech. Rep. ORNL/TM-2015/666, June 2015.

[225] "Efficiency requirements for residential central ac and heat pumps to rise in 2023," https://www.eia.gov/todayinenergy/detail.php?id=40232, accessed: 2021-12-06.

[226] J. Paige, C. McMillan, D. Steinberg, M. Muratori, L. Vimmerstedt, and M. Trieu, *Electrification Futures Study: End-Use Electric Technology Cost and Performance Projections through 2050.* National Renewable Energy Laboratory (NREL), Golden, CO, 2017.

Vita

Huangjie Gong, PhD Candidate

Department of Electrical and Computer Engineering, University of Kentucky

Huangjie Gong is a Ph.D. candidate in the SPARK Laboratory, Electrical and Computer Engineering Department at University of Kentucky (UK). He started his studies at UK in 2017 after receiving his M.S. degree in Control Theory and Engineering from Southwest Jiaotong University, Chengdu, China. At UK, he has been working as a Teaching Assistant and as a Research Assistant on projects sponsored by DOE, NSF, companies, utilities, including TVA and LG&E-KU, and EPRI. He is the main developer of an HPC-based large-scale co-simulation software framework for energy use in buildings and power flow in electric power distribution systems incorporating EnergyPlus and OpenDSS as computational engines. Huangjie also conducts research on machine and deep learning for human behavior and energy management in smart buildings. Additional research topics include: HVAC, water heater, EV, PV, and battery modeling and control, power system controls and protection, net-zero-energy (NZE) buildings, aggregate models for loads and DER in electric power distribution systems, and smart grids.